

**PERSPECTIVES IN FUNDAMENTAL  
AND APPLIED RHEOLOGY**



# **PERSPECTIVES IN FUNDAMENTAL AND APPLIED RHEOLOGY**

**Edited by:**

**Francisco José Rubio-Hernández**

*Universidad de Málaga (Spain)*

**Ana Isabel Gómez-Merino**

*Universidad de Málaga (Spain)*

**Carlos del Pino**

*Universidad de Málaga (Spain)*

**Luis Parras**

*Universidad de Málaga (Spain)*

**Laura Campo-Deaño**

*Universidade do Porto (Portugal)*

**Francisco José Galindo-Rosales**

*Universidade do Porto (Portugal)*

**José Francisco Velázquez-Navarro**

*Universidad de Málaga (Spain)*

Perspectives in Fundamental and Applied Rheology - 2nd Edition

Published by:

The Editors

Copyright © F.J. Rubio-Hernández, A.I. Gómez-Merino, C. Pino, L. Parras, L. Campo-Deaño, F.J. Galindo-Rosales and J.F. Velázquez Navarro

Málaga, 2013

ISBN 978-84-616-6551-8

# Preface

In the last years Rheology, defined as the science of deformation and flow of matter, has revealed as one of the most attractive and multidisciplinary scientific field in the current research activity. As it happens in other many scientific disciplines, Rheology can be classified in fundamental and applied research, in response to the different studies developed. Fundamental Rheology is made with the basic research carried out in laboratories using rheometry and other experimental methods to characterize the behavior of non-Newtonian fluids. As part of this research area, we should not forget the great advances obtained in both theoretical and computational Rheology, which have given us a new global perspective and new active branches in Fluid Mechanics. The Applied Rheology corresponds to the characterization of complex fluids (multiphasic systems and composites, biomaterials, biopolymers) and the study of several materials (foods, cosmetics and pharmaceuticals), paying special attention to its practical applications (e.g. formulation and product engineering).

The title of this book, *Perspectives in Fundamental and Applied Rheology*, clearly expresses the philosophy of its content, being its purpose to provide a wide overview of the trending topics among the rheologists engaged in both industrial and academic research from different countries. Its content results from the contribution of different international authors to a number of topics: Biomaterials and Biopolymers, Food, Cosmetics and Pharmaceutical Products, Formulation and Product Engineering, Multiphasic Systems and Composites, Non-Newtonian Fluid Mechanics, Polymer and Liquid Crystals, Rheometry and Experimental Methods, Suspensions and Colloids, which have been adequately structured.

We hope you enjoy with the reading of this book and gain a grasp of fundamental and applied aspects of Rheology in which research is currently focused.

The Editors



## **Preface to the 2<sup>nd</sup> edition**

This new edition includes some new contributions to Fundamental and Applied Rheology. Following major contributors suggestion we have published this second edition in electronic form with the new capabilities that it involves. We hope you found it interesting and useful .

The Editors



# Contents

<b><i>Part I: Biomaterials and Biopolymers</i></b>	<b>1</b>
1. Evaluation of acylation reactions to improve chitosan thickening and gelling properties in castor oil	3
2. Injection-moulded bioplastics from rice husk protein	9
3. Rheological characterization and thermogravimetric analysis of oleogels containing isocyanate-functionalized biopolymers as gelling agent	15
4. Characterisation of crayfish flour-based bioplastics processed by injection moulding	21
5. <i>Staphylococcus aureus</i> strains rheology during growth	27
6. Rheological study and physical stability of emulsions formulated with alpha-pinene and hydrocolloids.	31
7. Synovial Fluid Hyaluronate Characterization in Stagnation Point Extensional Flow	37
8. Skin viscoelasticity and hydration studies on the topical application of a surfactant free emulsion	45
9. Egg albumen/tragacanth gum based bioplastics plasticised with water/glycerol mixtures	51
10. Shear and elongational flow measurements of PCL/PLA blends	57
11. Development of protein-based composite materials by thermomechanical processing	63
12. Rheological characterization of chitosan solutions and chitosan/beeswax emulsions to be used in edible films	69

13. Rheological and thermogravimetric response of an acylated chitosan gel-like dispersion in castor oil and traditional lithium and calcium lubricating greases: a comparative study \_\_\_\_\_ 73

***PART II: Food, Cosmetics and Pharmaceutical Products* \_\_\_\_\_ 79**

1. Rheological study on wheat bread dough with Brewer's Spent Grain \_\_\_\_\_ 81
2. Texture analysis on wheat bread with Brewer's Spent Grain 87
3. Rheological characterization of Chia flour gels for culinary purpose \_\_\_\_\_ 93
4. Orientation effects during flow in clay/water suspensions \_ 99
5. Rheological and kinetic study of the influence of PEG-400 on a Hyaluronic acid polymeric matrix for topical metronidazole administration \_\_\_\_\_ 105
6. Influence of the preservative on rheological properties and on *in vitro* release profiles of topical gels containing AINES \_\_ 111
7. Rheological characterization of different toothpastes. Analysis of parameters with influence on the packaging process \_\_\_\_ 117
8. Rheology of fine particle size chestnut flour doughs with common bakery additives \_\_\_\_\_ 123
9. Fat replacement in biscuits by sunflower oil-water-cellulose emulsions. Effect in dough oscillatory and creep properties 129
10. Effect of high-pressure on the viscoelastic properties of aqueous glucomannan dispersions \_\_\_\_\_ 135
11. Influence of pH and type of acid anion on the linear viscoelastic properties of Egg Yolk \_\_\_\_\_ 143
12. Influence of Lipids on the Rheological Properties of Amimulsion – a new safe cosmetic emulsion \_\_\_\_\_ 149
13. Comparative effect of high-pressure and pH on the viscoelastic characteristics of aqueous glucomannan dispersions \_\_\_\_\_ 157

14. Rheological and texture properties of gels and emulsions prepared with pea protein isolate and proteins recovered from Cape hake by-products _____	165
15. Effect of high pressure treatment on thermal and rheological properties of chickpea ( <i>Cicer arietinum</i> L.) flour dispersions and pastes _____	173
16. Effect of temperature on the viscoelastic characteristics of San Simón da Costa cheese (PDO) _____	181
17. Effect of setting time on the rheological properties of suwari gels made with squid surimi with added Konjac glucomannan _____	189
18. Dependence on rheological properties of gluten-free doughs with flour processing: effect of temperature and particle load density during air drying _____	197
19. Topical application of lipid nanoparticle-containing gels: impact on skin viscoelasticity _____	205
20. Rheological behaviour and structure of food thickeners used for dysphagia treatment when dissolved in water and milk	211
21. Flow behaviour of citrus flavoured soy desserts. Influence of interaction between protein and starch _____	217
22. Rheological and microstructural study on food emulsions stabilized by tuna proteins: effect of emulsion pH _____	225
<b><i>PART III: Formulation and Product Engineering</i></b> _____	<b>231</b>
1. Influence of homogenization rate of O/W emulsions containing a mixture of green solvents and a polyoxyethylene glycerol ester. _____	233
2. Rheological behaviour and microstructure of NCO-terminated castor oil bituminous products _____	241
3. Rheological Characterization of $\alpha$ -pinene multiple emulsions formulated with two amphiphilic copolymers with different HLB and gellan gum. _____	247

4.	Modification of PVC plasticizers using ionic liquids _____	253
5.	Rheological characterization of lubricating greases based on vegetable oil-derived basestocks containing biodegradable and traditional thickeners agents _____	259
6.	Preparation, Rheology and Physical Stability of O/W emulsions formulated with a mixture of green solvents _____	265
7.	Influence of the presence of sodium bicarbonate on thermal and mechanical properties of soy-based plastics processed through injection moulding _____	271
8.	Relationship between protein stabilized emulsions properties and controlled emulsification process by a mixer type rheometer _____	277
9.	Effects of Nanoclay/MDI Modification on Bitumen Properties _____	285
10.	Rheology, microstructure and physical stability of limonene in water emulsions stabilized by PE9400 and rosin gum. Influence of surfactant concentration _____	291
<b><i>PART IV: Multiphasic Systems, Composites, Polymers and Liquid Crystals</i></b> _____		<b>299</b>
1.	Influence of the calcium sulfate source on the rheological behaviour of calcium sulfoaluminate cement pastes _____	301
2.	Rheological behavior of LDPE/montmorillonite nanoclays_	307
3.	Taking advance of dynamic viscoelastic measurements to investigate polyurethane/graphene nanocomposites _____	313
4.	The rheological behavior of concrete equivalent mortars when electric arc furnace slag is used as fine aggregated _____	319
5.	When Liquid Crystalline Cellulose Flows and Relaxes _____	325
<b><i>PART V: Non-Newtonian Fluid Mechanics</i></b> _____		<b>331</b>
1.	Numerical simulations of the flow through blood vessels with stenosis _____	333

2.	Velocity overshoots in rectangular rectilinear microchannels	339
3.	Torque measurements in Newtonian and non-Newtonian fluids in Couette-Taylor flow	345
4.	Numerical Investigation of Viscoelastic Instabilities in Taylor-Couette Flow with Counter-Rotating Cylinders	351
5.	Flow of Red Blood Cells in Microchannel Networks: <i>in vitro</i> studies	357
6.	Visualization of the cell-free layer (CFL) in a PDMS microchannel with a micro-stenosis	363
	<b><i>PART VI: Rheometry and Experimental Methods</i></b>	<b>369</b>
1.	New trends in Rheology and accesories.	371
2.	Blood flow in microchannels manufactured by a low cost technique: xurography	377
3.	Synthesis and rheological characterization of magnetic fluids: influence of the stabilizer agents	383
4.	Assessment of wall-depletion phenomena in dilute multiple emulsions	391
5.	Simultaneous Rheometry and FT-IR Spectroscopy or Polarization Light Microscopy	397
6.	Flow visualizations in a rotating vane rheometer	401
7.	Separation and deformation of red blood cells in PDMS microchannels	407
	<b><i>PART VII: Suspensions and Colloids</i></b>	<b>415</b>
1.	Rheology of ethylene glycol based TiO <sub>2</sub> (anatase and rutile) nanofluids at high concentrations	417
2.	Scouting the rheology of aqueous dispersions of a food-grade advanced performance xanthan gum	423
3.	Viscosity empirical model for suspensions considering the effects of the shear rate and the concentration of particles	431

***Author Index*** \_\_\_\_\_ **437**

# **PART I**

## **Biomaterials and Biopolymers**



## CHAPTER 1

# Evaluation of acylation reactions to improve chitosan thickening and gelling properties in castor oil

G. Alonso<sup>1</sup>, R. Sánchez<sup>1,2</sup>, C. Valencia<sup>1,2</sup>, J.F. Arteaga<sup>1</sup>, J.M. Franco<sup>1,2</sup>

<sup>1</sup>Departamento de Ingeniería Química, Química Física y Química Orgánica. Campus de “El Carmen”. Universidad de Huelva. 21071 Huelva. Spain. Campus de Excelencia Internacional Agroalimentario, ceiA3.

<sup>2</sup>Pro2TecS – Chemical Process and Product Technology Research Center. Universidad de Huelva. 21071 Huelva. Spain.

### Introduction

Chitin, a natural polysaccharide, is known to be the  $\beta$ -1,4-glycan of N-acetyl-D-glucosamine (GlcNAc) [1]. Chitosan is a linear polysaccharide of  $\beta$ -(1,4)-2-aminos-2-deoxy-D-glucopyranose (GlcN) and 2-acetamido-2-deoxy-D-glucopyranose (GlcNAc) residues. This is one of the most important partially deacetylated derivatives obtained from chitin [2].

The applications of chitosan were limited owing to the intra and/or intermolecular hydrogen bonding from the acetamido or primary amino group residues. Low solubility of chitosan in both water and organic solvents resulted in many studies aimed at making water-soluble or organic-soluble chitosan derivatives by chemical modification techniques owing to both the reactive amino and hydroxyl groups by means of quaternarization, carboxymethylation, graft modification, and N- and O-hydroxyalkylation [3].

Lubricating greases are generally described as structured colloidal suspensions where a solid thickener and/or gelling agent is dispersed in a lubricating oil. The main difference between lubricating greases and other lubricants is their characteristic rheological behavior, frequently referred as consistency in the lubricant industry, which results from the addition of the thickener [4].

The objective of this study was to evaluate the use of acylated chitosans containing acyl groups of different lengths to thicken castor oil in order to be proposed as biodegradable alternatives to traditional lubricating greases. The rheological and thermogravimetric response of these gel-like dispersions is analyzed in this work.

### Experimental

#### *Materials*

Chitosan ( $M_w = 2.29 \cdot 10^5$  g/mol; DD = 86.3%) purchased from Qingdao Fraken (China) was modified with stearyl, palmitoyl, lauroyl and decanoyl chloride supplied by Sigma-Aldrich. All other common reagents and solvents employed were purchased from Sigma-Aldrich. Castor oil (211 cSt at 40°C, Guinama, Spain) was used as base oil for oleogel formulations.

#### *Synthesis and characterization of acylated-functionalized chitosan*

Four different types of acyl chloride were used to functionalize chitosan. The introduction of the acyl groups was made through two different methodologies dealing with the reaction in both acid and basic media.

##### *1. Reaction in acid medium, N-acylation*

A mixture of chitosan (12 g) and aqueous acetic acid (600 mL, 0.12 M) was stirred for 24 h to ensure total solubility. The pH was adjusted to 7.2 by slow addition of 0.1 M NaOH with strong agitation, yielding a gel slurry. The acyl chloride (72.0 g) was added and the reaction volume diluted to 1 L with distilled water. After 6h, each preparation was neutralized (pH=7.00) and precipitated with acetone. The precipitate, collected by filtration, was washed with an excess of methanol and decanted. The washing process was repeated three times to eliminate free fatty acids. Finally, the products were dried with pure acetone to obtain the corresponding derivative powders [5].

##### *2. Reaction in basic medium, N- and OH- acylation*

Chitosan (12.0 g) was soaked in triethylamine (100 mL) and acetone (60 mL) for 6 h at 50°C. The acyl chloride (72.0 g) dissolved in acetone (40 mL) was added dropwise into the solution in 3h. This solution was filtered and poured into 400 mL of acetone for 5 min. Then, the precipitate was filtered and washed with an excess of methanol for three times. Finally, the products were dried in the oven at 40°C. This procedure was carried out with different acyl chlorides (stearyl, palmitoyl and lauroyl) [2].

#### *Processing of gel-like dispersions*

Processing of gel-like dispersions samples was performed in an open vessel, using a controlled-rotational speed mixer (60 rpm), equipped with a helical ribbon impeller. Thickener concentration in each formulation was 35%. Samples were heated at 100°C during 30 min. and then cooled down to room temperature by external natural convection, while continuously stirring the mixture in the same heating device.

### Thermogravimetric analysis (TGA)

Measurements of mass losses versus temperature were carried out by using a thermogravimetric analyzer, model Q-50 (TA Instrument Waters, USA) under N<sub>2</sub> purge. Typically, 5-10 mg of sample were placed on a platinum pan and heated from 30 °C to 600 °C, at 10 °C/min.

### Rheological characterization

Rheological characterization of gel-like dispersions was carried out with a rheometer (Physica MCR-501, Anton Paar, Austria). Small-amplitude oscillatory shear (SAOS) tests were performed inside the linear viscoelastic region, using plate-plate geometries (25 mm and 50 mm, and 1 mm gap), in a frequency range of 10<sup>-2</sup>-10<sup>2</sup> rad/s, at 25 °C. Measurements were done one day after gel-like dispersions preparation.

## Results and Discussion

As can be observed in Figure 1, thermal decomposition of acylated chitosan occurs in several stages, the main one appearing at the lower temperatures. For this main degradation step, the temperature where the maximum mass loss rate is reached ( $T_{max}$ ) increases with the length of the hydro-carbonate radical of the acyl group inserted in the chitosan. The characteristic onset temperatures obtained from TGA are listed in Table 1, generally following the same tendency as  $T_{max}$ .

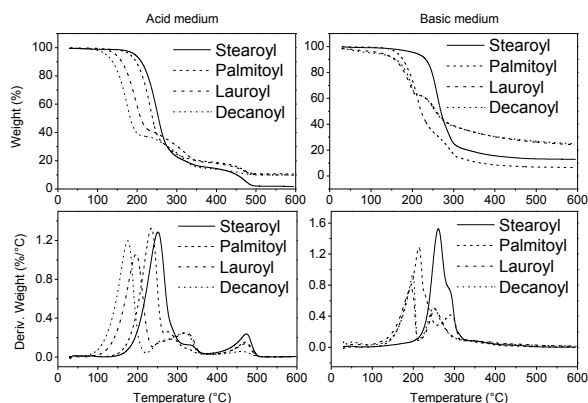


Figure 1. TGA thermograms for the different acylated chitosan studied

## Perspectives in Fundamental and Applied Rheology

Figure 2 shows the evolution of the SAOS functions with frequency for chitosan-based oleogels prepared using chitosan acylated with acyl groups of different length in the acid medium reaction. As can be observed, a “plateau” region of the mechanical spectrum is always noticed, similarly to that found in standard lubricating greases [6, 7]. A significant decrease in both moduli was also detected as the carbon chain length in the acyl group decreases excepting for the palmitoyl-functionalized chitosan-based gel-like dispersion, which exhibits the highest values of both moduli. The same evolution is also noticed in those oleogels thickened with chitosan molecules acylated in the basic medium (Figure 3). Whereas a significant decrease in both moduli is detected by changing the stearoyl fatty residue by the lauroyl one when the reaction occurred in the acid medium, in the case of acylating the chitosan in a basic medium the reduction of  $G'$  and  $G''$  is more gradual. As a result, stearoyl and palmitoyl acylated chitosans produced gel-like dispersions with higher SAOS functions when the acylation reaction was carried out in the acid medium. On the contrary, the chitosan acylation with lauroyl and decanoyl chloride in the basic medium yields oleogels with higher values of  $G'$  and  $G''$ . In this sense, an appropriate selection of the fatty chain and acylation medium allows to obtain modified chitosan molecules able to thicken castor oil in different degree.

*Table 1. TGA characteristic onset temperature for the different acylated chitosan studied*

Sample	$T_{\text{onset}} (^{\circ}\text{C})$	
	Acid medium	Basic medium
Stearoyl	215.7	236.8
Palmitoyl	201.9	181.3
Lauroyl	160.3	162.6
Decanoyl	141.3	173.4

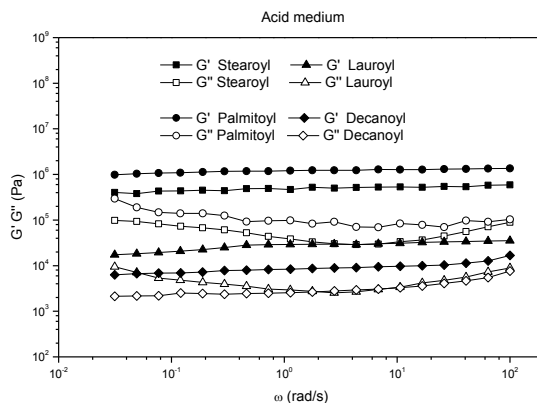


Figure 2. Rheological response of gel-like dispersions prepared with chitosan acylated in an acid medium

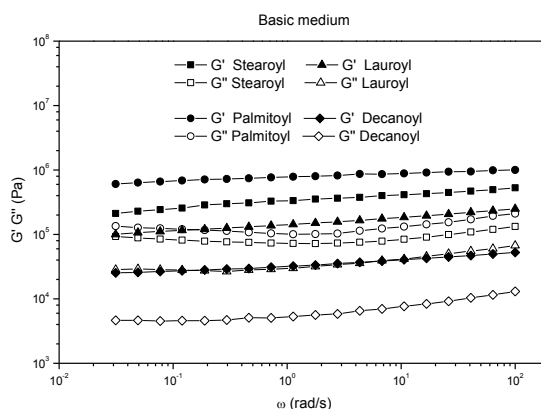


Figure 3. Rheological response of gel-like dispersions prepared with chitosan acylated in a basic medium

### Acknowledgements

This work is part of a research project (CTQ2010–15338) sponsored by a MEC-FEDER Programme. The authors gratefully acknowledge the financial support.

### References

1. Nagahama, H., Kashiki, T., Nwe, N., Jayakumar, R., Furuike, T. and Tamura, H. (2008). Carbohydr. Polym. 73, 456-463.
2. Ma, G., Yang, D., Kennedy J.F. and Nie, J. (2009). Carbohydr. Polym. 75, 390-394.

## Perspectives in Fundamental and Applied Rheology

3. Ma, G., Liu, Y., Kennedy, J.F. and Nie, J. (2011). *Carbohydr. Polym.* 84, 681-685.
4. Sánchez, R., Stringari, G.B., Franco, J.M., Valencia, C. and Gallegos, C. (2011). *Carbohydr. Polym.* 85, 705-714.
5. Le Tien, C., Lacroix, M., Ispas-Szabo, P. and Mateescu, M.A. (2003). *J. Controlled Release* 93, 1-13.
6. Madiedo, J.M., Franco, J.M., Valencia, C. and Gallegos, C. (2000). *J. Tribol.* 122, 590-596.
7. Delgado, M.A., Valencia, C., Sánchez, M.C., Franco, J.M. and Gallegos, C. (2006). *Ind. Eng. Chem. Res.* 45, 1902-1910.

### *Contact Address:*

*Gema Alonso (gema.alonso@diq.uhu.es)*

*Departamento de Ingeniería Química. Facultad de Ciencias Experimentales.*

*Campus de "El Carmen". Universidad de Huelva. 21071. Huelva. Spain.*

*Tel.:+34 959219998; Fax:+34 959219983*

## CHAPTER 2

# Injection-moulded bioplastics from rice husk protein

*A. Lucio-Villegas, M. Félix, A. Romero, A. Guerrero*

*Departamento de Ingeniería Química, Facultad de Química, Universidad de Sevilla (Spain)*

### Introduction

Plastic materials are currently considered essential because of their exceptional properties and higher performance to other materials such as metal or wood. There is an important demand to produce materials that are both environmentally friendly as they come from an alternative source to oil and eliminate the pressure on landfills with plastic solid wastes [1]. Bioplastics have been postulated as an alternative to using renewable biomass in the manufacture of high quality products, cost-competitive and biodegradable consumer goods as a means to reduce dependence on petrochemical feedstock and to diminish environmental pollution. In fact, the transition from a fossil-based economy to a bio-economy is an important target of the EU 2020 Strategy.

Bioplastics are constituted by different sources of biopolymers, such as proteins, lipids and polysaccharides. Proteins from rice, in view of the importance of the rice sector in Andalusia, could be seen as a fairly attractive raw material for the production of bioplastic. Rice protein is present in rice husk as the major by-product in the rice industry, which is currently treated as waste production and typically incinerated for energy purposes [2].

The objective of this work is to study the manufacture and characterization of high quality biodegradable rice protein biobased plastic materials processed by injection moulding. To achieve this objective, a previous mixing stage, using glycerol as a plasticizer, has to be carried out.

### Experimental

#### *Materials*

Rice protein concentrate from rice husk (RF), containing c.a. 80 wt% protein, was delivered from Remy Industries (Leuven-Wijgmaal, Bélgica). Glycerol (GL),

## Perspectives in Fundamental and Applied Rheology

sodium bisulfite (B) and glyoxal (GX) were purchased from Panreac Química, S.A. (Spain).

### *Preparation of samples*

Bioplastics were manufactured by a thermo-mechanical procedure including two stages:

Initially, selected blends were mixed in a two-blade counter-rotating batch mixer Haake PolyLab QC (ThermoHaake, Germany) at 25°C and 50 rpm for 60 min, monitoring the torque during mixing. RF/GL ratios of 60/40 and 70/30 were used in the absence or presence of a reducing agent B with or without GX at different additive concentration: 0-0.3 wt% for B and 0-3 wt% for GX.

Secondly, the dough-like materials obtained after mixing process were subsequently processed by injection moulding using a MiniJet Piston Injection Moulding System II (ThermoHaake, Germany) to obtain bioplastic specimens. The nozzle and mould temperatures were 85 and 130°C, respectively, with a residence time of 300 s in the mould and an injection pressure of 95 MPa. Lower pressure conditions, at 50 MPa (LPC), were also used for 70/30 specimens.

### *Mechanical measurements*

Dynamic Mechanical Thermal Analysis (DMTA) experiments were performed by triplicates with a RSA3 (TA Instruments, New Castle, DE, USA), on rectangular specimens using dual cantilever bending. Temperature sweeps were performed at a constant frequency (6.28 rad/s) and strain within the linear viscoelastic region. Heating rate was 3°C/min with temperature ranging from -30 to 160°C.

Tensile testing at room temperature was performed by means of an Insight 10 kN Electromechanical Testing System (MTS, Eden Prairie, MN, USA). All tensile tests were stroke controlled with a constant cross head speed of 10 mm/min. According to the standard ISO 527-3:1996, five tests were carried out for each sample.

## **Results and Discussion**

### *Preparation of blends*

Figure 1 shows torque as a function of mixing time for different selected systems.

Blends containing 40 wt% glycerol show much lower torque values showing too low consistency to be processed in the injection device. On the other hand, 70/30 blends show a remarkable shear-induced torque growth that reflects suitable potentials for further material processing. Moreover, addition of bisulphate leads to lower torque values over those corresponding to the additive-free blend, whereas

the combination of B and GX yields an anticipation of the increasing torque profile reaching a higher constant torque value.

A mixing time of 15 min was selected for the preparation of blends to be further processed by injection moulding. This time length is considered to be suitable to get fairly homogeneous blends while maintaining moderate torque values, thus avoiding premature network structure development before injection.

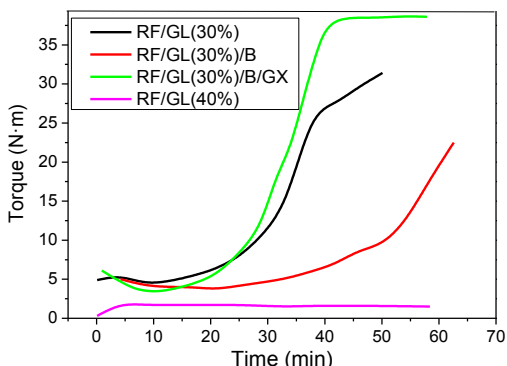


Figure 1. Evolution of torque over the mixing process for systems with different GL concentration (30 and 40 wt%) and additives (reducing agent, B, and reducing agent, B, plus aldehyde, GX).

### DMTA Measurements

Typical DMTA scans (complex modulus and loss tangent) from -30 to 160°C for bioplastic specimens are shown in figure 2.

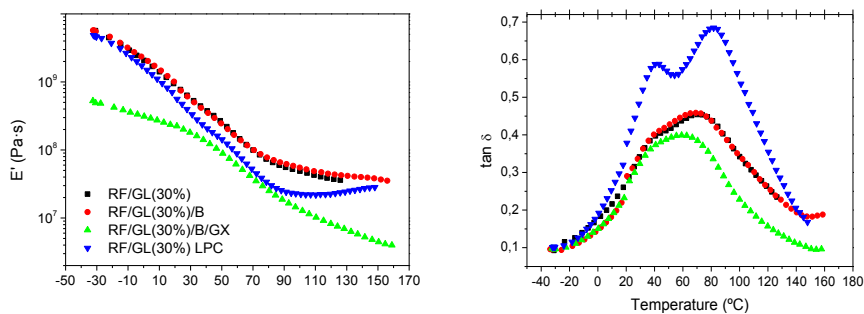


Figure 2. DMTA tests of selected specimens.

In general, bioplastic specimens show a rapid decay in elastic modulus with a change in the decay rate at a temperature around 60-70°C, coinciding with a maximum in the loss tangent, which could be related to a glass-like transition

temperature ( $T_g$ ). This region is followed by a rubber-like region where temperature shows much lower effect on viscoelastic properties. As may be observed, 70/30 specimens injected at 50 MPa (LPC) show much lower  $E'$  values than those injected at 90 MPa. In addition, two separate peaks were clearly shown for  $\tan \delta$  that suggests occurrence of a phase separation, reflecting an evident lack of compatibility between protein and plasticizer. Interestingly, a cross-linking thermosetting potential region was found for this system at high temperature. This effect suggests that cross-linking taking place during moulding is a consequence of the combination of both temperature and pressure, such that a decrease in pressure seems to cause a reduction in crosslinking density.

Addition of the reducing agent does not induce any significant effect on viscoelastic properties of specimens, whereas the combination of B and GX lead to a remarkable decrease in both  $E'$  and  $\tan \delta$ . In spite of this reduction, an apparent enhancement in the compatibility between protein and plasticizer may be also observed, as the peaks become overlapped. Similar results were reported by Sun et al [3] and Zarate-Ramírez [4].

### *Tensile strength measurements*

Regarding tensile strength measurements (Figure 3), Figure 4 shows values of some tensile parameters (elongation at break,  $\epsilon$ ; maximum tensile strength,  $\sigma_{\max}$ , and Youngs' Modulus,  $E$ ) obtained for selected specimens.

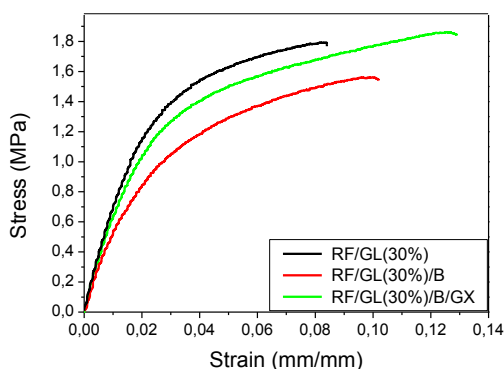


Figure 3. Stress-Strain curves for selected specimens.

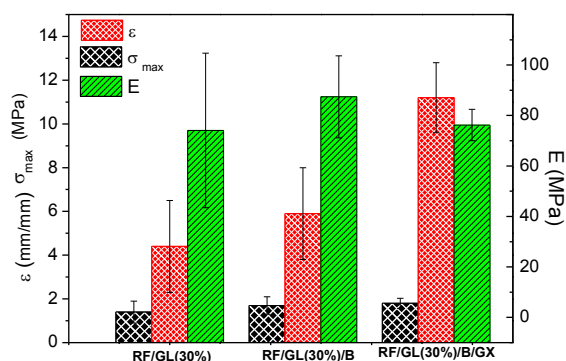


Figure 4. Parameters from tensile measurements: Elongation at break ( $\epsilon$ ); Maximum Stress ( $\sigma_{max}$ ) and Youngs' Modulus (E) for selected specimens.

Results evidence that although no significant differences were found in  $\sigma_{max}$ , and E values, bioplastics with added aldehyde show a marked increase in the elongation values (i.e. duplicating the value of aldehyde-free specimens), as corresponds to a ductility enhancement behaviour.

### Concluding Remarks

From the experimental results, it may be concluded that the 70/30 blends exhibit mechanical properties suitable for injection moulding. The effect of injection pressure has proven to be essential in the formation of crosslinks, together with the temperature of moulding. Thus, those specimens injected at low pressure displays a crosslinking enhancement potential that could be exploited either by increasing temperature or pressure. In fact, an increase in pressure leads to a remarkable increase in the elastic response, as well as to an increase in compatibility.

Although addition of sodium bisulphate do not yield any significant difference in DMA or tensile strength parameters, the combination of this reducing agent and glyoxal leads to a remarkable enhancement of the degree of compatibility between protein and glycerol, as well as to an extension of the elongation at break in comparison with the other systems.

### Acknowledgements

This work is part of a research project (MAT2011-29275-C02-02) sponsored by MEC-FEDER programs. The authors gratefully acknowledge their financial support.

### References

1. Madrid, R., Margarido, F., and Nogueira, C.A.(2012) Mat. Sci. Forum, 730-732. 659-664.
2. Alvarez-Chavez, C.R., Edward, S., Moure-Eraso, R., Geiser, K. (2012). J. Clean Prod 23, 47-56.
3. Sun, S., Song, Y., Zheng, Q. (2007). Food Hydrocolloid. 21, 1005-1013
4. Zárate-Ramírez L.S. (2011) Ph.D. thesis. Spain: University of Seville.

### Contact Address:

A. Guerrero ([aguerrero@us.es](mailto:aguerrero@us.es))

Dpto. Ingeniería Química, Facultad de Química, Universidad de Sevilla,

C/ Profesor García Gonzalez, 1-41012 Sevilla, Spain

Tel.:+34 954 557179; Fax:+34 954 556447

## CHAPTER 3

# Rheological characterization and thermogravimetric analysis of oleogels containing isocyanate-functionalized biopolymers as gelling agent

R. Gallego<sup>1</sup>, J. F. Arteaga<sup>1,2</sup>, C. Valencia<sup>1,3</sup>, J.M. Franco<sup>1,3</sup>

<sup>1</sup> *Departamento de Ingeniería Química, Química Física y Química Orgánica. Campus de "El Carmen". Universidad de Huelva. 21071 Huelva. Spain. Campus de Excelencia Internacional Agroalimentario, ceiA3.*

<sup>2</sup> *CIQSO – Center for Research in Sustainable Chemistry. Universidad de Huelva. 21071 Huelva. Spain.*

<sup>3</sup> *Pro<sup>2</sup>TecS – Chemical Process and Product Technology Research Center. Universidad de Huelva. 21071 Huelva. Spain.*

### Introduction

Nowadays, there is a general tendency to promote the replacement of non-renewable raw materials by renewable resources in order to avoid the impact that process technologies and products of different industrial sectors cause in the environment. The lubricant industry is especially involved in the minimization of the environmental impact caused by these materials [1,2]. Although vegetable oils are being increasingly used as lubricant base oils instead of mineral and synthetic oils, the substitution of traditional thickener agents, such as metallic soaps, in lubricating greases by others derived from renewable resources, like some biopolymers, is a complicated task due to the technical efficiency of the formers.

Some biopolymers like cellulose or chitin may present some advantages as biogenic thickeners in lubricating grease formulations [3,4]. In previous studies [4-6], some of these polymers were chemically modified in order to reduce the polarity and therefore increase the affinity by vegetable oils to form gel-like dispersions with acceptable properties to be used as lubricating greases. However, some weaknesses were observed regarding their physical and mechanical stabilities and thermal dependence. As it was previously reported [7], the role of ethyl cellulose, by modifying the rheological characteristics of vegetable oils, is essential to impart long-term physical stability to these oleogels. An alternative to improve physical stability is the functionalization of some of these polymers with reactive functional groups like isocyanate, as previously described for PVA [8], thus inducing a chemical reaction with some components of lubricating greases.

This work deals with the selective incorporation of reactive isocyanate groups into some biopolymers, such as methyl cellulose, chitin and chitosan, to be used as thickening agents in castor oil. Resulting chemical oleogels may have potential applications as green lubricating greases formulated from renewable resources.

### Experimental

#### Materials

Castor oil (Guinama, Spain) was selected as lubricant base oil to prepare oleogel formulations. Methyl cellulose (Sigma Aldrich, Germany), chitosan and chitin (Qingdao Fraken, China), were modified with 1,6-hexamethylene diisocyanate (Sigma Aldrich, Germany) in presence of triethylamine ( $\text{Et}_3\text{N}$ ) and toluene (Sigma Aldrich, Germany). Under inert atmosphere of argon and after 24 h of mixing at room temperature, different biopolymers were obtained, depending on the substrate and diisocyanate content (Table 1).

#### Preparation of oleogels

Oleogel samples (30% w/w) were prepared using an anchor impeller at 70 rpm for 24 h at room temperature to disperse the different biopolymers in the oil. The resulting dispersion was homogenized at 8800 rpm for 1 min.

Table 1. Molar ratios of the substrate, HMDI,  $\text{Et}_3\text{N}$  and toluene used in the functionalization reaction

Biopolymer	Substrate (equiv.) <sup>[1]</sup>	HMDI (equiv.) <sup>[1]</sup>	$\text{Et}_3\text{N}$ (equiv.) <sup>[1]</sup>	Toluene (ml)	Oleogel Code
MC-NCO-A	1.0 Methyl Cellulose	6.8	21	300	MC-NCO-A-30
MC-NCO-B	1.0 Methyl Cellulose	4.8	9.5	200	MC-NCO-B-30
MC-NCO-C	1.0 Methyl Cellulose	1.2	2.4	100	MC-NCO-C-30
CSAN-1	1.0 Chitosan	0.50	1.0	100	CSAN-1-30
CSAN-2	1.0 Chitosan	0.25	0.50	100	CSAN-2-30
CTIN-1	1.0 Chitin	0.25	0.50	100	CTIN-1-30

<sup>[1]</sup> Molar ratio between moles of free  $-\text{OH}$  and  $-\text{NH}$  groups present in each monomer of the starting substrate, and moles of each of the reagents employed.

*Thermogravimetric analysis (TGA)*

Measurements of mass losses versus temperature were carried out by using a Thermogravimetric analyzer, model Q-50 (TA Instrument Waters, USA), under N<sub>2</sub> purge, from 30 °C to 600 °C, at 10 °C/min.

*Rheological characterization*

Rheological characterization of oleogels was carried out with a Gemini controlled-stress rheometer (Bohlin, UK). Small amplitude oscillatory shear (SAOS) tests were performed inside the linear viscoelastic region, using a serrated plate-plate geometry (25 mm, and 1 mm gap), in a frequency range of 10<sup>-2</sup>-10<sup>2</sup> rad/s, at 25 °C. Measurements were done one day, one week, one month and four months after oleogel preparation. At least two replicates of each test were performed on fresh samples.

**Results and Discussion***Thermogravimetric analysis*

Thermal degradation of functionalized biopolymers and corresponding oleogels was studied by means of thermogravimetric analysis (TGA). Figure 1 shows TGA curves, in the form of weight loss vs. temperature derivative function, for selected biopolymers used as gelling agents. As can be observed, thermal degradation under nitrogen atmosphere occurred in several stages. Table 2 provides the temperature for the onset ( $T_{\text{onset}}$ ) of each stage for both biopolymers and oleogels. As can be observed, for isocyanate-functionalized methyl cellulose, chitosan and chitin, the inclusion of HMDI segments into the polymer structure reduces their thermal stabilities with respect to non-functionalized methyl cellulose ( $T_{\text{onset}}=347^{\circ}\text{C}$ ), chitosan ( $T_{\text{onset}}=281^{\circ}\text{C}$ ) and chitin ( $T_{\text{onset}}=343^{\circ}\text{C}$ ), respectively, with  $T_{\text{onset}}$  values for each stage that depends on the HMDI content.

Table 2. Characteristic temperatures of the biopolymers and formulations studied

<b>Biopolymer</b>	<b><math>T_{\text{onset}}</math> (°C)</b>	<b>Oleogel</b>	<b><math>T_{\text{onset}}</math> (°C)</b>
MC-NCO-A	123/310/440	MC-NCO-A-30	328
MC-NCO-B	117/311/440	MC-NCO-B-30	330
MC-NCO-C	95/323	MC-NCO-C-30	339
CSAN-1	122/240/292/429	CSAN-1-30	297
CSAN-2	107/283/431	CSAN-2-30	301
CTIN-1	106/275/363/439	CTIN-1-30	327/444

However, thermal decomposition of methyl cellulose and chitosan derivatives-based oleogels takes place in one main single stage at around 328-347°C and 297-481°C, respectively. This temperature range is broadened when using highly functionalized biopolymers.

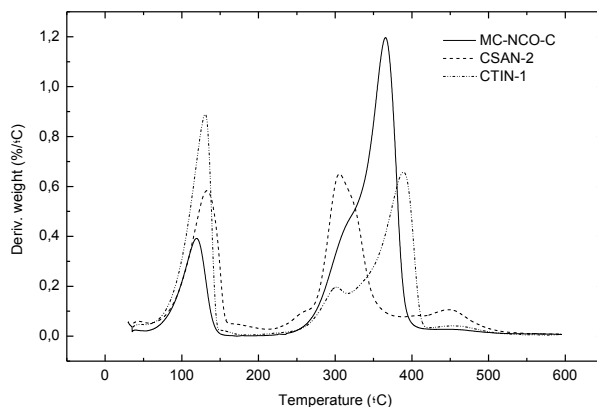


Figure 1. Thermal degradation curves, under inert atmosphere, for NCO-functionalized methylcellulose (MC-NCO-C), chitosan (CSAN-2) and chitin (CTIN-1).

### Rheological characterization

-NCO content in the functionalized biopolymer, able to originate cross-linking not only with the oil medium but also among polymeric chains, influences the rheological response of the oleogels (Figures 2-4).

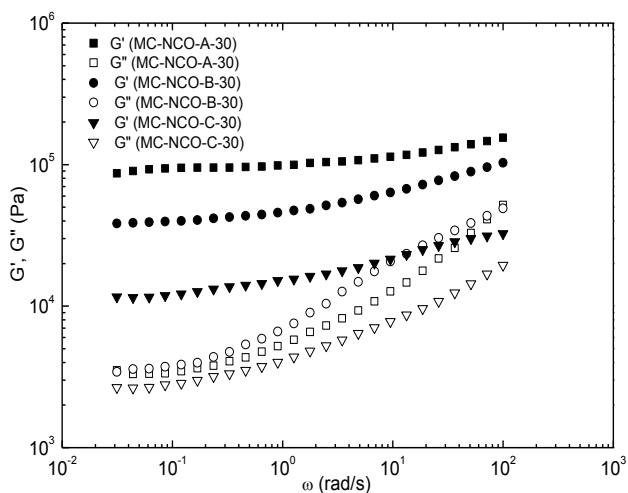


Figure 2. SAOS response of methylcellulose-based oleogels.

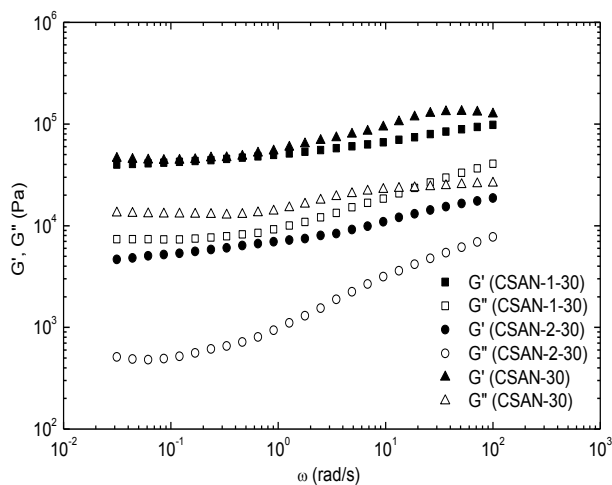


Figure 3. SAOS response of chitosan-based oleogels.

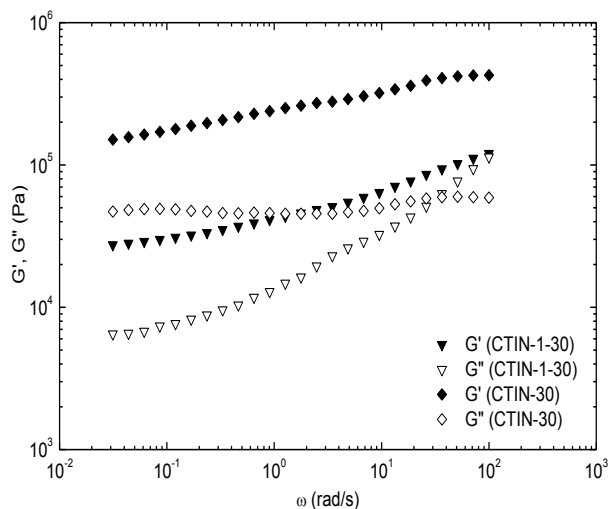


Figure 4. SAOS response of chitin-based oleogels.

As can be observed in Figures 1-3,  $G'$  is always higher than  $G''$  in the whole frequency range studied, and the plateau region of the mechanical spectrum followed by the beginning of the transition region was always noticed. In the case of the isocyanate-functionalized chitin oleogel (CTIN-1-30) (Figure 3) a crossover between both linear viscoelastic functions, at high frequencies, was achieved. Moreover, chitin and chitosan functionalization in a relatively low degree yields oleogels with significantly reduced values of the SAOS functions compared to the corresponding non-functionalized biopolymer-based oleogels.

However, as expected, SAOS functions for –NCO-functionalized biopolymers-based oleogels increase with the functionalization degree, attending to the higher degree of cross-linking produced by the higher –NCO content in the biopolymer. Figure 1 and 2 give evidence of this effect in functionalized methylcellulose and chitosan-based oleogels, respectively. Therefore, –NCO-functionalization may be considered a chemical tool to modulate the rheological response of chitin- and chitosan-based oleogels.

### Acknowledgements

This work is part of a research project (CTQ2010-15338) sponsored by a MEC-FEDER Programme. One of the authors (R. Gallego) has received a Ph.D. Research Grant from the “Ministerio de Ciencia e Innovación”. The authors gratefully acknowledge its financial support.

### References

1. Lea, C.W. (2002). *Ind. Lubric. Tribol.* 54, 268–274.
2. Wilson, B. (1998). *Ind. Lubric. Tribol.* 50, 6–15.
3. Nuñez, N., Martín-Alfonso, J. E., M. E. Eugenio, M. E., Valencia, C., Díaz, M. J., and Franco, J. M. (2011). *Ind. Eng. Chem. Res.*, 50, 5618-5627.
4. Sánchez, R., Franco, J. M., Delgado, M. A., Valencia, C., and Gallegos, C. (2011). *Carbohydr. Polym.*, 482, 151-158.
5. Martín-Alfonso, J. E., Núñez, N., Valencia, C., Franco, J. M., and Diaz, M. J. (2011) *J. Ind. Eng. Chem.*, 17, 818–823.
6. Núñez, N., Martín-Alfonso, J. E., Valencia, C., Sánchez, M. C., and Franco, J. M. (2012). *Ind. Crop. Prod.*, 37, 500–507.
7. Sánchez, R., Franco, J. M., Delgado, M. A., Valencia, C., and Gallegos, C. (2011). *Carbohydr. Polym.*, 83, 151–158.
8. Moreno, G., De Paz, M. V., Valencia, C., Franco, J. M. (2012). *J. Appl. Polym. Sci.*, 125, 3259–3267.

### Contact Address:

Rocio Gallego ([rocio.gallego@diq.uhu.es](mailto:rocio.gallego@diq.uhu.es))  
Departamento de Ingeniería Química  
Facultad de Ciencias Experimentales  
Campus de «El Carmen»  
Avenida de las Fuerzas Armadas, S/N.  
21071 Huelva  
Telf.: 959219998

## CHAPTER 4

# Characterisation of crayfish flour-based bioplastics processed by injection moulding

*M. Félix, M.J. Gutiérrez-Solís, C. Bengoechea, A. Romero*

*Departamento de Ingeniería Química, Facultad de Química, Universidad de Sevilla (Spain)*

### Introduction

Food industry typically produces a big amount of by-products that may yield a negative environmental impact. An example is the freshwater red-swamp crayfish (*Procambarus Clarkii*) which has undergone a fast widespread growth giving rise to a big amount of crayfish surpluses and the development of a strong local crayfish industry at the marshes of the Guadalquivir river [1]. A currently attractive way to valorise these by-products is the manufacture of protein-based plastic materials. Proteins are generally mixed with a plasticizer in order to reduce intermolecular forces among polymer chains, increasing mobility and reducing the glass transition [2]. Traditionally, protein films are processed by casting method, however classical polymer processing techniques are being increasingly used in this field. Among them, injection molding is a fairly attractive operation that has not received due attention yet. Typically in this process, polymeric materials are subjected to suitable thermal conditions, being injected at high pressure into the mould cavity [3]. Optimization of processing conditions is essential to achieve the desired properties of the final product. This is particularly relevant in protein-based materials that require thermoplastic mixing with a proper plasticiser but show a predominant thermoset character upon injection moulding. Besides, additives such as reducing agents may be helpful in order to reduce the average molecular weight of protein aggregates, thus facilitating both mixing and moulding processes.

The overall objective is to study the injection moulding process as an alternative to produce plasticized crayfish biobased plastic materials. Different protein/additive (either reducing or denaturant agent)/glycerol blends are mixed using a Haake PolyLab QC (ThermoHaake, Germany) recording torque and temperature over mixing. Rheological measurements of these blends are carried out by a Mars II rheometer (ThermoHaake, Germany) in order to select suitable processing

parameters (temperature and residence time in the pre-injection mixing chamber as well as the temperature of the mould).

### **Experimental**

#### *Materials*

Crayfish flour (CF), containing 65 wt% protein, was obtained from ALFOCAN S.A. (Isla Mayor, Seville, Spain). The only plasticizer: Glycerol (GL) and additives: sodium bisulphite (B) and urea (U) was purchased from Panreac Química, S.A. (Spain).

#### *Preparation of samples*

Bioplastics were manufactured by a thermo-mechanical procedure which includes two stages:

Initially, selected blends, containing 70 wt% CF and 30 wt% GL, were mixed in a two-blade counter-rotating batch mixer Haake PolyLab QC (ThermoHaake, Germany) at 25°C and 50 r.p.m. for 20 minutes, monitoring the torque and temperature during mixing.

Secondly, the dough-like materials obtained after mixing process were subsequently processed by injection moulding using a MiniJet Piston Injection Moulding System II (ThermoHaake, Germany) to obtain bioplastic specimens. The most suitable processing variables such as temperatures in the pre-injection mixing chamber or mould were selected after performing temperature ramp and DSC measurements.

#### *Temperature ramp tests*

Dough-like material was characterized by temperature ramp tests at 5°C/min from 20 to 90°C in linear viscoelastic range, using a Haake Mars II rheometer (ThermoHaake, Germany) and a plate geometry (dia: 25 mm) with a rough surface and a gap of 1 mm.

#### *Dynamic viscoelastic measurements*

Dynamic Mechanical Thermal Analysis (DMTA) experiments were performed by triplicates with a RSA3 (TA Instruments, New Castle, DE, USA), on rectangular specimens using dual cantilever bending. Temperature sweeps were performed at a constant frequency (6.28 rad/s) and strain within the linear viscoelastic region. The heating rate was 3°C/min with a temperature range from -30 to 140°C.

### Tensile strength measurements

Tensile testing at room temperature was performed by means of an Insight 10 kN Electromechanical Testing System (MTS, Eden Prairie, MN, USA). All tensile tests were stroke controlled with a constant cross head speed of 10 mm/min. According to the standard ISO 527-3:1996, five tests were carried out for each sample.

## Results and Discussion

### Preparation of blends

Different protein/additive/glycerol blends were prepared using a reducing agent (sodium bisulphite, B) and denaturing agent (urea, U), like additives at two different additive concentrations (3 and 30 mg/g protein).

Figure 1 shows torque and temperature as a function of mixing time for two different additive concentrations (3 and 30 mg/g).

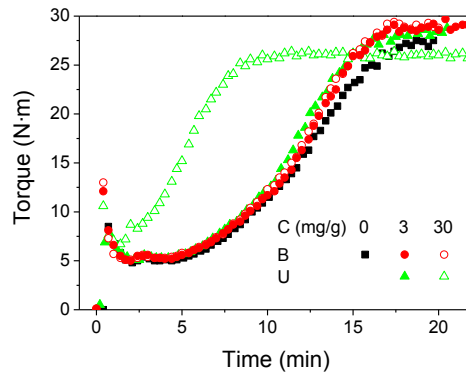


Figure 1. Evolution of torque over the mixing process for CF/additive/GL for two additive concentration (3 and 30 mg/g protein).

These results generally show that the use of reducing and denaturing agents anticipate the increase in torque, especially at the highest concentration of urea at which lower values in the final torque (plateau value) is also obtained.

### Thermal characterization of blends

Figure 2 shows the viscoelastic moduli ( $G'$  and  $G''$ ) for the reference system (CF/GL) and for systems with 3 mg/g protein of different additives (CF/sodium bisulphite, B, or urea, U/GL) as a function of increasing temperature.

As may be observed, the influence of temperature is moderate up to a value from which a continuous decrease in both moduli takes place. The maximum in  $\tan \delta$  reveals the occurrence of a glass-like transition at ca. 75°C. This transition may be also observed by DSC measurements (i.e. a  $T_g$  takes place at c.a. 60°C for

CG/GL blends). In addition, a reduction in viscoelastic properties is obtained when a reducing or denaturing agent is used. As a consequence, the addition of a reducing or denaturing agent leads to CF blends exhibiting enhanced processability in material moulding where rheological properties are a key factor, thus making these blends more easily injectable.

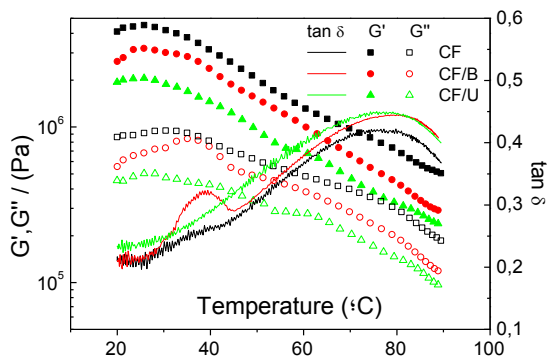


Figure 2. Viscoelastic moduli ( $G'$  and  $G''$ ) and loss tangent ( $\tan \delta$ ) for CF/GL and different CF/additives (3 mg per gram of protein)/GL blends subjected to thermoplastic mixing, as a function of temperature (from 20 to 100°C) at 5°C/min

According to these results, Table 1 shows the selected conditions for the injection moulding process for the blends studied in order to facilitate the mobility of the system in the barrel (lower viscosity of blend) and leaving temperature and pressure-induced protein crosslinking for the moulding stage.

A short residence time in the mould after injection is selected (20 s) in order to avoid protein degradation.

Table 1. Selected operation conditions for the injection moulding process.

	T (°C)	Time (s)
Pre-injection barrel	60	100
Injection pressure (MPa)	50	
Injection mould	100	20

#### Mechanical properties of specimens

Aiming to assess the mechanical response of bioplastics, DMTA and tensile tests were performed. From DMTA scans (from -30°C to 140°), two parameters ( $E'$  and

$\tan \delta$ ) have been selected at two different temperatures in order to compare the behaviour of bioplastics both under service conditions (20°C) and at high temperatures (130°C). Results from Table 2 evidence that addition of reducing (sodium bisulphite, B) and denaturing agent (urea, U) can under certain conditions increase the value of  $E'$  and decrease  $\tan \delta$ . However, whereas higher concentration of bisulphite (30 mg/g) is necessary to observe this effect, only a low concentration of urea (3 mg/g) is needed to increase  $E'$  and, consequently, decrease  $\tan \delta$ . In general, these structuring phenomena are more evident at higher temperatures (130°C).

Table 2. Elastic modulus ( $E'$ ) and loss tangent ( $\tan \delta$ ) at 20 and 130°C obtained from DMTA for CF/additives/GL specimens at two different additives concentration (3 and 30 mg/g protein)

	T (°C)	$E'$ (MPa)	$\tan \delta$
CF	20	139 ± 6	0.36 ± 0.02
	130	0.7 ± 0.1	0.89 ± 0.02
3mg/g B	20	137 ± 8	0.36 ± 0.02
	130	0.7 ± 0.1	0.89 ± 0.02
30mg/g B	20	143 ± 12	0.36 ± 0.02
	130	0.9 ± 0.1	0.58 ± 0.01
3mg/g U	20	157 ± 2	0.34 ± 0.01
	130	3.6 ± 2.8	0.88 ± 0.09
30 mg/g U	20	135 ± 9	0.38 ± 0.03
	130	1.2 ± 0.1	0.58 ± 0.05

Table 3: Parameters from tensile measurements: Elongation at break ( $\epsilon$ ), Maximum Stress ( $\sigma_{max}$ ) and Youngs' Modulus ( $E$ ) for CF/additives/GL specimens as two different additives concentration (3 and 30 mg/g protein)

	$\sigma_{max}$ (MPa)	$\epsilon$ (%)	$E$ (MPa)
CF	0.17±0.04	1.5 ± 0.2	20.3±2.3
3mg/g B	0.20±0.01	1.4 ± 0.1	26.0±5.9
30mg/g B	0.10±0.01	1.1 ± 0.1	51.8±13.2
3mg/g U	0.20±0.01	1.7 ± 0.1	22.0±0.9
30mg/g U	0.20±0.01	1.7 ± 0.1	27.4±13.1

Regarding the tensile properties, Table 3 shows the values of three parameters (maximum tensile strength,  $\sigma_{max}$ , elongation at break,  $\epsilon$ , and Youngs' Modulus,  $E$ ) obtained from tensile tests applied to CF/GL and CF/additive/GL bioplastics at

different additive concentration (3 and 30 mg/g). Results evidence no significant differences between systems with the exception of the system with higher concentration of bisulphite that leads to a system with higher  $E$  but lower  $\sigma_{\max}$  and  $\varepsilon$  that correspond to brittle bioplastics. Moreover, bioplastics containing urea show similar tensile results because no reactions related to structuring are implied.

### Concluding Remarks

From the experimental results, it may be concluded that mixing of protein-based flour, additives and plasticizer can be controlled by monitoring the torque in order to select the more suitable mixing time and formulation. Blends exhibit rheological properties that make them suitable for injection moulding processing and selected conditions can be selected in order to facilitate this process. The addition of reducing agent (sodium bisulphite) and, specially, denaturing agent (urea), like additives, influences the characteristics of the blend, yielding materials with different rheological properties that facilitate its processability. However, in general, the presence of additives (reducing or denaturing agents) in the final bioplastic formulation leads to better results in DMTA parameters (higher  $E'$  and lower  $\tan \delta$  values), depending of additive concentration, and no very important differences in tensile parameters, although results are dependent on additive concentration.

### Acknowledgements

This work was part of a research project sponsored by the Andalusian Government (Spain) (TEP-6134-2010) and the authors gratefully acknowledge their financial support.

### References

1. Kirjavainen, J., and Westman, K. (1999). *Aquat. Living Resour.* 12, 387-401.
2. Irissin-Mangata, J., Bauduin, G., Boutevin, B., and Gontard, N. (2008). *Eur. Polym. J.* 37 (8), 1533-1541.
3. Fernández-Espada, L., Bengoechea, C., Cordobes, F., and Guerrero, A. (2012). doi:10.1010/j.fbp.2012.11.009.

### Contact Address:

A. Romero (alromero@us.es)  
Dpto. Ingeniería Química, Facultad de Química, Universidad de Sevilla,  
C/ Profesor García Gonzalez, 1-41012 Sevilla, Spain  
Telf.:+34 954 557179; Fax:+34 954 556447

## CHAPTER 5

# ***Staphylococcus aureus* strains rheology during growth**

Raquel Portela<sup>1,2</sup>, Pedro L. Almeida<sup>3,4</sup>, Pedro Patrício<sup>3,5</sup>, Teresa Cidade<sup>4,6</sup>, Rita G. Sobral<sup>1,7</sup>, Catarina R. Leal<sup>3,4</sup>

<sup>1</sup>*Centro de Recursos Microbiológicos, Departamento de Ciências da Vida, Faculdade de Ciências e Tecnologia, Universidade Nova de Lisboa, Portugal.*

<sup>2</sup>*Laboratório de Genética Molecular, Instituto de Tecnologia Química e Biológica, Universidade Nova de Lisboa, Portugal.*

<sup>3</sup>*Instituto Superior de Engenharia de Lisboa, Área Departamental de Física, Portugal.*

<sup>4</sup>*CENIMAT/13N, Faculdade Ciências e Tecnologia, Universidade Nova de Lisboa, Portugal.*

<sup>5</sup>*Centro de Física Teórica e Computacional, Universidade de Lisboa, Portugal.*

<sup>6</sup>*Departamento de Ciência dos Materiais, Faculdade de Ciências e Tecnologia, Universidade Nova de Lisboa, Portugal.*

<sup>7</sup>*Departamento de Ciências da Vida, Faculdade de Ciências e Tecnologia, Universidade Nova de Lisboa, Portugal.*

### **Introduction**

The study of the mechanical properties of living bacteria in a liquid rich medium, environment commonly used in laboratorial settings, opens a new perspective on the bacterial physiology and behaviour during population growth. In this work, the human pathogen *Staphylococcus aureus* was used as a study model due to its coccoid shape and regular morphology: MRSA strain COL [1] and its mutant strain RUSAL9 [2], which presents a deficient daughter-cell separation mechanism. Cultures were grown under a mechanical stress solicitation in parallel with optical density monitorization. Complex viscoelastic behaviour was revealed by these bacterial systems [3]. In particular the shear viscosity measurement during growth time, for a constant shear rate, showed an unexpected behaviour that cannot be observed by common optical experimental techniques.

### **Experimental**

#### *Samples*

Planktonic cultures of MRSA strain COL [1] and strain RUSAL9 were grown at 37°C with aeration in tryptic soy broth (TSB), mainly composed of free amino acids,

oligopeptides, and to a lesser extent polysaccharides (Difco Laboratories, Detroit, USA).

### *Experimental Procedures*

Bacteria growth was followed by optical density at 620 nm, using a Ultrospec 2100 pro, at discrete time intervals. The starting inocula (OD = 0.005) was obtained from an overnight-grown liquid culture. Furthermore, the population's colony-forming units (cfu/ml), which provides an estimate of the viable cells, was determined over time.

Rheological measurements were performed in a controlled stress rotational rheometer, Bohlin Gemini HR<sup>nano</sup>, equipped with a steel plate/plate geometry with 40 mm diameter and gap of 2000  $\mu\text{m}$  to ensure a good signal; the viscosity was measured over time, at a constant shear rate of  $10 \text{ s}^{-1}$ , which mimics incubator conditions in biology laboratories, at  $37 \text{ }^\circ\text{C}$  (optimal growth temperature). A solvent trap was used in all measurements to avoid evaporation.

### **Results and Discussion**

OD<sub>620nm</sub> measurements during growth time are presented in Table 1, for the two strains, COL and RUSAL9, as well as the cfu/ml.

Three distinct phases can be identified: the *lag* phase, at short times (<300min), where the bacterial density is still low; the *exponential* phase, at intermediate times (300<t<425min) where the bacterial growth develops very rapidly and follows exponential time dependence; and finally the *late* phase (t>425min) where the bacteria still divide but at a smaller rate.

The viscosity growth curve, is represented in Figure 1, for both strains, COL and RUSAL9, showing a complex dependence with time.

For strain COL the viscosity increases with time and achieves a maximum value twenty times higher than the initial one (in the *exponential* phase of growth), presenting afterwards a dramatic decrease to values close to the initial one (in the *lag* phase). During a similar *exponential* phase, the viscosity for the strain RUSAL9 firstly presents a  $\sim 5\text{x}$  increase, followed by a steady decrease and again a final increase to a plateau of constant viscosity value, ten times higher the initial one. An hypothesis to explain this phenomena is that strain RUSAL9 the cells are not able to separate during cell division (due to a genetic mutation) and thus a self organized structure is not achieved as previously considered in the case of strain COL [3].

Table 1. *S. aureus* culture characterized by optical densities ( $OD_{620nm}$ ) and the population's colony-forming units, in arbitrary dimensions (cfu/ml); shadow separate distinct growth phases: lag, exponential, and late phases, respectively.

Time (min)	COL		RUSAL9	
	OD	cfu/ml	OD	cfu/ml
0	0	$1.38 \times 10^5$	0	$2.15 \times 10^5$
60			0.01	
80			0.04	$2.73 \times 10^5$
115	0.01	$4.76 \times 10^5$		
55			0.03	$4.60 \times 10^5$
190	0.08	$2.80 \times 10^6$		
135			0.11	$1.17 \times 10^6$
185			0.23	$1.34 \times 10^6$
275	0.48	$1.11 \times 10^7$		
225			0.41	$3.24 \times 10^6$
330	1.36	$3.28 \times 10^7$		
290			0.98	$4.56 \times 10^6$
405	3.07	$1.21 \times 10^8$		
365			2.42	$2.40 \times 10^7$
430			3.86	$3.70 \times 10^7$
480	5.21	$3.66 \times 10^8$	4.71	$1.01 \times 10^8$
500			7.30	$1.20 \times 10^8$

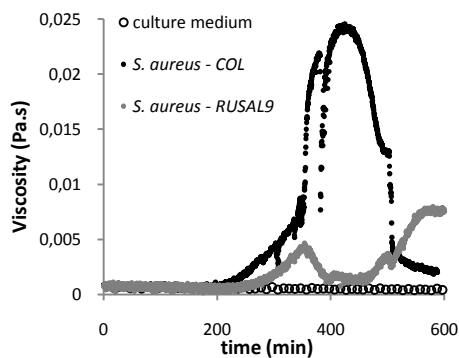


Figure 1. *S. aureus* cultures steady-state shear growth curve, measured at a constant shear rate of  $10 \text{ s}^{-1}$ ; culture medium – black open symbols; strain COL - black and strain RUSAL9 – gray full symbols (representative curves). All measurements were performed at  $37^\circ\text{C}$ .

## Acknowledgements

Strain COL was a kind gift from H. de Lencastre. We acknowledge the support from FCT (Portugal) through Grant No. PEst-OE/FIS/UI0618/2011 (CFTC), PEst-C/CTM/LA0025/2011 (CENIMAT/I3N), PEst-OE/BIA/UI0457/2011 (CREM), and through Project PTDC/BIA/MIC/101375/2008(awarded to RGS).

## References

1. Gill, S. R., et. al., (2005). J. Bacteriol. 187, 2426-38.
2. Oshida T. and A Tomasz, (1992). J. Bacteriol., 174, 4952-4959.
3. Portela, R., P. L. Almeida, P. Patrício, T. Cidade, R. G. Sobral and C. R. Leal (2013). Phys. Rev. E, 87, 030701-030705(R).

## Contact Address:

Catarina R. Leal ([cleal@adf.isel.pt](mailto:cleal@adf.isel.pt))  
Área Departamental de Física,  
ISEL – Instituto Superior de Engenharia de Lisboa  
Rua Conselheiro Emídio Navarro, 1, 1949-014 Lisboa, Portugal.  
Telf.:+351218317135; Fax:+351218317138

## CHAPTER 6

# Rheological study and physical stability of emulsions formulated with alpha-pinene and hydrocolloids.

*M. C. García, M. C. Alfaro, N. Calero, J. Santos, J. Muñoz.*

*Departamento de Ingeniería Química. Facultad de Química. Universidad de Sevilla (Spain).*

### Introduction

Many agrochemical formulations must be reformulated due to their high content in aromatic chemicals, such as xylene, naphthalene, deodorized kerosene, trimethylbenzene, etc. The use of these materials in agrochemical formulations and others is being progressively banned by the European Commission, which in turn is causing that many commercial products must be reformulated.

For this reason, the use of some essential oils as dispersed phase in O/W emulsions has raised hopes that eco-friendly pesticide emulsions may be developed. The overall aim of this project is to design emulsions which play the role of matrices for commercial products which may find applications in agrochemical formulations.

Alpha-pinene is a readily biodegradable terpenic solvent which may be obtained from renewable raw materials, such as pine resins and other conifers, as well as from essential oils derived from plants like juniper, rosemary and eucalyptus [1]. This solvent may be a good alternative to the above mentioned aromatic solvents. Emulsions are dispersions consisting of two or more immiscible liquid phases. Oil in water emulsions consist of dispersions of oil droplets dispersed in an aqueous phase, which are thermodynamically unstable.

Long-term physical stability of slightly concentrated O/W emulsions may be interestingly achieved by using suitable natural polysaccharides [2]. Adsorbing polysaccharides, such as gum Arabic or the gum exudates from *Acacia tortuosa*, *Cedrela odorata* or *Sterculia apetala*, have simultaneous emulsifying and stabilising properties [3]. On the other hand, non-adsorbing polysaccharides, like guar, locust bean or xanthan gum exhibit stabilising properties. These gums

increase the viscosity of the continuous phase of O/W emulsions and, as a consequence, enhance the long-term physical stability of emulsions against creaming.

Amphiphilic copolymers are quite interesting emulsifiers due to their ability to decrease the interfacial tension in addition to their high molecular weight [4]. The target of this work was to study the influence of the nature of polysaccharide (low-acyl gellan gum, xanthan gum or mixtures of both polymers) on the physical stability of a model emulsion, formulated with a green solvent ( $\alpha$ -pinene) and a mixture of amphiphilic copolymers as emulsifiers.

### Experimental

30 wt%  $\alpha$ -pinene Laevo-95 (Destilaciones Bordas-Chinchurreta) emulsions, containing 3 wt% emulsifier (2 wt% Atlas G-5000/1 wt% Atlox 4913) and 0.4 wt % polysaccharide were prepared with a T-50 Ultraturrax rotor-stator homogenizer followed by a High-pressure valve homogenizer (Emulsiflex C5, Avestin). EGG30/2/1, EXG30/2/1 and EGGXG30/2/1 stand for emulsions stabilized by gellan gum, xanthan gum and a 50% blend of these gums, respectively. Low-acyl gellan gum was kindly provided by CP-Kelco. Xanthan gum was purchased from Sigma-Aldrich and the amphiphilic copolymers used (block copolymer Atlas G-5000, HLB-16.9 and graft copolymer PMMA-PEG, Atlox 4913, HLB-11.5) were provided by Croda. Small amplitude oscillatory shear (SAOS) tests were conducted with a TA Instruments AR-2000 rheometer and flow curves with a Thermo-Haake MARS rheometer. Serrated parallel plates with gap=1 mm were always used. The measuring temperature was kept at  $20^{\circ}\text{C}\pm 0.1^{\circ}\text{C}$  with a cryostat-thermostatic Phoenix circulator (Thermo). Multiple light scattering (MLS) tests were carried out with a Turbiscan Lab-expert (Formulation) and droplet size distribution (DSD) measurements were determined by laser diffraction with a Malvern Mastersizer X. Transmitted light optical microscopy (Axio Scope A1, Carl Zeiss with a 63X objective) was used to obtain information on emulsions' microstructure.

### Results and Discussion

#### *Mechanical spectra*

Mechanical spectra exhibited different shapes for the three emulsions studied, which indicated the existence of different microstructures.

All emulsions studied showed clear viscoelastic properties with a predominance of the elastic component over the viscous one practically in all the frequency range studied.

The small angle oscillatory shear results obtained are presented using a log-log plot of the loss tangent against the angular frequency (Figure 1). This figure reveals a trend to a crossover of loss tangent values at low frequencies for emulsions stabilized with either xanthan gum or gellan gum. The lowest values of loss tangent at low (below 5 rad/s) frequencies will be reached by the emulsion stabilised with gellan gum. Thus, this emulsion would exhibit the highest ratio of elastic/viscous components at the lowest frequencies. It is noteworthy that the shape of the frequency dependence curve of the emulsion stabilized by the blend of polysaccharides was essentially governed by the presence of xanthan gum, except for the range of higher frequencies.

The relaxation spectra obtained from mechanical spectra revealed that the relaxation time of the emulsion stabilized by both gums is dominated by gellan gum at shorter times and by xanthan gum at longer times, which suggests the existence of thermodynamic incompatibility of both polysaccharides in the continuous phase.

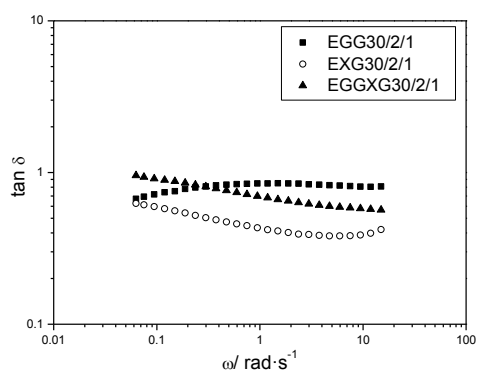


Figure 1. Frequency dependence of the loss tangent for  $\alpha$ -pinene emulsions stabilized by gellan gum, xanthan gum and a 50% blend of both gums.  $T=20^{\circ}\text{C}$ .

#### Droplet size distributions (DSD)

DSD were not significantly different to each other.  $D_{3,2}$ ,  $D_{4,3}$  mean diameters and span were on average 4.4  $\mu\text{m}$ , 8.6  $\mu\text{m}$  and 1.6. This demonstrates that the different mechanical spectra obtained can be mainly ascribed to the different structure formed by gellan, xanthan and the blend of both gums in the continuous phase.

*Multiple light scattering (MLS)*

MLS results were analysed as the percentage of backscattering at the centre of the measuring cell as a function of aging time. These results have been fitted to a first-order kinetic equation,  $BS = BS_e + (BS_0 - BS_e) e^{-Kt}$ , where,  $BS$  is the time-dependent backscattering value,  $BS_e$  is the corresponding equilibrium value,  $BS_0$  is the initial backscattering value and  $K$  is a 1st-order kinetic coefficient. The lowest value of the kinetic coefficient was obtained for the emulsion stabilised by gellan gum ( $1.7 \cdot 10^{-7} \text{ s}^{-1}$ ), which suggests that this emulsion was the most stable.

*Flow curves*

Figure 2 shows the flow curve results. Zero-shear viscosity values calculated from the Carreau-Yasuda equation supported the MLS results. The emulsions stabilised by gellan gum presented the highest zero-shear viscosity (4506 Pa·s), followed by the  $\eta_0$  provided by xanthan gum (3403 Pa·s). The emulsion stabilised by the blend of both biopolymers showed the lowest value (1144 Pa·s) confirming the thermodynamic incompatibility triggered by volume exclusion phenomena that take place in the continuous phase.

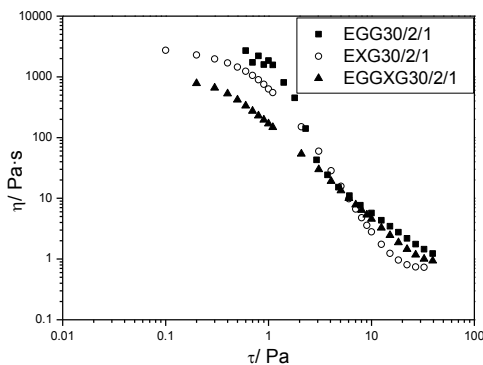
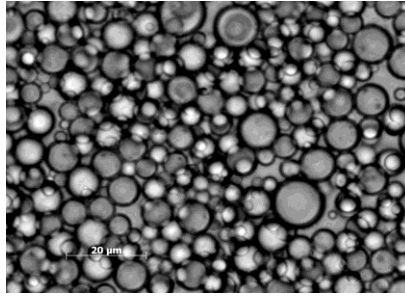


Figure2. Stress dependence of the viscosity for  $\alpha$ -pinene emulsions stabilized by gellan gum, xanthan gum and a 50% blend of both gums.  $T=20^\circ\text{C}$ .

*Optical microscopy*

The micrographs obtained by optical microscopy did not support the occurrence of structural differences for the three emulsions studied. Figure 3 shows the micrograph for the emulsion formulated with gellan gum.



*Figure 3. Micrograph obtained by optical microscopy for the emulsion stabilized by gellan gum.*

It is noted that all droplets showed spherical shape, which do not correspond to a closely-packed emulsion. A closely-packed structure is typically found in highly concentrated emulsions, where droplets tend to form polygonal structures [5]. The micrograph shown in Figure 3 supports the polydispersity of droplet sizes and the mean diameters calculated from results obtained by laser diffraction.

### **Concluding Remarks**

Slightly concentrated  $\alpha$ -pinene emulsions stabilized with biopolymers exhibit viscoelastic properties when gellan gum, xanthan or a blend of them are used at 0.4 wt%.

The low zero-shear viscosity value and the frequency dependence of the loss tangent shown by the emulsion stabilized by the blend of both biopolymers suggested the occurrence of thermodynamic incompatibility in the continuous phase.

The multiple light scattering and zero-shear viscosity results indicated that gellan gum provided the best physical stability.

### **Acknowledgements**

The financial support received (Project CTQ2011-27371) from the Spanish Ministerio de Economía y Competitividad (MINECO) and from the European Commission (FEDER Programme) is kindly acknowledged. The authors are also grateful to the following companies for providing materials for this research, Croda, CP Kelco and Destilaciones Bordas-Chinchurreta.

### References

1. Jäger, W. (2010). Metabolism of Terpenoids in Animal Models and Humans en Handbook of Essential Oils. Science, Technology and Applications, (Baser, K.H.C., and Buchbauer, G., eds.), pp.209-234, CRC Press, Boca Raton, USA.
2. Phillips, G.O., and Williams, P.A. (2009) Handbook of Hydrocolloids, 2nd edn, Woodhead Publishing Limited, New York.
3. Pérez- Mosqueda, L.M, Ramírez, P., M.C. Alfaro, M.C., Rincón, F.; Muñoz, J. (2013) Food Hydrocolloids 32, 440-446.
4. Reekmans, S. (1998). In Chemistry and Technology of Agrochemical Formulations, (Knowles, D.A., ed.). Kluwer Academic Publishers. The Netherlands.
5. Masalova, I.,Malkin, A.Ya. (2007) Applied Rheology.17, 4, 42250-1-42250-9.

### Contact Address:

*M.C. García (mcgarcia@us.es)*

*Dpto. Ingeniería Química,*

*Facultad de Química,*

*Universidad de Sevilla, C/ P. García González s/n, 41012, Sevilla (Spain)*

*Tel.:+34 954 557179 // Fax:+34 954 556447.*

## CHAPTER 7

# Synovial Fluid Hyaluronate Characterization in Stagnation Point Extensional Flow

*S.J. Haward*

*CEFT - Department of Chemical Engineering, Faculty of Engineering, University of Porto,*

### Introduction

The glycosaminoglycan hyaluronic acid, also known as hyaluronan, sodium hyaluronate, or simply HA, is a naturally-occurring high molecular weight linear polysaccharide. HA is found in high concentrations in the vitreous humor, umbilical cord, cockerel comb and joint synovial fluid and at lower concentrations in many other tissues. In healthy synovial fluid (SF) the HA concentration is typically a few thousand parts per million (ppm) and can have a molecular weight of several million Daltons [1]. SF has remarkable rheological properties, being very strongly shear-thinning in steady shear flow and also highly viscoelastic [2]. Recent extensional rheological measurements show that SF, and solutions of HA at physiological concentrations, are highly strain-hardening under elongational deformations [2].

It is clearly established that the high molecular weight and concentration of HA in SF contributes vitally to the SF rheological properties that provide effective lubrication and wear protection of human and animal joints. Also it is known that the concentration and molecular weight of HA in SF are degraded by degenerative joint diseases such as osteo-arthritis, impairing its ability to protect the joint and affecting mobility [3].

Viscosupplementation of arthritic joints is a pharmaceutical application of hyaluronic acid involving intra-articular injection of HA into the joint space in order to restore the SF rheological properties, relieving pain and increasing mobility [4]. The biocompatibility and rheology of HA in solution are also exploited in ophthalmic surgery and in consumer products such as skin creams and eye drops. The complete and thorough characterization of the rheology and dynamics of HA

in solution can thus provide benefits to a number of important applications. The analysis of the HA in SF also has potential as a diagnostic marker for joint disease.

In this article, measurements of the flow-induced birefringence in a stagnation point extensional flow field are used to characterize the response of dilute solutions of HA subjected to planar elongational flow. Extensional components occur in virtually all real flow fields, and may be of particular relevance to applications of HA in viscosupplementation and in the synovial fluid, where a strong biaxial extensional flow arises between cartilage surfaces approaching each other during compression (e.g. between the tibia and femur during locomotion) [5].

### Materials and Methods

Hyaluronic acid (HA) samples of molecular weight,  $M_w = 1.6, 2.6$  and  $4.8 \times 10^6 \text{ g mol}^{-1}$ , called (HA1.6, HA2.6 and HA4.8, respectively) are used in the study. The HA fibres are dissolved in phosphate-buffered saline (PBS) solution at concentrations  $0.01 \leq c \leq 0.08 \text{ wt\%}$ , at which the solutions can be considered dilute.

Additional tests are performed using porcine synovial fluid (PSF). The PSF is obtained from the tarsal joint of freshly slaughtered pig, is diluted by a factor of 20 $\times$  with PBS and subsequently centrifuged to remove cells and other extraneous matter. Also, 200 ppm  $\text{NaN}_2$  is added as a biocide.

Planar elongation flow fields are generated using microfluidic cross-slot devices (see Fig. 1 for an example). This allows access to high Weissenberg numbers  $Wi$  while inertial contributions to the flow are minimized.

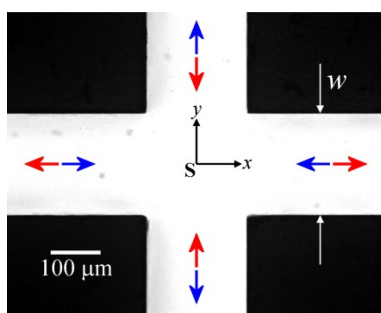


Figure 1. Photograph of the microfluidic cross-slot device with channel width  $w=200 \mu\text{m}$  and depth  $d=1\text{mm}$ .

The flow in the cross-slot device is driven using a system of oscillating piezo-electric micropumps described in ref. [6]. The coloured arrows in Figure 1 indicate the flow: red for inflow along the  $y$ -direction and blue for inflow along the  $x$ -direction. By symmetry, the cross-slot has a stagnation point at its centre (marked 'S' in Figure 1), where the flow velocity is zero. The resulting combination of high residence time and high  $Wi$  means that macromolecules can become highly stretched at the stagnation point and undergo a coil-stretch transition.

The oscillatory flow system has the advantage that small volumes of samples ( $\sim O(0.1\text{mL})$ ) are required, which allows scarce fluids such as SF to be tested that would not be possible in a continuous flow loop. Note that all the results presented subsequently are obtained for inflow along the  $y$ -direction, outflow along the  $x$ -direction.

The strain rate at the stagnation point of the cross-slot device is a linear function of the average flow velocity,  $U$ , in each of the four intersecting channels:

$$\dot{\epsilon} = \frac{aU}{0.5w}, \quad (1)$$

where the value  $a$  depends on the channel aspect ratio ( $\alpha = d/w$ ) and  $aU$  gives the flow velocity along the channel centreline. As the aspect ratio increases towards the 2D limit,  $a \rightarrow 1.5$ .

Flow-induced birefringence (FIB) is measured in the test fluids in the locality of the stagnation point as a function of the imposed strain rate. The measurements are made using the optical train and calibration methods described in ref. [6]. Birefringence arises in polymer solutions undergoing flow due to segmental orientation of the polymer chains, which causes the refractive index of the fluid to be different in the direction of and orthogonal to, the orientation direction. The magnitude of the birefringence can be related to the degree of segmental orientation and therefore to the macromolecular strain. Measurements with well-defined polymeric systems in stagnation point flows have indicated that macromolecules unravel and stretch to near their contour lengths when a critical strain rate ( $\epsilon_c$ ) is exceeded. In experiments, the value of the critical Weissenberg number ( $Wi_c$ ) for this coil-stretch transition to occur is roughly consistent with theoretical expectations, which show [7]:

$$Wi_c = \tau \dot{\epsilon}_c \approx 0.5 - 1 \quad (2)$$

where  $\tau$  is the characteristic relaxation time.

## Results and Discussion

With HA in PBS solutions, a birefringent strand becomes visible and increases in intensity as the strain rate in the cross-slot is increased (see Figure 2(a,b) for some examples obtained with HA4.8). The strand is localized along the outflow axis of the geometry ( $x$ -axis), which is a result of the high  $Wi$  and strains that are available to fluid elements that pass near to the stagnation point.

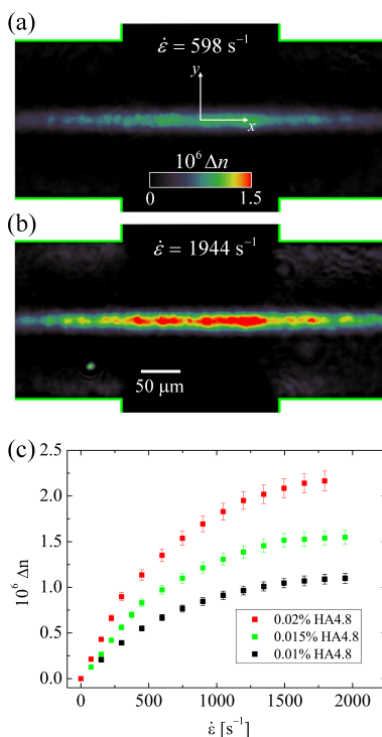


Figure 2. (a), (b) Birefringence ( $\Delta n$ ) observed with a 0.015 wt% solution of HA4.8 in the cross-slot at the strain rates indicated. (c) birefringence measured at the stagnation point for HA4.8 solutions over a range of strain rates.

The birefringence ( $\Delta n$ ) measured on the  $x = 0$  axis, close to the stagnation point is shown in Figure 2(c) for HA4.8 solutions of a range of concentration. The birefringence reaches a plateau value at high strain rate which scales very well with the polymer concentration, indicating the dilution of the fluids. The birefringence measured as a function of the strain rate for dilute HA solutions of various molecular weight is shown in Fig. 3(a). Points of inflexion on the curves

provide a measure of  $\dot{\varepsilon}_c$  and can be used in Eq. 2 to obtain the relaxation time,  $\tau \propto M_w^{9/5}$  (as shown by the inset figure).

Using  $M_w \propto \tau^{5/9} \propto \dot{\varepsilon}^{-5/9}$ , the data in Figure 3(a) can be converted into the molecular weight distributions shown in Figure 3(b). These are well-fitted by log-normal distribution functions from which the values of  $M_w$  and  $M_w/M_n$  can be extracted, see Table 1. The molecular weight parameters are in close agreement with the values specified by the suppliers of the HA samples.

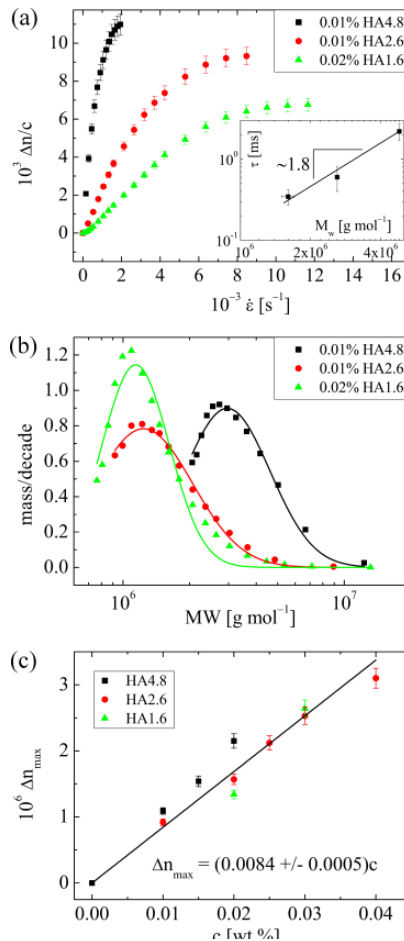


Figure 3. (a) Normalized birefringence as a function of strain rate for HA solutions of various MW (inset shows relaxation time as a function of the MW). (b) MW distributions determined from the data in shown in (a). (c) Maximum birefringence as a function of HA concentration, providing a linear relationship.

Table 1: Relaxation times, weight-average molecular weights and polydispersities of the various test fluid samples.

sample	$c$ [wt%]	$\tau$ [ms]	$10^{-6} M_w$ [g mol <sup>-1</sup> ]	$M_w/M_n$
HA1.6	0.02	0.35	1.45	1.17
HA2.6	0.01	0.60	2.07	1.41
HA4.8	0.01	2.25	4.38	1.30
PSF 20×	0.014	2.8	4.54	1.25

In Figure 3(c) the plateau value of the birefringence at high strain rate ( $\Delta n_{\max}$ ) is plotted as a function of the HA concentration for all the solutions tested. A closely linear relationship is found, with  $\Delta n_{\max} \approx 0.0084c$ .

Finally, the results of experiments with PSF diluted by 20× with PBS solution are presented in Figure 4.

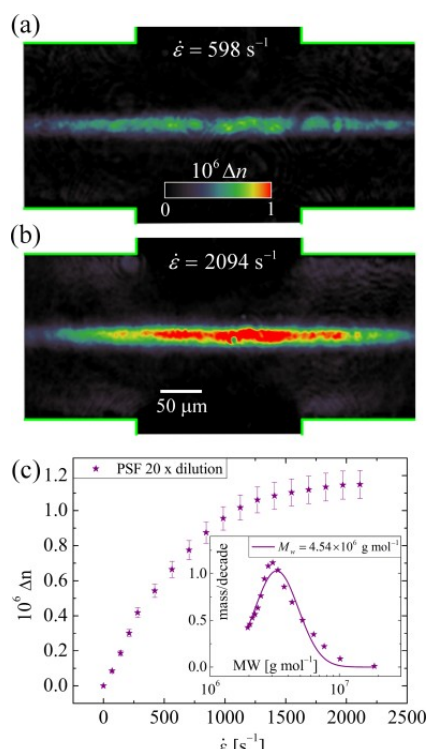


Figure 4. (a),(b) Birefringence observed in the cross-slot for the flow of diluted PSF. (c) Birefringence measured at the stagnation point for the diluted PSF over a range of imposed strain rates (inset shows the derived MW distribution).

The observed birefringence (Figure 4(a,b)) is qualitatively very similar to that observed in the HA4.8 solution, and follows a similar trend with strain rate, Figure 4(c). The plateau level of birefringence ( $\Delta n_{\max} \approx 1.2 \times 10^{-6}$ ) can be used to estimate the HA concentration at  $c \approx 0.014$  wt% (hence  $c \approx 0.28$  wt% in the undiluted PSF). The molecular weight distribution derived from the birefringence versus strain rate curve (Figure 4(c), inset) also yields parameters highly aligned with those expected for healthy synovial fluid (details are given in Table 1).

In conclusion, elongational flow in microfluidic cross-slot devices can be used for characterization of HA macromolecules based on their birefringence response at the stagnation point. The approach can be applied to assess the HA content and MW of diluted SF samples, yielding a potential novel analytical or diagnostic technique.

### Acknowledgements

Financial support from the European Commission Marie Curie action FP7-PEOPLE-2011-IIF grant 298220 is acknowledged.

### References

1. Kogan, G. Šoltés, L. Stern, R. and Gemeiner, P. (2007) *Biotechnol. Lett.* 29, 17-25.
2. Bingöl, A.Ö., Lohmann, D., Püschel, K. and Kulicke, W.M. (2010) *Biorheology* 47, 205-224.
3. Dahl, L.B., Dahl, I.M., Engstrom-Laurent, A. and Granath, K. (1985) *Ann. Rheum. Dis.* 44, 817-822.
4. Balazs, E.A. (2004) *Surg. Technol. Inter.* 12, 278-289.
5. Backus, C., Carrington, S.P., Fisher, L.R., Odell, J.A. and Rodrigues, D.A. (2002). In *Hyaluronan Volume 1* (Kenedy, J.F., Phillips, O.G., Williams, P.A. and Hascall, V.C., eds.), pp. 209-218, Woodhead Publishing Ltd, Cambridge, UK.
6. Haward, S.J., Sharma, V. and Odell, J.A. (2011) *Soft Matter* 7, 9908-9921.
7. De Gennes, P.G. (1974) *J. Chem. Phys.* 60, 5030-5042.

### Contact Address:

S.J. Haward ([shaward@fe.up.pt](mailto:shaward@fe.up.pt))  
Dpt. of Chemical Engineering, Faculty of Engineering, University of Porto  
Rua Dr. Roberto Frias sn 4200-465 Porto (Portugal)



## CHAPTER 8

# Skin viscoelasticity and hydration studies on the topical application of a surfactant free emulsion

J. Marto<sup>1,2</sup>, L. Gouveia<sup>1</sup>, F. Tonin, E. Oliveira<sup>b</sup>, A.J. Almeida<sup>1</sup> and H.M. Ribeiro<sup>1</sup>

<sup>1</sup>Research Institute for Medicines and Pharmaceutical Sciences (iMed.UL), Faculdade de Farmácia da Universidade de Lisboa, Lisboa, Portugal

<sup>2</sup>Laboratórios Atral S.A. (Grupo AtralCipan), Castanheira do Ribatejo, Portugal

### Introduction

Emulsion systems used in dermatopharmacy have to fulfil a number of requirements, e.g. acceptable physical stability, chemical inertness, satisfactory safety profile and efficacy, while maintaining optimal sensory attributes [1]. In order to provide all of these attributes to water-in-oil (w/o) cosmetic emulsions, several excipients need to be used, such as surfactants, fatty amphiphiles (e.g. alcohols), polymers and other excipients [2]. All these ingredients allow to re-establish, or to help maintaining *stratum corneum* (SC) emolliency as well as its global “rheological” properties.

The skin has viscoelastic properties: collagen and elastic fibres represent the elastic components, whereas friction between cells and collagen and other components of the dermal matrix accounts for the viscous part. Depending on its water and lipid contents, the epidermis presents a strong effect on the skin frictional resistance. An increase in skin hydration and lipid content improves the viscous resistance against deformation [3].

The present study was designed to investigate *in vivo* the influence of a w/o surfactant free emulsion on the biological parameters of the human skin, especially those concerning the biomechanical characteristics.

### Experimental

#### *Emulsion processing*

A surfactant-free w/o semi-solid Amimulsion (emulsion stabilized by solid particles –polymer - polysaccharide) was prepared using a modified cold emulsification

## Perspectives in Fundamental and Applied Rheology

process, as described elsewhere [2]. The emulsion contains well-known pharmaceutical excipients.

### Biological Studies

The biological effects of formulation were assessed in the ventral aspect of the human forearm skin (n=20, young healthy females, 20-30 years old, after previous informed consent) following a 14 days regular application (twice a day) of the formulation on predefined sites. All application sites, application sequence and measurements were randomised.

Biological characterisation included the non-invasive assessment of cutaneous water balance through the following variables:

- Epidermal capacitance (Corneometer® CM825) from CK electronics (Germany);
- Trans-epidermal water-loss (Tewameter® TM210) from CK electronics (Germany).

Biomechanical properties were assessed through a “suction method” – Cutometer 474SEM (CK electronics GmbH, Germany). The measuring principle is suction/elongation. In this study, the strain-time-mode was applied. A 2 mm opening probe was used and a pressure of 450 mbar was applied in order to suck the skin into the probe. Each measurement consisted of three suction cycles (1.30 s of suction followed by 1.30 s relaxation) and was performed in triplicate on the volar forearm.

The cutometer generates deformation versus time and six parameters were studied. The elastic deformation ( $U_e$ ), the total extensibility of the skin ( $U_f$ ), the elastic deformation recovery ( $U_r$ ), the total deformation recovery ( $U_a$ ) and the amount of deformation not recovered by the end of the stress-off period the stress ( $R$ ).

### Statistical analysis

Cross-correlation between variables (both independent and dependent) was calculated. As several significant cross-correlation were found, multivariate analysis was performed in order to reduce dimensionality of the data.

Principal component analysis (PCA) was performed on centred data to study the relationship between products (control and Amimulsion) and attributes ( $U_e$ ,  $U_f$ ,  $U_a$ ,  $U_v$  and  $U_r$ , pH, hydration level and TEWL).

## Results and Discussion

The skin is often exposed to surface-active agents like soaps, which may affect the skin barrier. Differences in the effects of emollients have been investigated using biophysical instruments [4,5].

A PCA was carried out with the control and Amimulsion as individuals and 8 attributes as variables. This analysis allowed a better evidencing of the differences among the control and Amimulsion, and also made possible to visualize relationships between attributes. The first two principal components accounted for 93% of the total variance. The loading plot of the variables shows that the vectors of specific variables are well represented, close to the correlation circle (Figure 1). PC1 is positively related to three attributes: hydration level (Corneo), time and formulation (Formul).

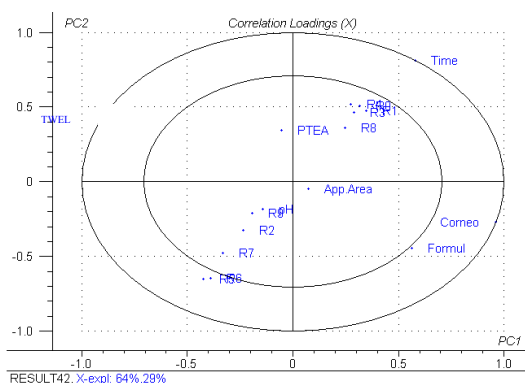


Figure 1 PCA:Loading plot of the attributes.

In a subsequent step, hierarchical cluster analysis performed on the centred data clearly reveals 4 clusters related to the time and formulation variables (Figure 2). These results are confirmed by PCA. In addition, the PCA also underlined that hydration level was correlated to the time and formulation (Figure 3.).

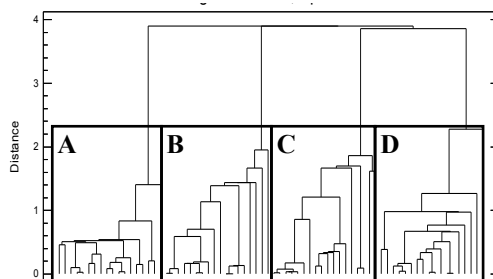


Figure 2 Hierarchical cluster analysis dendrogram based on multivariate statistical analysis. A – Control (t=0 day); B – Control (t=14 days); C – Amimulsion (t=0 day); D – Amimulsion (t=14 days).

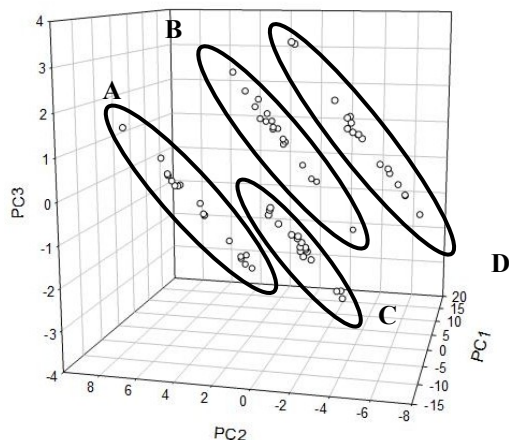


Figure 3 PCA loadings plot. A – Control (t=0 day); B – Control (t=14 days); C – Amimulsion (t=0 day); D – Amimulsion (t=14 days).

The SC water retention is a crucial factor in keeping the skin supple and flexible and influence skin permeability to molecules. The methodological procedure chosen, allowed the identification of positive results regarding skin water dynamics, expressed in terms of corneometry changes. However, Amimulsion did not decreased TEWL compared to the control (Figure 1).

An explanation may be that these last attributes are undoubtedly related to the mechanism of hydration. The major mechanisms of hydration are humectancy, emolliency, and occlusion. The hydration provided by emulsion is attributed to emollient (lipophilic emollient - triglycerides). In fact, emollients smooth the skin by filling spaces between skin flakes and adding a complementary occlusive activity, which contributes to SC hydration [6].

Regarding biomechanics, and considering the different complexities included in the interpretation of such indicators, the elastic portion of the suction part versus the elastic portion of the relaxation part ( $U_r/U_e - R_5$ ) and the portion of the viscoelasticity of the curve ( $U_v/U_e - R_6$ ) were considered as the most relevant variables (Fig.4 and Fig. 5) Furthermore,  $U_r/U_e$  and  $U_v/U_e$  were negatively loaded on PC1 and PC2 (Figure 4).

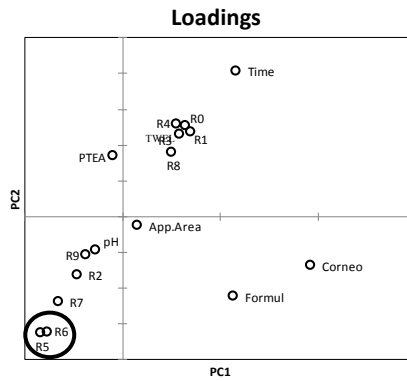


Figure 4 PCA:Loading plot of the attributes.

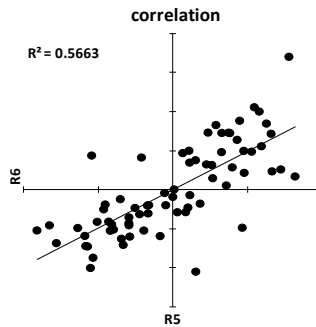


Figure 5. Scatter plot showing correlation between R5 and R6.

Nonetheless, these parameters slightly decreased during the period of time of the assay (14 days) for the formulation under use, which means that the skin became more viscoelastic. These results suggest the relative equivalence of biological impact for the formulations.

However, due to the young age of volunteers, effects upon the viscoelasticity of the skin were not significant. The statistical power (decreased by both the observed inter and intra variability) impairs the detection of the formulation influence on the biomechanics skin properties.

## Conclusions

Amimulsion appears to have an interesting impact on skin biology following a “long-term use” essay. Concluding, Amimulsion represent a highly effective carrier for topical application which is intended to increase skin hydration.

**References**

1. Eccleston G. (1997) Coll. Surf. A. 123-124: 169-182.
2. Raposo S., Salgado A, Eccleston G., Urbano M, Ribeiro MH (2013) Pharm. Dev. Technol. doi:10.3109/10837450.2013.788516, 2013.
3. Sylvia A. (2003) Eur. J. Pharm. Biopharm. 56:67-72.
4. Bárány E., Lindberg M., Loden M. (2000) Int. J. Pharm. 195: 189-195.
5. Bárány E., Lindberg M, Lodén M. (1999) Contact. Dermat. 40: 98-103.
6. Kraft N., Lynde C. (2005) Skin Ther. Lett. 10(5): 1-8.

*Contact Address:*

*J. Marto (jmmarto@ff.ul.pt)*

*iMed.Ul– Faculdade de Farmácia da Universidade de Lisboa. Av. Prof. Gama Pinto  
1649-003 Lisboa - Portugal*

*Tel: +351 217 946 400*

*Fax: +351 217 946 470*

## CHAPTER 9

# Egg albumen/tragacanth gum based bioplastics plasticised with water/glycerol mixtures

*López-Castejón<sup>1</sup>, L.; Bengoechea<sup>1</sup> C., Martínez<sup>2</sup>, I. ; García-Morales, M.<sup>2</sup>*

*1 Departamento de Ingeniería Química, Universidad de Sevilla, Facultad de Química. Calle Profesor García González 1, 41012 Sevilla Spain*

*2 Departamento de Ingeniería Química, Centro de Investigación en Tecnología de Productos y Procesos Químicos, Campus El Carmen, Universidad de Huelva, 21071, Huelva (Spain)*

### Introduction

Different types of proteins like wheat gluten, corn zein, soy protein, etc., have recently shown suitability for the manufacture of bioplastics [1,2]. Manufacture of these protein-based bioplastics generally involves the addition of plasticizers and, sometimes, a disrupting agent in the formulation [3,4]. Glycerol and water are among the most common plasticisers, as they facilitate the processing by reducing the intermolecular forces among the polymeric chains, which increases their mobility. In our case, a thermo-mechanical process was used, in which a dough-like material is obtained and further subjected to both heat and pressure [5]. Hence, materials with unique properties may be achieved by selecting adequate processing parameters and plasticizer nature and content [4].

Recent work by Jerez et al. [5,6] and González-Gutiérrez et al. [7] has revealed the feasibility of producing highly transparent bioplastics from egg white albumen. If compared to other common proteins, those bioplastics demonstrated suitable mechanical properties for the manufacture of biodegradable food packaging and other plastic stuffs by application of thermo-mechanical methods. However, for modified atmosphere packaging (MAP) applications, as oxygen scavenging and CO<sub>2</sub> emitting processes, bioplastics should not only possess adequate mechanical properties, but also may be required to be highly hydrophilic, as those processes are moisture dependent, and only occur after water has been absorbed from the food product or package atmosphere. Another point to consider is the degree of compatibility between glycerol and the protein matrix.

In this sense, tragacanth gum may be included in the base protein formulations, as preliminary studies have pointed out its effect on increasing the water absorption capacity of the resulting protein-based material. On the other hand, tragacanth gum has also shown an ability to prevent glycerol migration.

Thus, this research studies the effect of tragacanth gum, plasticizer and Relative Humidity (RH) control on the water uptake capacity and thermo-mechanical properties of albumen bioplastics.

### Experimental

#### *Materials and Formulations*

Spray-dried egg white albumen (designated EW; with 73 wt.% protein, 6 wt.% ashes and 8 wt.% moisture) provided by OVOSEC S.A. (Spain) was used. Tragacanth gum (T) was supplied by Sigma-Aldrich (USA). Glycerol, from Panreac Química, S.A. (Spain), and distilled water were designated G and W, respectively.

As far as formulations are concerned, a biopolymer/plasticizer ratio of 60:40 was set, with a 2:1 protein/gum ratio when gum was included, and the glycerol/water ratio within the plasticizer varying as 1:0, 3:1, 1:1, 1:3 and 0:1. These formulations allowed the effect of the plasticizer on the water uptake capacity and mechanical properties to be evaluated. Bioplastics were obtained through a thermo-mechanical process, which includes two stages:

- a) Mixing of ingredients in the kneading tool (Rheomix 600p) of a torque-rheometer (Polylab, Thermo Haake, Germany) at 50 rpm for 10 min.
- b) Compression-moulding: the resulting dough-like material was subjected to pressure of 100 bar and temperature of 120 °C for 10 min in a hot-plate press (8).

#### Testing

Water absorption tests, according to ASTM D570 (2005), were carried out by immersing the probes into distilled water for 24 hours, the water absorption percentage calculated as:

$$\text{water absorption} = \frac{\text{wet wt.} - \text{reconditioned wt.}}{\text{conditioned wt.}} \times 100 \quad (1)$$

the weight of the probe just after 24 h of water immersion; reconditioned weight, is the final weight of the wet sample after 24 h of drying in an oven at 50°C.

Dynamic temperature sweeps were performed from -30 to 140 °C at 3 °C/min at a constant frequency of 1 Hz and strains within the LVR with a RSA3 rheometer (TA Instruments, USA) in double cantilever bending mode.

Tensile tests were performed with a MTS Insight 10 kN (USA), according to D638 (2003), with an extension rate of 5 mm/min, at room temperature.

## **Results and Discussion**

### *Effect of the gum and type of plasticiser*

#### *Water uptake*

A remarkable increase in the water uptake capacity is apparent when tragacanth gum is included in the formulation. Thus, the inclusion of one third of gum in the biopolymer fraction (that is, EW/T ratio of 2:1) approximately duplicates the water uptake capacity if compared to the gum-free bioplastic, irrespective of the glycerol/water ratio in the formulation: increases in the water uptake from 92.60 up to 224.53% for the G/W 1:0 ratio; from 72.65 up to 152.80% for the G/W 1:1 ratio; and from 75.63 up to 141.08% for the G/W 0:1 ratio, were observed.

Plasticizer ratio clearly affects their water uptake capacity and mechanical properties. Thus, a change in the glycerol/water ratio from 1:1 to 1:0, always maintaining the total amount of plasticizer constant (40 wt.% of the bioplastic), generally produces an important increase in the water uptake capacity, being this parameter specially high for the sample with gum only containing glycerol as plasticizer (that is, ratio of 1:0).

#### *Dynamic Flexural moduli*

The presence of gum also seems to affect the bioplastics mechanical properties. In that sense, when dynamic flexural measurements in the LVR region are conducted, lower values of the elastic modulus are generally noticed if the gum is included in the formulation. Moreover, DMTA results shown in Figure 1 demonstrate the greatest values (elastic flexural modulus) for the sample that only contains water as plasticizer.

#### *Tensile Properties*

Tensile tests corresponding to bioplastics not containing tragacanth gum always reveal a larger elongation at break and, for two of the formulations, higher tensile strength than the respective gum-containing sample (Figure 2). Again, the sample which only contains water as plasticizer (G/W 0:1) is the one which presents the greatest value for mechanical properties (e.g. tensile strength at break).

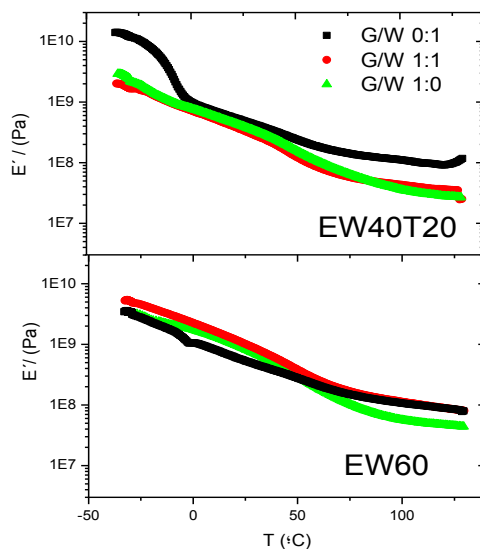


Figure 1. DMTA profiles at 1 Hz for EW probes with glycerol (G): water(W) ratios (0:1, 1:1, and 1:0 with tragacanth gum (EW40T20) and without tragacanth gum (EW60).

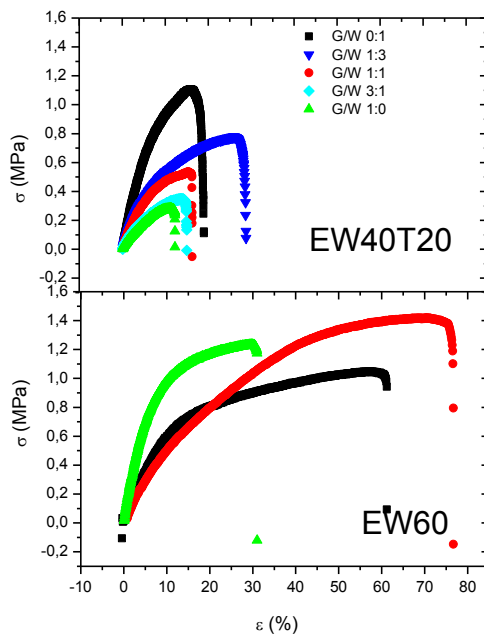


Figure 2. Influence of glycerol:water ratio (0:1, 1:3, 1:1,3:1, and 1:0) on stress-strain ( $\sigma$ - $\epsilon$ ) relationship for the of thermo-mechanically processed albumen bioplastics with tragacanth gum (EW40T20) and without tragacanth gum (EW60)

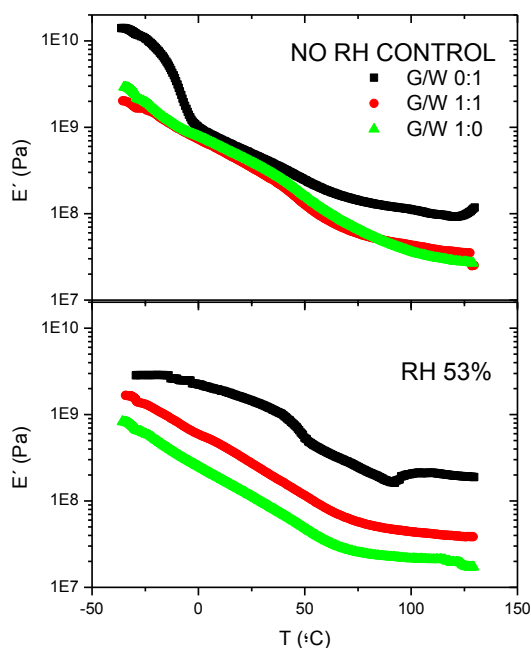


Figure 3. DMTA profiles at 1 Hz of thermo-mechanically processed egg white-tragacanth bioplastics containing different glycerol-water ratios (1:0, 1:1, and 0:1) not submitted to RH control (up); and submitted to RH control (down)

#### *Influence of Relative Humidity (RH)*

After preparation, some samples were stored in sealed glass containers at room temperature (no RH control, as previously) or placed in desiccators at relative humidity of 53% with a saturated solution of  $\text{Mg}(\text{NO}_3)_2 \cdot 6\text{H}_2\text{O}$  at room temperature (RH control) before testing.

#### *Water uptake*

When observing those probes without RH control, it seems that higher glycerol contents tend to induce greater water uptake after 24 hours. Water absorption values range from around 140 to 235% under these conditions, with the lowest value corresponding to the probe without glycerol. On the contrary, no apparent tendency is observed when the probes submitted to RH control (53%) are studied, with all water uptake values being in a narrower range (from around 150 to 208%).

### *Dynamic Flexural moduli*

Both the storage and loss moduli of all the EW/T/G/W bioplastics tend to decrease to a plateau region as temperature increases from -30 to 130°C for all the EW/T/G/W bioplastics. It may be noticed how lower values for  $E'$  (Figure 3) and  $E''$  are obtained when increasing the content of glycerol, due to its plasticizing effect.

Water loss seems to take place during equilibration under RH control for the sample containing only water as plasticizer (G/W 0:1), which results in a hardened probe. Thus, its corresponding  $E'$  curve show some discontinuities, as can be observed. Anyway, it is remarkable how when RH control is taken, the decay in the viscoelastic properties in the plateau region as glycerol content increases is much more pronounced than in the case of samples with no RH control.

### **References**

1. Gómez-Martínez D., Partal P., Martínez I., Gallegos C. (2009) *Bioresour. Technol.*, 100, pp. 1828–1832.
2. Kim S. (2008) *Bioresour. Technol.*, 99, pp. 2032-2036
3. Sothornvit, R. and Krochta, J. (2005) *Innovations in food packaging*. (Han J.H., ed.) pp. 403-433, Elsevier, Academic Press San Diego
4. Pommet, M.; Redl, A. ; Guilbert, S. y Morel, M.H. (2005) *J of Cereal Science*, 42: 81–91.
5. Jerez, A.; Partal, P; Martínez, I.; Gallegos, C. and Guerrero, A. (2007) *Rheologica Acta*, 46: pp. 711-720.
6. Jerez A., Partal P, Martínez I., Gallegos C., Guerrero A. (2007), *J. Food Eng.*, 82, pp. 608-617
7. Gonzalez-Gutierrez J., Partal P, Garcia-Morales M., Gallegos C. (2010) *Bioresource Technology*, 101, pp. 2007–2013

### **Acknowledgements**

Authors acknowledge financial support of this work by the Ministerio de Economía y Competitividad through the project MAT2011-29275-C02-02

### *Contact Address:*

C. Bengoechea ([cbengoechea@us.es](mailto:cbengoechea@us.es))  
Departamento de Ingeniería Química  
Facultad de Química, Universidad de Sevilla  
C/Profesor García González, 1, 41012  
Telf.: +34954 557 179

## CHAPTER 10

# Shear and elongational flow measurements of PCL/PLA blends

*Pedro Mejia, Itxaso Calafell and Antxon Santamaria*

*Department of Polymer Science and Technology and POLYMAT Institute  
The University of the Basque Country (UPV/EHU)*

### Introduction

In recent decades biopolymers, as well as biodegradable polymers, have attracted a great interest. One reason for this attention lies in the large number of potential applications, including the field of medicine. Furthermore, the use of mixtures of polymers makes possible to use the benefits of each of the two components to try to obtain a material tailored to specific applications.

The aim of this work is to establish a relationship between the morphology and the rheological behavior of Poly( $\epsilon$ -caprolactone) (PCL); Polylactic acid (PLA) homopolymers and its blends at different amounts of both components. Lactic acid monomer can be extracted from renewable resources (corn, sugar cane, wheat) and Poly( $\epsilon$ -caprolactone) is a polymer which possesses flexibility, thermal stability and biodegradability.

Blends of compositions ranging from 20 to 80 wt% PLA are investigated. In particular the following aspects are contemplated: a) Thermal characterization of the samples performed using Dynamic Mechanical Thermal Analysis (DMTA). b) Shear viscosity measurements under conditions similar to polymer processing. c) Elongational or tensile flow measurements using melt spinning experiments. d) Morphological analysis of the blends by SEM scanning electron microscopy.

### Experimental

Commercial samples, PCL (CAPA<sup>R</sup> 6800) and PLA (3052 D Biomer<sup>R</sup>) were used. Blends were prepared in a twin screw extruder Collin ZK-25 at a temperature of T=180°C.

A dynamic spectroscopy analysis on solid state was carried out in a Dynamic Mechanical Analyzer, Triton 2000 DMA from Triton Technology, Ltd. The samples were heated from -100 °C to 150°C at a constant heating rate of 4°C/min and a frequency of 1.0 Hz. The scans were performed under bending deformation mode. The surfaces of cryogenically fractured specimen were observed by Scanning Electron microscopy, SEM, in a Hitachi S-2700 electron microscope at an accelerating voltage of 15 kV.

Extrusion flow experiments were performed in a Göttfert Rheograph 2002 rheometer using a capillary die of dimensions  $R=0.5$  mm and  $L/D=30/1$ , at temperatures between 170 and 190°C. The end effects (usually corrected employing the so-called Bagley plots) should not be relevant for this high  $L/D$  value; viscosity curves involve, actually, apparent viscosity and apparent shear rate.

Melt spinning experiments were carried in a Rheotens unit (Gottfert) adapted to the Gottfert Rheograph 2002 rheometer.

### Results and Discussion

Temperature sweep tests carried out in the DMTA made it possible to obtain the glass transition temperature for pure polymers and its blends. The relaxation spectra, in particular the maxima observed in the loss tangent,  $\tan \delta$ , showed the existence of two glass transition temperatures, located very close to the respective glass transitions of PLA ( $T_g=70^\circ\text{C}$ ) and PCL ( $T_g=-44^\circ\text{C}$ ). A crystallization process was also observed at  $T_c= 103^\circ\text{C}$ , for pure PLA and the blends.

These results clearly indicate that the blends were immiscible, which is due to the semicrystalline nature of PLA [1]. The two-phase blends were analysed by SEM. The continuous and dispersed phase changed, as well as the size of the latter, depending on composition, as it is seen in Figure 1.

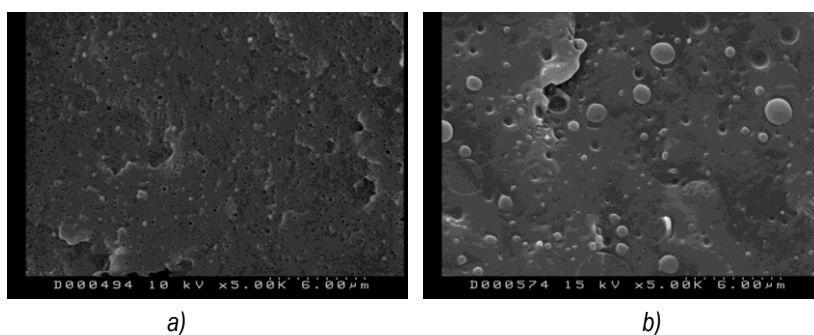


Figure 1. SEM microphotographs of blends a) 80%PLA/20%PCL, b) 20%PLA/80%PCL

The results of Figure 1b show that bigger dispersed drops (PLA) are formed in the blend which has PCL continuous phase, than in the opposite case. These morphologies, observed before blends were submitted to extrusion flow in a capillary rheometer, determine the viscosity results. As can be seen in Figure 2, drops, ellipsoids or fibers can be formed, depending on the value of the tensile stress and the diameter of the dispersed phase.

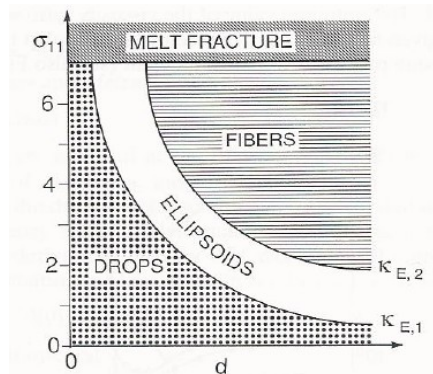


Figure 2. Map proposed by Yakovlev [2] to correlate the tensile stress,  $\sigma_{11}$ , (Y axis) and the diameter of the initial drop,  $d$ , (X axis) with the morphology of the dispersed phase.

Actually, during flow experiments in a capillary rheometer, a tensile stress component,  $\sigma_{11}$ , is developed at the entrance of the capillary, due to converging flow. In view of the map of Figure 2, the probability of reaching a fibril morphology (during extrusion) is considerably higher in the case of the blend 20% PLA/80%PCL than for 80%PLA/20%PCL, because the diameter of the drops is much bigger (Figure 1) in the former. This hypothesis lies on the base of the viscosity and melt elasticity results shown in Figure 3. The melt elasticity of the blends is expressed in terms of the extrudate swell,  $D_j/D$ ; where  $D_j$  is the diameter of the extrudate and  $D$  the diameter of the capillary.

We remark that for 80%PLA/20%PCL composition an enhancement of the viscosity is observed, as compared with pure PLA. This viscosity increase is compatible with the drop morphology that is expected during the extrusion of this blend, because the initial drops (Figure 1a) are too small to be transformed into fibers (Figure 2). However, in the case of 80%PLA/20%PCL composition, initial drops (Figure 1b) are relatively big and can transform into fibers according to the map of Figure 2. It is well known [2] that emulsion-like drop morphology brings about positive deviations with respect to the additive rule of the viscosity, whereas fiber-like morphology gives rise to a negative deviation: Both respective behaviours are observed in Figure 3. On the other hand, very high  $D_j/D$  values are

observed in particular for compositions which are prone to give emulsion-like drop morphology. The observed deviation is typical of immiscible polymer systems.

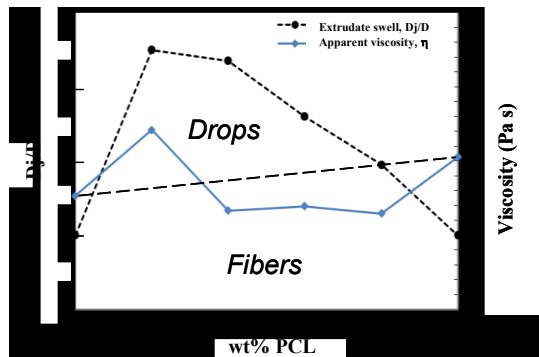


Figure 3. Viscosity (continuous line) and elasticity,  $D_j/D$ , (dotted line) results, taken at 100 1/s and  $T=170^\circ\text{C}$ , as a function of blend composition. Broken line represents the simple additive rule for viscosity.

On account of the importance of the capability of PLA and PCL to be used as threads for medical purposes, a study of the melt spinning behavior of their blends was carried out. Bearing in mind the technological importance of the “melt strength” and the “breaking stretching ratio” in melt spinning, we determined these parameters, as it is shown in Figure 4.

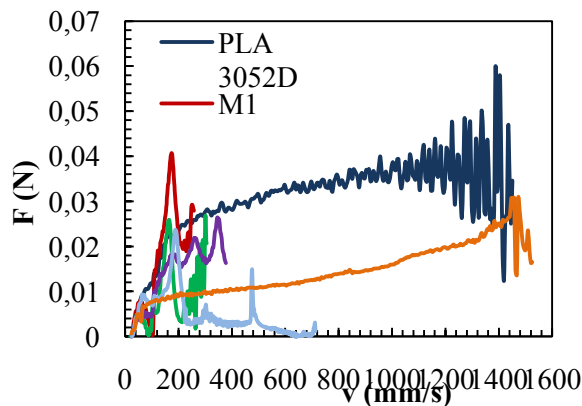


Figure 4. Tensile force as a function of stretching velocity. M1, M2, M3 and M4 stand, respectively, for blends of 80%, 60%, 40% and 20% PLA concentration. Draw resonance is observed for pure PLA (force oscillations)

The “breaking stretching ratio” is proportional to the maximum stretching velocity and the “melt strength” is given by the maximum tensile force. Both, pure polymers, PLA and PCL, give good results; better in the case of PCL, which requires less force to be stretched and does not show draw resonance.

On the contrary, very poor results are obtained for the blends, in terms of spinnability. Apparently, the constitution of two phases is reflected in the maxima observed for the blends in Figure 4. These results indicate that the blends studied in this contribution are not suitable to make yarns.

## References

1. Lopez-Rodriguez, N.; Lopez-Arraiza, A.; Meaurio, E.; Sarasua, J. R. (2006) Polym. Eng. Sci., 46, 1299-1308.
2. Utracki, L. (1989) Polymer Alloys and Blends, Hanser, New York

## Acknowledgements

This work has been done under the auspices of the UFI 11/56 of the UPV/EHU. Financial support from GIC IT-441-10 (Basque Government) is acknowledged

## Contact Address:

*Antxon Santamaria (antxon.santamaria@ehu.es)  
Polymer Science and Technology Department and POLYMAT Institute  
University of The Basque Country  
Centro Joxe Mari Korta  
Avenida Tolosa 72, 20018 Donostia-San Sebastián Spain  
Phone 943 018494, Fax number 943 01 7065*



## CHAPTER 11

# Development of protein-based composite materials by thermomechanical processing

*Diañez I., Martínez I., García-Morales M., Partal P.*

*Dpto. Ingeniería Química, Centro de Investigación en Tecnología de Productos y Procesos Químicos (Pro<sup>2</sup>TecS), Universidad de Huelva-Campus Excelencia CeIA3 (Spain)*

### Introduction

In the last few years there has been a growing interest in the development and use of biodegradable bioplastics from renewable sources, whose properties are able to compete, in many cases, with those of the traditional petroleum-based plastics, while reducing the environmental pollution caused by plastic waste. The main renewable sources of biopolymers are proteins, polysaccharides and lipids. Proteins are thermoplastic heteropolymers of both polar and non-polar amino acids that are able to form numerous intermolecular linkages, and undergo different interactions, yielding a wide range of potential functional properties [1]. Egg white protein (albumen) is known to be a suitable raw material because of its desirable properties, such as high transparency, an improved mechanical behaviour and an easy processing by moulding, among others [2,3]. However, in order to cover more demanding and specialized applications, enhanced and innovative features are needed. A way to accomplish this is by adding certain types of nanoparticles to the polymer matrix, obtaining bio-based composite materials, also known as nano-biocomposites. One of the most promising additives for this purpose are nanoclays, such as montmorillonites, that can be used either in their natural state or organically modified. These clays belong to the family of phyllosilicates, and are characterized by a layered structure: discs or platelets, with extension varying from 1  $\mu\text{m}$  to 10  $\mu\text{m}$  and a thickness of about 1 nm, which stack together, by Van der Waals forces, to form the primary particles of the material. In turn, these particles unite in aggregates whose size varies from 0.1 to 10  $\mu\text{m}$  (Fig.1).

A negative charge inside the clay platelet is naturally counter-balanced by inorganic cations like  $\text{Na}^+$ ,  $\text{Li}^+$ ,  $\text{Ca}^{2+}$ ,  $\text{K}^+$  or  $\text{Mg}^{2+}$ , located into the inter-layer space. At this point, the clay is considered to be in its natural state. However, with the aim of obtaining more compatible formulations, a chemical modification of the clay is often carried out. This process is known as organo-modification. The most

common technique of modifying nanoclays is the cationic exchange, which consists in the substitution of inorganic cations for organic ones (e.g.  $\text{NH}_4^+$ ,  $\text{MT}_2\text{EtOH}$ ) [4].

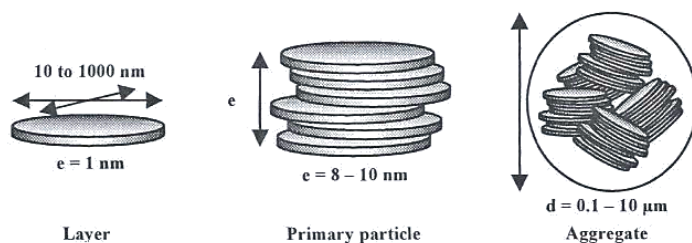


Figure 1. Phyllosilicate multi-scale structure [4]

The affinity between the nanoclay and the matrix, among other factors, will determine the behaviour of the nano-biocomposite. The improvements achieved so far are, in most investigations, enhanced mechanical and thermal properties. Nevertheless, barrier properties, membrane separation, UV protection, flammability resistance, polymer blend compatibilization, electrical properties and biomedical features have been also improved [5].

The morphology of the composite will also be influenced by the processing conditions, leading to different final properties. Up to now, three techniques have been mainly used to incorporate the nanoclays into the polymer matrix. These are the in-situ polymerization, the solvent intercalation and the melt intercalation process [4].

The aim of this work was to incorporate different types of nanoparticles into a protein-based matrix developed by a thermomechanical method, as well as to evaluate the effect of the nanoparticles on the thermo-mechanical properties and water absorption capacity of the bioplastics obtained.

### Experimental

The spray-dried egg white albumen used was provided by OVOSEC S.A. (Spain). Glycerol, from Guinama (Spain), and distilled water were used as protein plasticizers. With regard to the nanoparticles, two selected montmorillonites from Southern Clay Products, Inc. (USA) were used: a) Cloisite® Na<sup>+</sup> (MMT-Na) (natural sodium); and b) Cloisite® 30B (OMMT) (organo-modified).

Two different formulations, at 3 and 6 wt.% nanoclay, were prepared for each type. In these formulations, a plasticizer/protein ratio of 0.4 was always maintained, where the plasticizer consisted of a blend of glycerol (G) and distilled water (W) at

50 wt.%. A “control” formulation, with no nanoclay, was also studied. The final overall compositions are included in Table 1.

The thermomechanical processing includes two steps: a) mixing of the ingredients, for 10 min at room temperature, in the kneading tool (Rheomix 600p) of a torque-rheometer (Polylab, Thermo Haake GmbH, Germany) equipped with two counter-rotating rollers turning at 50 rpm [6]; b) Compression- moulding of the resulting dough-like material (100 bar, 120 °C, 10 min) into 50x10x3 mm<sup>3</sup> rectangular specimens [2].

DMTA tests were performed with a Seiko DMS 6100 (Seiko Instruments, Japan), in double cantilever bending mode. Temperature sweeps were performed at a constant frequency of 1 Hz within LVE region. A heating ramp of 2 °C/min was set between 30 and 170 °C.

For each formulation, water absorption was evaluated (after 2 and 48 h) by gravimetry, in samples immersed in 50 mL distilled water, at room temperature. Water absorption ( $Ab$ ) was calculated as:

$$Ab = \frac{W_1 - W_0 + W_{sol}}{W_0} \times 100 \quad (1)$$

where  $W_1$ ,  $W_0$  and  $W_{sol}$  are the weights of the wet specimen, dried specimen and water-soluble residue, respectively. All tests were done in triplicate.

Table 1. Final compositions of the samples studied

Sample	Composition (wt.%)			
	W	G	EW	Clay
0 wt.% Clay	20	20	60	0.0
3 wt.% Clay	19.4	19.4	58.2	3.0
6 wt.% Clay	18.8	18.8	56.4	6.0

## Results and Discussion

### *Thermo-mechanical behaviour*

The five protein-based composite materials were subjected to dynamic temperature sweeps in bending mode, at temperatures between 30 and 170 °C (Figure 2).

Figure 2 shows the evolution with temperature of the elastic modulus, which continuously decays as temperature increases. If compared to the neat matrix, the addition of 3 wt.% OMMT does not seem to have any effect on the thermo-mechanical behaviour of the bioplastic. On the contrary, the 3 wt.% EW/MMT-Na composite shows higher values of elastic modulus than the neat matrix.

However, similar  $E'$  values are observed if concentration is increased up to 6 wt.%.

In addition, all the  $\tan\delta$  curves exhibit a first peak, at about 55°C, corresponding to the gel-glasslike transition temperature ( $T_g$ ) of the egg white protein [3]. Likewise, all the curves present a second peak, located at about 150 °C, most probably related to an internal rearrangement of the material.

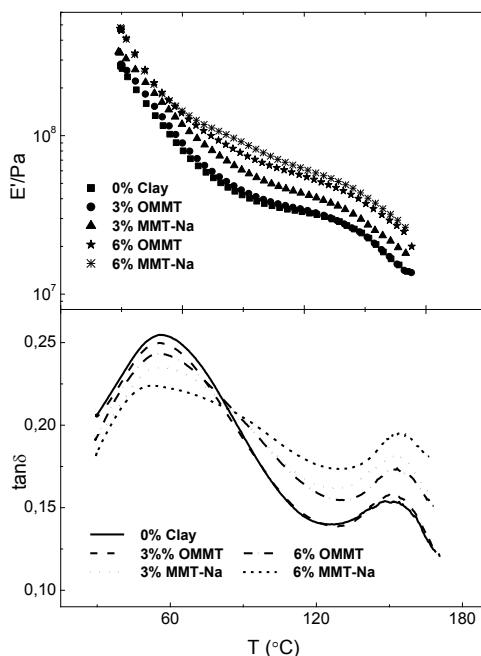


Figure 2. DMTA tests performed on the composite bioplastics obtained by moulding at 100 bar and 120 °C

No differences between the  $T_g$  values were found (Table 2). However, a less pronounced  $T_g$  peak is observed for the two bioplastics containing MMT-Na, which denotes that polymer chains mobility upon heating is more constrained by this type of nanoclay. Furthermore, EW/MMT-Na composites show a higher degree of elasticity in this temperature region. On the contrary, above 80 °C, these samples present higher values of  $\tan\delta$ , if compared to their OMMT counterparts, probably due to the weakening of the coulombic interactions associated with the presence of cations  $\text{Na}^+$ , while EW/OMMT samples seem to be reinforced by heating.

These results suggest a higher degree of compatibility between the natural clay (MMT-Na) and the bioplastic at the lowest temperatures tested, if compared to the more hydrophobic organo-clay (OMMT), for which large clay aggregates are observed. Hence, OMMT seems to act like a filler, and its effect is only significant

for the highest concentration studied (6 wt.%). On the contrary, MMT-Na most probably intercalates into the matrix, so that its modifying effect is notable even at the lowest concentration studied (3 wt.%).

#### *Water absorption capacity*

Table 2 presents the percentages of water absorbed, after 2 and 48 h, by the samples studied.

The addition of MMT-Na and OMMT to the egg white matrix is seen to reduce the water absorption, at the two immersion times studied. Thus, the presence of the organically modified clay (OMMT) has a larger effect after 48h. On the contrary, the degree of reduction in the water absorption of the samples containing MMT-Na was more significant after 2h.

*Table 2. Effect of the different nanoparticles on water absorption and  $T_g$  values of nano-biocomposites*

Composition	2h	48h	$T_g$ (°C)
	Ab (wt.%)	Ab (wt.%)	
0% Clay	41.76±2.69	51.89±0.66	56.45
3% OMMT	41.68±3.02	48.17±0.87	55.66
6% OMMT	40.39±2.58	45.02±1.68	56.73
3% MMT-Na	37.97±0.08	50.37±0.35	55.28
6% MMT-Na	38.39±0.24	53.54±2.26	53.05

#### **Concluding Remarks**

Bioplastics based on egg white protein exhibited enhanced mechanical properties and reduced water absorption (after 2h of immersion) after addition of a natural nanoclay (MMT-Na), at different concentrations.

The hydrophobic effect of the organically modified MMT on the water absorption was more significant after 48h of immersion. However, the mechanical properties of the resulting egg white-based materials were only improved at a concentration of 6 wt.%, what is most probably related to the poor affinity between the nanoclay and the matrix.

In no case, the glass transition temperatures were significantly altered.

## Acknowledgements

This work is part of a research project sponsored by “Ministerio de Economía y Competitividad” (Ref. MAT2011-29275-C02-01). The authors gratefully acknowledge its financial support.

## References

1. Song, Y.Zheng, Q. (2008). *Bioresour. Technol.* 99, 7665-7671.
2. Jerez, A., Partal, P., Martinez, I., Gallegos, C.Guerrero, A. (2007). *J. Food Eng.* 82, 608-617.
3. Gonzalez-Gutierrez, J., Partal, P., Garcia-Morales, M.Gallegos, C. (2011). *Carbohydr. Polym.* 84, 308-315.
4. Pollet, E., Avérous, L. (2010). *Advances in Polymer Nanocomposite Technology* (Vikas Mittal), pp. 315-354, Nova Science Publishers, Inc,
5. Paul, D.R., Robeson, L.M. (2008). *Polymer.* 49, 3187-3204.
6. Dealy, J.M. (1982). *Rheometers for Molten Plastics* pp. 255, Van Nostrand Reinhold, New York.

## Contact Address:

*Díaz I. (Isabel.díaz@alu.uhu.es)*

*Dpto. Ingeniería Química, Centro de Investigación en Tecnología de Productos y Procesos Químicos (Pro2TecS.) Universidad de Huelva. Avda. Tres de Marzo s/n, 21071 Huelva, Spain  
Telf.:+34 959219987; Fax:+34 959219983*

## CHAPTER 12

# Rheological characterization of chitosan solutions and chitosan/beeswax emulsions to be used in edible films

*Bernardo Ribeiro<sup>1</sup>, Sara Silva<sup>1</sup>, Adriana Godinho<sup>1</sup>, Isabel Sousa<sup>1</sup>,*

*Margarida Moldão-Martins<sup>1</sup>, Vítor D. Alves<sup>1\*</sup>*

*<sup>1</sup>CEER – Biosystems Engineering, Institute of Agronomy, Technical University of Lisbon, Portugal*

### Introduction

Chitosan is a natural biopolymer with excellent film-forming ability which has been object of considerable interest as edible film material, applied in the preservation of fruits and vegetables. However, one of the most important drawbacks of hydrophilic biopolymer-based films, namely those from chitosan, is their high sensitivity to water [1]. In food applications, the level of such sensitivity to water may limit the films applicability. In the last years several strategies have been proposed to enhance the resistance to water of chitosan matrices, namely the addition of lipids [2] (waxes or fatty acids) and reticulating agents (e.g. tripolyphosphate, citric acid [3]). Based on the literature and author's previous studies, citric acid is an excellent reticulating agent; once it reacts with chitosan amine groups to form an acyclic amide structure [3] enabling the development of chitosan films with improved the resistance to water. Still, the studies were focused mainly on the study of the effect of lipids and reticulating reactions separately. In this work, the effect of simultaneous addition of beeswax (as hydrophobic phase) and citric acid (as reticulating agent) to chitosan based formulations is studied. The rheological characterization of the new edible coating formulations is extremely important to understand its physical behavior, and to know how it will flow when applied on food products surfaces (to produce edible coatings), or on flat supports (to form stand-alone films).

### Experimental

#### *Preparation of chitosan edible coating formulations*

Chitosan purchased from Golden-Shell Biochemical Co.,Ltd., China (>85% deacetylation degree) was dissolved in an acetic acid (1%wt) solution, at a concentration of 2%wt. After stirring overnight at ambient temperature, glycerol (50%wt, mass of glycerol per mass of dried polymer) and tween 80 (0.15%wt) were added. For the preparation of chitosan/beeswax emulsions, solid beeswax was added (1%, 5% and 10%wt, mass of wax per mass of dried polymer) to the previous solution, under stirring at controlled temperature ( $T=70^{\circ}\text{C}$ ). The dispersion of the melted beeswax was promoted by vigorous magnetic stirring (1000 rpm) for 30 min. If necessary, air bubbles were removed in vacuum at room temperature. Chitosan/citric acid solutions and chitosan/citric acid/beeswax emulsions were also prepared (50%wt, mass of citric acid per mass of dried polymer).

#### *Rheological analysis of chitosan based formulations*

The rheology of all chitosan and chitosan/beeswax formulations was studied using a controlled stress rheometer (Haake RS-75, Germany), equipped with a cone and plate geometry (diameter 3.5 cm, angle  $2^{\circ}$ ). During the experiments, the shearing geometry was covered with paraffin oil in order to prevent water loss. A temperature sweep, in cooling conditions, at  $1^{\circ}\text{C}/\text{min}$  rate between  $70^{\circ}\text{C}$  to  $26^{\circ}\text{C}$  (to include the melted and solid phases of beeswax in the chitosan matrices), was performed at 1Hz frequency and 1Pa of shear stress, being measured  $G'$  and  $G''$  moduli. Flow curves were determined using a steady state flow ramp in the shear range of  $0.01\text{--}700\text{ s}^{-1}$ , at  $30^{\circ}\text{C}$ . The shear rate was measured point by point with consecutive 60s steps at constant shear rate. The viscosity was recorded for each point to obtain the flow curves. Frequency sweeps were carried out at a controlled stress of 1 Pa (shown by stress sweeps to give values within the linear viscoelastic region).

### Results and Discussion

A temperature sweep, in cooling conditions, at  $1^{\circ}\text{C}/\text{min}$  rate between  $70^{\circ}\text{C}$  to  $26^{\circ}\text{C}$  was performed for the formulations with beeswax, to evaluate the temperature at which the phase transition of the wax phase and its influence on the emulsions viscoelastic properties (Figure 1). It may be observed an increase of viscous modulus as the temperature decreased, being an step rise observed at around  $60^{\circ}\text{C}$  for all emulsions. By the contrary, no significant alteration of the storage modulus is detected.

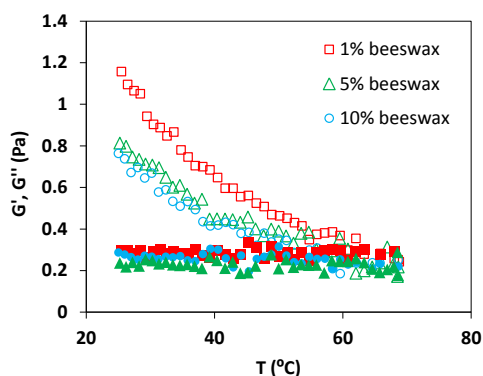


Figure 1. Temperature sweep of chitosan-beeswax emulsions:  $G'$  – full symbols,  $G''$  – empty symbols

All formulations tested (chitosan and chitosan-beeswax, with and without citric acid addition) presented a quasi-Newtonian shear-thinning behavior and an apparent viscosity suitable to be spread with a controlled thickness on a flat support. In addition, the respective mechanical spectra indicated a behavior typical of viscous materials composed of entangled macromolecules.

The rheological characterization of this study showed that citric acid and beeswax addition to chitosan solutions enables the production of formulations with high potential for the development of edible coatings and stand-alone films. It is expected these barriers to present an improved resistance to water, a quite important aspect when the main goal is to achieve a longer shelf-life in products with high water content.

### Acknowledgements

The authors would like to acknowledge FCT-MCTES, Portugal, for funding the project PTDC/AGR-ALI/114706/2009 – “New edible bioactive coatings for the improvement of food products quality”. Bernardo Ribeiro also acknowledges his research grant within the same project.

## References

1. Sebti, I., Chollet, E., Degraeve, P., Noel, C., and Peyrol, E. (2007). Water Sensitivity, Antimicrobial, and Physicochemical Analyses of Edible Films Based on HPMC and/or Chitosan. *J. Agric. Food Chem.* 55, 693–699.
2. Vargas, M., Albors, A., Chiralt, A., González-Martínez, C. (2009). Characterization of chitosan-oleic acid composite films. *Food Hydrocolloids.* 23 536 – 547.
3. Zheng Cui, Evan S. Beach & Paul T. Anastas (2011): Modification of chitosan films with environmentally benign reagents for increased water resistance, *Green Chemistry Letters and Reviews*, 4:1, 35-40

## Contact Address:

Vitor D. Alves ([vitoralves@isa.utl.pt](mailto:vitoralves@isa.utl.pt))  
CEER, Biosystems Engineering,  
Institute of Agronomy,  
Technical University of Lisbon  
Address: Tapada da Ajuda, 1349-017, Portugal  
Telf.: +351 21 3653546; Fax: +351 21 365 3195

## Chapter 13

# Rheological and thermogravimetric response of an acylated chitosan gel-like dispersion in castor oil and traditional lithium and calcium lubricating greases: a comparative study

*R. Sánchez, C. Valencia, J.M. Franco*

*Departamento de Ingeniería Química, Química Física y Química Orgánica. Campus de "El Carmen".  
Universidad de Huelva. 21071 Huelva. Spain.*

### Introduction

Nowadays, lubricating industry is focused on developing more environmentally friendly formulations since lubricant customers are aware of the negative effects that traditional lubricants exert on the environment. The use of vegetable oils in the lubricant formulations reduces environmental pollution because these are highly biodegradable [1]. Oil substitution has been satisfactorily addressed [2], however, fully biodegradable lubricating greases must also involve the replacement of the thickener agents obtained from renewable resources [3]. This substitution is a much more complex task to be solved due to the high technical efficiency of traditional metallic soaps. The main objective of this work was to develop and characterize a new formulation based on an acylated chitosan as thickener, with improved properties at high temperatures and suitable mechanical response. Thermo-gravimetric, rheological and tribological properties of this novel green formulation have been compared with those exhibited by two conventional greases thickened with lithium and calcium soaps, respectively.

### Experimental

#### *Materials*

Castor oil (Guinama, Spain) was used as base oil to prepare the acylated chitosan-based formulation. The average molecular weight and degree of deacetylation (DD) of the original chitosan (Qingdao Fraken, China) were  $2.29 \times 10^5$  g/mol and 86.3%, respectively. All other common reagents and solvents employed were purchased from Sigma-Aldrich.

## Perspectives in Fundamental and Applied Rheology

A commercial model lithium lubricating grease (Castrol Optipit, Germany) and one based on vegetable oil and calcium thickener (kindly supplied by Verkol, Spain) were used as benchmarks.

### *Methods*

#### Acylation of chitosan

The acylation reaction of chitosan was performed following the method described by Le Tien and coworkers [4]. A mixture of chitosan (12 g) and acetic acid (600 mL, 0.12 M) was stirred for 24 h. Then, the pH was adjusted to 7.2 by addition of 1 M NaOH. After that, decanoyl chloride (72 g) was added and the reaction volume was diluted to 1 L with distilled water. After 6 h, the reaction volume was neutralized and precipitated with acetone. The precipitate, collected by filtration, was washed with methanol and decanted. The washing process was repeated three times to eliminate free fatty acids. Finally, the acylated chitosan was placed in a desiccator during 12 h. Different batches of acylated chitosan were obtained following this procedure and blended to be used as oil gelling agent.

#### Manufacture of the biodegradable grease

The manufacture process was performed in an open vessel, using a controlled-rotational speed mixer (60 rpm), equipped with a helical ribbon impeller. Thickener concentration was previously optimized (35 % w/w) to provide physically stable formulation without observing significant oil bleeding. Initially, castor oil (130 g) was heating up to 90 °C and then the acylated chitosan (70 g) was slowly added under continuous agitation. The mixing process was maintained during 1 h and, finally, the system was cooled down to room temperature by external natural convection, maintaining the internal stirring, in the same heating device.

#### Thermogravimetric analysis (TGA)

Measurements of mass losses versus temperature were performed using a Thermogravimetric Analyzer, model Q-50 (TA Instrument Waters, USA), under N<sub>2</sub> purge. Typically, 5–10 mg of sample were placed on a Pt pan, and heated from 30 °C to 600 °C, at 10 °C/min.

#### Rheological characterization

Rheological characterization was carried out with a controlled-stress rheometer, Physica MCR-501 (Anton Paar, Austria). Small-amplitude oscillatory shear (SAOS) tests were performed inside the linear viscoelastic region in a frequency range of 10<sup>-2</sup>-10<sup>2</sup> rad/s, at different temperatures. Viscous flow tests were performed by applying a stepped shear-rate ramp in a shear rate range of 10<sup>-2</sup>-10<sup>2</sup> s<sup>-1</sup>. Rheological measurements were carried out using grooved plate-plate geometry (25 mm diameter, 1 mm gap).

### Tribological tests

Tribological tests were performed in a tribology measuring cell coupled with the rheometer dealing with a rotating ball on three 45° inclined plates geometrical combination, using a steel (1.4401 grade 100) measuring ball of 1/2" and steel (1.4301) plates. The stationary friction coefficient was obtained by applying a normal force of 10 N and setting a constant rotational speed (60 and 120 rpm) during 10 minutes at 25 °C.

### Results and Discussion

Characteristic onset temperatures for the beginning of significant mass losses, obtained from TGA tests, are listed in Table 1. As can be observed, the biodegradable formulation thickened with the acylated chitosan showed higher thermal resistance than lithium and calcium lubricating greases.

*Table 1. TGA characteristic onset temperature, activation energy values from equation (1) and consistency index from equation (2)*

Sample	$T_{\text{onset}}(^{\circ}\text{C})$	$E_a$ (J/mol)	$m$ ( $\text{Pa}\cdot\text{s}^{n-1}$ )
Li	286	5194/24412	684
Ca	325	7039/60469	726
Bio	345	7149	787

Figure 1 shows the mechanical spectra, obtained from SAOS measurements, at 25 °C, inside the linear viscoelastic range, for the different formulations studied. As can be observed, the so called "plateau" region of the mechanical spectrum is always noticed. The values of the linear viscoelastic functions and their evolution with frequency for the lithium-based commercial grease and the acylated chitosan-based oleogel are almost identical. On the other hand, the values of the storage and loss moduli are higher for the calcium-based grease, although the viscous modulus reaches similar values at high frequencies.

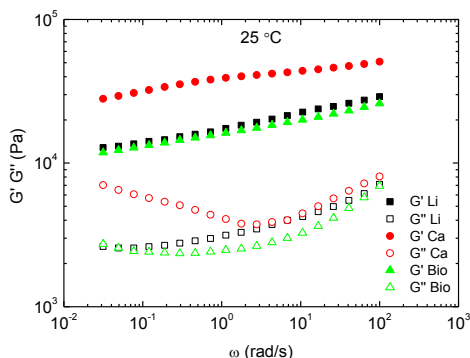


Figure 1. Evolution of SAOS functions with frequency for all formulations, at 25 °C

The influence of temperature on the SAOS functions was also analysed for all formulations by studying the evolution of the “plateau” modulus with temperature, which can be described by means of an Arrhenius-type equation:

$$G_N^0 = A \cdot e^{\frac{E_a}{R} \cdot \left(\frac{1}{T}\right)} \quad (1)$$

where  $E_a$  is a fitting parameter that gives information about the formulation thermal dependence, with a physical meaning similar to an activation energy (J/mol),  $R$  is the gas constant (8.314 J/mol·K),  $T$  is the absolute temperature (K), and  $A$  is the pre-exponential factor (Pa). As can be seen in Figure 2, Equation 1 can be used to fit fairly well ( $r^2 > 0.995$ ) the experimental “plateau” modulus values in different temperature ranges. In the case of non-biodegradable greases, two different sets of fitting parameters need to be used in order to cover all the temperature range in which these formulations show a linear viscoelastic region, until 175 °C for the lithium-based grease and 125 °C for the calcium-based grease, being this type of behaviour previously reported [5]. On the other hand, the evolution of the plateau modulus in the biodegradable grease has been satisfactorily fitted using only one set of Arrhenius parameters for the entire temperature range (0 to 125 °C).

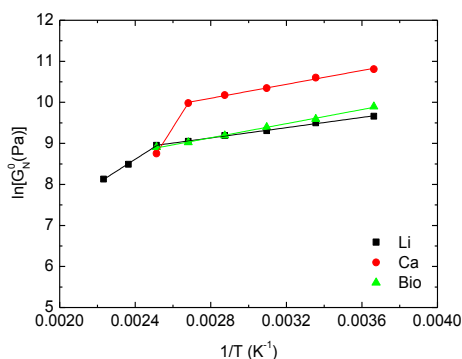


Figure 2. Evolution of the plateau modulus (symbols) with temperature, and Arrhenius' fitting (solid lines), for all samples

Table 1 includes the values of the activation energy deduced from Equation (1). In the case of commercial greases, the calcium-based system displays a higher value than the lithium-based one. On the other hand, acylated chitosan-based grease shows a very similar value of the activation energy than the calcium-based one in the low temperature range but much lower than that found in the high temperature range for commercial greases.

Figure 3 shows typical steady-state flow curves for the three formulations studied. A very similar viscosity values and flow behaviour may be observed in all cases, although higher shear rate dependence was obtained for the acylated chitosan-based oleogel. The Sisko model fits fairly well ( $r^2 > 0.995$ ) the shear thinning behaviour observed in the non-biodegradable greases:

$$\eta = m \cdot \dot{\gamma}^{n-1} + \eta_{\infty} \quad (2)$$

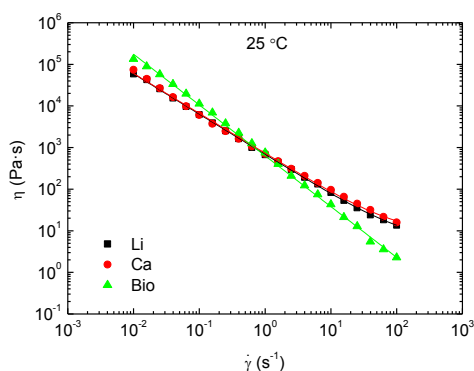


Figure 3. Flow curves (symbols) and Sisko or power law models fitting (solid lines) at 25°C

As can be observed in Table 1, the consistency index for the acylated chitosan-based oleogel is slightly higher than those obtained for the commercial greases studied but inside the typical range found in other types of greases [6].

Table 2 lists the friction coefficient values, obtained at 60 and 120 rpm and 25 °C, for the three formulations studied. The friction coefficient value measured at 60 rpm when using the acylated chitosan-based formulation in the lubricated contact is slightly higher than those obtained with the commercial greases. However, an intermediate value was found at 120 rpm. In the case of the lithium grease, when the rotational speed is increased, the friction coefficient is almost not affected, just detecting a slight increase. On the other hand, calcium- and acylated chitosan-based formulations exhibited reduced friction coefficient values when rotational speed was increased from 60 to 120 rpm.

Table 2. Friction coefficient at 60 and 120 rpm for all samples

Sample	Rotational speed (rpm)	Friction coefficient
Li	60	0.093
	120	0.096
Ca	60	0.099
	120	0.082
Bio	60	0.108
	120	0.086

## Acknowledgements

This work is part of a research project (CTQ2010–15338) sponsored by a MEC-FEDER Programme. The authors gratefully acknowledge the financial support.

## References

1. Beran, E. (2008). *Tribol. Int.* 41, 1212–1218.
2. Dresel, W. H. (1994). *Ind. Crops Prod.* 2, 281–288.
3. Sánchez, R., Stringari, G.B., Franco, J.M., Valencia, C. and Gallegos, C. (2011). *Carbohydr. Polym.* 85, 705-714.
4. Le Tien, C., Lacroix, M., Ispas-Szabo, P. and Mateescu, M.A. (2003). *J. Controlled Release* 93, 1-13.
5. Delgado, M. A., Valencia, C., Sánchez, M. C., Franco, J. M. and Gallegos, C. (2006). *Tribol. Lett.* 23, 47-54.
6. Delgado, M.A., Franco, J.M. and Kuhn, E. (2008). *Ind. Lubr. Tribol.* 60, 37-45.

## Contact Address:

R. Sánchez ([ruben.sanchez@diq.uhu.es](mailto:ruben.sanchez@diq.uhu.es))

Departamento de Ingeniería Química. Facultad de Ciencias Experimentales. Campus de "El Carmen". Universidad de Huelva. 21071. Huelva. Spain.

Tel.: +34 959219985; Fax: +34 959219983

## **PART II**

# **Food, Cosmetics and Pharmaceutical Products**



## CHAPTER 1

# Rheological study on wheat bread dough with Brewer's Spent Grain

C. Camacho<sup>1</sup>, S. Pinho<sup>2</sup>, S. Beirão-da-Costa<sup>1</sup>, I. Sousa<sup>1</sup>

<sup>1</sup>CEER - Biosystems Engineering Research Centre, Institute of Agronomy/Technical University of Lisbon, Tapada da Ajuda, 1349-017 Lisboa, Portugal

<sup>2</sup>Institute of Agronomy/Technical University of Lisbon, Tapada da Ajuda, 1349-017 Lisboa, Portugal

### Introduction

Brewer's spent grain (BSG) is a by-product from brewing industry, produced at 120 g per litre of full beer, and nowadays it goes straight to animal feed formulations. This is a material with high content of protein (23.1 %), fat (18.3 %) and crude fibre (13.1 %) and has a great potential to be valorised, since it has received little attention as a marketable commodity. Some studies have been conducted to evaluate the BSG incorporation in breads [1]. The Portuguese trend of bread consumption favours the use of this by-product as a raw material to add to doughs to produce high fibre functional bread.

The objective of the present study is to evaluate the characteristics of wheat dough enriched with BSG and the effect of the addition of sodium stearoyl lactilate (SSL), as emulsifier, on rheological parameters of the doughs.

### Experimental

#### *Materials*

Commercial wheat flour 65 type was kindly provided by Cerealis and BSG from Sociedade Central de Cervejas e Bebidas S.A. The BSG material with  $71.3 \pm 0.42$  % moisture was dried at 60 °C, during 48 hours, and then milled, obtaining a BSG flour (BSGf) with particle diameter up to 0.5 mm. SSL was gently provided by Unifine Iberia.

#### *Methods*

The rheological behaviour of wheat dough with BSGf addition was studied using a Central Composite Rotatable Design (CCRD) with two independent variables (% BSGf; % SSL) at 5 levels with three replications of the central point. Incorporation

## Perspectives in Fundamental and Applied Rheology

level varied between 0-0.5 % (w/w flour basis) for SSL and between 0-20 % for BSGf. The doughs were characterised for farinographic and extensographic parameters, as well as analysed by dynamic rheological tests at small amplitude shear stress (SAOS).

Farinographic characteristics: water absorption (%), gluten development and dough stability time (min) of the mixtures, were accessed in a Brabender farinograph. Then, doughs were prepared according to 54-10.01 AACC method [2] and analysed in a Brabender extensograph for the parameters: resistance, extensibility, energy consumption and resistance/extensibility (R/E) proportional number, calculated after 45, 90 and 135 minutes of proofing time (30 °C and 80 % moisture).

Dynamic rheological tests were conducted on a CS 75 controlled-stress rheometer (Haake, Germany) using serrated plates (35 mm diameter and 1.0 mm gap) to avoid slip.

Linear viscoelastic region was determined by stress sweep tests with tensions between 0.1 and 10,000 Pa for 0.1 and 1 Hz frequencies. These tests were conducted on doughs without BSGf and doughs with 20 % BSGf. Then, a frequency sweep at constant stress 10 Pa was conducted.

### *Statistical analysis*

Experimental data were analyzed using Statistic 7.0 software (StatSoft Inc.). Response Surface Method (RSM) was used to evaluate the effect of independent variables and their interactions.

## **Results and Discussion**

### *Mixtures Farinograph characterization*

Table 1 shows the farinograph data of the mixtures with BSGf incorporation.

Table 1. Mixtures farinograph parameters

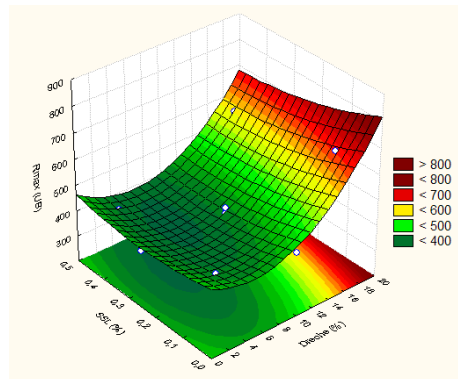
Parameters	BSGf levels (%)				
	0	2.9	10	17.1	20
Water (%)	59	59.5	62.5	64	65
Mixture time (min)	3	3	4	4	4
Stability time (min)	9.5	9	6.5	8	8

As BSGf incorporation increased, the water absorbed by the mixture also increased, since BSGf fibre has the ability to retain a considerable amount of water. Formulation with the maximum BSGf incorporation retained about 6 % more water than plain flour. With increasing BSGf addition, the mixture time slightly increased and stability time slightly decreased. This must be due to the presence of the BSGf protein and fibre that compete with gluten protein for the available water, taking some time to develop the protein network, reinforced by the protein and fibre from BSGf.

### *Extensograph tests*

The extensograph results showed that BSGf addition affects the dough resistance and extensibility, at all analyzed times. Figure 1 shows the dough resistance (BU) after 45 minutes proofing time and figure 2 the extensibility (cm) after the same time.

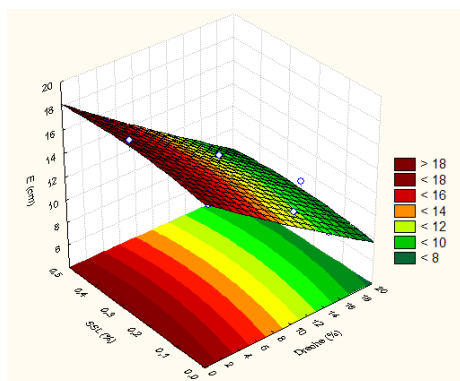
As the BSGf incorporation level increases, the resistance of dough to rupture also increases (figure 1) while their extensibility decreased (figure 2). After 90 and 135 minutes proofing times these general profiles were maintained.



$$\text{Resistance 45 minutes} = 465,33 - 16,25 * \text{BSGf} + 1,69 * \text{BSGf}^2 - 254,97 * \text{SSL} + 502,31 * \text{SSL}^2 - 13,15 * \text{BSGf} * \text{SSL}$$

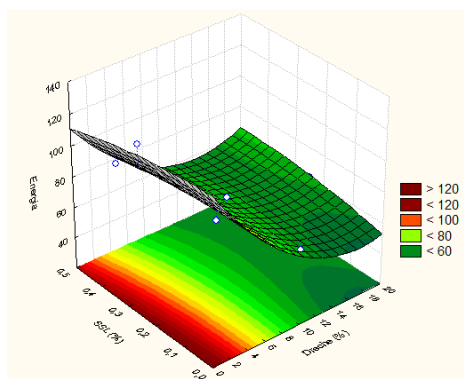
$$R^2 = 0,94; \text{ adjusted } R^2 = 0,88$$

*Figure 1. Response surface – dough resistance after 45 minutes proofing time*



$$\begin{aligned} \text{Extensibility 45 minutes} &= 17,70 - 0,547 * \text{BSGf} + 0,002 * \text{BSGf}^2 + 4,65 * \text{SSL} - 7,49 * \\ &\quad \text{SSL}^2 - 0,0003 * \text{BSGf} * \text{SSL} \\ R^2 &= 0,94; \text{adjusted } R^2 = 0,88 \end{aligned}$$

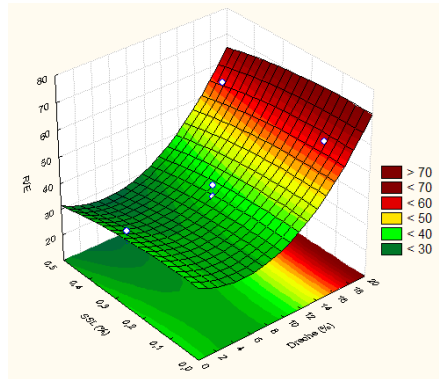
Figure 2. Response surface – dough extensibility (E) at 45 minutes proofing time



$$\begin{aligned} \text{Energy 135 minutes} &= 127,68 - 8,88 * \text{BSGf} + 0,26 * \text{BSGf}^2 - 9,81 * \text{SSL} - 48,46 * \text{SSL}^2 + \\ &\quad 2,96 * \text{BSGf} * \text{SSL} \\ R^2 &= 0,96; \text{adjusted } R^2 = 0,92 \end{aligned}$$

Figure 3. Response surface – dough energy to rupture after 135 minutes proofing time

As we can observe in figure 3, the total energy value needed to dough stretching was smaller for high levels of BSGf, being the difference more pronounced for higher levels of BSGf incorporation, mainly due to extensibility reduction. This is clear on figure 4 where the ratio R/E is increasing with BSGf incorporation.



$$\begin{aligned} \text{Resistance/Extensibility ratio} &= 37,36 - 1,79 * \text{BSGf} + 0,17 * \text{BSGf}^2 + 4,11 * \text{SSL} - 32,13 * \\ &\quad \text{SSL}^2 - 0,01 * \text{BSGf} * \text{SSL} \\ R^2 &= 0,87; \text{ adjusted } R^2 = 0,75 \end{aligned}$$

Figure 4. Response surface – dough ratio resistance/extensibility after 135 minutes proofing time

The BSGf incorporation levels had a significant influence ( $p < 0.05$ ) on extensograph tests. For all cases, SSL incorporation levels had no significant effect.

#### Dynamic tests

Concerning the dynamic testing, after analysis of storage and loss moduli ( $G'$  and  $G''$ ), it was found that both increased with frequency, and the storage modulus ( $G'$ ) was higher than loss modulus ( $G''$ ). When BSGf was added at 20 % an increase of both moduli of the order of almost a decade, keeping the frequency dependence, was observed (Figure 5).

These results are in agreement with the increase in resistance to extension. Therefore the BSGf incorporation can be regarded as a reinforcement of the internal structure of the dough.

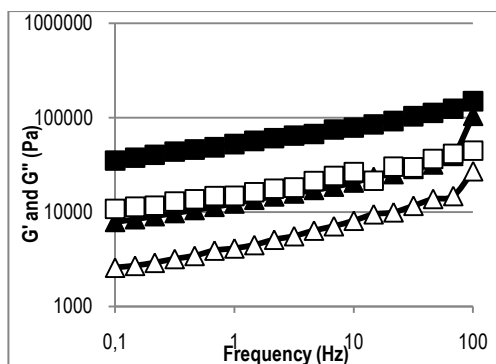


Figure 5. Frequency sweep. Symbols: triangles – 0 % BSGf/ 0.25 % SSL; squares – 20 % BSGf/0.25 % SSL. Solid symbols –  $G'$ ; Open symbols –  $G''$ .

### Concluding Remarks

The Brabender extensograph empiric tests showed that the addition of BSGf to wheat dough increased resistance and decreased extensibility. Furthermore, the dynamic tests showed a similar increase of both the elastic and the viscous components of the wheat dough. In conclusion, from the SAOS tests, a reinforcement of the dough structure is evident. This must be attributed to the BSGf protein and fibre contribution to the wheat gluten matrix.

### Acknowledgments

This work was supported by COMPETE program: QREN – Dreche project n. 23141\12 with Metalogonde, Lda. and Panicongelados, S.A.

### References

1. Stojceska V & Ainsworth P (2008) Food Chem., 110, 865-872
2. AACC International Method (1999) 54-10.01, Extensigraph Method, General, Physical Dough Tests

### Contact Address:

Isabel de Sousa ([isabelsousa@isa.utl.pt](mailto:isabelsousa@isa.utl.pt))  
CEER - Biosystems Engineering Research Centre  
Institute of Agronomy  
Technical University of Lisbon  
Tapada da Ajuda, 1349-017 Lisboa, Portugal  
Telf.: +351 213 653 246; Fax: +351 213 653 195

## CHAPTER 2

# Texture analysis on wheat bread with Brewer's Spent Grain

C. Camacho<sup>1</sup>, M.R. Coelho<sup>2</sup>, S. Beirão-da-Costa<sup>1</sup>, I. Sousa<sup>1</sup>

<sup>1</sup>CEER - Biosystems Engineering Research Centre, Institute of Agronomy, Technical University of Lisbon, Tapada da Ajuda, 1349-017 Lisboa, Portugal

<sup>2</sup>Institute of Agronomy, Technical University of Lisbon, Tapada da Ajuda, 1349-017 Lisboa, Portugal

### Introduction

The Brewer's spent grain (BSG) is a by-product from brewing industry of a quite low cost and high nutritive value and it has a strong potential to be used as an ingredient in bakery as a good source of protein (23 %), fat (18 %) and crude fibre (13 %), in the development of functional breads.

Previous studies have supported the use of BSG flour (BSGf) to enrich bread [1], and to produce extruded snacks [2].

The objective of this study was to evaluate the incorporation of BSG into wheat flour breads in order to obtain functional breads, meeting the expectations of the actual Portuguese consumer for functional and darker breads.

### Experimental

#### *Materials*

Commercial wheat flour 65 type was kindly provided by Cerealis. BSG came from Central de Cervejas e Bebidas S.A. The BSG material with  $71.3 \pm 0.42$  % moisture was dried at 60 °C during 48 hours. Due to its high granular aspect, it is not suitable for direct application, so BSG was milled obtaining a BSG flour (BSGf) with particle size smaller than 0.5 mm. The sodium stearyl lactilate (SSL) was gently provided by Unifine Iberia. The other materials, like salt and fresh compressed yeast, were purchased in local market.

#### *Methods*

To study the dependent variables, a Central Composite Rotatable Design (CCRD) was used with two independent variables (BSGf and SSL concentration) at 5

## Perspectives in Fundamental and Applied Rheology

levels with three replications of the central point. SSL incorporation level varied between 0-0.5% (w/w flour basis) and BSGf between 0-20 %.

Breads general appearance were visually analyzed. The dependent variables, analyzed by Response Surface Methodology, were: mass losses, specific volume, water activity, crumb colour, hardness of crust, hardness and elasticity of crumb. Texture indicators were evaluated at 24, 48 and 72 h after baking, using texture profile analysis (TPA) by a TA-XT2 Texturometer. TPA tests for crust and crumb were performed in compression (1 mm.s<sup>-1</sup> speed up to 11 mm strain) and, for crumb analysis, loaves were sliced by hand into slices of 2 cm thick and three pieces were obtained from each slice.

Colour parameters (L\*, a\* and b\*) were assessed by CIELAB, where L\* is the lightness and a\* and b\* are chromaticity responsible parameters. The colour tests were performed using a Chroma Meter CR-400 (Minolta Co., Japan).

### *Statistical analysis*

Experimental data were analyzed using Statistic 7.0 software (StatSoft Inc.). Response Surface Methodology (RSM) was used to evaluate the effect of independent variables and their interactions on analysis parameters.

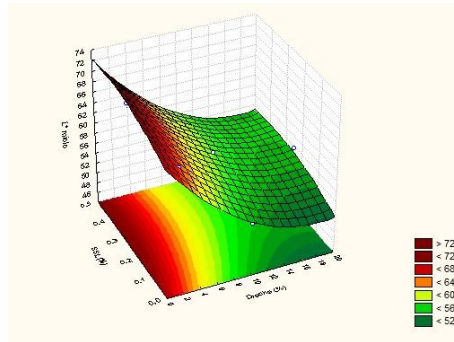
## **Results and Discussion**

### *Breads appearance*

High BSGf levels incorporation leads to a cracked bread crust appearance. This may be due to high fibre content that strengthens the matrix. It seems that crumb homogeneity is determined by SSL incorporation. It was observed that for high SSL levels, crumb alveolus size is higher and well distributed within the crumb representing also a texture improvement.

### *Crumb colour*

Figure 1 shows the effect of BSGf and SSL incorporation levels on bread luminosity. As can be seen, BSGf incorporation significantly affects ( $p < 0.05$ ) the crumb luminosity, a darker crumb is obtained as BSGf incorporation level increases (figure 1).



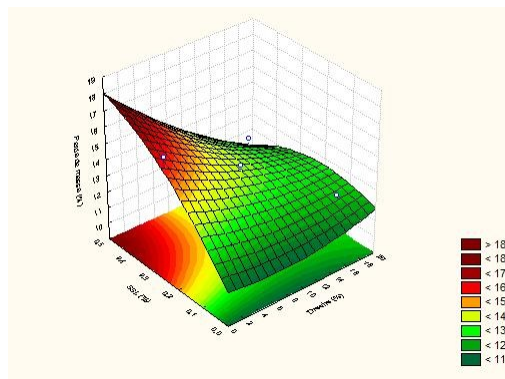
$$L^* = 68,56 - 1,97 * BSGf + 0,055 * BSGf^2 + 21,39 * SSL - 27,94 * SSL^2 + 0,03 * BSGf * SSL$$

$$R^2 = 0,99; \text{ adjusted } R^2 = 0,98$$

Figure 1. Response surface for crumb luminosity

### Mass losses after baking

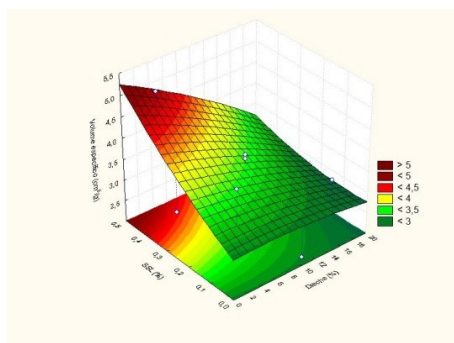
The baking process always leads to mass loss of the dough. Higher mass losses were observed for BSGf incorporations up to 8 % and high SSL incorporation levels. BSGf presences higher than 8 % counteract the effect, minor losses were assessed. This can be explained by the water absorption within the fibre and protein from BSGf.



$$\text{Mass loss (\%)} = 11,09 - 0,078 * BSGf + 0,01 * BSGf^2 + 22,86 * SSL - 17,88 * SSL^2 - 0,78 * BSGf * SSL$$

$$R^2 = 0,88; \text{ adjusted } R^2 = 0,77$$

Figure 2. Response surface for mass loss after baking



Specific volume (cm<sup>3</sup>/g)

$$= 2,95 + 0,01 * BSGf - 0,0009 * BSGf^2 + 3,34 * SSL + 2,51 * SSL^2 - 0,19 * BSGf * SSL$$

$$R^2 = 0,56; \text{ adjusted } R^2 = 0,12$$

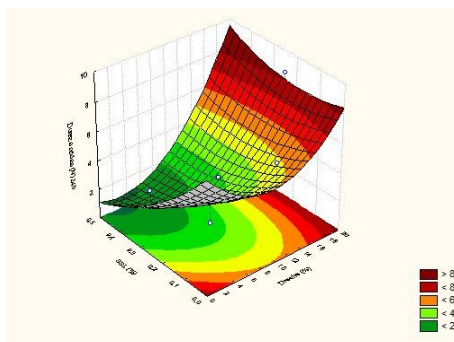
Figure 3. Response surface for bread volume

### Specific volume

The bread volume increased with SSL addition and decreased with BSGf incorporation, as we can observe in figure 3.

### Crust hardness

Above 8 % BSGf incorporation, bread crust hardness increased steeply with BSGf and slightly with SSL additions (Figure 4). 24 h after baking, hardness values lower than 2 N were obtained for 0.4 to 0.5 % SSL and BSG up to 8 %.

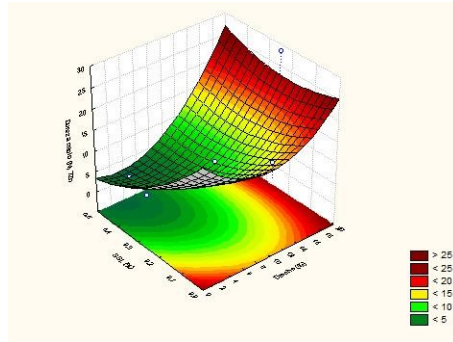


$$\text{Crust hardness (N) } 24h = 7,74 - 0,57 * BSGf + 0,03 * BSGf^2 - 20,55 * SSL + 14,43 * SSL^2 + 0,78 * BSGf * SSL$$

$$R^2 = 0,84; \text{ adjusted } R^2 = 0,68$$

Figure 4. Response surface for crust hardness after 24h baking

Crumb hardness



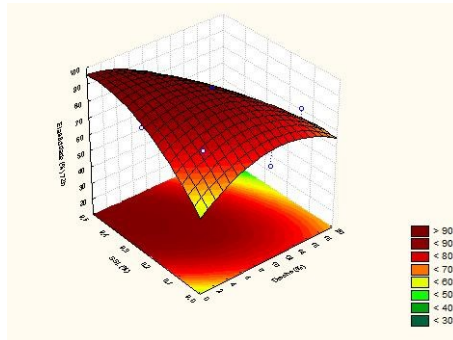
$$\text{Crumb hardness (N) } 72 \text{ h} = 23,57 - 1,68 * \text{BSGf} + 0,09 * \text{BSGf}^2 - 67,18 * \text{SSL} + 53,72 * \text{SSL}^2 + 2,19 * \text{BSGf} * \text{SSL}$$

$$R^2 = 0,81; \text{ Adjusted } R^2 = 0,62$$

Figure 5. Response surface for crumb hardness after 72h baking

Crumb elasticity

The major differences detected between formulations, in respect to crumb hardness, were observed during staling, being the best fitted results observed 72 h after baking (figure 5). The softer crumb formulations were observed with BSGf levels below 6 % and SSL up to 0.4 %. Concerning bread crumb elasticity, formulations without SSL and 20 % of BSG had the lower elasticity values (about 80, 60 and 65 % after 24, 48 and 72 h of baking). Bread with BSG until 5 % and 0.5 % SSL presented elasticity values around 95 % at 72 h after baking (figure 6).



$$\text{Crumb elasticity (\%)} 72 \text{ h} = 55,64 + 3,63 * \text{BSGf} - 0,16 * \text{BSGf}^2 + 177,59 * \text{SSL} - 195,27 * \text{SSL}^2 - 7,55 * \text{BSGf} * \text{SSL}$$

$$R^2 = 0,87; \text{ Adjusted } R^2 = 0,73$$

Figure 6. Response surface for crumb hardness after 72h baking

### **Concluding Remarks**

Altogether, the results indicate that BSGf could be added up to 10 % to a bread formulation and SSL had a positive effect compensating for the volume of the bread. It can be said that there was some sort of texture improvement and shelf-life potential increase of these novel functional (richer in protein and fibre) breads.

### **Acknowledgments**

This work was supported by COMPETE program: QREN – Dreche project n. 23141\12 with Metalogonde, Lda. and Panicongelados, S.A.

### **References**

1. Stojceska V & Ainsworth P (2008) Food Chem., 110, 865-872
2. Ainsworth et al. (2007) J Food Engineering, 81, 702-709

### *Contact Address:*

*Isabel de Sousa (isabelsousa@isa.utl.pt)  
CEER - Biosystems Engineering Research Centre,  
Institute of Agronomy, Technical University of Lisbon  
Tapada da Ajuda, 1349-017 Lisboa, Portugal  
Telf.: +351 213 653 246; Fax: +351 213 653 195*

## CHAPTER 3

### Rheological characterization of Chia flour gels for culinary purpose

S. Ramos<sup>1</sup>, P. Fradinho<sup>2</sup>, P.Mata<sup>1</sup>, A.Raymundo<sup>2</sup>

<sup>1</sup> REQUIMTE, Faculdade de Ciências e Tecnologia – UNL, 2829-516 Caparica (Portugal)

<sup>2</sup> NIEAB. Instituto Piaget. Quinta da Arreinelha de Cima, 2800-305 Almada (Portugal)

#### Introduction

Chia (*Salvia hispanica L.*) is an herbaceous plant from tropical regions. The consumption of chia seeds, with high contents of dietary fibres, antioxidants and polyunsaturated fatty acids can enhance cardiovascular and digestive health, contributing to the prevention of obesity problems [1;2].

Due to its ability to swell when absorbing water, which occurs due to the presence of carbohydrates (cellulose, hemicellulose, lignin, pectin, among others), the addition of dietary fibre to a food matrix can affect its texture, playing a role as texturing and stabilizing agent. Soluble fibre contributes to the stabilization of the food structure through gel formation or by thickening the continuous phase. Generally, insoluble fibre increases the firmness of food stuffs and provides a highest fat absorption capacity [3].

The functional and physicochemical properties of chia have already been studied and its potential to stabilize emulsions [4] and to produce edible films [5] was proved.

The present work intends to access the gelling properties of chia flour (from grind chia seeds) with the purpose to study its potential for the development of functional food stuffs and culinary applications of the gel matrixes.

#### Experimental

Chia seeds “Midzu” (from Peru, provided by Efeito Verde, Lda) were grinded and only the 0.5-1mm fraction was used for gel preparations. For texture measurements, chia flour gels with concentrations ranging from 1 to 15% (w/w) were prepared dispersing the flour in water, under mechanical stirring (Eurostar Digital, IKA-WERKE), 350 rpm for 30 min. The suspensions were poured into glass

containers (35mm height, 32mm diameter) and heated at two different gelation temperatures (50°C or 90°C), during 30 min, in a water bath.

Texture analysis of chia flour gels was performed in a TA.XT-plus texturometer (Stable Microsystems), at 20°C, in a temperature-controlled room. Texture Profile Analysis tests (TPA) was performed, using a 10 mm cylindrical probe in a penetration mode, which allowed to determine the firmness, cohesiveness and adhesiveness of gels. The texture measurements were carried out 24h after preparation to achieve the gel maturation.

Small amplitude oscillatory shear measurements (SAOS) were performed to characterize gelation process of chia flour. The rheological characterization of 10%, 13% and 15% chia flour gels was performed using a controlled stress rheometer (Haake, RS-300) coupled to an UTC-Peltier system, with a serrated parallel plate (PP 35S) with 1 mm gap. The chia flour suspensions, after hydration during 30 min were transferred to the bottom plate to promote de gelation *in situ*.

The suspensions were heated from 20 to 90°C (heating rate 2°C/min), maintained at this temperature for 30 min, and then cooled down to 5 °C, at three different cooling rates (0.5, 2 and 5°C/min). The gel maturation was performed at this temperature, during 120 min to ensure the full gel maturation. Then the mechanical spectra were obtained, within the viscoelastic linear range.

Each formulation was tested at least in triplicate. Experimental data were analysed by means of one-way ANOVA or Kruskal-Wallis test. When the former analysis indicated differences among means, a Scheffé test or pairwise comparison was performed to differentiate means with 95% confidence ( $p \leq 0.05$ ). All statistical treatments were done using SPSS Statistics (v.20, IBM SPSS Statistics, New York, USA).

### Results and Discussion

The critical concentration for gelation of chia flour was previously tested. The gel formation was verified for concentrations above 10%. Figure 1 presents the main texture parameters used to characterize chia gels – firmness, adhesiveness and cohesiveness.

The gel firmness and adhesiveness increases with chia content, for both temperatures studied. The temperature used for the gels preparation also modified the texture, giving a slight rise to firmness and adhesiveness values for 90°C, although with no statistical significance ( $p > 0.05$ ).

The presence of a high content of polysaccharides from chia seeds (hemicellulose, cellulose, lignin) influences the structure of the gel, leading to the formation of a more structured gel matrix, as described by Elleuch et al.[6].

Regarding gel cohesiveness, it was observed a decrease of this attribute with chia content. No dependence of this parameter with temperature of gel preparation was observed.

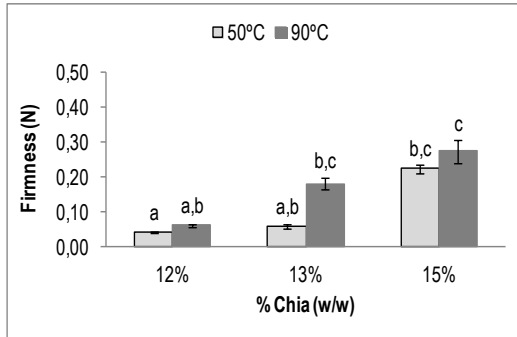


Figure 1a. Firmness of chia flour gels prepared at 50°C and 90°C. Different superscript letters indicate significantly different values at  $p \leq 0.05$  level.

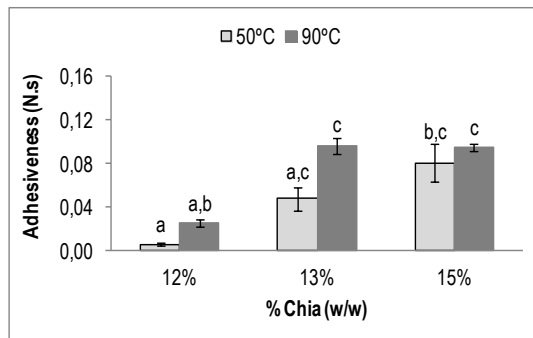


Figure 1b. Adhesiveness of chia flour gels prepared at 50°C and 90°C. Different superscript letters indicate significantly different values at  $p \leq 0.05$  level.

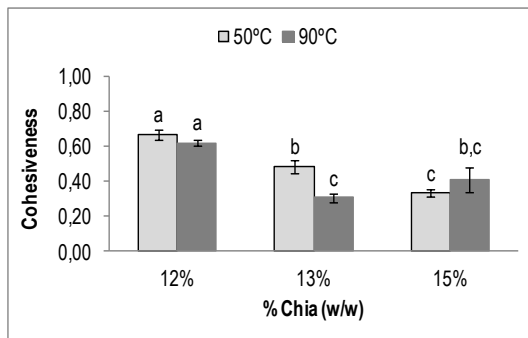


Figure 1c. Cohesiveness of chia flour gels (12%-15%) prepared at 50°C and 90°C. Different superscript letters indicate significantly different values at  $p \leq 0.05$  level.

Overall, from the TPA analysis, it was observed that gels with 13% (w/w) chia flour showed the most properly texture to the development of culinary applications, considering the commercial properties of gels as standard (comparison not shown). Nevertheless, the preparation of gels with lower content of chia take in advantage the global cost of the formulation, considering the high market price of chia seeds.

The mechanical spectrum of chia gels with 10, 13 and 15% (w/w) obtained after the heating/cooling cycle previously described is depicted in figure 2.

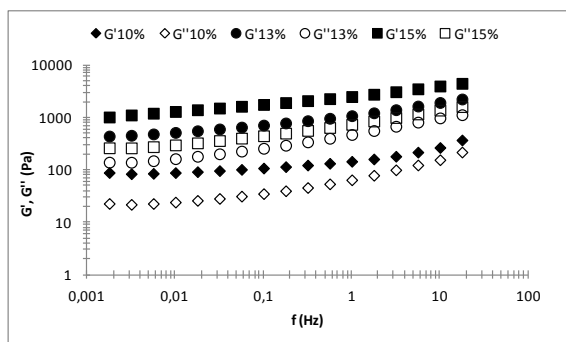


Figure 2. Mechanical spectra of chia flour gels with different concentrations (cooling rate of 2°C/min).

From the mechanical spectra, it is observed that all gels presented weak gel like structure, as  $G'$  is always higher than  $G''$  but both moduli showed a frequency dependence, as it was observed by Moreira et al. [7] for this type of gels. A similar pattern was observed for the three concentrations, with a clear increase in the linear viscoelastic functions with chia content. This reflects an increase in the level of gel structure and is in agreement with the texture results.

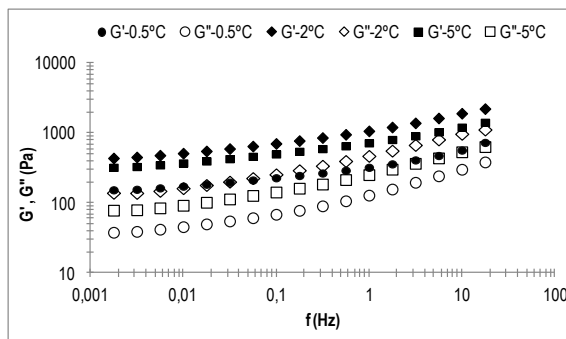


Figure 3. Frequency sweeps of chia flour gels (13%) at different cooling rates (-0.5°C/min, -2°C/min and -5°C/min).

The cooling rate affects the dynamic of formation the gel structure, as it was previously studied for several authors [8]. In order to optimize the cooling process of chia gels, three cooling rates were tested (Figure 3) for 13% (w/w) chia gels: 0.5°C/min, 2°C/min and 5°C/min. It is evident that the highest cooling rates (2 and 5 °C/min) promoted an increasing level of gel structure, expressed as higher values of the linear viscoelastic functions. In addition, a cooling rate of 2°C/min should be considered the optimum cooling rate to promote a structured gel system.

### Concluding remarks

From the texture and rheological measurements of chia flour gels, it is promising the application of this food ingredient in the preparation of several food stuffs, as an alternative to the usual thickening and gelling agents.

Chia is suitable for incorporation in different types of food matrixes, as sauces and soups, as well as desserts and drinks [9], resulting from its high fibre content (about 55%), mainly composed by insoluble dietary fibre, associated with high swelling power (20 g/g water at 25°C).

The chia flour concentration induces different degrees of gel structure that can be applied in the production of a large variety of food products (sweet, salty, etc), making chia a custom made food ingredient.

### References

1. Taga, M.S., Miller, E.E., Pratt, D.E. (1984). *JAACS*, 61 (5), 928-931.
2. Reyes-Caudillo, E., Tecante A., Valdivia-López M.A. (2008). *Food Chemistry*, 107, 656–663.
3. Oreopoulou, V., Tzia, C. (2007). In *Utilization of by-products and treatment of waste in the food industry* (Oreopoulou, V. and Russ, W., eds.), Vol.3, pp.209-232, Springer, USA.
4. Capitani, M.I., Spotorno, V., Nolasco, S.M., Tomás, M.C. (2012). *LWT - Food Science and Technology*, 45, 94-102.
5. Muñoz, L.A., Aguilera, J.M., Rodríguez-Turiénzo, L., Cobos, A., Diaz, O. (2012). *Journal of Food Engineering*, 111, 511–518.
6. Elleuch, M., Bedigian, D., Roiseux, O., Besbes, S., Blecker, C., Attia, H. (2011). *Food Chemistry*, 124, 411–421.
7. Moreira, R., Chenlo, F., Torres, M.D. (2013). *LWT -Food Science and Technology*, 50, 160-166.
8. Nunes, M.C., Raymundo, A., Sousa, I. (2006). *Food Hydrocolloids*, 20, 106-113.
9. Thebaudin, J.Y., Lefebvre, A.C., Harrington, M., Bourgeois, C.M. (1997). *Trends in Food Science & Technology*, 8, 41-48.

## Perspectives in Fundamental and Applied Rheology

### *Contact Address:*

*A.Raymundo (araymundo@almada.ipiaget.org)  
NIEAB, Instituto Piaget,  
Quinta da Arreínela de Cima,  
2800-305 Almada (Portugal)  
Telf.:+351 212946274;Fax:+351 212946251*

## CHAPTER 4

### Orientation effects during flow in clay/water suspensions

*Mercedes Fernández<sup>1</sup>, María Eugenia Muñoz<sup>1</sup>, Jose Ramón Leiza<sup>2</sup> and Antxon Santamaría<sup>1</sup>*

<sup>1</sup> *Department of Polymer Science and Technology and POLYMAT Institute, University of the Basque Country UPV/EHU (Spain)*

<sup>2</sup> *Department of Applied Chemistry and POLYMAT Institute, University of the Basque Country UPV/EHU (Spain)*

#### Introduction

The complex nonlinear behaviour of colloidal suspensions is linked to the suspension microstructure at rest, which depends on the particle interactions and its deformation under stress. In the case of natural clays, highly non spherical colloidal particles, the rheology differs from that of spheres at the same volume fractions. One of the most important property characterizing clay particles is their ability to form yield stress materials when dispersed in water, that make them valuable ingredients in the processing of many industrial materials, such as paper, ceramics, food, paints, cosmetics, etc. The adequacy to an application is often controlled by rheometric methods and many studies have focused on the rheology of aqueous clay suspensions, highly dependent on the nature of the clay, suspension preparation, concentration, pH, ionic strength and so forth. Typically clay suspensions show high viscosity even at low concentration due to the ability of rotation of the particles and effective space filling and also due to specific particle interactions related to the charged nature of the clay particles [1]. Once the stress starts to exceed the interparticle forces, the dispersions become highly shear thinning and a shear fluidification occurs. The rheological features have been interpreted by two different models: The so-called “house of cards” model that assumes attractive interactions between faces and edges of the platelets, and a model based on the formation of an oriented network stabilized by repulsive forces caused by interacting double layers. Interpretations for both attractive interactions and gel structure were provided in several studies [2].

## Perspectives in Fundamental and Applied Rheology

In this work, the viscoelastic behaviour of concentrated suspension of Bentonite and Kaolinite have been investigated in the linear and non linear regime as a function of solid content and in the presence of polyphosphate as dispersing agent. Attention has been paid to the large amplitude oscillatory shear behaviour with the aim of studying the microstructural organization that confers peculiar flow properties to these colloidal systems.

### Experimental

#### *Clay crystalline structure*

Bentonite is a 2:1 smectite clay composed mostly of montmorillonite. It consists of an alumina octahedral sheet being sandwiched by two tetrahedral silica sheets. Bentonite is a swelling clay that absorbs water and swells considerably forming a yield stress gel at very low solids concentration, below 5 wt.%. Kaolinite has a two layered, crystalline structure: Alumina octahedral and tetrahedral silica sheets bonded by hydrogen. The clay is non-swelling due to its tight bonds and resistance to substitution within the lattice structure (Figure 1).

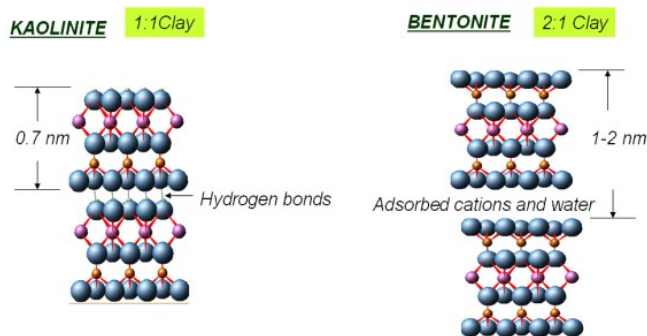


Figure 1. Kaolinite and bentonite crystalline structure

#### *Preparation of colloidal suspensions*

Bentonite (Sigma-Aldrich) and Kaolinite (Fluka) were used to prepare the clay water dispersion by mixing the powder with distilled water in continuous magnetic stirring for 2 hours at a speed of 100 rpm. The suspensions were aged 24 h prior to the measurement. 5-15 wt% Bentonite suspension and 40-60 wt% Kaolinite suspensions were prepared. A Sodium Polyphosphate (Panreac) was tested as dispersant within the concentration 0.1-1 wt%.

#### *Rheological measurements*

Rheological measurements were carried out at room temperature on a strain controlled rheometer (ARES, Rheometric Scientific) using parallel plate serrated fixture to prevent slip. Dynamic strain sweep test at angular frequency of 0.1, 1 and 10 Hz were performed. Sinusoidal strain at several shear strain amplitudes  $\gamma_0$ , in the range from 0.01 % to 1000% was applied and the responsive stress was recorded. 12 cycles were repeated for each  $\gamma_0$ . For the Fourier-transform, the stress was transferred from time domain to the frequency domain using the software developed by Whilhem [3]. The Lissajous curve analysis was processed with the software developed by Ewoldt et al. [4] [MITLaos program, *Software Supplied by MITLaos@mit.edu*].

### Results and Discussions

For the kaolinite and bentonite concentrated suspensions investigated in this work,  $G'$  (elastic modulus)  $>G''$  (viscous modulus) was obtained in the frequency range from 10 to 0.1 Hz indicating a gel-like behaviour due to the structure of colloidal aggregates. According to Lagaly [5] the microstructure of bentonite clay slurries is “card-house” or edge (+)/face (-) interaction at low pH and “overlapping coins” or face–face interaction forming band-like structures at high pH. The same model was also proposed for kaolin clay slurries.

The addition of dispersant modifies the rheological behaviour so that they can reduce or enhance the attractive forces among particles, thus promoting dispersion or aggregation, respectively. This was related to the mechanism of dispersion based on both electrostatic repulsion and steric stabilization [6]. A critical concentration of the polyphosphate was determined for optimum deflocculating effectiveness

Figure 2 shows the elastic modulus  $G'$  and viscous modulus  $G''$  obtained at  $\omega=1\text{Hz}$  as a function of the shear amplitude,  $\gamma_0$  ranging from 0.01 to 500% for the Kaolinite 60 wt% and Bentonite 10 wt%, without dispersing agent. A different transition from elastic gel-like behaviour to viscous-like flow was found for both suspensions. Kaolinite suspensions was characterized by a similar reduction of both moduli and a slight “hump” in  $G'$  and  $G''$  curves at a certain strain. This result is consistent with the breakdown by shear of the open “card house” structure evolving to an organized close-packed structure of neighbouring domains. These structures have been observed using electron cryomicroscopy for very concentrated suspensions of kaolinite by Moan et al [7]. The authors suggested a competition between shear forces that tend to align domains and interactions between neighbouring domains that oppose to their mutual alignment.

On the contrary, Bentonite suspensions were described by  $G'$  decrease and “hump” in  $G''$  curve. In this case the behaviour could be related to a more isotropic structure expected to be favoured for these large particles in low ionic strength [8].

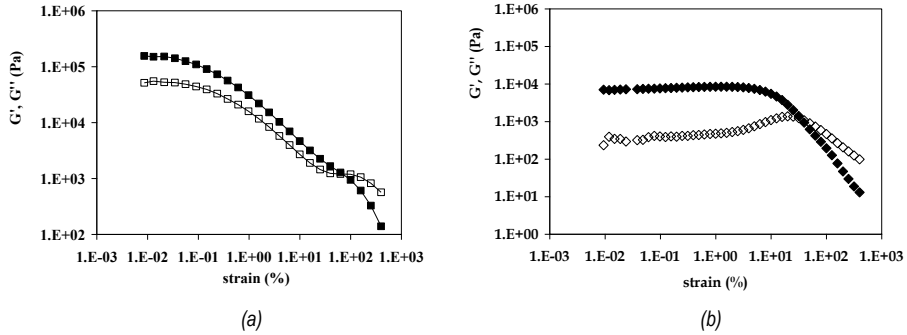


Figure 2.  $G'$  and  $G''$ -strain amplitude curves. a) Kaolinite 60wt% suspension and b) Bentonite 10 wt% suspension.

Both responses were clearly distinguished by the Laos analysis. The viscoelastic non linearity interpreted by Fourier Transform of the responsive stress results in a series of odd harmonics. The intensity of the third harmonic related to the primary one,  $I_{3/1}$ , is plotted as a function of the oscillatory strain amplitude,  $\gamma_0$ . Figure 3 compares the results obtained for Bentonite and Kaolinite suspensions. The intensity of the third harmonic in the Kaolinite reached a maximum and then decreased with strain amplitude before slightly increasing again with further increase of the strain amplitude. This result is similar to the hump in  $I_{3/1}$  observed for carbon black filled rubber compounds, emulsions and rigid polymer dispersions described in the review of Hyun *et al.* [9].

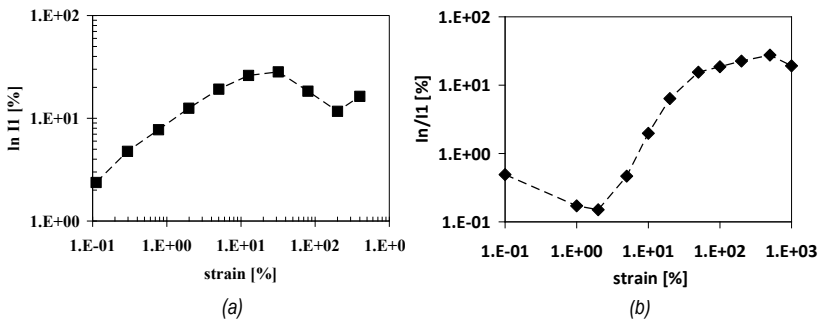


Figure 3. Intensity of the third harmonic as a function of strain amplitude from analysis of FT spectra. a) Kaolinite 60 wt% suspension b) Bentonite 10 wt% suspension

By analogy, we may consider that the minimum and subsequent increases in the intensities are related to the alignment and rupture of domains at intermediate strain amplitudes. Bentonite suspensions were characterized by third harmonic increase as a function of strain amplitude before approaching a plateau value. The result was also found for different hard gel system described in the review of Hyun *et al.*[9]

The decomposition of the total stress into their elastic and viscous components provides the Thickness and Stiffness index defined by Ewoldt *et al* [4] Intracycle non linearities were indicated by nonzero values and the nature of nonlinearity is given by their signs:  $S > 1$ , strain stiffening;  $S < 1$ , strain softening and  $T > 1$ , shear thickening,  $T < 1$ , shear thinning.

The evolution of these parameters as the strain was increased reflects the structural changes under shear in the kaolinite and bentonite suspensions. The Stiffness parameter,  $S$ , approached the value  $S=1$  typical for plastics materials. The Thickness parameters,  $T$ , distinguished both clays. Bentonite was strongly shear thinning after yielding, whereas kaolinite shown a minimum at intermediate deformation that could also be related to the orientation induced by flow.

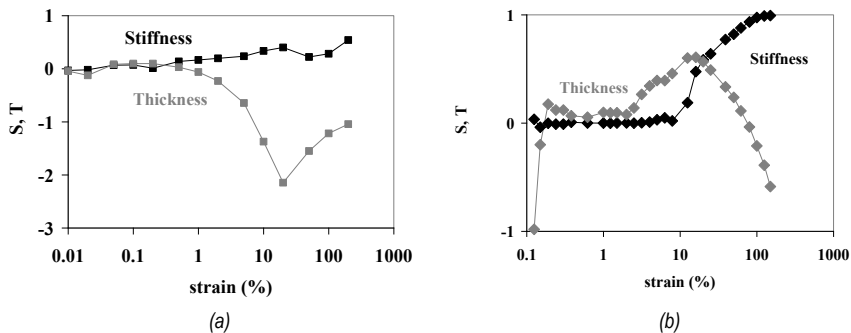


Figure 4. Intracycle viscoelastic non linearities. Stiffness and Thickness as a function of strain amplitude obtained from MitLAOS analysis. a) Kaolinite 60wt% and b) Bentonite 10wt%

The evolution of the non linearity parameters was found to be affected by preshear conditions, solid content and dispersant agent addition, as they could favour or not the tendency of plate like particles to align. Despite the effect of these variables, LAOS main features for kaolinite and bentonite suspensions remained unaltered. LAOS test provides useful information on microstructure of these complex fluids. In particular allow us distinguish the behaviour of soft gel of

kaolinite concentrated suspensions, from the hard gel behaviour that characterized the bentonite concentrated suspensions studied in this work.

### Acknowledgements

The Spanish Ministerio de Ciencia e Innovación and the Fondo Europeo de Desarrollo Regional are greatly acknowledged for their support through project VECLADES (IPT-010000-2010-032)

### References

1. Brinke *et al* (2007) *Soft Matter*, 1145-1162.
2. Michot L.J *et al.* (2009) *Langmuir* 25, 127-139
3. Wilhelm, M. (2002) *Macromol Mater Eng*, 83-105
4. Ewoldt, R. *et al* (2008) *J Rheol* 52, 1427-1458.
5. Lagaly, G., (1989) *Appl. Clay Sci.* 4, 105-123
6. Papo, A. *et al* (2002) *Colloids and surfaces A: Phys. and Eng. Aspects* 201, 219-230.
7. Moan, M. *et al* (2003) *J Rheol* 47(6), 1493-1504
8. Bossard, F. *et al* (2007) *J Rheol.* 51(6), 1253-1270.
9. Hyun, K. *et al* (2011) *Progress in Polym. Sci.* 36(12), 1697-1753

### Contact Address:

Mercedes Fernández ([mercedes.fernandez@ehu.es](mailto:mercedes.fernandez@ehu.es))  
Polymer Science and Technology Department and POLYMAT Institute.  
University of The Basque Country (UPV/EHU)  
Joxe Mari Korta Centre, Av Tolosa 72, 20018 Donostia-San Sebastián Spain  
Phone 943 018494, Fax number 943 01 7065

## CHAPTER 5

# Rheological and kinetic study of the influence of PEG-400 on a Hyaluronic acid polymeric matrix for topical metronidazole administration

Rodríguez Belenguer P<sup>1,3</sup>., Nácher A<sup>1,3</sup>., Hernández MJ<sup>2</sup>., Díez-Sales O<sup>1,3</sup>.

<sup>1</sup>Department of Pharmacy and Pharmaceutical Technology, Faculty of Pharmacy, Univ. Valencia (Spain).

<sup>2</sup>Department of Earth Physics and Thermodynamics, Faculty of Physics, Univ. Valencia (Spain).

<sup>3</sup>IDM, Polytechnic Univ. Valencia (Spain)

### Introduction

In recent years, much attention has been focused on biopolymers and particularly on Carbopol, Chitosan and Hyaluronic acid (HA) because of their biomedical and pharmaceutical potential applications [1,2,3]. HA is a polysaccharide recognized to be produced by bacteria *Streptococcus zooepidemicus*. HA has regenerative properties in several mucous areas of the body such as gastrointestinal, vaginal or mouth areas amongst others. It is a linear polyelectrolyte based on  $\beta$ 1,4- D-glucuronic acid and  $\beta$ 1,3-N-Acetyl-D-glucosamine alternated in the repeat unit [4]. Its physicochemical properties are influenced by pH of final formulation [5]. Hyaluronic acid-polyethylene glycol 400 matrix systems have been considered as potential vehicles in topical dosage forms. Topical administration is a good alternative to the oral route because there is less risk of adverse events, drug interactions or antibiotic resistance and it is also a comfortable route.

Polyethylene glycol is an excipient used as a humectant agent, antiseptic and plasticiser [6].

The selected drug has been metronidazole which is used on various types of bacterial and parasitic infections, including bacterial vaginosis and rosacea. Metronidazole inhibits DNA synthesis on *T.vaginalis*, restoring the vaginal pH=4 under non pathogenesis [7].

The objective of this work was to study the effect of PEG proportion and pH on rheological properties of HA-PEG400 systems, as they are very important for the characterization of these matrices [4,5,8]. Metronidazole release was studied in pH 4 formulations for a possible vaginal application.

### **Experimental**

#### *Formulation of gels*

HA, lactate and PEG-400 were obtained from Guinama (Valencia, Spain). Metronidazole was supplied by Acofarma (Valencia, Spain). Purified water by reverse osmosis (MilliQ®, Millipore Spain) with a resistivity above 18,2 M $\Omega$ ·cm was used.

Metronidazole (0.75%) solutions with different proportions (0%, 5%, 10% and 20%) of PEG were prepared by dissolving both products in water. Afterwards HA is added. Matrix systems were left to stand for 24 h at room temperature for complete hydration of the polymer and removal of the bubbles. Formulations were adjusted to the corresponding pH with lactic acid.

#### *Rheological measurements*

Rheological tests were carried out with a controlled stress rheometer Rheostress 1 (ThermoHaake, Germany) with data acquisition software (Rheowin 4.0.1). Cone plates (2°, 35 mm and 60 mm) and serrated parallel plates (35 mm) were used. All measurements were performed in duplicate at 25 °C and 600 s of rest after loading.

Step flow curves in CS mode (30 s each point) were recorded.

In order to determine the linear viscoelastic range, stress sweeps at a frequency of 1 Hz were performed. Frequency sweep tests at 1 Pa were performed from 0.01 to 10 Hz. Also creep at 1 Pa (300 s) and recovery (300 s) tests were performed.

#### *Diffusion tests*

The cumulative amounts,  $Q$ , of Metronidazole released from HA-PEG 400 were determined using 0.45  $\mu$ m cellulose-acetate membrane filters in Franz type cells with an available diffusion area of 0.784 cm<sup>2</sup>, placed in a heating/stirring device. The volume of the receptor compartment was 6 mL and it was filled with distilled water. The HA-PEG 400 (1 g) was placed on the artificial membrane and covered with parafilm to prevent any evaporation. During 24 h at predetermined time intervals, 200  $\mu$ L samples were taken from the receptor and replaced by the same volume of fresh distilled water to maintain a constant volume. The samples (n=6) were analyzed by HPLC (Perkin-Elmer LC Binary pump) using a C18 column (4.6mmx150mmx5 $\mu$ m) and a acetonitrile-water (60:40 v/v) as mobile phase at a

flow rate of 1 mL min<sup>-1</sup>. Ultraviolet detection was made at 320 nm. The calibration curve was linear over a concentration range from 7.5 to 0.15 mg/mL with a dilution 1/10.

## Results and discussion

All the formulations studied had a shear thinning behaviour (Fig 1 and 3), so flow curves were fitted to Carreau model [9]:

$$\eta = \frac{\eta_0}{\left(1 + \frac{\dot{\gamma}}{\dot{\gamma}_c}\right)^s} \quad (1)$$

Where  $\eta_0$ , is zero-shear viscosity,  $\dot{\gamma}_c$ , critical shear rate, and  $s$  is shear thinning index.

When analyzing pH dependence, it is interesting to point out that all the formulations with pH>3, had a similar behaviour with zero shear viscosity between 1-5 Pa and critical shear rate between 15-40 s<sup>-1</sup>. However, for pH 2.5 viscosity highly increased reaching values even some orders of magnitude greater than those for systems with higher pHs (Figure 1).

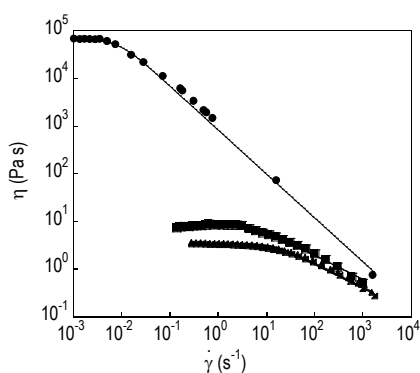


Figure 1. Flow curves for the systems 20% PEG-400 at different pH:  $\blacktriangle$  2.5;  $\blacksquare$  3.5;  $\blacktriangleleft$  4;  $\blacktriangle$  5

Oscillatory tests showed a viscous behaviour for formulations with pH between 3 and 7, as loss modulus ( $G''$ ) were greater than storage modulus ( $G'$ ) and both moduli were strongly dependent on frequency [1,2] (Figure 2). However, for systems with pH 2.5 a gel-like behavior, with  $G' > G''$  and a low dependence with frequency was observed. This effect could be due to an isoelectric point located

around pH=2.5. The reduction of the carboxylic group dissociation favours the H-bond formation, but also the protonation of the -NH- group giving a positive net charge able to complex with the negative charge of few -COOH.

On the other hand dynamic moduli values were greater when PEG-400 concentration was increased.

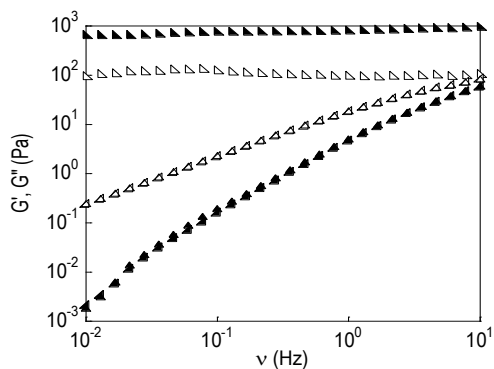


Figure 2. Viscoelastic moduli as a function of frequency for the systems with 20% PEG-400. Open symbols  $G''$  and close symbols  $G'$ , pH:  $\blacktriangle$  2.5;  $\blacksquare$  4;  $\blacktriangle$  5

These results are in accordance with creep tests, as compliance values were fitted to Maxwell model in viscous, non-structured systems (pH>3) and Burger model on structured systems (pH<3).

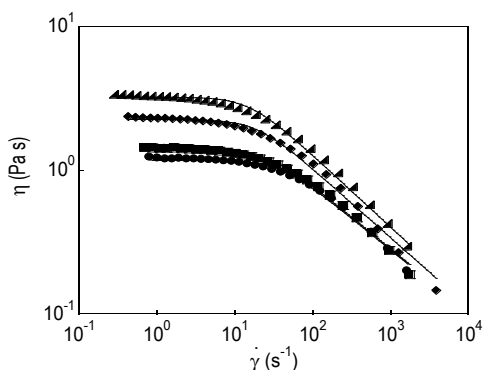


Figure 3. Flow curves for the systems at pH 4. PEG 400 concentrations:  $\bullet$  0%;  $\blacksquare$  5%;  $\blacklozenge$  10%;  $\blacktriangle$  20%

As indicated before, formulation with pH 3-7 exhibited a Newtonian behaviour up to shear rate of 15-40  $s^{-1}$ . For a fixed pH, viscosity of formulations slightly increased when increasing PEG 400 concentration (Figure 3).

All formulations at pH 4 could be fitted to the Maxwell model because they had a viscous behaviour (Figure 4). Moreover, maximum strain was inversely proportional to PEG-400 proportion.

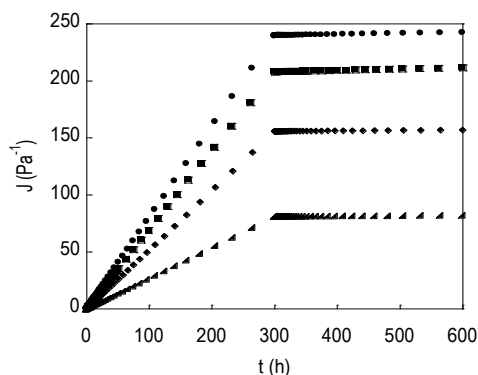


Figure 4. Creep and recovery for the systems at pH 4. PEG 400 concentrations. ● 0%; ■ 5%; ◆ 10%; ▲ 20%

It seems that the drug was diffusing in non structured viscous solutions (formulations at pH4), with a Newtonian viscosity (in the range of diffusion rates), dependent on PEG concentration.

Metronidazole release was expected to be related to viscosity of these formulations. Cumulative amounts measured as a function of time are plotted in Figure 5. Metronidazole release was faster at the beginning of tests, while release rate decreased significantly after 8 hours. In order to obtain diffusion coefficients,  $D$ , release profiles of Metronidazole were fitted to Higuchi model [10]:

$$Q = 2C_0(Dt / \pi)^{1/2} \quad (2)$$

Where  $Q$  corresponds to the cumulative amounts per unit surface area that reach the receptor solution at a given time,  $t$ , and  $C_0$  is the initial concentration of Metronidazole.

$Q$  values seemed to be higher for the less viscous systems, with lower concentration of PEG. However, ANOVA (one way, non-parametric, T-3 Dunnett) performed showed there were not statistically significant differences for diffusion coefficients obtained. Therefore, we can conclude that diffusion of the drug is not really dependent on concentration of PEG-400 at pH 4. The mean value obtained for  $D$  was  $(8.0 \pm 1.4) \times 10^{-6} \text{ cm}^2/\text{s}$ .

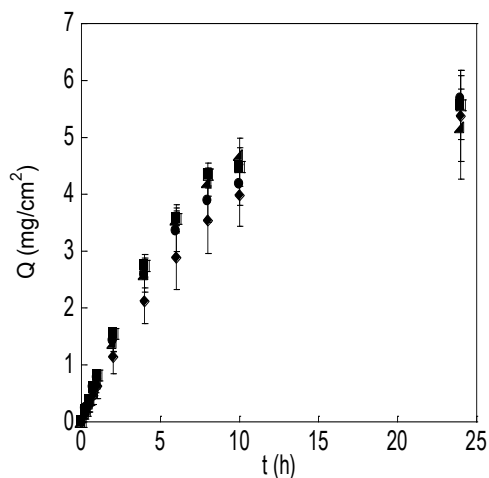


Figure 5. Release profiles of Metronidazole of the systems studied (pH 4) PEG 400: ● 0%; ■ 5%; ◆ 10%; ▲ 20%

## References

1. Bonacucina, G., Martelli, S., Palmieri, GF. (2004). *Int J. Pharm.* 282, 115-130.
2. Xian, X., Amit, JK., Harrington, D., Farach, MC. (2012). *NIH.* 8, 3280-3294.
3. Malhotra, M., Tomaro, C., Saha, S., Kahouli, I., Prakash, S. (2013). *Int J Nanomedicine.* 8, 2041-2052.
4. Fusco, S., Borzacchiello, A., Micio, L. (2008). *Biorheology.* 44, 403-418.
5. Gatej, L., Popa, M., Rinaudo, M. (2005). *Biomacromolecules.* 6, 61-67.
6. Alemdar, A., Güngör, N., Ece, O.I., Atici, O. (2005). *J. Materials Sci.* 40, 171-177.
7. Lorenzo, P., Moreno, M., Leza, J.C., Lizasoain, I., Moro, M.A., Portolés, A. (2008). *Farmacología básica y clínica.* 18 edn. Médica Panamericana, Madrid.
8. Nyström, B., Kjoniksen, A.L., Beheshti, N., Maleki, A., Zhu, K., Knudsen, K.D. (2010). *Adv Colloid Interface Sci.* 158, 108-118.
9. Barnes, H.A., Hutton, J.F., Walters, K. (1993). *An introduction to rheology.* 1 edn. Elsevier Science Publishers, Amsterdam.
10. Higuchi, W.I. (1967). *Pharm. Sci.* 56, 315-324.

## Contact adress:

Amparo Nácher Alonso ([amparo.aacher@uv.es](mailto:amparo.aacher@uv.es))  
 Department: Pharmacy and Pharmaceutical Technology  
 University of Valencia  
 Address: Av. Vicente Andrés Estellés s/n, Burjassot, Valencia, España 46100.  
 Telf.: 963543319

## CHAPTER 6

# Influence of the preservative on rheological properties and on *in vitro* release profiles of topical gels containing AINES

*J. Marto*<sup>1,2</sup>, *M. Militão*<sup>1</sup>, *L. Gouveia*<sup>1</sup>, *E. Oliveira*<sup>2</sup> and *H. M. Ribeiro*<sup>1</sup>

*1 Research Institute for Medicines and Pharmaceutical Sciences (iMed.UL), Faculty of Pharmacy, University of Lisbon, Portugal*

*2 Laboratórios Atral S.A., Portugal.*

### Introduction

In normal conditions, when the skin is treated with altering substances, it recognises that its barrier function has been impaired and rapidly restores itself by synthesising lipids to replace those that have been extracted [1]. Therefore, ideal penetration enhancers should specifically promote the permeation of drugs across the skin without exhibiting irreversible effects on its properties. Skin enhancers are, thus, part of the pharmaceutical formulations and they alter the diffusional gradient of the drug across the skin by altering the partitioning of the drug from the delivery system into the stratum corneum. Therefore, it is the pharmaceutical development of topical formulations' challenging duty to find ways to overcome this barrier, when it is needed, for instance, to deliver drugs to the skin to treat health related issues [2]. The release of a therapeutic agent from a formulation is dependent upon the physico-chemical properties of both the drug and the vehicle.

The present study was conducted in order to study the effect of preservative on the release patterns of AINE from topical gels and compare the formulation's drug releases to the commercial formulation.

### **Experimental**

#### *Gels processing*

Gels containing AINE were prepared differing on the concentration of the preservative agent (ethanol) used: GA 10% (w/w); GB 15% (w/w); GC 20% (w/w); GD 25% (w/w); GE 30% (w/w); GF 35% (w/w).

And we compare all formulations with the commercial formulation (R).

Gels GD and GE were selected for subsequent studies due to the similarity of the rheological profiles to the commercial formulation.

### **Rheological analysis**

The rheological characterization and apparent viscosity was determined using a Brookfield viscometer, Model RVT DV II, using a spindle 7, at 25°C. A sample of each formulation was put into an appropriate container and the rheograms were obtained with a shear rate from 0.6 to 122s<sup>-1</sup> followed by decreasing the shear rate from 122 to 0.6s<sup>-1</sup>.

#### *In Vitro Release Studies*

*In vitro* drug release profile was determined using vertical Franz cells (n=12) through hydrophilic polysulfone membrane (Tuffryn®-0,45µm) and silicone membrane with a diffusion area of 1cm<sup>2</sup>. Membranes were activated for 30mins with receptor phase before use, to enhance the simulation of the skin's lipophilicity and to reduce the membrane's porosity. The receptor phase contained a mixture of 3:2 phosphate buffer/ethanol. Sink conditions were maintained throughout the experiment. The temperature of fluid was maintained at 37°C ±1°C and stirring was maintained at 200 rpm. Samples (200µL) were withdrawn through the sampling part from the diffusion cell at prefixed time interval (1, 2, 3, 4, 6 and 12h) and replaced with an equal volume of fresh receptor medium maintained at the same temperature. The receptor samples were analysed by HPLC to determine the amount of drug released/permeated.

### **Statistical analysis**

Two-way analysis of variance (ANOVA) with replication was done (p<0.05) to detect differences among the formulations.

## Results and Discussion

### *Rheological analysis*

Continuous shear experiments measure the ability of each system to resist structural breakdown during the standardized shearing procedure. Representative plots are shown in figure 1 with apparent viscosity values calculated at the apex of the loop (122,36 s<sup>-1</sup>) also shown in the table 1. The yield values for each gel are shown in the table 2.

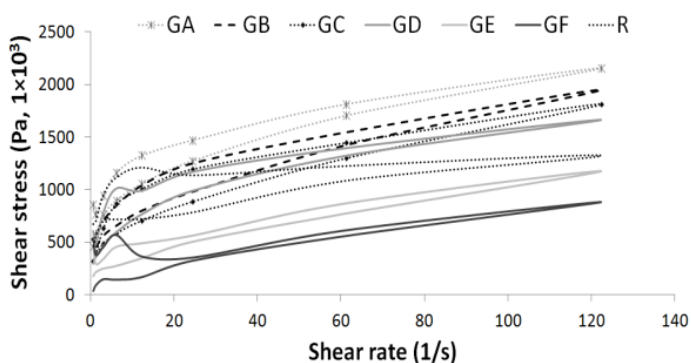


Figure 1. Shear stress as function of shear rate of all gels. (Mean  $\pm$  SD, n=3)

Table 1. Results of apparent viscosity of different formulations (Shear Rate at 122,36 1/s)

Gel	Apparent viscosity (Pa.s)
R	10.8
GA	17.6
GB	15.9
GC	14.8
GD	13.6
GE	9.6
GF	7.2

Table 2. Results of yield values of different formulations.

Gel	Yield values (Pa.s)
R	1100
GA	1400
GB	744
GC	864
GD	984
GE	728
GF	872

When the apparent viscosity decreases with the increase in shear rate the fluid is considered shear thinning. Moreover, they immediately recover their non sheared viscosity once shear is removed [3]. The shear thinning behaviour which means that the material will gradually recover the original internal structure after shear, indicating good applicability onto skin.

Apparent viscosity values provide a comparison of the resistance to structural breakdown between the gels and the loop areas compare the amount of structure that fractures in the standardised cycle. The GD, GE, GF and commercial formulation showed complex flow with a spur on the up-curve. Such complex flow curves are typical for high viscosity gels where the spur, although in part instrumental, is a function of significant elasticity [4, 5]. The flow curves clearly demonstrate that incorporation of higher percentage of preservative partially destroys the structural elements of the gel (decreasing the spur). Thus, GF presented the lower apparent viscosity. This decrease in viscosity was due to the addition of ethanol. Ethanol was used in different concentrations and we compare all formulations with the commercial formulation (R).

Yield value indicates the minimum force (the yield stress) that must be applied to a liquid to start disrupting the structure imparted by the rheology modifier, so that flow can occur. All samples showed different yield values and thixotropic flow behaviour (Figure 1 and Table 2). These values confirm that substantial amounts of stress are required before the topical gels can start to flow.

Gels GD and GE were selected for subsequent studies due to the similarity of the rheological profiles.

*In Vitro Release Studies*

In the release studies, using Tuffryn® membrane, we verified that the amount of ethanol affected the drug release when comparing GD to GE ( $p < 0.05$ ). The mechanism might be due to the disruption of the stratum cornea integrity through extraction of hydrophobic alcohols, raising the drug penetration [1].

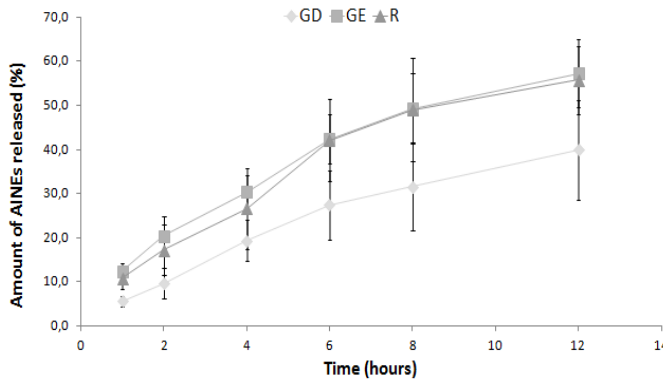


Figure 2. Release profile through Tuffryn® membrane for gels GD, GE and R (mean  $\pm$  SD,  $n=12$ ).

The formulation GD presented a release profile similar to R ( $p > 0.05$ ). This result was confirmed in a second release study using silicone membranes for GE and R ( $p > 0.05$ ). After 12 hours both formulations had released around 18.6%  $\pm$  1.1 of initial concentration.

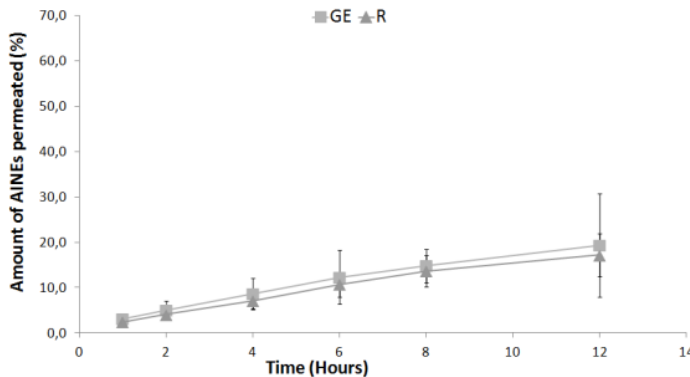


Figure 3. Permeation profile through silicone membrane for gels GE and R (mean  $\pm$  SD,  $n=12$ ).

### Conclusions

The results showed that the amount of ethanol influenced the viscosity and the release of AINEs from topical gels. Consequently, the selection of the preservative and its amount is an important aspect in development topical formulations.

### References

1. Walker R. B., et. al. (1996) *Advanced Drug Delivery Reviews*. 18:295-301.
2. Trommer H. et.al. (2006) *Skin Pharmacol Physiol*. 19:106–121.
3. Chen, H. (2007). *Food Hydrocolloids*. 21, 1201-1208.
4. Barry, B.W. and Saunders, G.M. (1970) *J. Colloid Int. Sci*, 34, 300-315.
5. Davis, S.S., Shotton, E. and Warburton, B., (1968) *J. Pharm Pharmacol*, 157S-167S

### Contact Address:

*J. Marto (jmmarto@ff.ul.pt)*

*NanoDDs*

*iMed.UL– Faculdade de Farmácia da Universidade de Lisboa.*

*Av. Prof. Gama Pinto 1649-003 Lisboa - Portugal*

*Tel: +351 217 946 400; Fax: +351 217 946 470.*

## CHAPTER 7

### Rheological characterization of different toothpastes. Analysis of parameters with influence on the packaging process

A. Sánchez-Vicent<sup>1,2</sup>, J. A. Picó<sup>1</sup>, J. Peris<sup>1</sup>, M. J. Hernández<sup>2</sup>

<sup>1</sup> Research and Development, KOROTT, SL. Polígono Santiago Payá, 03801 Alcoy (Spain)

<sup>2</sup> Dep. of Earth Physics and Thermodynamics. Fac. of Physics, Univ. of Valencia, 46100 Burjassot, Valencia (Spain)

#### Introduction

The present study is focused on the relationship between the rheological properties of toothpastes and their behaviour in an innovative packaging system recently implemented at the company Korott SL (Alcoy, Spain).

The production process is performed in a 3000 L reactor with continuous stirring and homogenization. Once manufactured, toothpaste is distributed through 100 mm diameter pipes. Different pressures are applied to push the toothpaste until it reaches the filling machine. Lobular pumps and a pigging system exert an average pressure of  $2 \cdot 10^5$  Pa up to the hopper of the filling machine, where toothpaste comes to rest for a few minutes. Finally a strong and fast extrusion is produced when the toothpaste passes through a hose in order to fill the final container.

The behaviour of some similar toothpastes seems to be different during the final filling process. For this reason, the aim of the study is trying to relate the rheological properties of the toothpastes to the differences observed.

#### Experimental

##### *Toothpastes*

Three kinds of commercial toothpastes have been analysed: "Total" (T), "Fresh" (F) and "Whitening" (W). The main ingredients are humectants such as sorbitol and water. The variability in the concentration of thickeners and abrasives (silica) gives a different texture to each toothpaste. All of them include Cellulose gum in their composition, but only "Total" contains Xanthan Gum.

### *Rheological measurements*

Experiments were carried out at 20°C in a control stress rheometer DHR-1 (TA Instruments) with a Peltier plate for temperature control. Serrated and smooth 40 mm diameter parallel plates (1 mm gap) were used. All measurements were repeated at least twice.

Apparent yield stress values were obtained from flow curves with steady-state sensing from 10 to 10000  $\mu\text{Nm}$ .

Frequency sweep tests were performed at a stress within the linear viscoelastic region, varying the frequency from 0.1 Hz to 100 Hz.

The linear viscoelastic region, LVR, was previously determined in an amplitude sweep measurement at a frequency of 1 Hz.

Apart from viscoelastic moduli and shear thinning properties, other kind of parameters of interest in packaging and extrusion have been analysed, such as recovery time of viscosity and the structural regeneration after an interval of high-shear conditions. This allows us to analyse the toothpaste behaviour at rest after the flow process.

3 steps viscosity recovery test: In first step a low constant shear rate (0.01  $\text{s}^{-1}$ ) was applied until a constant viscosity is reached. After applying a higher shear rate for 90 s, viscosity is recorded again at the initial shear rate.

3 steps Structural regeneration test: An oscillatory time sweep (at 1 Hz and constant amplitude in the LVR) was followed by applying a constant high shear rate of 20  $\text{s}^{-1}$  for 90 s. Finally, another time sweep under the same conditions of the first step was carried out.

Before starting each experiment stability of the sample was checked using an oscillatory time sweep.

## **Results and Discussion**

### *Characterization*

Yield point has been determined by means of flow curves. There is a sharp fall in viscosity at 200 Pa for T and W, and at 400 Pa for F, what corresponds the yield point value. Moreover, viscosity is slightly higher for the samples T and W (Figure 1).

The three toothpastes have a gel structure ( $G' > G''$ ), i.e., the sample displays a viscoelastic behavior with a dominant solid portion (Figure 2). This is an important requirement for a clean extrusion. In particular, F is stiffer than T and W for the reason of having a greater  $G'$ . The LVR is defined as the zone in which  $G'$  is constant with a tolerance of 5%. The upper limits of the LVR are 2.5 Pa for F, 10

Pa for T and 8 Pa for W. Therefore, F seems to be the stiffest toothpaste and in turn the most fragile.

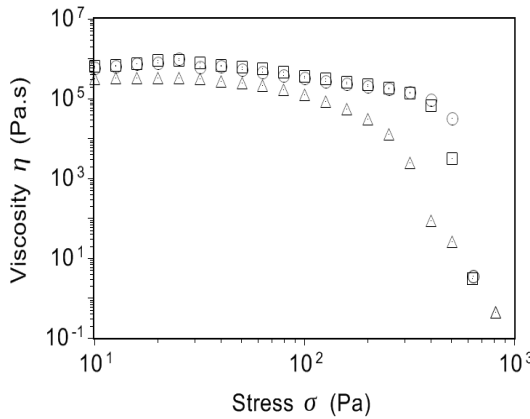


Figure 1. Flow curves for all three toothpastes analysed.

△ Fresh, □ Whitening, ○ Total.

The frequency sweep within LVR gives information about the structure at rest of the three samples. As loss angle,  $\delta$ , is between 10 and 20° for the entire frequency range tested, a solid-like behaviour is predominant. It is interesting to point out that F pastes have a different behaviour for  $f < 1$  Hz (Figure 3).

Therefore, it can be inferred that W and F are quite similar in regards to viscosity and structure. However, their response in the packaging process is very different.

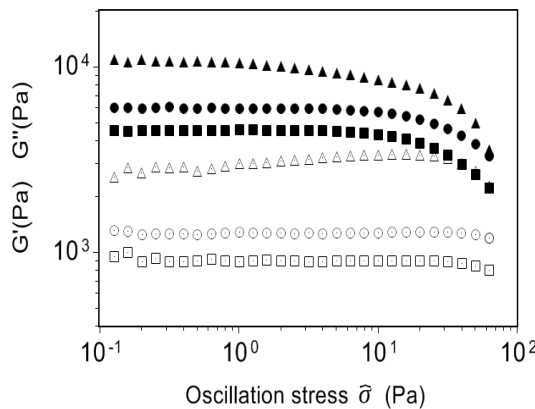


Figure 2. Stress sweeps at 1 Hz for the three toothpastes analysed. △ Fresh,

□ Whitening, ○ Total.

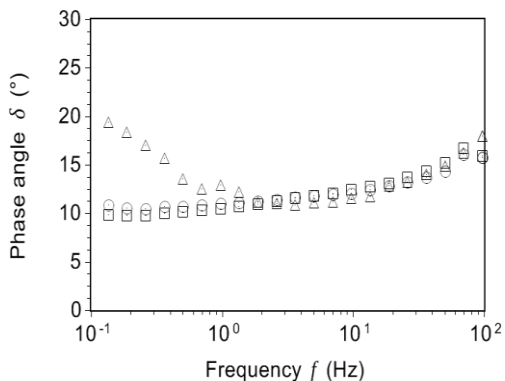


Figure 3. Frequency dependence of the loss angle  $\delta$  at 2 Pa for three kinds of toothpastes.  $\triangle$  Fresh,  $\square$  Whitening,  $\circ$  Total.

### Viscosity Recovery

The packing process implies that toothpaste has undergone a large amount of shear stresses. Since toothpastes are shear-thinning fluids, their viscosity decreases along the pipes.

A viscosity recovery test as the one described in Experimental Section can be useful in determining the time that the sample takes to recover viscosity. The evolution of viscosity after the previous shear was recorded during 300 s, since this is approximately the maximum time the material can remain at rest in the hopper.

As seen in Figure 4, the evolution of viscosity after a shear of  $20 \text{ s}^{-1}$  is different for each sample (the viscosity varies by about one decade), although the viscosity in the first step of the experiment (at  $0.01 \text{ s}^{-1}$ ) was approximately the same for all three (about  $10^4 \text{ Pa}\cdot\text{s}$ ).

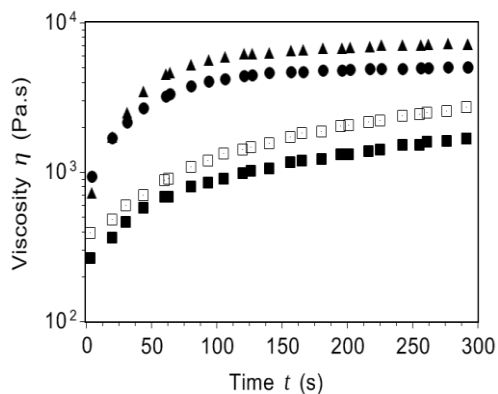


Figure 4. Evolution of viscosity at  $0.01 \text{ s}^{-1}$  after shearing the samples at  $20 \text{ s}^{-1}$  during 90 s.  $\triangle$  Fresh,  $\square$  Whitening,  $\circ$  Total.  $20^\circ\text{C}$  (filled symbols) and  $10^\circ\text{C}$  (empty symbols).

The evolution is more stable after 100s, but viscosity did not reach the initial value. The sample W is more sensitive to shear than the others, as viscosity loss is more pronounced.

An additional measurement for W at 10°C was performed, in order to observe whether these packaging conditions could promote viscosity recovery. Resulting improvement turned to be not significant.

### *Structural Regeneration*

When toothpaste is extruded in the container, there is a cut in cross section. The elasticity of the material should be highly enough to assure a clean cut. It was observed that in the final extrusion, toothpastes F and T have a cleaner cut than W.

This phenomenon was examined using a test of structural recovery described in Experimental Section, since a high value of elasticity promotes a cleaner cut.

Figure 5 shows the recovery of the elastic modulus  $G'$  after a shear of  $20 \text{ s}^{-1}$ . The experiment shown is an oscillation time sweep at 2 Pa and 1 Hz. The  $G'$  value of T and F rises faster than the  $G'$  value of W. Therefore T and F display a faster structural regeneration after a high-shear. Before high-shear is applied, the value of  $G'$  for W is 4500 Pa (Figure 2). After 300 s after the shear, this value is 650 Pa. It can be considered too low, since at least the value of  $G'$  for an optimum cutting is 1850 Pa, which corresponds to T after 300 s.

Analogous experiments have been performed at a temperature of 10°C in order to determine whether temperature influences packaging. However, its effect on T and F is negligible, whereas for W, the elastic modulus is greater than T after 100s.

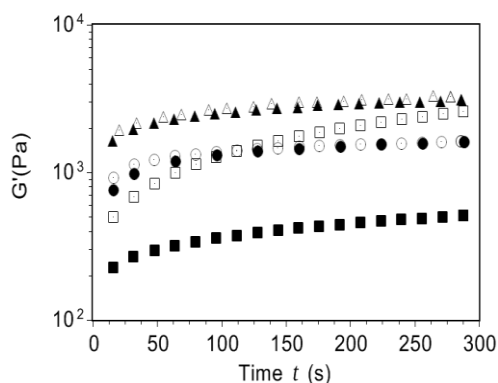


Figure 5. Structural regeneration after a shear of  $20 \text{ s}^{-1}$  during 90 s.  $\triangle$  Fresh,  $\square$  Whitening,  $\circ$  Total. 20°C (filled symbols) and 10°C (empty symbols).

In summary, W is different from T and F in terms of viscosity recovery and structural regeneration, though it is not in its characterization. Hence, these

## Perspectives in Fundamental and Applied Rheology

parameters, along with temperature, seem to be variables that have influence in packaging process.

### References

1. Hernández, M.J., Picó, J.A., Díez-Sales, O., Peris, J., Dolz, M. (2012). Rheological properties of liquid toothpastes: comparison between different products from several trademarks. XVIth International Congress on Rheology., pp. 455
2. Ardakani, H.A., Mitsoulis, E., Hatzikiriakos, S.G. (2011). Thixotropic flow of toothpaste through extrusion dies. *J Non-Newtonian Fluid Mech.*, pp. 1262-1271
3. Pader, M. (1988). Oral hygiene products and practice. *Cosmetic science and technology series*, vol. 6. Marcel Dekker, Inc., New York.
4. Barnes, H. A. (1999). The yield stress—a review or ‘παντα ρει’—everything flows? *J. Non-Newtonian Fluid Mech.*, pp. 133-178

### Contact Address

*J.A Picó (japico@korott.com)*

*Korott, S.L.*

*Polígono Santiago Payá, 03801 Alcoy (Spain)  
Telf.: 0034 966526550; Fax.: 0034 966522718*

## CHAPTER 8

# Rheology of fine particle size chestnut flour doughs with common bakery additives

*M.D. Torres, B. Rama, F.Chenlo, R. Moreira*

*Departamento de Enxeñaría Química, Escola Técnica Superior de Enxeñaría, Universidade de Santiago de Compostela, Campus Vida, E-15782 Santiago de Compostela, Spain.*

### Introduction

Chestnut flour (CF) doughs show lack of viscoelastic properties and the improvement of these characteristics depend greatly on the particle size distribution and composition of the flour, the water amount added and content of other ingredients [1]. New gluten-free sources of flours and natural additives are a goal for food industry and consumers. Several ingredients such as salt, sugars, oils or different types of hydrocolloids are commonly employed in bakery products. These additives show special functions in gluten-free doughs in order to help to mimic the gluten properties [2]. To achieve CF formulations comparable to other standard flours like wheat or rice is necessary to evaluate in detail the influence of additives particle size distribution.

This study aims to contribute to the current knowledge in this field by addressing the rheological properties of CF doughs with typical particle size distribution of standard flours in the presence of several additives usually employed in bakery such as sodium chloride (NaCl), sucrose, olive (OO) or sunflower (SO) oils. For this purpose, the rheological properties by means of steady-shear, oscillatory and creep-recovery measurements of all assayed formulations were carried out. Furthermore, the effect of these ingredients on the thermal behaviour of CF doughs was also studied.

### Experimental

Chestnut flour with low particle size (average particle size,  $76.8 \pm 3.0 \mu\text{m}$ ), CF1, was employed as control sample, CS. CF1 was elaborated by mixing of different sieved fractions (employing several standard sieves: 200, 125, 80, 63 and  $40 \mu\text{m}$ ) from commercial CF (Naiciña SL, Spain) with particle size lower than  $200 \mu\text{m}$ .

Moisture content of CF1 was  $12.5 \pm 0.3\%$ , dry basis (d.b.), according to ICC-Standard Method 110/1 [3]. The chemical composition of assayed flour and the corresponding protocols employed were previously reported [4].

The employed ingredients (NaCl, sucrose, OO and SO) were purchased in a local market (Galicia, Spain). CF1 doughs in the presence of NaCl (0.6-1.8%, flour basis, f.b.), sucrose (0.6-5.0%, f.b.), OO or SO oils (6.0-12%, f.b.) were prepared to determine the corresponding mixing and thermorheological properties.

Mixing tests carried out using Mixolab® apparatus consists on dough mixture at constant speed (80 rpm) at 30 °C during 30 min. Flour or flour blends are initially put into the Mixolab® bowl and the apparatus adds water to achieve the target consistency ( $C1:1.10 \pm 0.07$  Nm). At this moment, the rheological analysis of all studied doughs is carried out, taking a dough sample to the controlled stress rheometer (Anton Paar MCR 301). Steady-shear ( $0.01$  to  $10$  s<sup>-1</sup>), oscillatory ( $1$  to  $70$  rad s<sup>-1</sup> at  $0.1\%$  strain) and creep-recovery (loading of  $50$  Pa for  $60$  s) measurements at  $30^\circ\text{C}$  were conducted with parallel plate ( $50$  mm diameter,  $2$  mm gap). All dough samples were placed between the plates, coated with paraffin and remained in rest time ( $15$  min) before measuring. All tests were performed by triplicate.

Cross model Eq. (1) and power model, Eqs. (2-3), were used to correlate steady-shear and oscillatory data, respectively:

$$\eta = \eta_{\infty} + \frac{\eta_0 - \eta_{\infty}}{1 + \left( k \dot{\gamma} \right)^{(1-n)}} \quad (1)$$

$$\log G' = \log a' + b' \log \omega \quad (2)$$

$$\log G'' = \log a'' + b'' \log \omega \quad (3)$$

being  $\eta$  (Pa s) the apparent viscosity;  $\dot{\gamma}$  (s<sup>-1</sup>) the shear rate;  $\eta_0$  and  $\eta_{\infty}$  (Pa s) zero and infinite shear rate viscosities, respectively;  $k$  (s) the time constant and  $n$  the flow index;  $G'$  and  $G''$  (Pa) storage and loss moduli;  $\omega$  (rad s<sup>-1</sup>) the angular frequency and  $a'$ ,  $a''$ ,  $b'$  and  $b''$  fitting parameters. Creep and recovery data were described through creep compliance ( $J(t)$  (1/Pa) =  $\gamma/\sigma$ , where  $\gamma$  is the strain (-) and  $\sigma$  (Pa) the loaded stress) parameters like  $J_{\max}$  and  $J_r$  are the maximum and recovery compliance, respectively. Thermal behaviour of CF doughs was analysed using temperature sweep ( $30$  to  $100^\circ\text{C}$ ) tests (rheometer) and complete tests (Mixolab®). Last tests involve a mixing step ( $8$  min) followed by a heating-cooling steps ( $37$  min). In both measurements, gelatinisation temperatures and gelatinisation rates,  $\beta$ , of doughs were measured. Additionally, complete tests

allowed the evaluation of the rate of proteins network weakening,  $\alpha$ , enzymatic activity,  $\gamma_e$ , and retrogradation effects by means of C2, C3, C4 and C5 parameters [4]. Goodness of fittings was evaluated by coefficients of determination,  $R^2$ , and standard deviations. Significant differences among doughs parameters values were identified by one-factor analysis of variance (ANOVA), followed by Duncan test ( $p \leq 0.05$ ) (SPSS 18.0 statistical package).

## Results and Discussion

### *Mixing behaviour*

Water absorption (WA) was significantly modified in the presence of studied ingredients when compared to CF1 (56.4%), except for sucrose (at 0.6%) and NaCl addition where significant variations were not found. WA values decreased statistically regarding to CF1 with increasing sucrose (54.6%), OO (53.5%) and SO (53.8%) content. Development time (DT) values increased significantly with salt (1.33 min), sucrose (1.51 min), OO (1.86 min) and SO (1.61 min) addition. The highest influence on the DT of CF1 doughs was noticed with OO above 10%. Stability (St) values also increased when ingredients were added. Namely, St values rose with sucrose above 3.4% and oil in all tested concentration range, which improve notably the strength of CF1 doughs.

### *Rheological behaviour*

CF1 doughs exhibited a Newtonian plateau ( $< 0.02 \text{ s}^{-1}$ ), which was slightly shifted to lower shear rates by increasing ingredient amount. After this initial small plateau, all studied CF1 doughs showed shear thinning behaviour. The apparent viscosity decreased at each shear rate with increasing ingredient content when compared with CF1 doughs. The highest reduction was noticed with OO at the highest assayed content, followed by SO. The presence of NaCl in tested concentration range or sucrose below 3.4% varied slightly the apparent viscosity values. In all cases, flow index,  $n$ , can be considered low (from 0.25 to 0.40) corroborating the strong shear-thinning behaviour of these doughs. The values of time constant,  $k$ , also rose with increasing ingredients content. Lower  $k$  values can be related to higher shear rate for the Newtonian plateau range when  $n$  values vary in a narrow range. The presence of sucrose, NaCl or OO at the highest content showed the highest values of time constant.

The values of  $G'$  modulus increased with increasing  $\omega$  from 1 to 100  $\text{rad s}^{-1}$ , and decreased with respect to CF1 with increasing additives content at each  $\omega$ . The presence of the studied additives into CF doughs modified significantly the  $\tan \delta$  values when compared with CF1 doughs (Figure 1) and, therefore, the viscoelastic behaviour of the doughs. The  $\tan \delta$  data for CF1 doughs with studied

ingredients were lower than unit in all cases. Low values of  $\tan \delta$  indicate stiff characteristics of these doughs.

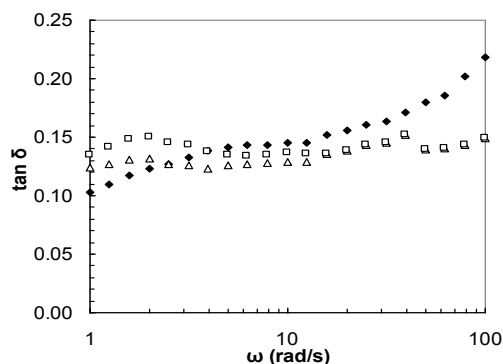


Figure 1. Values of  $\tan \delta$  for CF1 doughs without (CS:  $\blacklozenge$ ) and with the maximum tested amounts (% f.b.) of NaCl ( $\circ$ : 1.8%), sucrose ( $\diamond$ : 5.0%), OO ( $\square$ : 12%) and SO ( $\triangle$ : 12%). \*NaCl and sucrose symbols are hidden behind CS ones.

The highest modifications in  $\tan \delta$  were noticed with oils addition in the whole range of  $\omega$ . Likewise, the presence of sucrose in CF1 doughs not varied notably the  $\tan \delta$  behaviour regarding to CF1 doughs. Oils addition involved a slight increasing of the elastic contribution at higher  $\omega$  values. Nevertheless, a reverse trend was identified with NaCl addition. Particularly, in the case of salt, sucrose and oils addition the  $\tan \delta$  featured slight modifications with increasing additives content in the assayed concentration range.

The flow curves and mechanical spectra were successfully fitted using Cross ( $R^2 > 0.996$  and  $s < 0.008$  Pa s) and power ( $R^2 > 0.994$  for  $G'$  and  $R^2 > 0.980$  for  $G''$ ) models, respectively. The shape of creep-recovery curves and the values of compliance parameter,  $J(t)$ , were higher (below 0.011 1/Pa) than those found for other gluten-free formulations (below 0.005 1/Pa) [5]. The highest variations in creep-recovery curves were identified with oils addition. The low  $J_r/J_{max}$  ratio values (20.1%) obtained for CF1 doughs, which give information about the low elasticity values of this type of doughs, were enhanced when oils (SO:40.1 or OO:44.7% at 12%) were added, improving the non-linear viscoelastic properties of these doughs.

#### Thermal behaviour

The studied ingredients suppressed the gelatinization process and, consequently the gelatinization temperatures were delayed regarding CF1 doughs, except for NaCl at 0.6%, OO at 6.0% and SO below 8.0% where no significant variations

were found. The highest influences in delaying of gelatinization temperatures were noticed with sucrose.

Mixolab's complete curves did not vary significantly in the presence of NaCl and sucrose in the assayed concentration range. Both ingredients did not improve the behaviour of the CF1 doughs subjected to heating-cooling steps. C3, C4 and C5 values rose significantly with increasing OO below 8.0%. C4/C3 ratios for CF1 doughs with OO at 12% were within the range to those reported for soft (1.02) and hard (1.05) wheat flours [6]. Analysing mixing and thermal properties, the best effects on CF1 doughs seem to be achieved with OO at 12%. Many differences were found when compared with reported data for the effect of these ingredients in CF doughs with higher particle size ( $168.6 \pm 6.6 \mu\text{m}$ ) [1]. Higher specific surface of CF1 seems to promote interactions between components and ingredients during mixing processes, modifying mixing and rheological parameters.

### Concluding Remarks

CF1 doughs showed low stability and elasticity. Development time and stability increased with tested ingredients. Rheological properties were modified in the presence of SO and OO, whereas no noticeable changes were observed with sucrose and NaCl. The values of apparent viscosity at each shear rate and the values of storage and loss moduli at each angular frequency drop with oils addition. Creep-recovery data showed that OO and SO improved doughs elasticity.

### Acknowledgments

Authors acknowledge the financial support to Ministerio de Ciencia of Spain and FEDER (CTQ 2010-15309/PPQ). M.D. Torres thanks to the Ministerio de Educación of Spain for her FPU grant (AP 2007-04397).

### References

1. Moreira, R., Chenlo, F., Torres, M.D., Prieto, D.M. (2010). *J. Food Eng.*, 100, 270–277.
2. Moreira, R., Chenlo, F., Torres, M.D. (2011). *Food Hydrocolloids*, 25, 1041-1050.
3. ICC (2008). *ICC-Standard Methods*.
4. Moreira, R., Chenlo, F., Torres, M.D. (2011). *Food Hydrocolloids*, 25, 1361-1371.
5. Lazaridou, A., Duta, D., Papageorgiou, M., Belc, N., Biliaderis, C. (2007). *Journal of Food Engineering*, 79, 1033-1047.
6. Moreira, R., Chenlo, F., Torres, M.D., Prieto, D.M. (2012). *Food Biopr. Tech.*, 5, 2301-2310.

## Perspectives in Fundamental and Applied Rheology

### *Contact Address:*

*Ramón Moreira ( ramon.moreira@usc.es)  
Chemical Engineering Department, ETSE  
Universidade de Santiago de Compostela  
Rua Lope Gómez de Marzoa, s/n, 15782 Santiago de Compostela.  
Telf.: +34 881 816 759.*

## CHAPTER 9

# Fat replacement in biscuits by sunflower oil-water-cellulose emulsions. Effect in dough oscillatory and creep properties

*Paula Tarancón<sup>1</sup>, Teresa Sanz<sup>1</sup>, María Jesús Hernández<sup>2</sup> & Ana Salvador<sup>1</sup>*

*<sup>1</sup> Instituto de Agroquímica y Tecnología de Alimentos (CSIC), Apartado de Correos 73, 46100, Burjassot (Spain)*

*<sup>2</sup> Departament de Física de la Terra i Termodinàmica, Universitat de València, 46100, Burjassot, Valencia( Spain)*

### Introduction

Fat mostly employed in biscuit manufacturing contain a high percentage of saturated fatty acids, which confer a solid consistency necessary for biscuit manufacture [1]. Due to health reasons the reduction of saturated fatty acids and trans fatty acids is desired [2]. An emulsion composed of sunflower oil, water and cellulose ether is employed in this work to completely replace the conventional fat of a short dough recipe.

The aim of the present work was to characterize the differences in biscuit dough structure induced by the replacement of conventional fat by the sunflower oil cellulose emulsions by means of the study of the linear viscoelastic properties by using oscillatory and creep tests. The effect of the methoxyl and hydroxypropyl content of the cellulose was evaluated and the results were also related to final biscuit dimensions and texture.

### Experimental Methods

#### *Formulation of dough*

Dough ingredients were soft wheat flour 100%, shortening (total fat: 78.4%, saturated fatty acids: 51%, monounsaturated fatty acids: 20%, polyunsaturated fatty acids: 6%, trans fatty acids < 2%) or shortening replacer 32.15%;, sugar 29.45%, milk powder 1.75%, salt 1.05%, sodium bicarbonate 0.35, ammonium hydrogen 0.2% and tap water 9%. In the formulations with a shortening replacer, glycerol (3.2%) was also added to control the water activity.

## Perspectives in Fundamental and Applied Rheology

Four oil-water-cellulose ether emulsion with different cellulose ethers were used as shortening replacer [3]. Cellulose ethers with thermogelling ability and the same viscosity (4000 mPas) (2 % aqueous solution at 20 °C) were employed.

### *Rheological measurements*

Oscillatory and creep and recovery tests were performed at 25°C in a controlled stress rheometer (AR-G2, TA Instruments, Crawley, England) with the temperature controlled by a Peltier system. The rheometer was equipped with a 20mm roughened parallel plate with a gap of 3.5 mm. Dough test-pieces of 23.3 mm internal diameter were placed on the rheometer and kept in the measurement position for a 10 min for equilibration time. To protect against dehydration, vaseline oil was applied to the exposed surfaces of all the samples.

Stress sweeps were carried out at a frequency of 1 Hz to determine the extension of linear viscoelastic response. A stress amplitude of 3 Pa was chosen in order to perform frequency sweeps from 10 to 0.01 Hz. Storage modulus ( $G'$ ), loss modulus ( $G''$ ) and loss tangent ( $\tan\delta = G''/G'$ ) values were recorded.

To perform the creep test, an instantaneous shear stress ( $\sigma_0$ ) was applied in dough sample and the sample strain was recorded as a function of the creep time. The results were expressed as compliance  $J(t)$  [1/Pa], by the following formula:  $J(t) = \gamma(t) / \sigma_0$ . The shear stress applied during the creep phase was selected within the linear viscoelastic region (3 Pa) and maintained for 1200s.

### *Statistical analysis*

One way-ANOVA was applied to study the differences among formulations and creep and rheological parameters were correlated with texture properties.

A Principal Component Analysis (PCA) was used to correlate the creep and rheological parameters with dough texture properties. These analyses were performed using the statistical software XLSTAT, 2009.4.03 (Addinsoft, Barcelona, Spain).

## **Results and Discussion**

### *Creep tests*

The conventional dough and the dough prepared with the different cellulose emulsions showed different viscoelastic properties. The cellulose emulsion dough's showed higher values of compliance during the creep test, indicating higher deformability than the control dough. Conversely, the lower compliance values in control are indicative of lower deformation ability and thus a stronger matrix structure (Figure 1).

The higher  $J(t)$  values for the cellulose emulsion dough's may be associated to the employment of a liquid oil as a fat source, as the lubrication effect of fat has been associated with the liquid oil fraction in the shortening. The creep data ( $0 \leq t \leq 1200$  s) were satisfactorily fitted to the Burger model made up of four components.

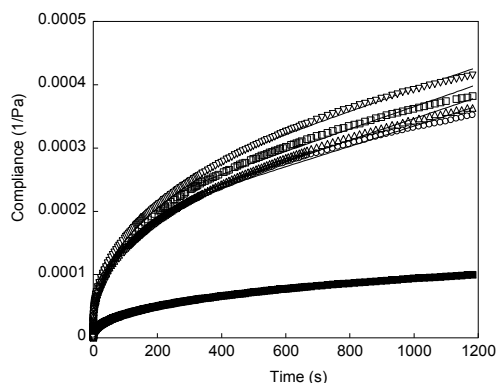


Figure 1. Compliance versus time in the creep test for the different formulations. ■ Control, □ HPMCE, △ HPMCF, ▽ HPMCK, ○ MCA.  $T=25^{\circ}\text{C}$ . Continuous lines represent adjustment to the Burger model.

### Oscillatory tests

Differences in the evolution of  $\tan \delta$  with the frequency were observed in control and cellulose emulsion dough's (Figure 2). This suggests that the replacement of shortening by the cellulose emulsion induces a change in the network structure of the dough. In particular at the low frequency range  $\tan \delta$  values were noticeable lower than in control sample (Figure 2). This result shows a notable increase of the elastic nature of cellulose emulsion dough's, which could be related with the glycerol that has been added in the product formulation. So, the glycerol may increase the number of hydrogen bonds with water and with cellulose emulsion providing the structural stabilization which is observed better at higher oscillation times (low frequency).

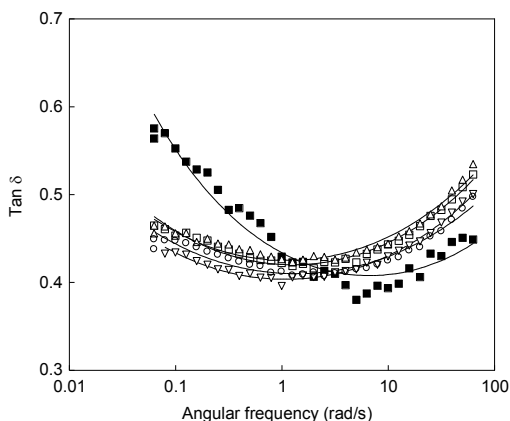


Figure 2.  $\tan \delta$  as a function of frequency for the different formulations  $\blacksquare$  Control,  $\square$  HPMCE,  $\triangle$  HPMCF,  $\nabla$  HPMCK,  $\circ$  MCA.  $T=25^{\circ}\text{C}$ .

*Correlations between creep and oscillatory results, dough texture, biscuit texture and spread properties*

To better understand the relationship among the creep and oscillatory results and the values of the dough texture, the biscuit texture and the biscuit dimensions measurements obtained in a previous work [3], a principal component analysis (PCA) was carried out (Figure 3).

The first component that explains 80.7% of the variance clearly separates the cellulose doughs from the control. All the cellulose doughs appear in the positive part of PC1, while the control dough appears separated in the negative part (Figure 3a).

The cellulose doughs are related to the creep parameters  $G_1$  and  $\eta_0$  and with the biscuit diameter and thickness. The texture dough parameters cohesiveness and springiness also appear separated in the positive part of PC1.

In the negative part of PC1, associated to control sample, appear the creep parameters  $G_0$  y  $\eta_1$ , the oscillatory parameters ( $G'$  and  $G''$ ) and the dough texture parameter hardness.

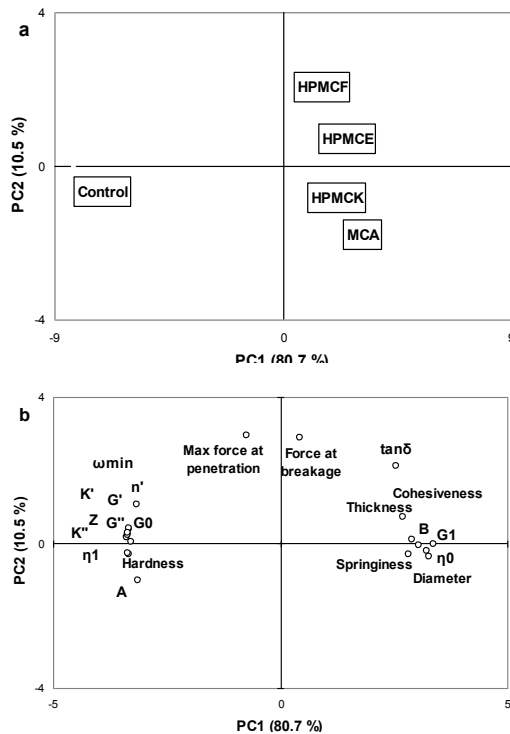


Figure 3. Two-dimension PCA plot of the variations in rheological parameters, textural parameters and dimensions among control dough and cellulose ethers dough.

The similarity in the biscuit texture properties among the control and the cellulose doughs' is one of the positive aspects of the employ of the cellulose emulsion as fat substitute, as reduction of fat content has always been associated with a negative increase in biscuit hardness. Therefore the differences in dough rheology and texture can only explained the biscuit dimension parameters.

### Concluding remarks

Clear differences in the viscoelastic properties among the control dough and the dough formulated with the cellulose emulsion were found. The type of cellulose did not exert a significant influence in the viscoelastic properties.

In the creep tests, the cellulose emulsion dough's showed significantly higher deformability. The oscillatory test reveals a notable structural stabilization at lower frequencies due to the greater elastic component relative to the viscous. The higher deformation of the cellulose dough's is compatible with the highest elastic nature at larger time scales and was associated to higher spreadness and diameter in the final biscuit.

### References

1. Lee, J. H., Akoh, C. C., & Lee, K. (2008). Physical properties of trans-free bakery shortening produced by lipase-catalyzed interesterification. *JAOCS, J Am Oil Chem Soc*, 85(1), 1-11.
2. Akoh, C.C. (1998). Fat replacers. *Food Technol.* 52, 47–53.
3. Tarancón, P., Salvador, A. and Sanz, T. (2012). Sunflower Oil–Water–Cellulose Ether Emulsions as Trans-Fatty Acid-Free Fat Replacers in Biscuits: Texture and Acceptability Study. *Food Bioprocess Tech*, DOI 10.1007/s11947-012-0878-6.

### Contact Address:

*Teresa Sanz (tesanz@iata.csic.es)*  
*Instituto de Agroquímica y Tecnología de Alimentos (CSIC)*  
*Avda. Agustín Escardino 7, 46980-Paterna (Valencia)*  
*Telf.: +34963900022*  
*Fax: +3496636301*

## CHAPTER 10

# Effect of high-pressure on the viscoelastic properties of aqueous glucomannan dispersions

V. Bargiela<sup>1</sup>, B. Herranz<sup>2</sup>, A.J. Borderías<sup>2</sup> C. A. Tovar<sup>1</sup>

<sup>1</sup> Dpto. Física Aplicada, Facultad de Ciencias de Ourense. Universidad de Vigo (Spain).

<sup>2</sup> Departamento de Productos, Instituto de Ciencia y Tecnología de los Alimentos y Nutrición (CSIC), (Spain).

### Introduction

Konjac glucomannan (KGM), a neutral polysaccharide derived from the tuber of *Amorphophallus konjac* C. Koch [1], can be used to improve the fish protein functionality lost in processing. KGM forms a time-stable gel after addition of 0.6 N KOH as alkaline coagulant [2]. Gelation occurs through the formation of a three-dimensional network by junction zones stabilized principally by hydrogen bonds and other physical interactions such as coulombic, dipole-dipole, van der Waals and hydrophobic interactions [3]. Previous papers explored the influence of thermal conditions [4, 5] and KGM concentration [6] on the rheological and structural characteristics of aqueous glucomannan dispersions (AGD). These studies provided an ample view of thermal effects on the transient properties of physical networks. Temperature acts via increases of both kinetic energy and free volume. It may therefore be useful to analyse how the pressure affects the dynamic behaviour of KGM molecules in AGD dispersions, since pressure mainly affects system volume and has a large range of applications in the food industry. Besides reducing the initial microbial load, high pressure (HP) improves the functional properties of muscle proteins [7] and induces denaturation, aggregation or gelation of myofibrillar proteins depending on the pressure level, time and temperature of the pressure treatment [8]. It could therefore offer an alternative process to induce gel formation, without heating, to obtain products resembling raw fish [9].

This work is the first step of a study whose objective is to determine the influence of high pressure on viscoelastic properties of AGD depending on pH in order to use HP treatment for making restructured seafood products. In particular,

the aim of the present chapter is to explore the effect of increasing pressure on the viscoelastic characteristics of AGD dispersions with 3% KGM and pH 9.36 (near the point of gelation), in order to choose the most suitable pressure conditions for making restructured seafood products.

### Experimental Methods

Aqueous glucomannan dispersions (3%) (w/v) from konjac (glucomannan purity 100%, Guinama, Valencia, Spain) were prepared by continuous stirring for 30 min at low speed in a vacuum homogenizer (Stephan UM5, Stephan u. Söhne GmbH & Co., Hameln, Germany) at 60 °C. Then KOH (Panreac Química, S. A., Barcelona, Spain) was added to increase the pH to 9.36, mixing for 1 minute at 50 rpm to induce gel formation. Cylindrical plastic containers were then filled with this mixture and left to set, for 1 hour at 30 °C and then 4 hours at 5 °C. Once the samples had set, they were placed in a 0.2 M citrate-phosphate buffer at pH 5 for 20 hours.

Gels were then subjected to HP of 100 MPa (lot A), 200 MPa (lot B), 400 MPa (lot D) and 600 MPa (lot E), all for 10 min at 25 °C. In addition, an unpressurized lot (lot C) was made. Small amplitude oscillatory shear (SAOS) data were gathered using a Bohlin CVO controlled stress rheometer (Bohlin Instruments, Inc. Cranbury, NJ) and a RS600 Haake rheometer (Thermo Electron Corporation Karlsruhe, Germany). In both rheometers the measurements were carried out using a parallel plate (20 mm in diameter and 1 mm gap). The temperature of the lower plate was kept at 25.0±0.1 °C. Stress sweeps were obtained from 1 to 800 Pa at frequency 1 Hz. Frequency sweeps were performed over the range 0.01–10 Hz, keeping  $\gamma=1\%$  constant within the linear viscoelastic (LVE) region. Transient tests were carried out under constant stress ( $\sigma$ ) within LVE range for 600 s, followed by a further 600 s recovery time to obtain the reformation curve.

### Results and Discussion

#### *Linear viscoelastic (LVE) range*

Stress sweeps were used to determine the influence of increasing HP on the limit values of the LVE range: stress ( $\sigma_{max}$ ) and strain ( $\gamma_{max}$ ) amplitudes and rigidity ( $G^*$ ) for 3% AGD. These showed that the rigidity ( $G^*$ ) of pressure-treated AGDs was significantly higher ( $p<0.05$ ) than in the control (C) (Table 1).  $G^*$  in B was slightly

higher than in the rest, indicating non-linear dependence between HP and rigidity of pressurized AGDs.

Table 1. High pressure effect on the limit parameters of the LVE range for 3% aqueous glucomannan dispersions (AGD). Stress amplitude,  $\sigma_{max}$ , strain amplitude,  $\gamma_{max}$  (%) and complex modulus,  $G^*$ . T=25 °C.

Sample	$\sigma_{max}$ (Pa)	$\gamma_{max}$ (%)	$G^*$ (kPa)
<b>C</b>	87±9 <sup>a</sup>	11.4±1.9 <sup>c</sup>	0.79±0.11 <sup>e</sup>
<b>A</b>	105±11 <sup>a</sup>	10.5±0.89 <sup>c</sup>	1.01±0.09 <sup>f</sup>
<b>B</b>	194±19 <sup>b</sup>	18.1±1.5 <sup>d</sup>	1.08± 0.08 <sup>f</sup>
<b>D</b>	158±16 <sup>b</sup>	15.3±1.9 <sup>d</sup>	1.05±0.13 <sup>f</sup>
<b>E</b>	178±18 <sup>b</sup>	17.4±0.56 <sup>d</sup>	1.02±0.03 <sup>f</sup>

<sup>a-f</sup> Different letters in the same column indicate significant differences with high pressure effect ( $P<0.05$ ).

In the case of  $\sigma_{max}$  and  $\gamma_{max}$ , there was a particular increase of firmness and structural stability at 200 MPa (B), as evidenced by the fact that  $\sigma_{max}$  and  $\gamma_{max}$  were significantly higher than in C and A (Table 1). This indicates that ~200 MPa is a high enough pressure to improve conformational stability and molecular flexibility [10]. HP causes a reduction of the free volume in the KGM matrix, resulting in increased polymer-polymer contacts due to hydrogen bonds, van der Waals and hydrophobic interactions [3]. Moreover, it is possible that HP produces partial disruption of junction zones, reducing the number of KGM chains that act cooperatively in junctions. Thus, HP could reduce the molecular association (cross-linking level) in junction zones and so reduces the degree of order in the AGD superstructure. This contributes to a reduction of the junction thickness, consequently enhancing the conformational flexibility of pressurized AGDs, as evidenced by the fact that  $\sigma_{max}$ , and  $\gamma_{max}$  were higher in B (more noticeable), D and E than in C, (Table 1). This rheological behaviour is compatible with the increase of  $G^*$  in pressurized AGDs with respect to C (Table 1), since the chain fragments resulting from the partial breakage of junctions may reorganize. These molecular fragments detached from the principal network could also form new cross-links among themselves, increasing the overall rigidity of A, B, D and E relative to C.

*Mechanical spectra*

Viscoelastic moduli have been fitted to the power law (eq. 1 and 2).

$$G' = G'_0 \cdot \omega^{n'} \quad (1)$$

$$G'' = G''_0 \cdot \omega^{n''} \quad (2)$$

Experimental values of  $G'$  and  $G''$  moduli varied depending on the frequency range selected.

From 10 to 0.15 Hz,  $G'$  was somewhat higher and more frequency-dependent than  $G''$ , indicating weak solid-like behaviour. The gel-sol transition was registered between 0.10 and 0.06 Hz (crossover interval) where  $G' \approx G''$ . After the transition zone, at frequencies lower than 0.06 Hz,  $G''$  was slightly higher than  $G'$  (Figure 1), indicating loss of molecular connectivity resulting in the predominance of viscous response in AGD samples. However, there was no sign that high pressure significantly influenced these results.

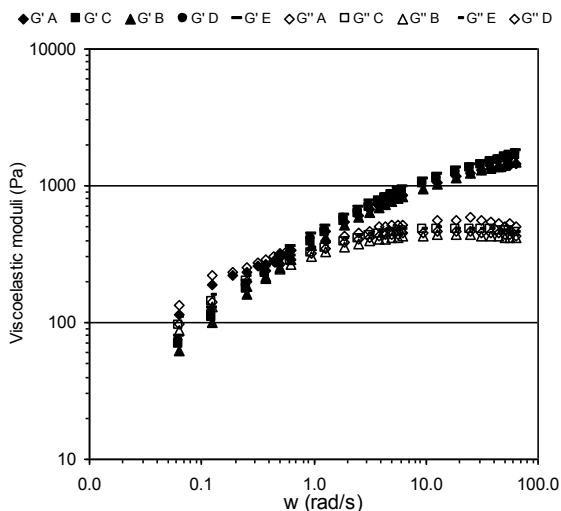


Figure 1. Influence of high pressure on Mechanical spectra of the AGDs.  $T=25^{\circ}\text{C}$ .

In the case of frequency dependence,  $G'$  showed two trends irrespective of pressure treatment: one, between 10 and  $\sim 0.15$  Hz where  $G'$  presented less frequency-dependence,  $n' = 0.290 \pm 0.008$  (similar for all AGDs); and another, from the crossover to the lowest frequency, where  $n'$  significantly increased

( $n' \approx 0.630 \pm 0.011$ ), indicating that the AGD matrix was more time-dependent and less stable conformationally in the low frequency range, which is consistent with the sol state at low frequencies.

However, the frequency-dependence of  $G''$  moduli was noticeably different from  $G'$ . In the high-frequency range (from 0.15 to 10 Hz),  $G''$  values flattened, while, in the low-frequency range (from 0.01 to 0.2 Hz)  $G''$  decreased continuously to the lowest frequency (Figure 1) more slowly ( $n'' \approx 0.430 \pm 0.020$ ) than  $G'$  ( $n' \approx 0.630 \pm 0.011$ ) in the same frequency range. Thus, the viscoelastic response in the low frequency range reflects structural changes which are characteristic of the phase transition in this case from gel (high frequencies) to sol (low frequencies). Since any (quelquer) gelation process is a critical phenomena where the transition variable is the connectivity [10]. In these AGDs, the degree of connectivity was progressively reduced as the frequency decreased due to the shear stress which broke some physical links, as evidenced by  $n' \gg n''$ , irrespective of the HP value.

#### Creep and Recovery Compliances

Creep experiments are conducted by applying constant stress ( $\sigma_0$ ), within the LVE range. The shear deformation  $\gamma(t)$  is recorded with time [11], which gives the time-dependent compliance  $J(t)$  on larger time scales. This is a measure of the softness of samples [12].

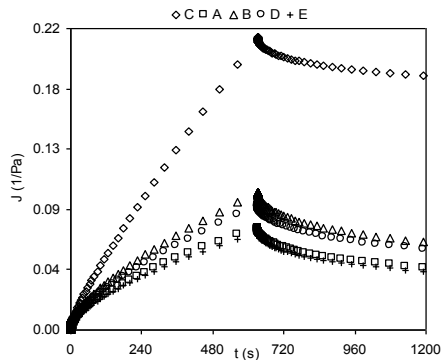


Figure 2. Influence of high pressure on creep and recovery compliances of the AGD samples.  $T=25^{\circ}\text{C}$ .

In the case of the control sample,  $J(t)$  values were highest during both creep and recovery times. This indicates that during loading there may be a more intense and irreversible junction scission, lowering the structural resilience, as evidenced

by the high  $J(t)$  through the recovery time. However when HP was applied, creep-recovery  $J(t)$  data significantly decreased in samples A (100 MPa) and E (600 MPa) similarly, and more effectively than in the others (Figure 2). Pressure reduces the free volume in the system, thus increasing the inter-chain attractions and probably inducing mechanical aggregation of KGM chains, which would increase the firmness of AGDs. However, this HP-induced aggregation may be partially reversible due to the physical nature of hydrogen bonds and electrostatic interactions, since they can mechanically break and recombine [13]. This fact could explain the non-linear dependence between rigidity of AGD and the HP value, which is consistent with the transient nature of the physically cross-linked networks [2].

### Conclusions

The effect of high-pressure treatment on the viscoelastic properties of 3% aqueous glucomannan dispersions varied depending on the kind of test. Mechanical spectra were practically pressure-independent, but they showed that at pH=9.36, there was a phase transition from gel to sol with decreasing frequency in the glucomannan dispersions. In the case of stress sweeps and creep-recovery tests, there was a considerable increase of rigidity and conformational stability in the pressurized samples, as evidenced by the fact that their complex modulus and stress and strain amplitudes were higher than in the control. Moreover, creep-recovery compliances were lower than in the control. All these viscoelastic data were mutually consistent, indicating that high pressure reinforced molecular packing of KGM chains; this caused the formation of new thin junctions, originating more flexible and stable AGDs mechanically stabilized by physical cross-linkings. Stress sweeps indicated that 200 MPa was a suitable pressure for improving the consistency and structural flexibility of glucomannan dispersions.

### Acknowledgements

Thanks to the Xunta de Galicia for its financial support under the Consolidation and restructuring program of competitive research units: Strategic Research Partnerships (2009/060) and project AGL2011-24693.

### References

1. Nishinari, K., Williams, P. A., and Phillips, G. O. (1992). *Food Hydrocolloids* 6, 199–222.
2. Herranz, B., C. A. Tovar, Solo-de-Zaldivar, B., and Borderias, A. J. (2012a). *Food Hydrocolloids* 27(1): 145–153.

## Part II: Food, Cosmetics and Pharmaceutical Products

3. Lapasin, R., and Prici S. (1999). *Rheology of Industrial Polysaccharides: Theory and Applications*. Gaithersburg: Aspen Publishers.
4. Herranz B., Borderias, A. J., Solo-de-Zaldívar, B., Solas, M. T., & Tovar, C. A. (2012b). *Food Hydrocolloids*, 29(1), 85-92.
5. Herranz B., Borderias, A. J., Solas, M. T., and Tovar, C. A. (2012c). *Food Res. Int.* 48, 885-892.
6. Herranz B., Tovar, C. A., Solo-de-Zaldívar, B. and Borderias, A. J. (2013). *LWT-Food Sci. and Technol.* 51, 500–506. .
7. Marcos, B., Kerry, J. P. and Mullen, A. M. (2010). *Meat Sci.* 85, 115–120.
8. Uresti, R. M., Velazquez, G., Vázquez, M., Ramírez, J. A. and Torres, J. A. (2005). *Food Hydrocolloids* 19, 964-973.
9. Uresti, R. M., Velazquez, G., Ramírez, J. A., Vázquez, M., and Torres, J. A. (2004). *J. Food Sci. and Agric.* 84, 1741–1749.
10. Rao, M. A. (2007). *Rheology of Fluid and Semisolid Foods. Principles and Applications* (2nd ed.). New York: Springer.
11. Mezger, T. G. (2006). *The Rheology Handbook*. Vincentz Network, Hannover.
12. Sperling, L. H. (2001). *Physical Polymer Science*. John Wiley and Sons. Canada.
13. Tanaka, F. and Edwards, S. F. (1992). *J. Non-Newtonian Fluid Mech.* 43, 247–271.

### Contact Address:

*Beatriz Herranz Hernández (beatriz.herranz@ictan.csic.es)*

*Departamento de Productos, Instituto de Ciencia y Tecnología de los Alimentos y Nutrición (CSIC), (Spain).*

*Tel.: +34 91 549 2300. Fax: +34 91 549 3627*



## CHAPTER 11

# Influence of pH and type of acid anion on the linear viscoelastic properties of Egg Yolk

*Aguilar, J.M., Cordobés, F., De la Fuente, J., and Fernández-Espada, L.*

*<sup>1</sup> Departamento de Ingeniería Química, Facultad de Química, Universidad de Sevilla (Spain)*

### Introduction

The native conformation of a protein can be explained in terms of a net balance between attractive and repulsive forces. Proteins present a maximum stability at the isoelectric point. Thus, any change in the environmental conditions (as pH or chaotropic salts) can modify and modulate the functional properties of proteins to a large extent.

Extreme pH values cause a high net charge leading to electrostatic repulsion between neighbour molecules and modifying the charge distribution among the amino acid side chains. As a consequence, changing pH to extreme values is a well known method for protein denaturation at low temperature [1].

Ion effects in biological systems were firstly investigated by Hofmeister and co-workers. They published a series of papers in which they showed that salts could be classified according to their salting-in and salting-out behaviour against proteins precipitation [2]. Nowadays, this specific ion effects make up the Hofmeister phenomena and the series of cations and anions are usually given in terms of the ability of the ions to stabilize the structure of proteins [3]. However, there is not a single and unique Hofmeister series, and, in general, cation effects are less pronounced than specific anion effects [4].

The objective of this study is to assess the influence of pH, as well as the contribution of each anion to the linear viscoelastic properties of egg yolk.

### Experimental

#### *Materials*

Egg Yolk (EY) was obtained from grade A, type L (63-73 g) fresh chicken eggs according to EU specifications. Any cracked or damaged egg was discarded and

the yolk was carefully extracted from the eggs by the Harrison & Cunningham preparation method [5]. Analytical grade Hydrochloric acid (37%) was obtained from Fisher Scientific (France). Chemically pure grade (purissimus) Citric acid anhydrous and Orthophosphoric acid (85%) were obtained from Panreac (Spain).

*Methods*

EY dispersions were obtained by dilution of native EY (50-52 wt% in solid content). The native pH of the system (ca. pH 6) was modified using solutions (1-5 M) of citric, or hydrochloric, or orthophosphoric acid. Samples with pH values 2-6 were prepared by adding the suitable acidulant and demineralised water in order to reach the desired pH ( $\pm 0.2$  pH units) in a EY dispersion with a 45 wt% in solids content. Samples were refrigerated overnight at 4°C.

Frequency sweep tests of egg yolk dispersions containing 45 wt% in solids at different pH values were performed by means of an AR-2000 (TA Instruments, UK) using a low-inertia 60 mm aluminium plate-plate geometry with 1 mm gap. As the viscoelastic response is different in the experimental frequency range ( $10^{-2} - 10^2$  rad/s), it was subdivided in several intervals overlapping at the ends of the range. Any measurement was carried out at 20 °C and at a stress clearly lower than the critical value for linear viscoelasticity. All samples were placed at room temperature for 30 min before their loading on the sensor. Afterwards, they were sealed with vaseline oil to prevent their drying during the test of samples. At least two replicates were performed for each rheological test.

**Results and Discussion**

Figure 1 shows stress sweep tests of EY (45 wt%) at 1 rad/s. It can be clearly seen that the three dispersions exhibit a predominantly viscous behaviour at pH 4.

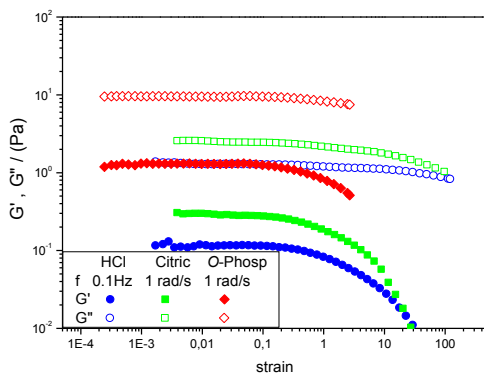


Figure 1. Stress Sweep Tests at 1 rad/s and 2 °C for EY (45 wt%) acidified until pH 4 using different acids.

A wide LVR is always found, although the critical strain depends on frequency, pH and the type of acid (i.e. a slightly smaller value may be observed in Fig. 1 when ortho-phosphoric acid is used).

Figure 2 and 3 compare mechanical spectra of EY dispersions for the three acids studied, at pH 4 and 2, respectively. The native EY (45 wt% at pH 6) is also plotted in both figures as no acid. As may be appreciated the ortho-phosphoric acid leads to moderate changes in the viscoelasticity behaviour of native EY, that become more apparent at low pH.

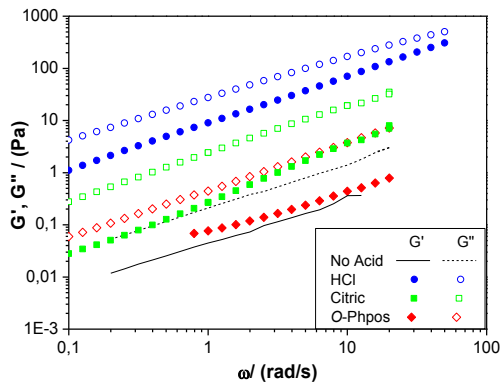


Figure 2. Mechanical Spectra at 20 °C for EY dispersions (45 wt% solids content) acidified until pH4 using different acids.

All the mechanical spectra plotted in Fig. 2 correspond to a predominantly viscous behaviour in which  $G''$  is always higher than  $G'$  within the experimental frequency range. This behaviour is typical of relatively dilute dispersions such as that corresponding to the native EY. Only a certain tendency to find a crossover between both moduli at high frequency may be noticed for the HCl-acidified dispersion.

On the other hand, the behaviour shown by EY at pH 2 (acidified by HCl or citric acids) is completely different to that one exhibited at pH 4 or 6. Both acids lead to a gel behaviour characterized by values of  $G'$  being much higher than  $G''$  where both functions show almost no dependence on frequency. This behaviour contrasts with the fluid-like behaviour displayed by the dispersion acidified with ortho-phosphoric acid.

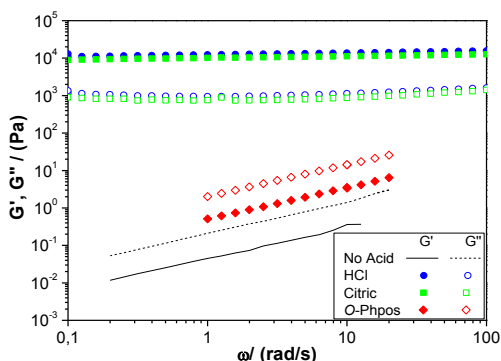


Figure 3. Mechanical Spectra at 20 °C for EY dispersions (45 wt% solids content) acidified until pH 2 using different acids.

Figure 4 shows the evolution of the complex modulus at 1 rad/s ( $G_1^*$ ) as a function of pH for EY dispersions (45 wt% solids content) using the three acids under study. The higher values of this parameter correspond to the use of hydrochloric acid, whereas the use of *o*-phosphoric acid produced the lower values. In any case, all studied acids exhibit an increase of this parameter as the pH decrease. However, a higher slope can be observed when the pH decrease from moderate pH values (3 or 4) to pH 2. This effect is still more pronounced for citric and hydrochloric acids, for which the complex modulus,  $G_1^*$ , increases in several orders of magnitude. However, it should be noted that this evolution doesn't correspond to the original sequence established by Hofmeister, according to which, citric and *o*-phosphoric acid should exhibit a higher structure-making effect, thus limiting the amount of available water to hydrate protein molecules. This difference may be related to the fact that under the experimental conditions, proteins present a positive surface charge, whereas in the original sequence the protein surface was negatively charged. This difference may be regarded as responsible for the inversion of the sequence, which would explain the higher values (except for pH 2) corresponding to hydrochloric acid.

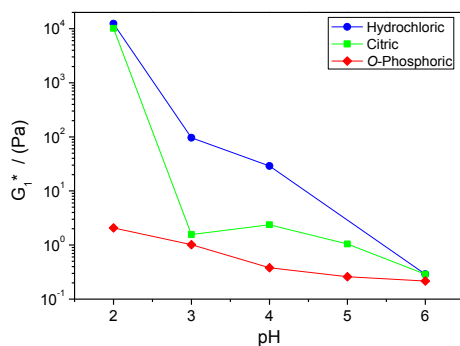


Fig. 4 Evolution of complex modulus values at 1 rad/s for EY (45 wt%) dispersions as function of pH and type of acidulant.

Furthermore, citric acid is hardly dissociated at pH 2 and present low ability to neutralize the charged protein residues, whereas hydrochloric, being a strong acid, is fully dissociated at all pH values. As for the *ortho*-phosphoric acid, it exhibits a unique anionic species in the experimental pH range. The sharply  $G_1^*$  profile found for citric acidified EY has to be related to a higher amount of anionic species with increasing pH.

The evolution of loss tangent at 1 rad/s as a function of pH is plotted in Figure 5. As shown, most of the systems under study exhibit a clearly predominant viscous component over the elastic one, with loss tangent values between 3 and 9. However, when the pH value decreases to 2, the values of this parameter fall to values less than one, leading to a predominantly elastic behaviour.

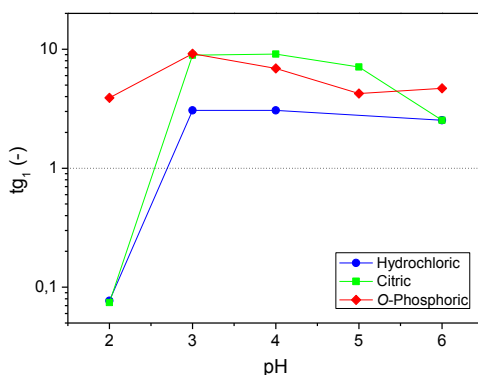


Fig. 5 Evolution of loss tangent values at 1 rad/s for EY dispersions (45 wt%) as a function of pH and type of acid.

## Conclusions

The reduction of pH media leads to an increase on the viscoelastic properties of EY dispersions for the three acids under study. This increase depends on the pH value and the type of acid used.

The addition of Hydrochloric or Citric acid showed a similar behaviour leading to a gel formation when the pH 2 is reached. But, this change is more sharply when the citric acid is used, which may be related to the different dissociation pattern of its ionic species.

On the other hand, the addition of *ortho*-Phosphoric acid showed a more moderate dependency of the viscoelastic properties on the pH values, without any sol-gel transition taking place within the experimental pH range. These results suggest that dihydrogen-phosphate anion exerts a certain inhibition effect on the hydrophobic interactions and hydrogen bonds between protein segments.

## Acknowledgements

Authors acknowledge financial support of this work by the Andalusian Government through the project TEP-6134-2010.

## References

1. Damodaran, S. (2010). In: Fennema Química de los alimentos (Damodaran, S., Parkin, K.L., and Fennema, O.R.), Vol. 5, pp. 215-325, 3rd edn, Acribia, Zaragoza.
2. Kunz, W., Henle, J., and Ninham, B.W. (2004). *Curr Opin Colloid & Interface Sci.* 9, 19-37.
3. Vrka, L., Jungwirth, P., Bauduin, P., Touraud, D., and Kunz, W. (2006). *J. Phys. Chem. B* 110, 7036-7043.
4. Kunz, W. *Curr. Opin. in Colloid & Interface Sci.* 15, 34-39.
5. Harrison, L.J., and Cunningham, F.E. (1986). *Poultry Sci.* 65, 915-921.

## Contact Address:

*J.M. Aguilar (jmaguilar@us.es)*

*Department of Chemical Engineering, Faculty of Chemistry*

*University of Seville*

*Campus de Reina Mercedes, c / Profesor García González, s/n, 41012 - Sevilla*

*Telf.: +34 954557179 ; Fax: +34 954556447*

## CHAPTER 12

# Influence of Lipids on the Rheological Properties of Amimulsion – a new safe cosmetic emulsion

*J. Marto<sup>1,2</sup>, M.T. Cidade<sup>2</sup>, L. Gouveia<sup>1</sup>, E. Oliveira<sup>3</sup>, A.J. Almeida<sup>1</sup> and H.M. Ribeiro<sup>1</sup>*

*<sup>1</sup>Research Institute for Medicines and Pharmaceutical Sciences (iMed.UL), Faculdade de Farmácia da Universidade de Lisboa, Lisboa, Portugal*

*<sup>2</sup>Cenimat/13N, Departamento de Ciência dos Materiais, Faculdade de Ciências e Tecnologia, FCT, Universidade Nova de Lisboa, 2829-516 Caparica, Portugal*

*<sup>3</sup>Laboratórios Atral S.A. (Grupo AtralCipan), Castanheira do Ribatejo, Portugal*

### Introduction

Cosmetic water in oil emulsions are complex multiple-phase systems which may contain a number of interacting surfactants, fatty amphiphiles (e.g. alcohols), polymers, and other excipients as structuring agents [1]. Understanding the forces and mechanisms of interactions in disperse systems, as well as knowing the morphology, size, charge and stability of self-assembled aggregates, is a central point in developing new materials and improving the effectiveness of the already available materials [2,3]. Studying their complex structure is quite a difficult task, which entails great care. The presently available methods give information about the presence of the multiple droplets, about their structure and size distribution directly or indirectly. Microscopic techniques can be used as direct method for droplet analysis [4].

In this work, the rheological behaviour and the microscopic analysis of two w/o semi-solid emulsions, differing only in the lipid used (Amimulsion EA and Amimulsion EB), intended for topical application and prepared using a cold emulsification process, were studied.

### Experimental

#### *Emulsion processing*

Two surfactant-free w/o semi-solid Amimulsions (emulsions stabilized by solid particles - polymer) were prepared using a modification of a cold emulsification

process, as described elsewhere [5]. The Amimulsions contain well-known pharmaceutical excipients differing only in the lipid used:

Amimulsion EA (lipophilic emollient - triglycerides);

Amimulsion EB (lipophilic occlusive - hydrocarbons).

### *Microscopy*

A computerised image analysis device coupled to an Olympus microscope (Olympus BX51, Germany), was used for the microscopic observations, in bright field to determine emulsions' droplet size. Samples were examined one day after preparation. Droplet samples were photographed and slides were made so that droplets ( $n \geq 625$ ) could be measured [6]. The droplet size was statistically analysed in order to assess the size distribution and to determine the geometric standard deviation ( $\sigma_g$ ).

### *Rheological analysis*

The rheological measurements were obtained using a Bohlin Gemini HR<sup>Nano</sup> Rheometer (Malvern, UK) using cone and plate geometry (truncated cone angle 2.0° and radius 20 cm), at two different temperatures, 25°C and 37°C. All samples were tested 1 month after preparation and storage at 25°C, at least in triplicates using fresh samples.

Steady state shear measurements were performed for shear rates ( $\dot{\gamma}$ ) between 1 and 1000 s<sup>-1</sup>.

Oscillation frequency sweep tests were performed over a frequency range from 1 and 100 rad s<sup>-1</sup>.

## **Results and Discussion**

### *Microscopy and particle size analysis*

The light microscopy images and the plot of the particle size distribution revealed that the size of droplets and the microstructure of the systems depended on the lipid used (Fig. 1 to Fig. 4).

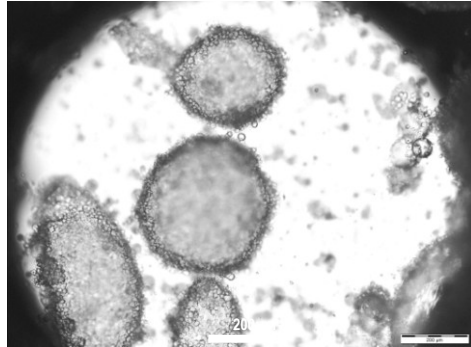


Fig.1 Photomicrographs of Amimulsion EA (magnification 100x).

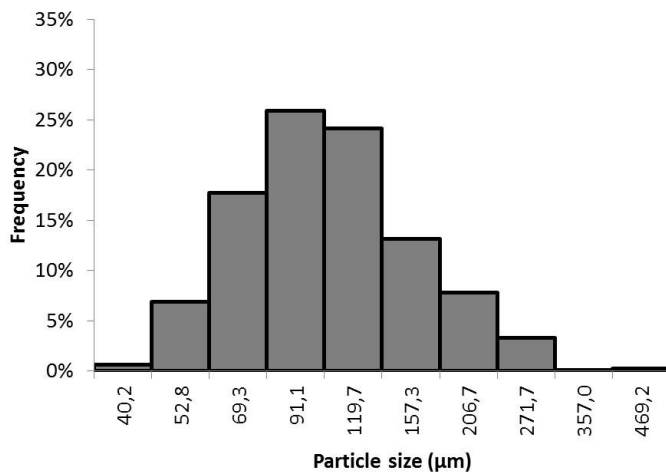


Fig. 2 Droplet size distribution of Amimulsion EA. Median particle size = 125.2  $\mu\text{m}$  and  $\sigma_g = 188$ .



Fig.3 Photomicrographs of Amimulsion EB (magnification 100x).

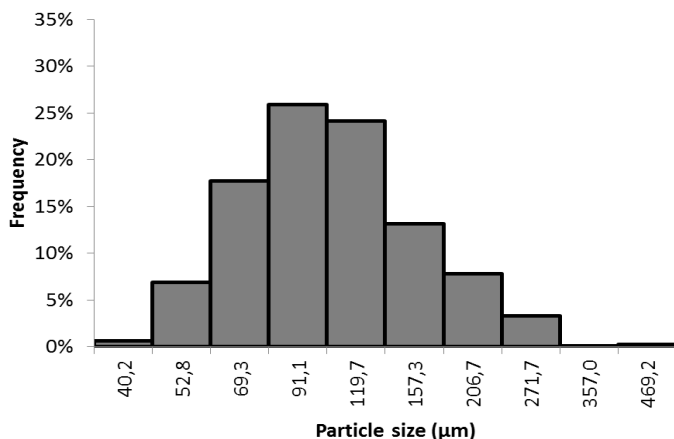


Fig. 4 Droplet size distribution of Amimulsion EB. Median particle size= 103.3 µm and  $\sigma_g=180$ .

In the case of Amimulsion EA bigger inner droplets with a non-homogeneous size were observed (Fig. 1 and Fig. 2). Amimulsion EB presented several small inner droplets of water in the oil phase. The droplets presented a symmetric and a well defined microstructure (Fig. 3 and Fig. 4). Droplet size differences between these emulsions are probably due to affinity of the lipids for the internal phase.

*Rheological analysis*

Continuous shear experiments measure the ability of each system to resist structural breakdown during the standardized shearing procedure. Representative flow curves are shown in Fig. 5 and Fig. 6 for both emulsions at the same temperature (25°C and 37°C, respectively).

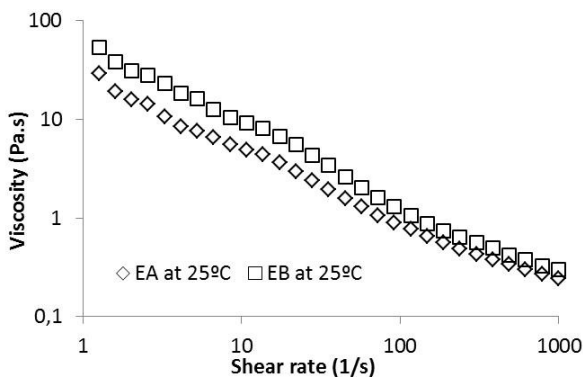


Fig. 5 Viscosity as function of shear rate for both Amimulsions at 25°C (average from 3 experiments).

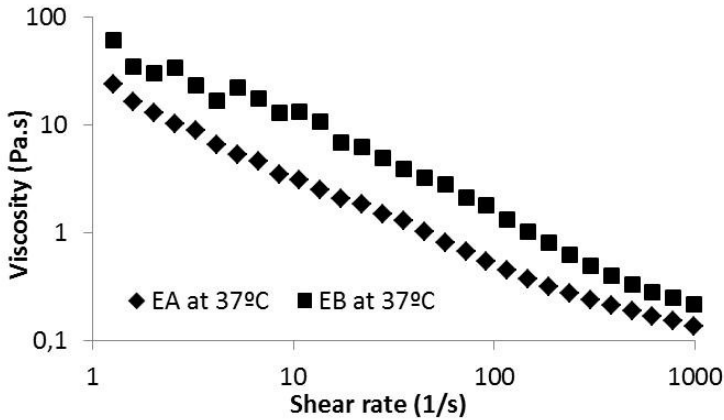


Fig. 6 Viscosity as function of shear rate for both Amimulsions at 37°C (average from 3 experiments).

The steady state shear viscosity decreases with the increase of the shear rate, showing a shear-thinning behaviour for both emulsions. Amimulsions EA and EB at 25°C had viscosities essentially the same as, or slightly higher than, Amimulsions EA and EB at 37°C.

In order to obtain information about viscoelastic behaviour of the investigated systems and the network structure formed by particle–particle interactions, an oscillation frequency sweep test was conducted at a strain in the linear viscoelastic regime, previously determined.

The viscoelastic properties are expressed with the following dynamic parameters: (1) storage modulus ( $G'$ , Pa), characterizing the elastic behaviour and representing the energy stored by the system; (2) loss modulus ( $G''$ , Pa), characterizing the viscous (plastic) behaviour, representing the energy dissipated by the system [7,8].

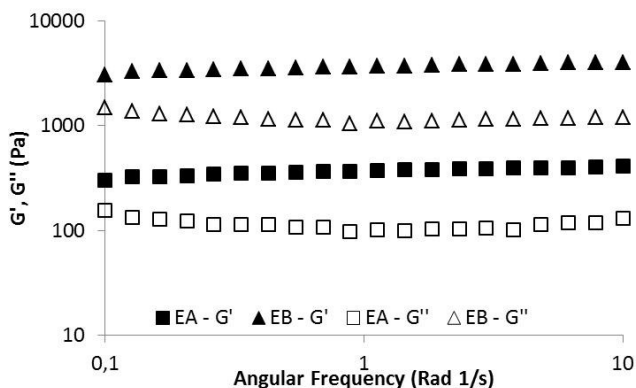


Fig. 7 Storage and loss modulus as a function of angular frequency for both Amimulsions at 25°C (average from 3 experiments).

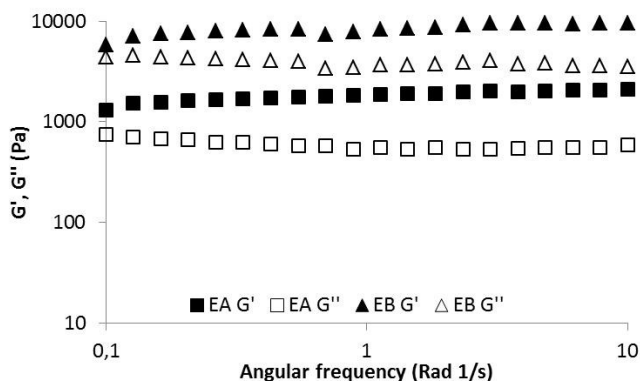


Fig. 8 Storage and loss modulus as a function of angular frequency for both Amimulsions at 37°C (average from 3 experiments).

For the two Amimulsions,  $G'$  is must higher than  $G''$ , meaning a dominant elastic behaviour of both emulsions. Also, in both cases, the slope of the curve  $G'$  vs.  $\omega$  is very small meaning that both systems are well structured. As expected, the  $G'$  and  $G''$  increased with temperature, probably due to the onset gelatinization of the polymer that stabilized the inner droplets. Fig. 7 and Fig. 8 indicate that EB presents higher  $G'$  and  $G''$  moduli than EA.

These findings are in accordance with the previous results of droplet size and distribution, emphasizing the influence of lipids in the structure of these Amimulsions. The Amimulsion containing hydrocarbons presented a slightly stronger and organized structure.

## Conclusions

Structure analysis of the systems, stabilized by solid particles, confirmed a strong microstructure, suggesting that the Amimulsions are stable vehicles with a high potential for topical application.

## References

1. Brummer R., (2006) Rheology Essentials of Cosmetic and Food Emulsions, Springer, Germany.
2. Eccleston, G., (1997). Colloids Surf. 123-124, 169-182.
3. Villari, V., Micali, N., (2008). J. Pharm. Sci. 97, 1703-1730.
4. Kovács, A. et al (2005). J. Therm. Anal. Cal. 82, 491-497.
5. Raposo S. et. al. (2013). Pharm Dev Technol. doi:10.3109/10837450.2013.788516.
6. BS 1377: 1990 British Standard Institution, part 2.
7. Gašperlin, M., Tušar, L., Tušar, M., Kristl, J., Šmid-Korbar, J., (1998). Int. J. Pharm. 168, 243–254.
8. Ribeiro, H.M., Morais, J. A., Eccleston, G. M. (2004) Int. J. Cosm. Sci. 26, 47-59.

### Contact Address:

Joana Marto ([jimmarto@ff.ul.pt](mailto:jimmarto@ff.ul.pt))

*iMed.UL– Faculdade de Farmácia da Universidade de Lisboa. Av. Prof. Gama Pinto  
1649-003 Lisboa - Portugal*

*Tel: +351 217 946 400; Fax: +351 217 946 470*



## CHAPTER 13

# Comparative effect of high-pressure and pH on the viscoelastic characteristics of aqueous glucomannan dispersions

V. Bargiela<sup>1</sup>, C. A. Tovar<sup>1</sup>, A.J. Borderías<sup>2</sup>, B. Herranz<sup>2</sup>

<sup>1</sup> Dpto. Física Aplicada, Facultad de Ciencias de Ourense. Universidad de Vigo (Spain).

<sup>2</sup> Dpto. de Productos, Instituto de Ciencia y Tecnología de los Alimentos y Nutrición (CSIC), (Spain).

### Introduction

Konjac glucomannan (KGM) has been reported as a novel alternative for making restructured fish products owing to its capacity to form thermo-resistant gels when KGM is deacetylated by addition of an alkaline agent. Deacetylation produces a three-dimensional network in which fish particles with little or no protein functionality can be held as a filler. These networks are formed by locally ordered regions (junction zones) which are stabilized mainly by hydrogen bonds and other non-covalent interactions such as dipole–dipole and hydrophobic interactions. The number and size of these can fluctuate with time and temperature [1], so that the lifetime of these networks is finite (“transient networks”) [2]. Previous papers reported that the stability of these networks was affected by temperature [3] and successive high pHs (increasing deacetylation) [4]. The study of these parameters offered an idea of the optimal KGM gelation conditions for designing gels with adequate texture for use in technological treatments like cooking and pasteurization. Nowadays isostatic high pressure (HP) is widely used in the manufacture of surimi gels and restructured fish products [5, 6]. Such HP can affect molecular interactions (hydrogen bonds, hydrophobic and electrostatic interactions) and protein conformation, leading to protein denaturation, aggregation and gelation [7]. Hence, KGM network stability could also be seriously compromised by HP, necessitating a comprehensive analysis of network stability before it can be used in the manufacture of restructured fish products.

This chapter is part of a study whose object is to determine the influence of HP on the structural characteristics of aqueous glucomannan dispersions (AGD) (3%) (w/v) at several pHs, in order to choose the most suitable HP conditions for the

manufacture of restructured fish products. In this chapter, the effect of increasing HP on the viscoelastic properties of 3%

AGD at two pHs close to the point of gelation (9.1 and 9.4) is examined to elucidate the differences produced by the alkalization level.

### Experimental Methods

Aqueous glucomannan dispersions (3%) (w/v) from konjac glucomannan (purity 100%, Guinama, Valencia, Spain) were prepared by continuous stirring for 30 min at low speed in a vacuum homogenizer (Stephan UM5, Stephan u. Söhne GmbH & Co., Hameln, Germany) at 60 °C. Then KOH (Panreac Química, S. A., Barcelona, Spain) was added to increase the pH to 9.1 and 9.4, mixing for 1 minute at 50 rpm to induce gel formation. Cylindrical plastic containers were then filled with this mixture and left to set, for 1 hour at 30 °C and then 4 hours at 5 °C. After that they were placed in a 0.2 M citrate-phosphate buffer at pH=5 for 20 hours. Both samples, pH= 9.1 (lot A) and pH=9.4 (lot B), were then subjected to high pressure (HP) treatments (100, 200, 400 and 600 MPa) for 10 min. Samples A1 (100 MPa), A2 (200 MPa), A4 (400 MPa) and A6 (600 MPa) were prepared at pH=9.1 (lot A), and samples: B1 (100 MPa), B2 (200 MPa), B4 (400 MPa) and B6 (600 MPa) were prepared at pH=9.4 (lot B), all at 25 °C.

Small amplitude oscillatory shear (SAOS) data were gathered using a Bohlin CVO controlled stress rheometer (Bohlin Instruments, Inc. Cranbury, NJ) and a RS600 Haake rheometer (Thermo Electron Corporation Karlsruhe, Germany). For both rheometers the measurements were carried out using a parallel plate (20 mm in diameter and 1 mm gap). The temperature of the lower plate was kept at  $25.0 \pm 0.1$  °C. Stress sweeps were obtained from 1 to 800 Pa at frequency 1 Hz. Frequency sweeps were performed over the range 0.01–10 Hz, keeping  $\gamma=1\%$  constant within the linear viscoelastic (LVE) region. Transient tests were carried out under constant stress ( $\sigma$ ) within LVE range for 600 s, followed by a further 600 s recovery time to obtain the reformation curve.

### Results and Discussion

#### *Linear viscoelastic (LVE) range*

Stress sweeps were used to determine the influence of HP on the limit parameters within the LVE range, such as strain amplitude ( $\gamma_{max}$ ) and rigidity ( $G^*$ ) of AGDs at pH= 9.1 and 9.4. The stress sweeps were recorded at 1 Hz, where the AGD behaves as a weak gel, close to the gel–sol transition phase (at lower frequencies) as indicated by mechanical spectra (next section). In A samples (pH=9.1) the effect of HP on  $\gamma_{max}$  was irregular and noticeably stronger than in B (pH=9.4) (Figure 1).

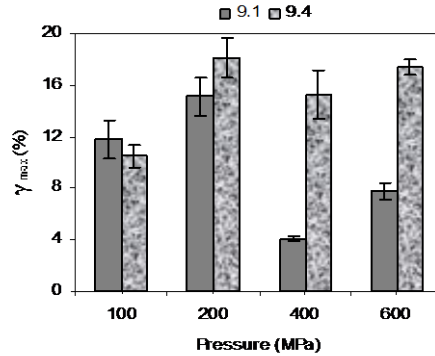


Figure 1. Influence of high pressure on strain amplitudes of the LVE range in AGD at two pH.  $T=25^{\circ}\text{C}$  and  $\nu=1\text{Hz}$ .

$\gamma_{max}$  was highest in A2 (200 MPa) and lowest in A4 (400 MPa) (Figure 1).  $G^*$  was higher in A4 (400 MPa) (Figure 2) than in all the other AGDs (lot A) under different HP. This fact suggests that in A4, HP increased the number and size of the junctions in the AGD matrix, since the progressive development of a physical structure is reflected by a substantial narrowing of the  $\gamma_{max}$  value (1) (Figure 1), indicating a more rigid and less flexible structure (8). However, in samples at pH=9.4 (lot B) there was a significant increase in  $\gamma_{max}$  only between 100 (B1) and 200 MPa (B2). Beyond this pressure, from HP=200 (B2) to 600 MPa (B6),  $\gamma_{max}$  values remained practically constant with little dependence on HP (Figure 1). Note also that in lot B (pH=9.4) HP did not significantly affect the  $G^*$  data (Figure 2).

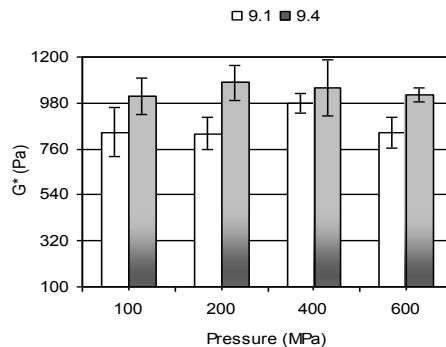


Figure 2. Influence of high pressure on the limit complex modulus in the LVE range in AGD at two pH.  $T=25^{\circ}\text{C}$  and  $\nu=1\text{Hz}$ .

These results indicate that the viscoelastic response in the LVE range under the same HP was very much dependent on the alkalinity of the AGDs and consequently also on the deacetylation ratio [4]. Thus, at pH 9.1 there were more acetyl groups in KGM chains (less polymer-polymer association), resulting in more free volume within the AGD matrix. The resulting structures were consequently more sensitive to pressure-treatment, as shown in Figures 1 and 2.

Increasing HP in the lower range (100–200 MPa) caused a similar rheological response irrespective of pH. Thus,  $\gamma_{max}$  significantly increased in both A1–A2 and B1–B2 (Figure 1), and in both cases  $G^*$  did not change (Figure 2). This suggests that between 100 and 200 MPa, stability and molecular flexibility were enhanced in AGDs without this affecting the overall rigidity of the matrix. However, if we compare the effect of pH on  $G^*$  in the same HP range (100–200 MPa), we find that  $G^*$  was greater in B1–B2 (pH=9.4) than in A1–A2 (pH=9.1), indicating that the degree of cross-linking was greater at the higher alkalinity than at the lower. Thus, when the deacetylation ratio increased, both the number of chain segments acting cooperatively (junction thickness) and the extent of the KGM associations (junction length) increased, reinforcing the final structure in the AGD matrix.

*Mechanical spectra*

Figure 3 shows mechanical spectra of AGDs from lot A (pH=9.1). The corresponding results at pH=9.4 were practically indistinguishable from these, and are not shown in Figure 3 for the sake of clarity.

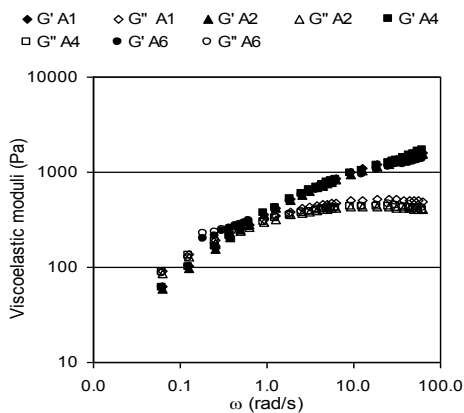


Figure 3. Influence of high pressure on mechanical spectra in AGD at pH=9.1 (A1-A6). T=25°C.

From 10 to 0.20 Hz,  $G'$  was somewhat higher and more frequency-dependent than  $G''$ , indicating weak solid-like behaviour. The crossover interval ( $G' \approx G''$ ) was

located between 0.10 and 0.06Hz, corresponding to the gel-sol phase transition. At frequencies lower than 0.06 Hz,  $G''$  was slightly higher than  $G'$  (Figure 3), indicating the predominance of liquid-like behaviour in AGD samples. HP did not significantly influence mechanical spectra at either pH.

### Creep and Recovery tests

Comparative effects of HP on creep and recovery compliances  $J(t)$  of AGDs at both pH=9.1 and 9.4 are shown in Figure 4.

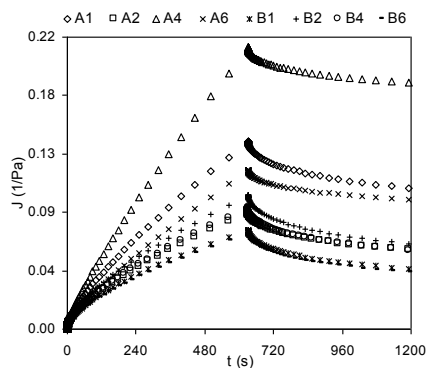


Figure 4. Influence of high pressure and pH on creep and recovery compliances in the LVE range of AGD at pH=9.1 (A1-A6) and pH=9.4 (B1-B6)  $T=25^{\circ}\text{C}$ .

An irregular (non-linear) trend was identified between  $J(t)$  data and HP. This is a consequence of the weak and random nature of the physical cross-links that form the junction zone, producing transient, heterogeneous aggregates which form a network of super-strands in polysaccharide gels [1]. There were no pH-dependent differences in compliance curves during either creep or recovery steps. Thus, while at the higher pH (9.4; lot B) the results were practically independent of HP, at the lower pH (9.1; lot A) there were significant differences depending on the HP applied (Figure 4). For example, A4 (400 MPa) showed the highest values of both creep and recovery compliances, and conversely A2 (200 MPa) presented significantly smaller  $J(t)$  during both loading and recovery processes; these last values were practically indistinguishable from those in B2. Where the increase of  $J(t)$  was small, as in samples B1–B6, A2 and A6, there was likewise little breakage of cross-links in the AGD matrix, suggesting that the size (length and thickness) of the junction zone in AGDs is homogeneous, and hence suitable for the formation of more flexible and cohesive networks. Thus, the degree of molecular stabilization in A2 and A6 (with more acetyl groups in KGM chains) was comparable to that in more deacetylated dispersions like B1–B6 pH (9.4),

irrespective of HP. In short, for less alkalized AGDs, 200 MPa is enough pressure to improve time-stabilization to levels similar to those found in more deacetylated networks (B1–B6).

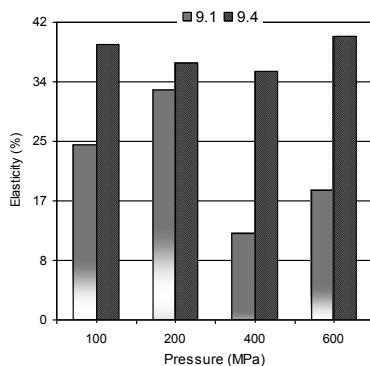


Figure 5. Influence of high pressure on elasticity from creep and recovery tests of the AGD at pH=9.1 and 9.4 T=25°C.

These results were corroborated by the elasticity values calculated, as reported by Herranz [9]. The more deacetylated AGDs (lot B) were generally more elastic than the less deacetylated AGDs (lot A) (Figure 5). However, when HP= 200 MPa in A2, there was a considerable increase in elasticity, only slightly less than in B2 (Figure 5). This indicates that 200 MPa is a suitable pressure for improving the internal structure of less deacetylated samples. This makes for more stable networks with an optimum junction size, providing flexible, elastic structures similar to B samples. Conversely, 400 MPa (A4) was too high a pressure for AGDs at lower pH, making for more compact and less elastic networks as reflected in the minimum values of both  $\gamma_{max}$  (Figure 1) and elasticity (Figure 5).

## Conclusions

Small differences in alkalization levels of 3% aqueous glucomannan dispersions (AGD) produce strong rheological responses in terms of the effect of HP on their viscoelastic characteristics. In the case of less deacetylated AGDs (pH=9.1), the effect of HP was greater than in more deacetylated samples (pH=9.4). Creep and dynamic tests at 25 °C converged, leading to the same conclusion: namely, that HP=200MPa is an optimal value for HP treatment to induce mechanical and viscoelastic stabilization of 3% AGDs at low levels of alkalization.

### **Acknowledgements**

Thanks to the Xunta de Galicia for its financial support under the Consolidation and restructuring program of competitive research units: Strategic Research Partnerships (2009/060) and project AGL2011-24693.

### **References**

1. Lapasin, R., and Pril S. (1999). *Rheology of Industrial Polysaccharides: Theory and Applications*: Aspen Publishers, Inc. Gaithersburg.
2. Tanaka, F., and Edwards, S. F. (1992). *Biomacromolecules*, 25, 1516–1523.
3. Herranz B., Borderías, A. J., Solas, M. T., and Tovar, C. A. (2012a). *Food Res. Int.* 48, 885–892.
4. Solo-de-Zaldívar, B., Tovar, C. A., Borderías, A. J., and Herranz, B. DOI:10.1016/j.foodhyd.2013.04.009 .
5. Pérez-Mateos, M., and Montero, P. (1997). *J. Agric. Food Chem.*, 45, 44–49.
6. Moreno, H.M., Cardoso, C., Solas, M.T., and Borderías A.J. (2009). *J. Aquatic Food Product Technol.*, 18, 312–330.
7. Messens, W., Van Camp, J., and Huyghebaert, A. (1997). *Trends in Food Science Technology* 8, 107–112.
8. Mezger, T.G. (2006). *The Rheology Handbook*. Vincentz Network, Hannover.
9. Herranz, B., C. A. Tovar, Solo-de-Zaldivar, B., and Borderias, A. J. (2012b). *Food Hydrocolloids* 27(1): 145–153.

### **Contact Address:**

*Beatriz Herranz Hernández (beatriz.herranz@ictan.csic.es)*

*Departamento de Productos, Instituto de Ciencia y Tecnología de los Alimentos y Nutrición (CSIC), (Spain).*

*Tel.: +34 91 549 2300. Fax: +34 91 549 3627*



## CHAPTER 14

# Rheological and texture properties of gels and emulsions prepared with pea protein isolate and proteins recovered from Cape hake by-products

Tomé, A.S.<sup>1</sup>; Pires, C.<sup>2</sup>; Batista, I.<sup>2</sup>, Sousa, I.<sup>1</sup> Raymundo, A.<sup>1,3</sup>

<sup>1</sup>NIEAB - ISEIT Almada, Instituto Piaget, Quinta da Arreínela de Cima, 2800-305 Almada, Portugal.

<sup>2</sup>IPMA, IP, Instituto Português do Mar e da Atmosfera, Av. de Brasília 1449-006 Lisboa, Portugal.

<sup>3</sup>CEER, Instituto Superior de Agronomia/Technical University of Lisbon, Tapada da Ajuda, 1349-017 Lisboa, Portugal.

### Introduction

The search for alternative sources of protein, obtained from by-products of the food industry can have high environmental and economic impact. The use of fish protein deserves special attention due to their nutritional properties. As pointed out by [1], the fishing by-products can potentially be used in foods, as binders, emulsifiers and gelling agents. Furthermore, the use of vegetable proteins as a substitute for egg protein in traditionally food stuffs as in the stabilisation of mousses, mayonnaises and puddings, has also been studied in different systems such as foams [2], emulsions [3] and gels [4], with important advantages from the nutritional and technological point of view. The properties of gel formation and emulsifying capacity of Cape-hake were also studied in a previous work [3]. This study demonstrated that it is feasible to produce fish proteins from Cape hake by-products by pH-shift process. Their production represents a possibility for the upgrading of these by-products. These proteins can be considered a good source of high quality due to the content of essential amino acids. The rheological behaviour of the gels, with different HPP concentrations, showed a typical pattern of myofibrillar protein networks. The emulsifying capacity and solubility of HPP were relatively low, but had high fat absorption. Higher protein concentration induced an increase in the complexity of the gel structure and an increase of the viscoelastic functions and zero shear rate limiting viscosity of the o/w emulsions. Sensory evaluation of the gels and emulsions obtained only with Cape-hake

protein showed a limited sensory acceptance, whereby the use of mixtures with other proteins can be a way to increase the consumer's acceptance.

In the present work, the gelling and emulsification properties of mixed systems of recovered proteins from Cape-hake by-products (HPP) and pea protein (PPI) was studied in order to evaluate the potential of these systems for the development of new food products with commercial advantages.

### Experimental

#### *Materials*

Frozen Cape hake (*Merlucciuscapensis*) by-products resulting from the fish portioning from Gelpexe (Portugal), were used as raw material to prepare protein isolate (HPP) [5]. Pea protein isolate (PPI) Pisane HD was kindly provided by Cosucra, S.A. (Belgium). Commercial vegetable oil was purchased in the local market.

#### *Methods*

For gels preparation the formulations were calculated based on the percentage of HPP and PPI addition. The total protein powders added were adjusted to 20% (w/w). The formulations tested were: 100 % PPI, 80 % PPI + 20 % HPP, 50 % PPI + 50 % HPP, 20 % PPI + 80 % HPP and 100 % HPP. The isolates HPP and PPI were previously rehydrated with distilled water (77.5 %) and sodium chloride was added (2.5 %). The pH of suspensions was adjusted to 7.0 and suspensions were placed into glass flasks (2.5 cm diameter, 4.5 cm height) and heated at 90 °C for 30 min, to assure sufficient protein unfolding. Gels were kept at 5 °C overnight to reach maturation structure, before performing the texture measurements.

For rheological measurements, the protein suspensions were immediately poured into the rheometer measuring system to promote the gelation in situ and the heating and cooling process were followed.

Oil-in-water emulsions were prepared with total 3 % (w/w) protein in the same proportions considered for gels, 65 % (w/w) oil and 32 % (w/w) water. The protein mixtures were dispersed in distilled water with magnetic stirring for 30 min, at room temperature (20–22°C), followed by pH adjustment to 3.8 or 7.0. The emulsification was carried out at 13500 rpm for 5 min with an Ultra Turrax T-25 rotor-stator homogenizer (Ika, Germany). The emulsions were stored in cylindrical glass flasks (60 mm  $\phi$ , 45 mm height) and preserved at 5°C, for 24 hours, to reach the equilibrium state. The textural and rheological properties of the emulsions were evaluated at 20°C temperature and replicated at least three times.

Texture evaluation of gels and emulsions was performed by a texture profile analysis carried out in a texturometer TA-XT2iPlus (Stable Micro System, U.K.).

Penetration tests were performed with a perspex cylindrical probe (10 mm and 38 mm of diameter for gels and emulsions, respectively) with a load cell of 5000 g and 2 mm/s of crosshead speed. From texturograms, parameters such as firmness and adhesiveness were calculated.

The rheological behaviour of gels and emulsions was studied in a controlled-stress rheometer (RS-300, Haake, Germany). All tests were replicated at least three times and a constant shear stress within the linear viscoelastic region was applied in all tests. Gels were characterized by small-amplitude oscillatory shear measurements (SAOS), using serrated plate-plate geometry (20 mm Ø). Protein suspensions were placed on the rheometer measuring device at 20 °C and heated to 90 °C at 1 °C/min, kept at 90 °C for 30 min and further cooled down to 5 °C at 1 °C/min. Gel kinetics was investigated at 5 °C for 600 min ( $f = 1$  Hz), to ensure that gel equilibrium was reached, followed by frequency sweep tests. Emulsions were also characterized by SAOS and steady state flow behaviour, at 20 °C temperature. Frequency sweep tests were performed with a cone and plate sensor system (35 mm Ø, 2° angle). For steady-state flow measurements a serrated parallel plate sensor system (20 mm Ø) was used to overcome the slip effect. From flow curves the Carreau model was adjusted to obtain the zero-shear rate limiting-viscosity ( $\eta_0$ ) [3].

A general linear model - one-way ANOVA - was used to determine significant differences ( $p \leq 0.05$ ) between samples, followed by post-hoc Tukey HSD test, using STATISTICA® from StatSoft, Inc. (Tulsa, OK, USA - v 6.1, 2003).

## Results and Discussion

With respect to the gels obtained with mixtures of Cape hake (HPP) and pea (PPI) protein, firmness of gels significantly increased ( $p < 0.05$ ) with increasing levels of HPP in the mixtures (Table 1). The presence of pea protein within the fish protein network contributes to a less firm gel. Similar results were reported by [5] with gels prepared with myofibrillar and pea protein mixtures. However, in terms of adhesiveness results are inexpressive, since this parameter has higher errors associated to this type of materials.

The increase of gel firmness with the content of HPP in the system is consistently followed by an increase of the level of the gels structure. The rheological studies revealed that a gel network was rapidly formed upon heating from 20 to 90 °C, and when cooling down to 5 °C, the gel structure was reinforced as interactions between the proteins were strengthened. In Figure 1, the mechanical spectrum obtained for the gels prepared with different proportions of HPP and PPI are represented, after the described heat treatments. For all samples,  $G'$  value is

always higher than  $G''$ , in the frequency range studied, and both moduli are frequency dependent, which is a characteristic behavior of a weak gel [8,11].

Table 1: Firmness and adhesiveness of gels obtained with the mixtures of PPI and HPP at pH 7.0.

	Firmness (N)	Adhesiveness (N.s)
100PPI	0.43±0.12 a	0.36±0.18 a,b
80PPI+20HPP	0.56±0.11 a	0.62±0.24 b
50PPI+50HPP	1,76±0.63 b	0,44±0.23 a,b
20PPI+80HPP	2,96±0.82 c	0.10±0.06 a
100HPP	6,68±0.78 d	0.10±0.07 a

Different letters mean statistically different averages ( $p < 0.05$ ).

Regarding the emulsions obtained with mixtures of PPH and PPI, a distinct behavior at both pH values studied (Table 2) was observed. At pH 7.0 a synergetic effect is evident between the two proteins, in stabilizing the emulsion structure, as higher values of firmness and adhesiveness are obtained for binary systems than when using each proteins alone. This synergetic effect is not visible for pH 3.8, a pH value common in food applications.

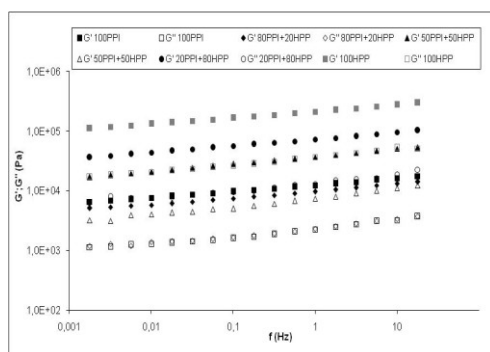


Figure 1 - Mechanical spectra of HPP and PPI gels at 5°C and pH 7.0, within the linear viscoelastic range, obtained after the heating/cooling and maturation cycle: denaturation (30 min at 90°C), cooling from 90 °C to 5 °C at 1 °C/min and maturation 5 °C for 600 min ( $f = 1$  Hz).

The linear viscoelastic behaviour of the emulsions prepared at pH 7.0 and 3.8 was typical of protein-stabilized emulsions, where an elastic network developed due to the occurrence of an extensive flocculation process.  $G'$  was higher than  $G''$  in the frequency range studied and the evolution of  $G'$  with increased frequency showed a tendency to the development of a plateau region, followed by a minimum  $G''$  [3]. The Plateau modulus  $G_N^0$  was the parameter used to compare emulsions. This parameter can be considered as a measure of the intensity of the entangled network developed between the adsorbed and not adsorbed protein molecules [7, 8]. Hence,  $G_N^0$  can be estimated as the value of  $G'$  obtained for the minimum value of  $\tan \delta$  [9] and respective values are summarized on Table 3.

The highest values obtained for  $G_N^0$  correspond to the emulsions 50PPI+50HPP and 20PPI+80HPP obtained at pH 3.8., which should correspond to the systems with a more entanglement network developed between protein molecules and consequently with greater stability.

From the steady-state flow curves, a clear shear-thinning behaviour was noticed for all the emulsions studied and the Carreau model is well fitted [6]. From the  $\eta_0$  values (Table 3), it is evident that the emulsion prepared with the 20PP+80HPP mixture presented the highest  $\eta_0$  at pH 7.0, whereas at pH 3.8 the highest  $\eta_0$  was obtained for the emulsion prepared with 100HPP. This is in agreement with the previous described synergetic effect developed by pea and hake protein in the stabilisation of the emulsions structure at pH 7.0.

### Concluding Remarks

From mixtures of hake protein recovered from by-products of fishing industry with pea protein isolate it is possible to obtain gels and emulsions with commercial potential and promising rheological characteristics.

## Perspectives in Fundamental and Applied Rheology

Table 2 - Firmness and adhesiveness of emulsions obtained with the mixtures of PPI and HPP at pH 7.0 and 3.8.

	Firmness pH 7.0 (N)	Adhes. pH 7.0 (N.s)	Firmness pH 3.8 (N)	Adhes pH 3.8 (N.s)
100PPI	0.18 ± 0.03 <sup>a</sup>	0.44 ± 0.09 <sup>ij</sup>	0.14 ± 0.02 <sup>a,b</sup>	0.17 ± 0.09 <sup>ij,k</sup>
80PPI+ 20HPP	0.38 ± 0.01 <sup>a</sup>	0.92 ± 0.02 <sup>i</sup>	0.10 ± 0.01 <sup>b,c</sup>	0.01 ± 0.01 <sup>k,l</sup>
50PPI+ 50HPP	0.72 ± 0.17 <sup>a,b,c</sup>	1.36 ± 0.53 <sup>ij,k</sup>	0.25 ± 0.01 <sup>e</sup>	0.48 ± 0.11 <sup>l,m</sup>
20PPI+ 80HPP	0.7 ± 0.14 <sup>b,c</sup>	1.88 ± 0.20 <sup>ij,k</sup>	0.41 ± 0.07 <sup>d,e</sup>	0.79 ± 0.31 <sup>m</sup>
100HPP	0.47 ± 0.09 <sup>c</sup>	0.89 ± 0.32 <sup>l</sup>	0.44 ± 0.15 <sup>c,d</sup>	1.16 ± 0.33 <sup>k,l</sup>

Different letters mean statistically different averages ( $p < 0.05$ ).

Table 3 – Plateau modulus ( $G_N^0$ ) and zero-shear-rate limiting viscosity ( $\eta_0$ ) of emulsions prepared at pH 7.0 and pH 3.8.

	$G_N^0$ pH7.0 (Pa)	$G_N^0$ pH 3.8 (Pa)	$\eta_0$ pH7.0 (Pa.s)	$\eta_0$ pH 3.8 (Pa.s)
100 PPI	366.55	217.91	1.51E+05	7,20E+04
80PPI+ 20HPP	680.50	452.50	1.41E+05	2,03E+04
50PPI+ 50HPP	1084.00	1797.43	3.97E+05	1,38E+05
20PPI+ 80HPP	1542.25	1867.75	5.75E+05	2,23E+05
100HPP	653.21	1946.75	2.46E+05	2,78E+05

## References

1. Sathivel, S., Bechtel, P.J., Babbitt, J.K., Prinyawiwatkul, W., Negulescu, I.I., Reppond, K.D. (2004) J. Agric. Food. Chem. 52, 5040–5046.
2. Raymundo, A.; Empis, J. Sousa, I. (1998). Z. Lebensm.Unters.Forsch.207: 91-96.
3. Franco, J. Raymundo, A.;Sousa, I. & Gallegos, C. (1998a). Journal of Agric. Food. 46: 3109 – 3115.
4. Nunes, C., P. Batista, A. Raymundo, M.M. Alves, Sousa, I. (2003). Food Colloids, Biopolymers and Materials Special Issue.31: 1-4.
5. Pires, C., Costa, S., Batista, A.P., Nunes, M.C., Raymundo, A., Batista., I. (2012). Journal of Food Engineering. 108 (2): 268-275.
6. Raymundo, A. Franco, J.M., Partal, P., Sousa, I., Gallegos, C. (1999). JSD - AOCS. 2, 4: 545 - 551.
7. Sun, XD; Arntfield, S.D. (2010). Food Research International, 43: 509-515.
8. Romero, A., Cordobés, F., Puppo, M.C., Villanueva, A.; Pedroche, J.; Guerrero, A. (2009). Food Hydrocolloids. 23,3: 964-972.
9. Wu, S., (1989). J. Polym. Sci. 27:723.

### ContactAddress:

A.Raymundo ([anabelaraymundo@gmail.com](mailto:anabelaraymundo@gmail.com))



## CHAPTER 15

# Effect of high pressure treatment on thermal and rheological properties of chickpea (*Cicer arietinum* L.) flour dispersions and pastes

W. Canet, R. Fuentes, M.D. Olivares, M.D. Álvarez

*Department of Characterization, Quality and Safety, Institute of Food Science, Technology and Nutrition (ICTAN-CSIC) (Spain)*

### Introduction

Chickpea is a crop of economic importance and also an important source of protein in the diet of people in numerous countries [1]. Dispersions of chickpea flours are used in the production of several convenience foods including fried snacks and sweets [2], as well as in emulsified meat products [3]. It is still desirable to develop chickpea based products or partially substitute wheat flour by chickpea flour in different food products. High hydrostatic pressure (HHP) provides the possibility to produce foods with novel textures [4]. To achieve the desired product functionality and texture, the understanding of pressure-induced gelatinization of starch is vital for applications of HPP treatment in starch-containing products. Rheology and differential scanning calorimetry (DSC) provide information at physical and macroscopic level indicating changes associated with gelatinization or denaturation processes [5]. The objective of this work was to evaluate the effect of HHP treatment on rheological and thermal properties of chickpea flour slurry. HHP treated dispersions were studied as function of pressure level (0, 150, 300, 450 and 600 MPa), slurry concentration (with 1:5, 1:4, 1:3 and 1:2 flour-to-water ratios) and temperature. For that, flour-water suspensions were pre-treated with pressure and subsequently analyzed for changes in their properties by an isothermal heating process carried out at 75 °C for 15 min and at 90 °C for 5 min.

### Experimental Methods

#### *Materials*

Spanish chickpea (cv. Castellano) flour used was a commercially available product donated by the flour miller industry *Los Pisones* (Zamora, Spain).

## Perspectives in Fundamental and Applied Rheology

Chickpea flour was supplied packed in polyethylene pouches (500 g) and stored in watertight cabins (10 °C and 73 ± 3% relative humidity) until use.

### *Sample preparation*

Rice flour slurries were prepared at four concentrations yielding 1:5, 1:4, 1:3 and 1:2 flour-to-water ratios. At each case, the measured quantity of water was added in small portions and the flour was initially stirred using a glass rod, to break the lumps and to form a smooth suspension [6]. Next, the sample was kept for half-an-hour at room temperature for hydration, stirring constantly at 900 rpm before subjecting it to rheological or thermal measurements. Slurries (200 mL) were vacuum packaged in flexible bags type Doypack® (Polyskin XL, Amcor Flexiblehispania, Granollers, Spain), introduced into the pressure unit filled with pressure medium (water) and then treated by high-pressure (150, 300, 450, 600 MPa/25 °C/15 min). HHP treatments were performed using a Stansted Fluid Power Iso-lab 900 High Pressure Food Processor (Model: FPG7100:9/2C, Stansted Fluid Power Ltd., Harlow, Essex, UK), with 2000 mL capacity, maximum pressure of 600 MPa, and maximum temperature of 60 °C.

### *Dynamic rheological measurements*

A Bohlin CVR 50 controlled stress rheometer (Bohlin Instruments Ltd., Cirencester, UK) was used to conduct rheological measurements in combination with a four-bladed cruciform vane geometry (diameter = 25 mm and height = 40 mm), which rotates inside a 27-mm-diameter serrated cup with 0.5 mm deep serrations, and a solvent trap to minimize moisture loss during tests. SAOS isothermal measurements were carried out at three selected temperatures (25, 75 and 90 °C). Sample temperature was internally controlled via a computer using a Bohlin Rheology fluid circulating bath KTB-30 (also from Bohlin Instruments Ltd.). In order to induce a paste, flour dispersions were isothermally heated in the vane geometry to 75 and 90 °C by using the pre-condition option for 15 and 5 min, respectively with controlled stress at 0 Pa before the actual measurements. Frequency sweep oscillatory tests were performed at variable frequencies over the range 0.1-100 rad s<sup>-1</sup>, keeping the amplitude stress at a constant value within the LVE region.

### *Thermal properties*

A DSC (TA Q1000, TA Instruments, New Castle, DE, USA) was employed and calibrated with indium and sapphire for temperature and heat capacity values. Slurry samples, weighing around 15 mg (±0.002) were capsulated in hermetically sealed aluminum volatile pans. Thermal scans were performed from 25 to 100 °C at a heating rate of 10 °C min<sup>-1</sup>. An empty pan was used as a reference and dry nitrogen at a flow rate of 50 mL min<sup>-1</sup>, was used as the purge gas. Thermal transitions were measured in terms of onset ( $T_0$ ), peak ( $T_p$ ) and conclusion ( $T_c$ )

gelatinization temperatures. The gelatinization temperature range ( $R$ ) was computed as  $(T_c - T_0)$ . The enthalpy ( $\Delta H_{gel}$ ) of the transition was calculated from the area of the peak endotherm. The peak height index (PHI) was calculated by the ratio  $\Delta H_{gel}/(T_p - T_0)$ , as described by Kaur and Singh [1].

## Results and Discussion

### *Rheological properties*

In order to investigate the HHP effect on the flour slurries, samples were analyzed directly after treatment. The viscoelastic behavior of the chickpea flour slurries with 1:2 flour-to-water ratio at 25 °C is illustrated in Fig. 1. The behavior of unpressurized and pressurized dispersions at 25 °C resembled that of an entangled system, with  $G'' > G'$  until the crossover frequency was reached. Slurries underwent significant increases in both moduli with flour concentration and applied pressure. Following increasing trends of both  $G'$  and  $G''$ , there was a systematic increase in  $\eta^*$  with applied pressure treatment indicative of the presence of higher entanglement density, demonstrating that the treatment of chickpea slurries with increasing pressure causes increasing gelatinization of starch. Pressure-induced melting of sorghum starch granules started at pressures  $> 300$  MPa and complete gelatinization was obtained after treatment with 600 MPa [4]. It was also clear that the swelling of starch granules was correlated with the increase in  $\eta_{initial}$  [7].

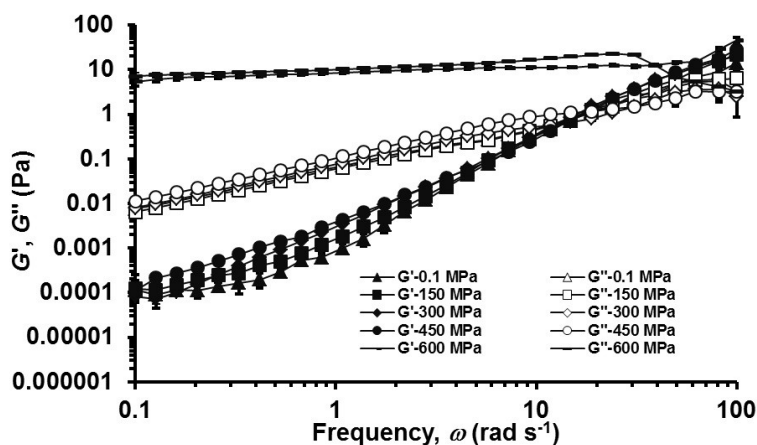


Figure 1. Effect of HHP treatment on mechanical spectra of 1:2 chickpea flour slurry at 25 °C

A dispersion can be converted into a paste under various conditions, such as temperature change. Mechanical spectra of heat-induced pastes at 75 °C for 15 min (for samples of 1:5 and 1:3 flour-water slurries) before and after HPP

treatments are presented in Figs. 2 and 3. Similar results were obtained for heat-induced pastes at 90 °C for 5 min (not shown).

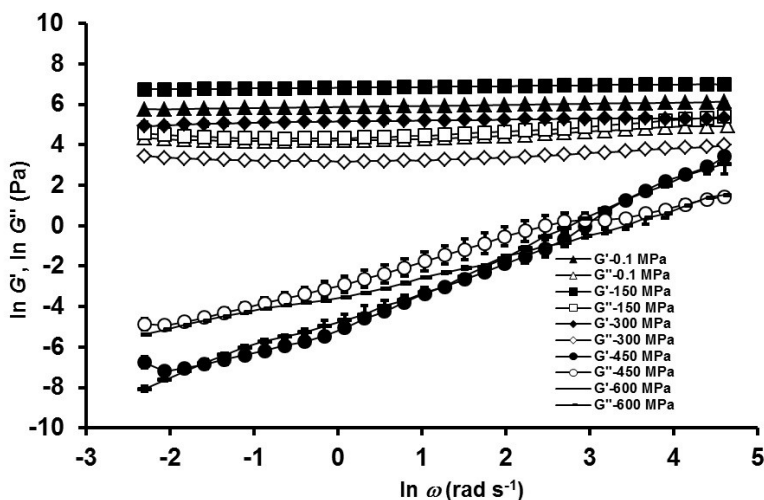


Figure 2. Effect of HHP treatment on mechanical spectra of 1:5 chickpea flour paste induced at 75 °C for 15 min

Elasticity ( $G'$ ) of thermally induced flour paste increased as function of chickpea flour concentration and decreased with increasing applied pressure in proportion with the extent of high-pressure-induced gelatinization of starch. It is well known that gelatinization is an irreversible melting phase transition [4]. Consequently, in the subsequent heating process weaker pastes are formed with increasing the amount of pre-gelatinized starch and after only melting of the remaining crystallites. The effect of HHP treatment was also more pronounced at the higher water contents. Even due to earlier pressure-induced gelatinization, weak gel behavior was not observed for pressure treated (600 MPa) samples of 1:5 flour-water slurry (Fig. 2). Certainly, frequency sweeps provides information on physical changes that can indicate the degree of gelatinization.

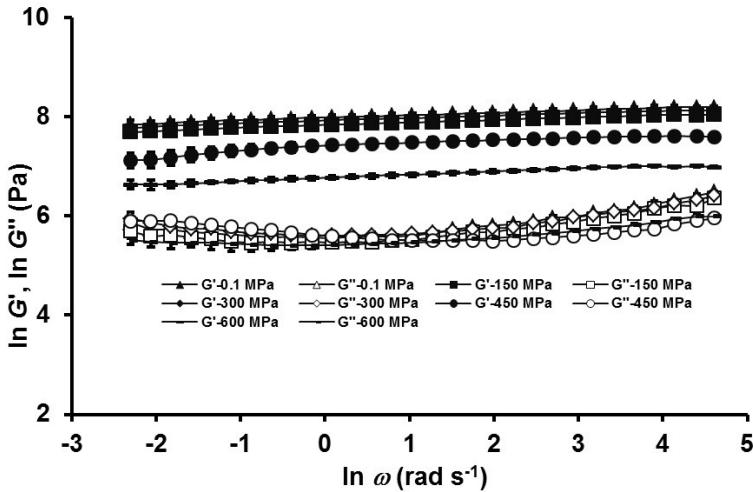


Figure 3. Effect of HHP treatment on mechanical spectra of 1:3 chickpea flour paste induced at 75 °C for 15 min

#### Thermal properties

The melting enthalpies of the pressure-treated slurries showed progressive gelatinization of starch as either concentration or pressure levels increased. The enthalpy value increased as concentration increased. It was also found that the enthalpy decreased with increasing pressure level. Conversely, chickpea flour dispersions subjected to 600 MPa for 15 min showed no peak and hence no enthalpy value, suggesting complete HHP-induced gelatinization of starch. Stolt et al. [8] found a complete loss of birefringence in barley starch after treatment at 600 MPa for 15 min.

#### Concluding Remarks

Chickpea flour dispersions were partial or totally gelatinized under pressure but the quality of the yielded pastes was falling with increasing pressure level. It may be hypothesized that the addition of HHP-treated chickpea slurries (600 MPa, 15 min) in unpressurized similar batter based products can offer easier flow characteristics during heating, preparation and handling. On the other hand, data presented provide a useful fingerprint of rheological behavior, which plays an important role in optimizing sensory quality of final food products.

Table 1. Effects of HHP treatment and concentration on thermal properties of chickpea flour slurry

HPP/Ratio	$\Delta H_{gel}$ (J/g)	PHI
0.1 MPa/1:5	1.14±0.01 <sup>aC</sup>	0.15±0.00 <sup>a,bB,C</sup>
150 MPa/1:5	1.41±0.27 <sup>aC</sup>	0.17±0.05 <sup>aC</sup>
300 MPa/1:5	1.12±0.01 <sup>aD</sup>	0.10±0.00 <sup>a,bD</sup>
450 MPa/1:5	1.15±0.01 <sup>aC</sup>	0.08±0.00 <sup>bC</sup>
600 MPa/1:5	ND	-
0.1 MPa/1:4	1.32±0.06 <sup>cC</sup>	0.13±0.01 <sup>cC</sup>
150 MPa/1:4	3.24±0.03 <sup>aB</sup>	0.54±0.00 <sup>aB</sup>
300 MPa/1:4	1.70±0.01 <sup>bC</sup>	0.18±0.00 <sup>bC</sup>
450 MPa/1:4	0.71±0.01 <sup>dD</sup>	0.07±0.00 <sup>dC</sup>
600 MPa/1:4	ND	-
0.1 MPa/1:3	1.79±0.16 <sup>cB</sup>	0.19±0.03 <sup>cB</sup>
150 MPa/1:3	3.32±0.02 <sup>aB</sup>	0.47±0.00 <sup>aB</sup>
300 MPa/1:3	2.48±0.02 <sup>bB</sup>	0.37±0.00 <sup>bB</sup>
450 MPa/1:3	1.93±0.02 <sup>cB</sup>	0.19±0.00 <sup>cB</sup>
600 MPa/1:3	ND	-
0.1 MPa/1:2	2.50±0.09 <sup>dA</sup>	0.29±0.01 <sup>cA</sup>
150 MPa/1:2	4.21±0.03 <sup>aA</sup>	0.64±0.01 <sup>aA</sup>
300 MPa/1:2	3.19±0.03 <sup>bA</sup>	0.40±0.00 <sup>bA</sup>
450 MPa/1:2	2.79±0.02 <sup>cA</sup>	0.37±0.00 <sup>bA</sup>
600 MPa/1:2	ND	-

<sup>a-d</sup>For the same concentration, parameter means without the same letter are significantly different ( $P < 0.01$ ). <sup>A-D</sup>For the same HHP treatment, parameter means without the same letter are significantly different ( $P < 0.01$ ).

### Acknowledgements

The authors wish to thank the Spanish Ministry of Economy and Competitiveness for financial support (AGL2011-28569).

## References

1. Kaur, M., and Singh, N. (2005). *Food Chem.* 91, 403–411.
2. Ravi, R., and Bhattacharya, S. (2004). *J. Food Eng.* 65, 619-624.
3. Sanjeewa, W.G.T., Wanasundara, J.P.D., Pietrasik, Z., and Shand, P.J. (2010). *Food Res. Int.* 43, 617-626.
4. Vallons, K.J.R., and Arendt, E.E. (2009). *Innov. Food Sci. Emerg. Technol.* 10, 449-456.
5. Ahmed, J., Ramaswamy, H.S., Ayad, A., Alli, I., and Alvarez, P. (2007). *J. Cereal Sci.* 46, 148-156.
6. Bhattacharya, S., Bhat, K.K., and Raghuveer, K.G. (1992). *J. Food Eng.* 17, 83-96.
7. Oh, H.E., Hemar, Y., Anema, S.G., Wong, M., and Pinder, N.D. (2008). *Carbohydr. Polym.* 73, 332-343.
8. Stolt, M., Oinonen, S., and Autio, K. (2001). *Innov. Food Sci. Emerg. Technol.* 1, 167-175.

### Contact Address:

*W. Canet (wenceslao@ictan.csic.es)*

*Department of Characterization, Quality and Safety, Institute of Food Science, Technology and Nutrition (ICTAN-CSIC), José Antonio Novais 10, 28040 Madrid (Spain)*

*Tel.:+34 915492300 ; Fax:+34 915493627*



## CHAPTER 16

# Effect of temperature on the viscoelastic characteristics of San Simón da Costa cheese (PDO)

V. Bargiela<sup>2</sup>, I. Franco<sup>1</sup>, J. Carballo<sup>1</sup>, C.A. Tovar<sup>2</sup>

<sup>1</sup>Área de Tecnología de Alimentos, Facultad de Ciencias de Ourense. Universidad de Vigo (Spain)

<sup>2</sup>Departamento de Física Aplicada, Facultad de Ciencias de Ourense. Universidad de Vigo (Spain)

### Introduction

San Simón da Costa cheese is a traditional smoked variety produced in the north-west of Spain from cow's milk and protected by a Protected Denomination of Origin (PDO) since 2004 [1]. It is semi-hard, firm, creamy, slightly acid and without eyes. The rind is well defined, smooth, bright and amber in colour. It has a characteristic shape between a spinning top and a bullet. Cheese is a viscoelastic gel. The pH and proteolysis are critical parameters that influence the textural and physical properties of cheeses [2]. Its texture is important because it is the property by which the consumer first identifies and judges the specific variety. In previous studies it has been analyzed the relationship of textural attributes of these cheeses with manufacturing and compositional parameters at ambient temperature [3]. The melting properties of cheese are interesting functional attributes that influence the final quality of cooked food as pizza, burgers and cheese sticks [2].

The aim of this work is to analyze the effect of heating process from 20 to 90 °C on the viscoelasticity of San Simón da Costa cheese (PDO), under small deformations. The thermal response of cheeses will be related with the physicochemical parameters.

### Experimental Methods

Sixteen cheeses were manufactured by eight factories following the industrial method described by [3,4] in compliance with the regulations of PDO. Each sample was split into two halves; one was ground and held in an air-tight

container at  $-40\text{ }^{\circ}\text{C}$  until biochemical analysis, while the other was directly subjected to the rheological test on the same day. The water soluble nitrogen (WSN) and pH were determined according to the methods described by [4].

The temperature-dependent behaviour at constant dynamic mechanical conditions was gathered using a RS600 Haake rheometer (Thermo Electron Corporation Karlsruhe, Germany). The measurements were carried out using a parallel plate (20 mm in diameter and 1 mm gap). The temperature of the lower plate was controlled by Peltier system ( $\pm 0.1\text{ }^{\circ}\text{C}$ ). The temperature sweeps are oscillatory tests which are performed at constant values of frequency (0.1 Hz), and strain amplitude:  $\gamma=0.5\%$  within the linear viscoelastic (LVE) region. The heating rate was  $1^{\circ}\text{C}/\text{min}$ , slow enough to ensure temperature equilibration throughout the sample and the measuring system [5]. The measuring curves are semi-logarithmic diagrams, so they are presented with the temperature on the x-axis on a linear scale, the storage ( $G'$ ) and loss ( $G''$ ) moduli are shown on the first y-axis with the same logarithmic scale. Also the phase angle ( $\delta$ ) is displayed on a second y-axis on the logarithmic scale.

Each dynamic-mechanical thermo-analysis (DMTA) test has been repeated seven times at least and the viscoelastic parameters were presented as mean values. Trends were considered significant when means of compared sets differed at  $P<0.05$  (Student's t-test).

## Results and Discussion

### *Biochemical parameters*

The differences in manufacturing (rennet dose, scalding temperature, fineness of the curd, duration of stirring, etc.) among the factories are evidenced by different pH and WSN values (Table 1). These values are within the range described for the same cheese by other authors [4]. The sample 6B showed a significantly ( $P<0.05$ ) lower level of pH. The WSN contents observed indicate that proteolysis is not very marked in this cheese variety [3,4] though we can see significant differences between factories.

### *DMTA diagrams*

Figure 1 shows the thermal profiles of the cheeses in terms of changes of  $G'$ ,  $G''$  and  $\delta$  values during heating from 20 to  $90\text{ }^{\circ}\text{C}$ . The values of both dynamic moduli decreased and  $\delta$  increased with the increasing T from 20 to  $\sim 65\text{ }^{\circ}\text{C}$ . Conversely, from  $T>70\text{ }^{\circ}\text{C}$   $G'$  and  $G''$  increased and  $\delta$  decreased with T. In general, at high temperatures a minimum was apparent for  $G'$  values while  $G''$  has a less-pronounced minimum, their values even flattened (Figure 1bcfgh).

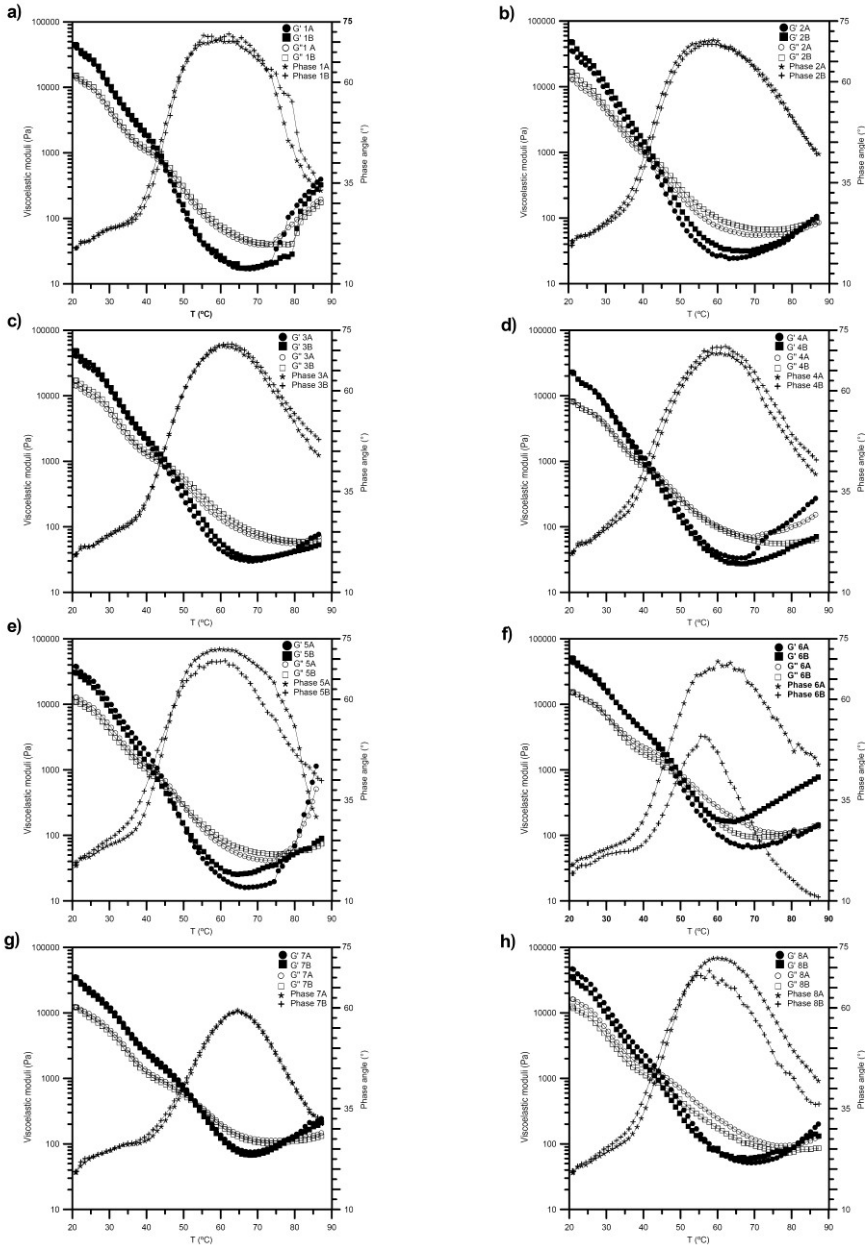


Figure 1. Comparison among the DMTA diagrams of the San Simon da Costa cheeses.

The  $\delta$  values increased following two trends: a) more slowly from 20 to 40 °C (before crossover point) and b) faster among 40 and ~55 °C (principally after the crossover point). In the first step (20<T<40 °C) cheeses are stable gels showing solid-like character ( $G'>G''$ ), hence  $\delta < 45^\circ$ , but losing progressively the gel state, due to breakage of weaker polar interactions as electrostatic and van der Waals interactions, so flexibility increased resulting in some lost of packing capability into the micellar networks, therefore  $\delta$  slightly increased. In the second step, (40<T<55°C) the decrease rate of  $G'$  values is higher than that of  $G''$ , so the first crossover point ( $G'=G''$ ) is reached ( $\delta=45^\circ$ ). This is the beginning of melting process: the gel-sol transition, which is a characteristic point of the viscoelastic materials associated with the structural properties as molecular rigidity, structural regularity and packing ability [6].

From DMTA diagrams of Figure 1 it can be obtained graphically the melting temperature ( $T_m$ ) for each factory, which can be a useful tool for the Regulator Council to distinguish the structural quality of the cheeses. In general for samples 1, 2, 3, 4, 5 and 8 (A and B)  $T_m \sim 45^\circ\text{C}$  was similar between A and B samples.  $T_m$  value was higher than the corresponding to the complete melting point of milk fat [7]. However for samples 6 there were noticeable differences: being  $T_m$  for the sample 6A similar to the other samples, but 6B had higher  $T_m \sim 53^\circ\text{C}$  (Figure 1f). This result showed that the micellar network of sample 6B was more rigid with higher and stronger connectivity among casein micelles due to its lowest pH, which is near to the isoelectric point of caseins which lowers the density of electrostatic charge resulting in a more packed network [3]. In addition samples 7(A-B) were completely different than the remainders, because these are the most proteolysed cheeses (Table 1) but  $T_m \sim 53^\circ\text{C}$  was higher in both 7(A-B) samples and undistinguishable between them (Figure 1g). This result shows that the proteolysis provides a particular structural regularity resulting in a thermal stabilization of casein networks for samples 7 (A and B), as can be noted in the higher  $T_m$  (Figure 1g).

In general, from  $T_m$  to ~65 °C, the softening of samples continued, the samples showing fluid-like behaviour ( $G''>G'$ ) increasing  $\delta$  values from 45 to  $\delta_{\max} \sim 70^\circ$ , reaching the maximum value within the small temperature range, between 55 and 65 °C approximately. In this temperature range, the number of hydrogen bonds decreases contributing to the network weakening [7]. Again the exceptions were sample 6B and samples 7 (A and B) whose  $\delta_{\max}$  were lower than the remainders 50 and ~60° respectively, thus, heating caused less fluidity indicating a greater thermal stability in their micellar networks, even at high temperatures.

From  $T>70^\circ\text{C}$  a new structural strengthening can be noted, because  $G'$  increased faster than  $G''$  with  $T$ , consequently  $\delta$  decreased, achieving a second crossover point ranged around 80-85 °C. This second transition point, from fluid-like ( $G''>G'$ ) to a solid state ( $G'>G''$ ) could be considered as another characteristic parameter of cheeses. The increase of elastic character at high temperatures may be caused by the hydrophobic interactions, which are reinforced until ~70 °C, and could

favour the caseins denaturation, increasing the casein-casein contacts by disulfide bonds at high temperatures.

The thermal profile of San Simon da Costa cheese was similar to Cheddar [8].

*Temperature-dependent complex viscosity. Flow activation energy ( $E_a$ )*

The thermal response of cheeses may be done in terms of the temperature effect on the complex viscosity ( $\eta^*$ ). In general,  $\eta^*$  decreased with increasing T from 20 to ~60 °C. The  $\eta^*$  values were fitted to Arrhenius relation (Eq. 1):

$$\eta^* = A \cdot e^{(E_a / R \cdot T)} \quad (1)$$

With T in Kelvin and the material constants: A (Pa·s),  $E_a$  (kJ·mol<sup>-1</sup>) is the flow activation energy,  $R=8.314 \cdot 10^{-3}$  (kJ·mol<sup>-1</sup>·K<sup>-1</sup>).  $E_a$  describes the potential barrier for the molecules are able to move against the internal flow resistance (liquid-specific energy barrier), caused by the friction between the neighbouring molecules [5]. Table 1 contains  $E_a$  values at two temperature intervals ( $\Delta T_1$  and  $\Delta T_2$ ). Corresponding both, to the two trends before and after the crossover temperature respectively, analyzed above.

In general the  $E_a$  values calculated for  $\Delta T_1=20-40$  °C range were lower than for  $\Delta T_2=40-55$  °C. This thermal effect could be explained because in the first interval there is naturally low capability of flow (time-continuous deformation), due to the predominant elastic over viscous character of the micellar matrix. Therefore, within the system the fluidity depends basically of the small quantity of loose molecular fragments from the breakage of weaker interactions (van der Waals and electrostatic), so the potential barrier is low and consequently  $E_a$  is low. However for the second  $\Delta T_2$  range, after crossover temperature, the viscous character of micellar networks remarkably increase ( $\delta$  increase), and the breakage of stronger polar interactions as hydrogen bonds, contribute to the increase of molecular friction among the loose structures from the matrix, increasing the flow resistance, being needed more  $E_a$  to overcome the internal friction within a weaker matrix.

However it was found two exceptions: a) samples 7 (A and B), whose  $E_a$  values were low and undistinguishable in both intervals ( $\Delta T_1$  and  $\Delta T_2$ ). These cheeses were the most proteolysed (Table 1), so their micellar networks are weaker (more porous), less cohesive and with minor connectivity degree, so they content naturally more free molecular segments, which possess higher motion ability facilitating the internal flow, thus their  $E_a$  values were lower than the other samples (Table 1). b) Conversely, samples 8A and 8B had the opposite trend for  $E_a$  in the same  $\Delta T$  intervals, being  $E_a$  higher at the low ( $\Delta T_1$ ) range. This result could be reasoned because samples 8 (A and B) had the highest pH values (Table 1), thus in their micellar networks there are more quantity of ions which increase the number of the electrostatic interactions, which are broken principally in this

## Perspectives in Fundamental and Applied Rheology

temperature range (20-44 °C), resulting in a major quantity of ionic fragments which are loosed making difficult the molecular flow, increasing  $E_a$ .

Table 1. pH values and WSN contents (g/100 g Nitrogen) and comparison between  $E_a$  (kJ·mol<sup>-1</sup>) parameters from equation 1 for San Simón da Costa cheeses at  $\Delta T_1 = 20-40^\circ\text{C}$  and  $\Delta T_2 = 40-55^\circ\text{C}$ .

Sample	$E_a^{20-40}$	$E_a^{40-55}$	pH	WSN
1A	129.2±2.6fS	165.2±2.5oT	5.72±0.03ah	15.43±0.12a
1B	127.1±3.0efS	163.9±2.5oT	5.70±0.00ac	14.03±0.77b
2A	130.9±3.2fQ	148.7±2.8nR	5.76±0.03be	6.78±0.05c
2B	131.3±2.7fQ	144.8±1.8nR	5.68±0.01cg	5.08±0.61d
3A	119.5±3.8dO	129.7±1.3lP	5.79±0.01bdh	16.73±1.28e
3B	121.2±3.7deN	121.8±1.2jN	5.82±0.03d	16.99±0.60e
4A	111.1±3.8cG	126.5±1.1kH	5.70±0.01ac	8.95±0.39fg
4B	118.9±3.8dl	122.0±1.4jl	5.73±0.02ae	9.19±0.19f
5A	118.7±2.9dJ	165.8±2.4oK	5.69±0.00acg	12.98±0.29b
5B	123.3±3.4deL	132.1±0.9mM	5.69±0.03acg	9.34±0.75f
6A	94.6±2.1aA	126.9±1.5kB	5.70±0.02ac	7.88±0.03cg
6B	104.2±2.8bC	130.3±3.9lmD	5.39±0.00f	8.30±0.09fg
7A	101.6±2.9bE	102.0±2.3gE	5.66±0.01g	21.28±0.31h
7B	104.4±2.5bE	100.3±1.9gE	5.76±0.02eh	17.98±1.15e
8A	120.5±2.7dF	110.3±1.0hG	5.98±0.00i	11.00±0.05i
8B	121.1±2.3dF	112.9±1.3iG	5.89±0.01j	11.33±0.15i

<sup>a-p</sup> Different small letters in the same column indicate significant differences among samples from different factories ( $P < 0.05$ ).

<sup>A-T</sup> Different capital letters in the same row indicate significant differences between both  $\Delta T_1$  and  $\Delta T_2$  for each sample ( $P < 0.05$ ).

## Conclusions

The thermal profiles of the viscoelastic parameters can be a useful tool for the Regulation Council of San Simon da Costa cheese to distinguish the structural quality of cheese from different factories. The thermal profiles were similar for six of the eight factories analyzed. There were two exceptions: samples 6 and 7 whose differences among the pH and proteolysis values respectively in relation to the others, justify the differences found in their thermal profiles. Proteolysis caused thermal stabilization in their weak micellar networks, lowering the flow ability at high temperature. The lowest pH value provides a micellar matrix stronger, more cohesive and less sensible to temperature changes.

## Acknowledgments

This work was financially supported by the Xunta de Galicia (Consolidation and Structuring of Competitive Research Units - Strategic Groups mode, 2009/060).

## References

1. Xunta de Galicia (2004). Diario Oficial de Galicia. 231, 16311-16321.
2. Lucey, J.A., Johnson, M.E., and Horne, D.S. (2003). J. Dairy Sci. 86, 2725–2743.
3. Bargiela, V., Franco, I., and Tovar, C.A. (2011). Queso San Simón da Costa (DOP). Editorial Académica Española, Saarbrücken.
4. Nhuch, E.L., Prieto, B., Franco, I., Bernardo, A., and Carballo, J. (2008). Aust. J. Dairy Technol. 63, 68–76.
5. Mezger, T.G. (2006). The Rheology Handbook. Vincentz Network, Hannover.
6. Sperling, L.H. (2001). Physical Polymer Science. John Wiley and Sons. Canada.
7. Lucey, J.A., Mishra, R., Hassan, A., and Johnson, M.E. (2005). Int. Dairy J. 15, 645–653.
8. Udayarajan, C.T., Lucey, J.A., and Horne, D.S. (2005). J. Text. Stud. 36, 489–515.

## Contact Address:

Clara Asunción Tovar Rodríguez ([tovar@uvigo.es](mailto:tovar@uvigo.es))  
Dpto. Física Aplicada, Facultad de Ciencias de Ourense. Universidad de Vigo, As Lagoas s/n,  
32004, Ourense (Spain)  
Telf.:+34 988387241; Fax:+34 988387001.



## CHAPTER 17

# Effect of setting time on the rheological properties of suwari gels made with squid surimi with added Konjac glucomannan

C.A. Tovar<sup>1</sup>, B. Herranz<sup>2</sup>, A.J. Borderías<sup>2</sup>

<sup>1</sup> Dpto. Física Aplicada, Facultad de Ciencias de Ourense. Universidad de Vigo (Spain).

<sup>2</sup> Departamento de Productos, Instituto de Ciencia y Tecnología de los Alimentos y Nutrición (CSIC), (Spain).

### Introduction

Surimi, consisting of a concentrate of salt-soluble myofibrillar proteins, has gelling properties that make it useful as a base in gel-based food products. Alaska pollock (*Theragra chalcogramma*) is the species that produces the best nominal quality of surimi [1]. Research has shown that a cephalopod such as giant squid (*Dosidicus gigas*) may also be used if it is subjected to specific chemical treatments [2]. Two patents have been reported dealing with squid surimi [3,4], the first based on acid solubilization followed by isoelectric protein precipitation, and the second on muscle washing with an acid solution. The rheological characteristics of surimi gels depend on the temperature and heating time applied to the minced muscle after mixing with NaCl to solubilize the proteins. When subjected to  $T < 40$  °C, the resulting gel, called “suwari”, is soft, elastic and cohesive. This kind of gel preserves the flavour and colour of raw fish muscle. During setting in this temperature range, myosin heavy chain (MHC) becomes polymerized through the formation of non-disulphide covalent cross-links, catalysed by an endogenous transglutaminase (TGase) [1].

Gelling characteristics of surimi from giant squid (*D. gigas*) can be enhanced using an aqueous dispersion of a polysaccharide, such as Konjac glucomannan (KGM). Moreover Iglesias-Otero et al. (2010) [5] reported that addition of 1% of an aqueous dispersion of KGM-10% wt (ADK) at pH=8.5 in squid surimi noticeably

improved the thermal gelation profile. A previous paper [6] analysed the effect of the T increase at a fixed heating time. The aim of the present study was to determine the influence of setting time at a fixed T=40 °C on the rheological properties, under large and small deformations, of suwari gels made with giant squid (*D. gigas*) surimi processed by isoelectric precipitation with 1% added ADK (10% wt).

### Experimental Methods

The squid surimi was produced by a method patented by [3]. Alaska pollock (*T. chalcogramma*) surimi (grade A) was supplied by a local factory and was analysed as a reference of a very good gel. The suwari gels used in this study were: A samples are neutral suwari gels from A. pollock surimi grade A; B samples are from giant squid (*D. gigas*) surimi + 1% ADK at pH=8.5 (this preparation is described in (5)), and C are control samples, i.e. neutral suwari gels made from squid surimi without ADK. The raw pastes were placed in cylindrical steel cells in a water-bath (Mettler WB 10.) at 40 °C for 0.5, 1, 2 and 4 hours. Afterwards the cells with the sample inside were placed in a water-ice slurry and finally kept refrigerated at 7 °C for one day.

Puncture tests were performed at 20 °C to breaking point, using a TA-XT2 Texture Analyser (SMS, Surrey, UK) with a 5 mm-diameter round-ended metal probe. Crosshead speed was 1 mm/s, and a 2 kg load cell was used. The load as breaking force (BF) and the depth of depression as breaking deformation (BD) were recorded. From these data we calculated the ratio BF/BD; this gives the fracture constant ( $K_f$ ), which provides a measure of relative rigidity of gels at the failure point. All determinations were carried out on at least six replicates.

Small amplitude oscillatory shear (SAOS) data were gathered using a Bohlin CVO controlled stress rheometer (Bohlin Instruments, Inc. Cranbury, NJ). The measurements were carried out using a parallel plate (20 mm in diameter and 1 mm gap). The temperature of the lower plate was kept at 10.0 °C  $\pm$  0.1. Frequency sweeps were performed over the range 0.1–10 Hz, keeping the  $\gamma=0.5\%$  constant within the LVE region. Transient tests were carried out applying a constant shear stress ( $\sigma$ ) within the linear viscoelastic (LVE) range for 600 s; after that, when removing the load other 600 s was the recovery time to obtain the reformation curve.

## Results and Discussion

### *Effect of setting time on textural properties of suwari gels*

Figure 1 shows the effect of setting time on the rigidity of suwari gels A, B and C. The rigidity of B samples continuously increased with increasing setting time. In C gels,  $K_f$  values also increased at longer times, particularly 4 hours. Conversely, in A suwari gels  $K_f$  values were practically independent of heating time. B and C gels (squid surimi) were more rigid than A gel (A. Pollock) at any setting time. The addition of 1% of ADK (B gel) at any fixed time caused a much greater increase of rigidity, as evidenced by the notable increase of  $K_f$  in B with respect to C suwari gels, which was significant for 1, 2 and 4 hours (Figure 1). This increase of rigidity with time showed the particular packing effect caused by the KGM in squid-suwari gels. However in A suwari gels heated at 40 °C the overall rigidity was independent of the setting time. It therefore seems that non-disulphide covalent protein-protein bonds like  $\epsilon$ -( $\gamma$ -glutamyl) lysine dipeptide rendered the firmness of the A suwari-network equally time-stable.

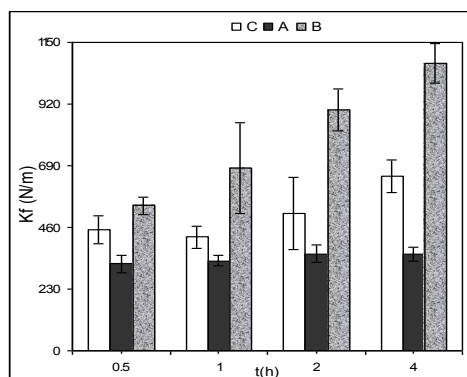


Figure 1. Influence of setting time on the fracture constant of suwari gels C (control) A (A.p.surimi), B (squid surimi+1%ADK).  $T=20^{\circ}\text{C}$

### *Linear viscoelastic (LVE) range*

Stress sweeps were used to determine the limit values of stress ( $\sigma_{max}$ ) and strain ( $\gamma_{max}$ ) in suwari gels for each setting time. Note that during the first hour of setting there were two opposite trends in samples A and B relative to those at 0.5 h: on the one hand, in A suwari gel  $\sigma_{max}$  and  $\gamma_{max}$  both significantly increased ( $p < 0.05$ ), reflecting an improvement in the rheological quality of suwari gel A. Conversely, in samples B the same time produced a significant decrease in both  $\sigma_{max}$  (Table 1) and  $\gamma_{max}$  (Figure 2), indicating an increase of stiffness in the B suwari gel, resulting in a less flexible and more unstable network (7).

Table 1. Setting time effect on the stress amplitudes,  $\sigma_{max}$  (kPa), of suwari gels made with the three kinds of surimi.  $T=10^{\circ}\text{C}$ .

t(hour)	A	B	C
0.5	0.365±0.037 <sup>aA</sup>	1.40±0.14 <sup>eB</sup>	1.22 ± 0.12 <sup>fB</sup>
1	0.719±0.072 <sup>bC</sup>	0.982±0.098 <sup>dD</sup>	1.31 ± 0.13 <sup>fE</sup>
2	0.456±0.046 <sup>cF</sup>	1.28±0.13 <sup>eG</sup>	1.18 ± 0.12 <sup>fG</sup>
4	0.467±0.047 <sup>cH</sup>	1.44±0.14 <sup>eI</sup>	1.14 ± 0.14 <sup>fJ</sup>

<sup>a-f</sup> Different small letters in the same column indicate significant differences with setting time for each sample ( $P<0.05$ ).

<sup>A-J</sup> Different capital letters in the same row indicate significant differences among samples at fixed setting time ( $P<0.05$ ).

However, in samples C,  $\sigma_{max}$  and  $\gamma_{max}$  remained practically constant over the same time (1 hour). From  $t>1$  hour to 2 hours the trends of  $\sigma_{max}$  for A and B samples were again opposite, but in a different sense than during the first hour: in A sample  $\sigma_{max}$  and  $\gamma_{max}$  decreased, while in B suwari gel both parameters increased (Table 1 and Figure 2). In C suwari gel  $\gamma_{max}$  significantly decreased (Figure 2) while  $\sigma_{max}$  remained almost constant (Table 1).

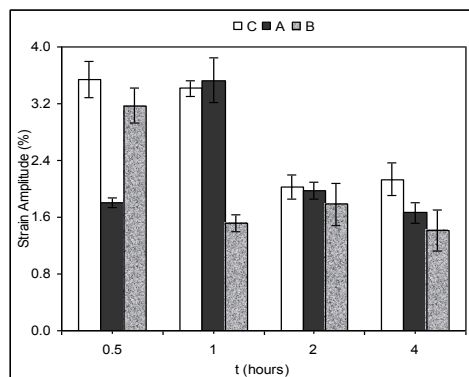


Figure 2. Influence of setting time on the strain amplitudes of C (control) A (A.p.surimi), B (squid surimi+1%ADK).  $T=10^{\circ}\text{C}$

*Mechanical spectra*

Experimental values of  $G'$  and  $G''$  moduli (data not shown) have been fitted to the power law (Eq. 1 and 2)

$$G' = G_0' \cdot \omega^{n'} \quad (1)$$

$$G'' = G_0'' \cdot \omega^{n''} \quad (2)$$

The quality factor  $Q$ , which is a useful parameter to distinguish the gel characteristics of different samples, can be calculated from  $G_0'$ ,  $G_0''$ ,  $n'$  and  $n''$  at frequency 1 Hz [8].

The highest value of *factor*  $Q$  was found in A suwari gel after 1 hour of setting (Figure 3). This result, together with the high  $\gamma_{max}$  (Figure 2), shows that 1 hour was an optimum setting time to improve the functional properties of actomyosin in A. pollock surimi and so make suwari gels of better quality. The benefit of adding 1% of ADK as an ingredient to squid surimi (B gel) can be seen already at 0.5 h of setting, in that the factor  $Q$  was significantly higher in B gel than in C gel. In B sample, from  $t \geq 1$  h factor  $Q$  retained practically the same value as at 0.5 h. (Figure 3), showing the time stability effect exerted by ADK during heating. Conversely, in C sample between 1 and 2 h, factor  $Q$  diminished dramatically, increasing finally at 4 h (Figure 3). This behaviour showed the structural instability of the C suwari network due to initial aggregation of myofibrillar protein [5].

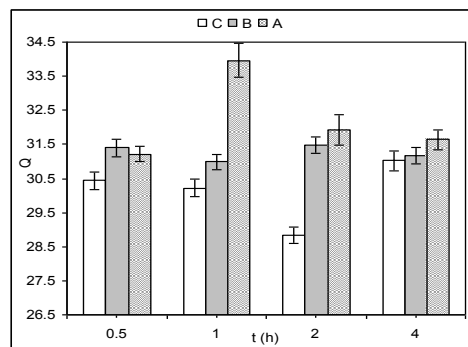


Figure 3. Influence of setting time on Quality factor of the three suwari gels.  
 $\nu=1\text{Hz}$ ,  $T=10^\circ\text{C}$

## Perspectives in Fundamental and Applied Rheology

### Creep and Recovery Compliances

The relaxation moduli  $G(t)$  can be derived from creep compliances  $J(t)$  (data not shown) Thus, the equation of Winter and Chambon [9] can be used to calculate other parameters related to gel strength ( $S$ ), and also to the relaxation exponent

$$G(t) = S \cdot t^{-n} \quad (3)$$

Where  $S$  ( $\text{Pa} \cdot \text{s}^n$ ) depends on the strength of the network and  $n$  is related to the connectivity degree in gels [10].

Table 2. Setting time effect on  $S$  ( $\text{kPa} \cdot \text{s}^n$ ) parameters from equation 3 for the three suwari gels.  $T=10^\circ\text{C}$ .

t(hour)	A	B	C
0.5	16.71±0.85	38.5±2.3	29.48± 0.77
1	19.9±3.8	48.7±4.1	34.4± 4.1
2	21.4±2.3	57.0±5.1	45.8± 4.1
4	23.2±2.2	89.8±8.4	46.8± 3.9

Values are given as mean values ± standard deviation of fit parameters

In general, from 0.5 to 4 hours, the gel strength increased with increasing setting time, proportionately least in samples A (39%), followed by C (59%), and most in B suwari gels (133%) (Table 2). This indicates that 1% of ADK with increased heating time produced a stronger network, which is consistent with the fact that  $K_f$  was highest in puncture tests (Figure 1) and  $\gamma_{\max}$  was lowest in stress sweeps (Figure 2). The explanation for this result may be that after 4 hours at  $40^\circ\text{C}$ , a large number of polymer-water hydrogen bonds had been broken, resulting in a new rearrangement of water molecules in the network. Thus, 1% ADK may help to reinforce protein-protein hydrophobic interactions even with low-temperature setting [1].

Table 3. Setting time effect on  $n$  values (Equation 3) for the three suwari gels.  $T=10^{\circ}\text{C}$ .

t(hour)	A	B	C
0.5	0.164±0.002	0.139±0.002	0.161± 0.002
1	0.156±0.002	0.150±0.002	0.167±0.002
2	0.164±0.002	0.157±0.002	0.173±0.002
4	0.163±0.002	0.162±0.002	0.165±0.002

Values are given as mean values  $\pm$  standard deviation of fit parameters

Thus, ADK could form a parallel network within the principal (actomyosin) network in *B* suwari gel. Increasing time may help the KGM network to settle, resulting in a strong structure with little order and high gel strength. The low level of conformational order is reflected in the high  $n$  value in *B* suwari gel (similar to *A* and *C* samples) after 4 hours of heating (Table 3). When the number of cross-links diminishes  $n$  increases, and so a discontinuous and heterogeneous protein-polysaccharide matrix may form at high setting-times. Conversely, in *B* sample,  $n$  was the lowest after 0.5 hour of setting (Table 3). This result corroborates the fact that 1% ADK improved the degree of connectivity in the suwari network at shorter times. Thus, 0.5 hour is a long enough setting time to improve suwari gels made from squid surimi.

## Conclusions

0.5 hour setting at  $T=40^{\circ}\text{C}$  was an optimum time for improving the structural quality of suwari gels made with squid surimi (which has poor gelling ability) +1% of a 10% aqueous dispersion of glucomannan at  $\text{pH}=8.5$ . One hour was the best setting time for suwari gels made from Alaska Pollock surimi.

## Acknowledgements

Thanks to the Xunta de Galicia for its financial support under the Consolidation and restructuring program of competitive research units: Strategic Research Partnerships (2009/060).

### References

1. Park, J.W. (2005). Surimi and surimi seafood, Marcel Dekker, Inc. New York.
2. Sánchez-Alonso, I., Careche, M., and Borderias A.J. (2007). Food Chem. 100, 48–54.
3. Careche, M., Sánchez-Alonso, I., and Borderias, A.J. (2005). Patent ES2208105. CSIC.
4. Careche, M., Borderias, A.J., and Sánchez-Alonso, I. (2006). Patent E·S2231023. CSIC.
5. Iglesias-Otero, M.A., Borderias, J., and Tovar, C.A. (2010). J. Food Eng., 101, 281–288.
6. Tovar, C.A., Herranz, B., and Borderias, J. (2011). Rheology Trends: from nano to macro Systems. ISA Press. Lisbon.
7. Mezger, T.G. (2006). The Rheology Handbook. Vincentz Network, Hannover.
8. Campo-Deaño, L., Tovar, C.A., and Borderias, J. (2010). J. Food Eng. 97, 457–464.
9. Nijenhuis, K. (1997). Thermoreversible networks. Viscoelastic properties and structure of gels, Advances in Polymer Sciences, Springer, Berlin.
10. Gabriele, D., de Cindio, B., and D'Antona, P. (2001). A weak gel model for foods. *Rheol. Acta*, 40, 120–127

### Contact Address:

Clara Asunción Tovar Rodríguez (tovar@uvigo.es)

Dpto. Física Aplicada, Facultad de Ciencias de Ourense. Universidad de Vigo, As Lagoas s/n, 32004, Ourense (Spain)

Tel.:+34 988387241; Fax:+34 988387001.

## CHAPTER 18

# Dependence on rheological properties of gluten-free doughs with flour processing: effect of temperature and particle load density during air drying

B. Rama<sup>1</sup>, S. Arufe<sup>1</sup>, M.D. Torres<sup>1</sup>, F. Chenlo<sup>1</sup>, R. Moreira<sup>1</sup>

<sup>1</sup>*Departamento de Enxeñaría Química, Escola Técnica Superior de Enxeñaría, Universidade de Santiago de Compostela (Spain)*

### Introduction

In recent years, the gluten-free formulations demand is growing and for this reason it is necessary the utilization of new raw materials in food industry [1]. Chestnut fruit, due to the absence of toxic prolamines, can be used as an alternative source for preparing gluten-free products for celiac people. The chestnut fruit is rich in carbohydrates, mainly starch and sucrose, and also a good source of essential fatty acids [2]. In the case of starchy foodstuff, like chestnut flour, the product properties depends on convective air-drying conditions such as temperature [3] and particle load density, among others due to starch transformation during this process. Starch gelatinisation takes place in a range of temperatures depending on starch source, moisture content, among others. After drying operation, milling is necessary to obtain flours with adequate average particle size due to the influence of this parameter on the dough rheology [4].

Rheological properties of doughs determine its behaviour during bakery processes. It is important to know the effect of previous processing conditions of chestnuts on rheology of chestnut flour doughs.

The main aim of this work is to relate the drying conditions of chestnut particles with the rheology of chestnut flour doughs.

### Experimental

Chestnuts (*Castanea Sativa Mill*) were purchased from a local market (Galicia, Spain) and stored at 4°C until its utilization.

## Perspectives in Fundamental and Applied Rheology

### *Pretreatment*

Chestnuts were manually selected, dehulled and peeled, and then cut in cubes with average size of 6 mm<sup>3</sup> using a laboratory blender (Waring, Model HGBTWT, USA).

### *Drying*

Chestnut particles were air-dried at several temperatures (45°C, 65°C, and 85°C) with air velocity of 2 m/s, relative humidity of 30% and at two different particle load densities, low particle load density (LLD, 2.63±0.26 kg/m<sup>2</sup>), and high particle load density (HLD, 6.13±0.10 kg/m<sup>2</sup>) in a pilot-plant tray dryer (Angelantoni challenge 250, Italy).

### *Milling and sieving*

Dried particles were milled using an ultra-centrifugal mill (ZM200 Retsch GmbH, Germany) and then sieved from 40 to 200 µm using standard sieves (Cisa, Standard ISO-3310.1, Spain) providing a flour powder surface mean diameter of 36 µm (45°C, LLD), 47 µm (65°C, LLD), 46 µm (85°C, LLD), 36 µm (45°C, HLD), 38 µm (65°C, HLD) and 39 µm (85°C, HLD). It should be notice that most particles passed the sieve of 40 µm.

### *Starch characterization*

Starch characterization was carried out by means of total starch (TS, % g starch/g dry flour), measured as total starch in flour without previous gelatinisation, and damaged starch (DS, % g damaged starch/g flour) measurements using a "Total Start Assay Kit" [5] and a "Starch Damage Kit" [6] respectively.

### *Mixing behaviour*

The mixing and kneading behaviour of doughs was determined using Mixolab® apparatus (Mixolab® Chopin Technologies, France) following the protocol Chopin S (T 30°C, time 30 min, speed 80 rpm and target consistency 1.1±0.07 Nm) explained in detail in the bibliography [7]. During this experiment, water is added to flour in order to reach the target consistency of the dough. The obtained water absorption or hydration (H, % w/w) was related to the rheological behaviour.

### *Rheological characterization*

The rheological characterization was carried out at 30°C using a controlled stress rheometer (MCR 301, Anton Paar Physica, Austria) equipped with a high-

performance chamber (CTD 450, Anton Paar Physica, Austria) using a plate-plate geometry (50 mm, 2 mm gap). Three different tests were performed at least in duplicate:

- Mechanical spectra (1–100 rad/s, 0.1% strain).
- Flow curves (0.001–0.1 s<sup>-1</sup>).
- Temperature sweep (30–180°C, heating rate 4°C/min at 0.1% strain).

## Results and Discussion

The chemical characterization indicated that chestnuts dried at low particle load density exhibited different total starch content with drying temperature. In this case, total starch decreased with increasing temperatures (Table 1). However, this fact did not happen in chestnut dried at high particle load density. At these conditions, no significant changes with air drying temperature were observed. It is clear that air drying conditions modify the total starch content of chestnut flours.

Table 1. Total starch (TS) content of chestnut flour.

T (°C)	TS (% w/w)	LD
45	61.7 ± 10.1	LLD
65	51.5 ± 6.6	LLD
85	31.6 ± 3.1	LLD
45	49.2 ± 2.3	HLD
65	44.0 ± 9.5	HLD
85	45.5 ± 5.2	HLD

The mixing behaviour determined by Mixolab® indicated that doughs with high damaged starch values needed more water absorption to reach the target consistency (Table 2).

Table 2. Hydration (H) and damaged starch (DS) of chestnut flour made from chestnuts dried at different temperatures and particle load densities.

T (°C)	DS (% w/w)	H (% w/w)	LD
45	8.0±1.7	56.1±0.1	LLD
65	4.4±0.1	46.6±1.7	LLD
85	11.3±0.1	69.9±0.7	LLD
45	4.4±0.3	48.2±0.2	HLD
65	6.1±1.7	52.1±0.1	HLD
85	7.6±0.1	57.3±0.4	HLD

Figure 1 shows experimental data of hydration (H) versus damaged starch (DS) of chestnut flours. A linear relationship was observed for both low and high load densities during chestnut particles drying.

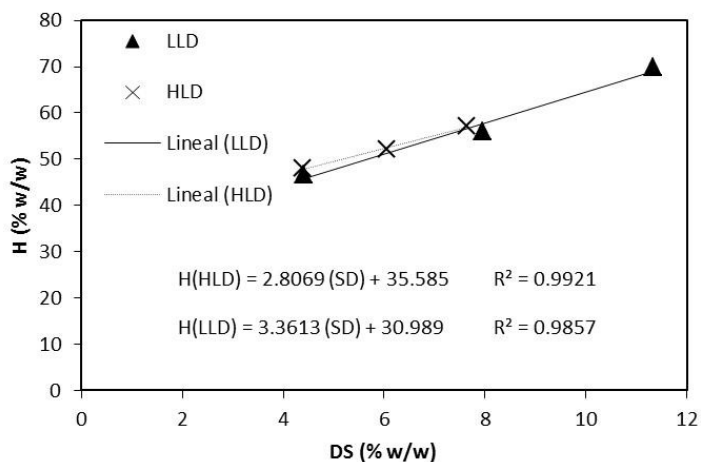


Figure 1. Experimental data of hydration (H) versus damaged starch (DS) for chestnut flour doughs made from chestnuts dried at high (HLD) (X) and low (LLD) (▲) particle load densities.

Doughs were rheologically characterised at the target consistency achieved using Mixolab®. All studied doughs depicted strong shear-thinning behaviour as it can be

noticed in the flow curves tests ( $0.001\text{--}0.1\text{ s}^{-1}$ ). Figures 2 and 3 show the experimental data of storage ( $G'$ ) and loss ( $G''$ ) moduli versus the angular frequency ( $\omega$ ) for tested doughs made from chestnut dried at different load densities and temperatures. All tested doughs exhibited  $G'$  values larger than  $G''$  at the same  $\omega$  indicating that the elastic character prevails over the viscous character. These results are consistent with those previously reported [8]. Nevertheless, viscoelastic characteristics of the doughs were simultaneously modified by the temperature and load density during drying operation.

Figure 2 shows the influence of the particle load density on the  $G'$  and  $G''$  moduli values varied in different way with particle load density as function of temperature. In example, Figure 2 shows results at  $45^\circ\text{C}$  where no effect was observed. Nevertheless, at  $65$  and  $85^\circ\text{C}$  of drying temperature both moduli decreased with increasing load density.

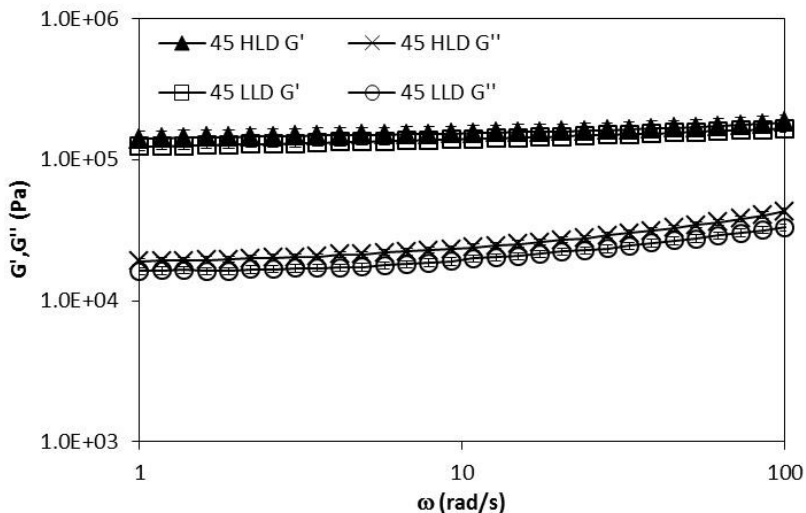


Figure 2. Experimental data of  $G'$  and  $G''$  moduli versus angular frequency ( $\omega$ ) for chestnut flour doughs made from chestnuts dried at  $45^\circ\text{C}$  at high particle load density (HLD) ( $\times$ ,  $\blacktriangle$ ) and at  $45^\circ\text{C}$  and low particle load density (LLD) ( $\square$ ,  $\circ$ ).

Figure 3 shows that both  $G'$  and  $G''$  moduli decreased when chestnut flours were obtained at drying temperature above ( $85^\circ\text{C}$ ) and at below ( $45^\circ\text{C}$ ) gelatinisation temperature of starch at LLD.

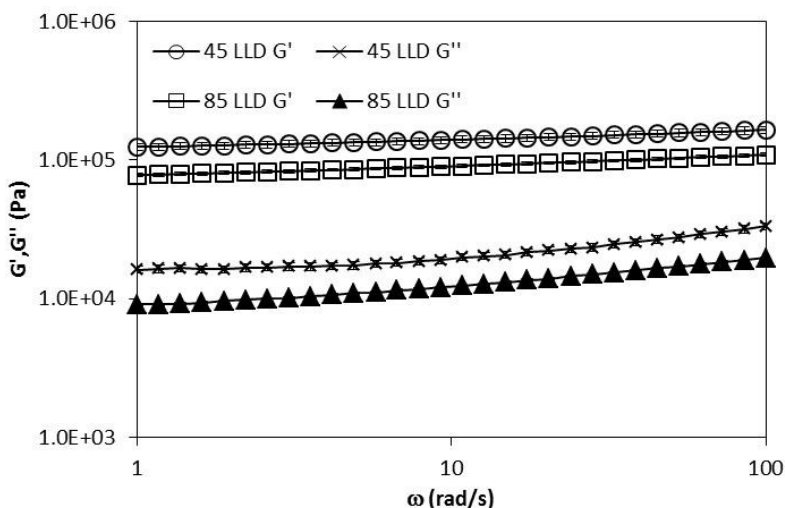


Figure 3. Experimental data of  $G'$  and  $G''$  moduli versus angular frequency ( $\omega$ ) for chestnut flour doughs made from chestnuts dried at different temperatures and LLD, 45°C ( $\circ, X$ ) and 85°C ( $\square, \blacktriangle$ ).

Temperature sweep tests allowed the determination of onset ( $T_0$ ) and end ( $T_1$ ) gelatinisation temperatures of the starch.  $T_0$  was calculated as the temperature when  $G'$  began to rise, and  $T_1$  was viewed as the temperature when the first derivative ( $dG'/dT$ ) was zero. These tests also revealed differences on gelatinisation temperatures of the samples starch. Doughs made from chestnuts dried at low particle load density showed high hydration levels and consequently lower gelatinisation temperatures of the starch even at different dried temperatures. This behaviour is not so clear for chestnuts dried at high load density (Table 3).

This fact indicates that drying temperature is not the main factor that causes the differences on hydration values and therefore on onset gelatinisation temperatures but the most influential parameter on the starch gelatinisation temperature is the damaged starch content owing to the linear dependence between damaged starch and hydration of dough (Figure 1).

Table 3. Gelatinisation temperature ranges ( $T_0$  and  $T_1$ ) of chestnut starch for chestnuts dried at different temperatures and particle load densities (LLD and HLD).

LLD		
T (°C)	$T_0$ (°C)	$T_1$ (°C)
85	46.9±0.9	73.7±0.1
65	62.5±2.6	76.2±0.4
45	55.8±0.5	76.4±0.6
HLD		
T (°C)	$T_0$ (°C)	$T_1$ (°C)
85	62.2±3.1	78.0±0.1
65	58.6±1.3	78.6±0.1
45	57.6±1.7	79.5±0.6

## References

1. Lamsal, B., Koegel, R., Gunasekaran, S. (2007). Food Science and Technology. 40, 1520-1526.
2. Borges, O.P., Carvalho, J.S., Correia, P.R., Silva, A.P. (2007). Journal of Food Composition and Analysis. 20, 80-89.
3. Correia, P., Beirão da Costa, M.L. (2012). Food Bioproducts Processing. 90, 284-294.
4. Moreira, R., Chenlo, F., Torres, M.D., Prieto, D.M. (2010). Journal of Food Engineering. 100, 270-277.
5. Total starch assay procedure. Megazyme International Ireland Limited 2009.
6. Starch damaged assay procedure. Megazyme International Ireland Limited 2008.
7. Rosell, C.M., Collar, C., Haros, M. (2007). Food Hydrocolloids 21, 454-462.
8. Moreira, R., Chenlo, F., Torres, M.D., Rama, B. (2013). Foods and Bioproducts Processing. 91, 7-13.

**Acknowledgments**

Authors acknowledge the financial support to Ministerio de Ciencia of Spain and FEDER (CTQ 2010-15309/PPQ). M.D. Torres thanks to the Ministerio de Educación of Spain for her FPU grant (AP 2007-04397).

*Contact Address:*

*Ramon Moreira (ramon.moreira@usc.es)  
Chemical Engineering Department,  
School of Engineering, ETSE  
Universidade de Santiago de Compostela  
Rua Lope Gómez de Marzoa, s/n, 15782 Santiago de Compostela.  
Telf.: +34 881 816 759.*

## CHAPTER 19

# Topical application of lipid nanoparticle-containing gels: impact on skin viscoelasticity

Mancini G.<sup>1,2</sup>, Gonçalves LMD.<sup>1</sup>, Gouveia L.<sup>1</sup>, Bica A.<sup>2</sup>, Ribeiro HM.<sup>1</sup>, Almeida A.<sup>1</sup>

<sup>1</sup> iMed.UL (Research Institute for Medicines and Pharmaceutical Sciences) – Nanomedicine and Drug Delivery, FFUL;

<sup>2</sup> Laboratório de Estudos Farmacêuticos (LEF) Lisboa, Portugal.

### Introduction

Increasing skin hydration and improving its viscoelasticity are important factors in the cosmetic products research [1]. These biological effects may be modulated by an adequate vehicles election. The skin hydration is raised by the use of occlusive, moisturizers and humectants topic products. Once that many of the topic formulations have an occlusive effect, their appearance is aesthetically undesirable, as petrolatum for example, and thus the research on new occlusive products is increasing nowadays.

The skin presents viscoelastic properties. Collagen and elastic fibers represent its elastic components [2,3], while the cell-to-cell friction and also collagen represent skin viscous part [4]. An increase in skin hydration and lipids content improve skin resistance against viscous deformation. Skin biomechanical properties are also influenced by age, gender and anatomic region, among others.

The Solid Lipid Nanoparticules (LNP) were introduced primarily as carriers systems for drugs and cosmetics “active ingredients”. When applied on the skin, LNP present *in vitro* occlusive properties, which depend on particle size, crystalline state and lipid concentration [6]. This is due to the fact that LNP form an intact skin superficial film reducing the transepidermal water loss.

The present study was aimed to investigating the moisturizing properties of LNP incorporated in a suitable gel formulation when compared with a liquid suspension of the same LNP and with the gel without LNP (Blank formulation). The biomechanical skin properties were assessed during this study.

### Experimental Methods

Three topical formulations were prepared and tested: a) a topical gel containing nanoparticles (LNPGel); b) a blank gel prepared without LNP (BlankGel); and c) a liquid aqueous LNPSuspension.

The gel composition is hydroxypropyl methylcellulose, propylene glycol, ethanol and menthol.

Skin viscoelasticity was assessed in the ventral aspect of the human forearm skin of young healthy females with 18 to 25 years old, after previous informed consent (n=10), following a 12 days regular application of the formulation on predefined sites. Application sites, applications sequence and measurements were randomized. A control area with no product (not treated) was used as control.

The biomechanical properties were assessed using the “suction method” (Cutometer 474SEM;CK electronics GmbH, Germany). The measuring principle is suction/elongation. An optical system detects the decrease of infrared light intensity depending on the distance the skin is being sucked into the probe. The time/strain mode was applied, using an elementary load cycle of a 300 mBar strain instantaneous deformation. This was maintained for 1.30 s and then released, followed by a 1.30 s relaxation period.

The following parameters obtained by skin deformation are shown on Figure 1, and then analyzed:  $U_f$  ( $R_0$ ), the final distension at the end of the first vacuum period;  $R_2$  (equal to the difference of  $U_f-U_a$ ), residual deformation at the end of a measuring cycle (resilient distension); and  $U_v/U_e$  ( $R_6$ ), value of the ratio between viscoelastic and elastic distension [3].

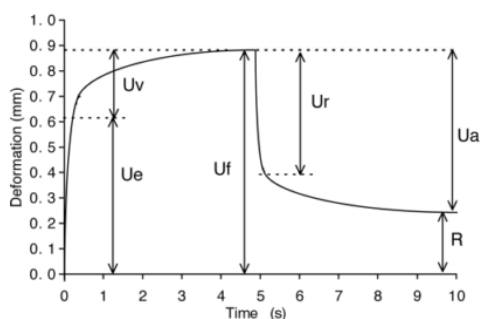


Figure 1. Curve obtained with cutometer. [3]

The curves of the obtained skin deformation values were analyzed using the Software Cutometers MPA 580, and the  $R_0$  to  $R_9$  parameters could be deduced from the  $U$  parameters:  $R_0$ , the final distension of the first curve ( $U_f$ );  $R_1$ , the ability to return to the original state ( $U_f-U_a$ );  $R_2$ , the overall elasticity of the skin, including

creep and creep recovery ( $U_a/U_f$ ); R3, the last maximum highest point of the last curve; R4, the last minimal lowest point of the last curve; R5, the net elasticity ( $U_r/U_e$ ); R6, the ratio of viscoelastic to elastic extension, also called the viscoelastic ratio ( $U_v/U_e$ ); R7, the ratio of elastic recovery to the total deformation ( $U_r/U_f$ ); R8, the  $U_a$  of the first curve; and R9, the residual deformation at the end of the measuring cycle ( $R3-R0$ ) [6].

### Statistical analysis

The significance of the difference of each of the parameters among the three formulations was analyzed by repeated measures ( $n=3$ ) using ANOVA for the paired data.

A level of  $P < 0,05$  was statistically considered significant.

### Results and Discussion

Throughout the 14 days of study, the final distension at the end of the first vacuum period, which is set by parameter  $U_f$ , diminishes for formulations LNPGel and LNPSuspension in a more pronounced way when compared to BlankGel and control. BlankGel also presents a lower value of  $U_f$  when compared to control but those are less evident when compared to the other formulations. This parameter is related with the skin tension, thus lower values of  $U_f$  are a result of a tighter skin.

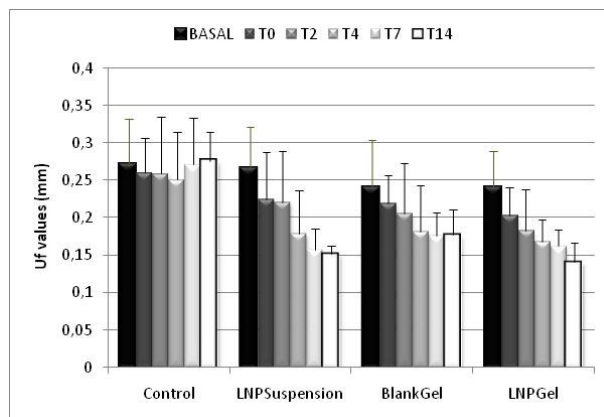


Figure 2.  $U_f$  values measured throughout the study ( $n=20$ ; Mean  $\pm$  SD)

Another key parameter studied was R1, which is the residual deformation at the end of a measuring cycle (resilient distension). A R1 value close to 0, after the application of a force, means that a tight and moisturized skin has to come back to its original (Table 1).

Table 1. R1 values measured throughout the study(n=20; Mean±SD).

	T0	T30'	T2	T4	T7	T14
Control	0.030	0.040	0.010	0.070	0.010	0.060
LNPSuspension	0.040	0.010	0.010	0.010	0.010	0.000
BlankGel	0.024	0.039	0.017	0.014	0.005	0.012
LNPgel	0.050	0.010	0.000	0.000	0.000	0.000

As shown in Table 1, there is an improvement of R1 related with both formulations when compared to BlankGel and control. This result shows that, the skin, upon application of the formulations becomes tighter since after application of a force the skin returns to its original form without biomechanical modifications.

The  $U_v/U_e$  represents the value of the ratio between viscoelastic and elastic distension. This parameter suffered an increase along the study (Figure 3). A more pronounced value was obtained for LNPgel formulation. This enhancement is related with an interstitial fluid reduction that results in higher water levels. The water accumulation in the dermis diminishes the friction between fibers and favors the interstitial fluid movement, enhancing skin moisture.

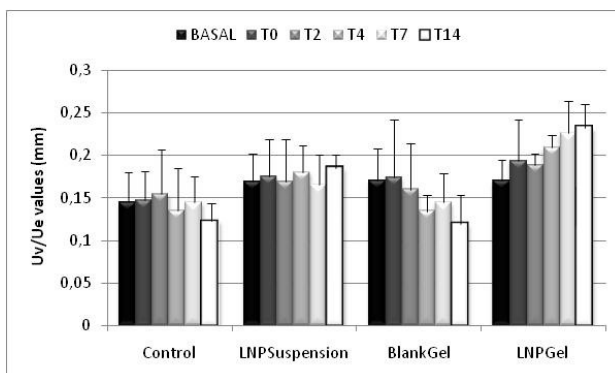


Figure 3.  $U_v/U_e$  values measured throughout the study (n=20; Mean±SD)

### Conclusions

With this study we can conclude that Solid Lipid Nanoparticles enhance slightly skin elasticity after continued topical application.

### Acknowledgements

This work is supported by the Ministry of Science (FCT-MCTES), Portugal (SFRH/BDE/33975/2009) and Laboratório de Estudos Farmacêuticos.

## References

1. Edwards C. et al. Evaluation of biomechanical properties of human skin.(1995) Clin.Dermatol. 13 (4) 375–380.
2. Cua A.B. et al. Elastic properties of human skin: relation to age, sex and anatomical region. (1990) Arch. Dermatol. Res. 282 283–288.
3. Elsner P. et al. Mechanical properties of human forearm and vulvar skin. (1990) Br. J. Dermatol. 122 607–614.
4. Vogel H.G. et al. Directional variations of mechanical parameters in rat skin depending on maturation and age. (1981) J. Invest. Dermatol. 76 493–497.
5. S.A. Wissing et al. Investigations on theocclusive properties of solid lipid nanoparticles (SLN). (2001) J. Cosmet. Sci. 52 313–324.
6. Hyo S.R. Influence of age and regional differences on skin elasticity as measured by the Cutometer. (2008) Skin ResTechnol 14: 354–358.

### *Contact Address:*

*G. Mancini (gmancini@ff.ul.pt)*

iMed.UL (Research Institute for Medicines and Pharmaceutical Sciences)

*Faculty of Pharmacy*

*University of Lisbon*

*Av. Prof. Gama Pinto*

*1149-003*

*Lisboa- Portugal*

*Telef: 217946400/ ext 14248; Fax: 217946470*



## CHAPTER 20

# Rheological behaviour and structure of food thickeners used for dysphagia treatment when dissolved in water and milk

A. Moret-Tatay<sup>1</sup>, J. Rodríguez-García<sup>2</sup>, E. Martí-Bonmatí<sup>3</sup>, I. Hernando<sup>2</sup>, M.J. Hernández<sup>1</sup>,

<sup>1</sup> Department of Earth Physics & Thermodynamics. Applied Rheology Laboratory. Universitat de València (Spain)

<sup>2</sup> Research Group of Food Microstructure & Chemistry. Dep. Food Technology. Univ Politècnica de València (Spain).

<sup>3</sup> Dep Artificial Nutrition. Hospital General Universitario. Valencia (Spain)

### Introduction

People with dysphagia have a reduced control of the bolus during swallowing. To compensate this and avoid the risk of food aspiration, they must be fed with thickened food and beverages [1-3]. Modified starches are the hydrocolloids most widely used in commercial thickeners, although some of them include gums [2,4]. Because of the physical treatment of the starch (pre-gelatinization) they are soluble in cold liquids and do not form lumps.

These thickeners are used to increase viscosity of different liquids as water, coffee, tea, juices or milk [1,2,3]. Depending on the medium in which they are dissolved, the final consistency could be affected [1,2,4].

In this work differences in structure and viscoelasticity in two food matrix (water and milk) of two commercial thickeners with different composition were analysed.

### Experimental Methods

Commercial thickeners with different composition were supplied by the Hospital General of Valencia: Nutilis Nutricia® (modified maize starch, xanthan, tara and guar gum) and Nestlé Resource® (modified maize starch). Two concentrations corresponding to the consistencies of nectar-syrup and pudding (0.05 g/mL and 0.09 g/mL) were dissolved in two food matrix: water and whole milk (Central Lechera Asturiana). Controlled stirring at room temperature was applied (400 rpm during 3-4 min) and samples were kept at rest for 30 min before measuring.

Rheological measurements were carried out with a controlled stress rheometer RS1 (Thermo-Haake). All samples were measured at 25 °C, after 900 s resting between sensors (60 mm serrated plates and cone-plate 60 mm/2°). Four measurements were made in samples prepared in two different days. Reproducibility was assured.

Step flow curves in control stress mode were performed. Storage modulus and loss modulus (in linear viscoelastic region) were measured as a function of frequency.

A light microscope (LM) Nikon Eclipse 80i (Nikon, Japan) was used to observe the samples stained with lugol.

### Results and Discussion

Dynamic spectra for Resource pastes corresponded to a weak gel, typical of starch pastes, as it was expected. However, for Nutilis pastes both moduli were more dependent on frequency, indicating a less structured internal network (Fig 1).

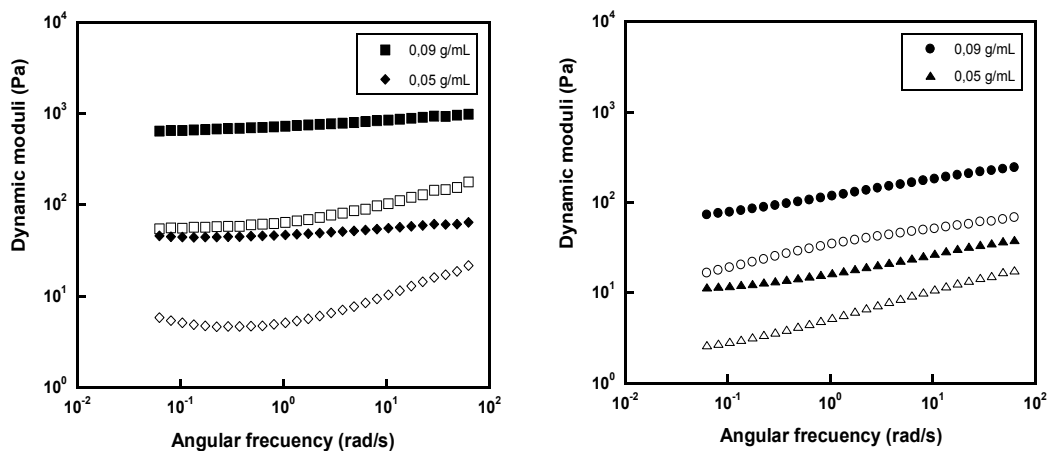


Figure 1. Dynamic spectra for the two thickeners dissolved in WATER at concentrations indicated. Filled symbols: Storage modulus,  $G'$ ; empty symbols: loss modulus,  $G''$ .

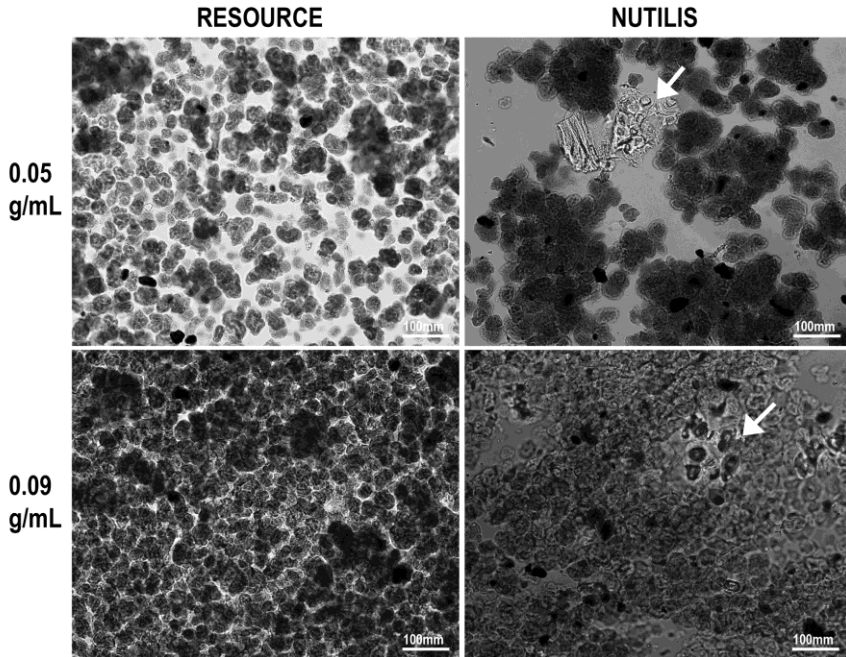


Figure 2. LM images for the two thickeners dissolved in WATER at concentrations indicated. Arrows: gums.

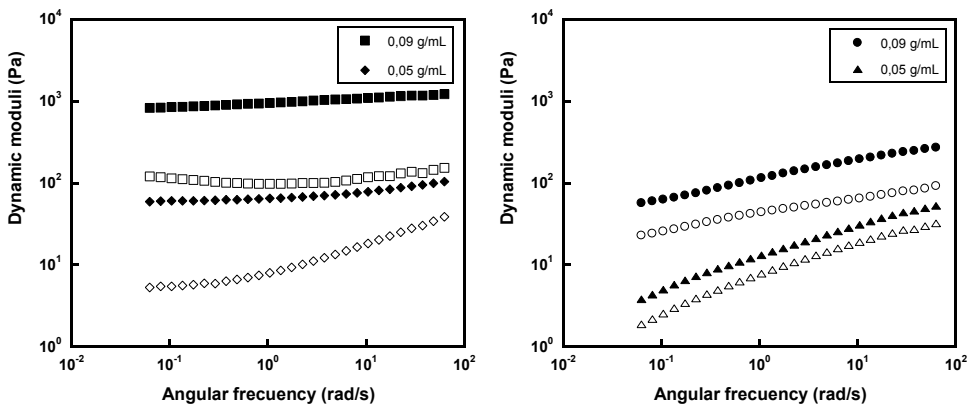


Figure 3. Dynamic spectra for the two thickeners dissolved in MILK at concentrations indicated. Filled symbols: Storage modulus,  $G'$ ; empty symbols: loss modulus,  $G''$ .

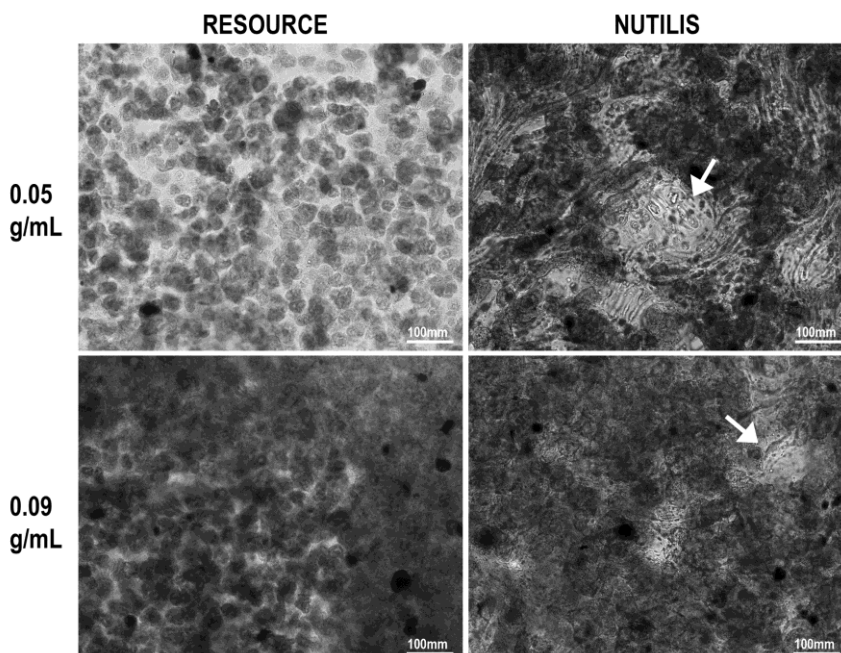


Figure 4. LM images for the two thickeners dissolved in MILK at concentrations indicated. Arrows: gums.

On the other hand, Resource thickener dissolved in water showed similar viscoelastic properties than when it was dissolved in milk (Fig 3). However, for Nutilis thickener viscoelastic moduli were significantly affected when changing the food matrix (Fig 3). Loss tangent,  $\tan \delta$ , presented higher values than those corresponding to water pastes, especially for the lowest concentration.

These results could be related with microscopy observations. Resource samples were characterized by an even distribution of dispersed swollen starch granules, and the structure of Resource samples in milk and water were similar. On the contrary, the microstructure of Nutilis samples were characterized by the disruption of the starch granules dispersion by gums, mainly in milk samples (Fig 2 and 4).

Both thickeners dissolved in water provided more viscous fluids than when they were dissolved in milk (Fig 5).

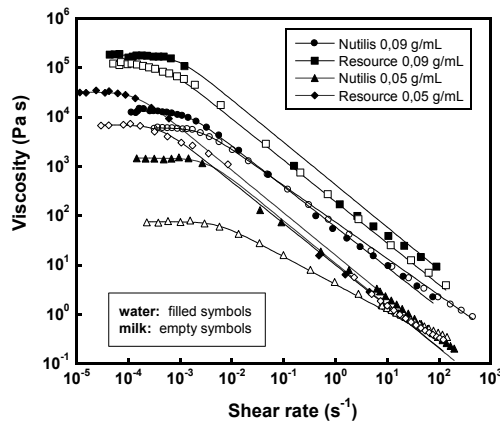


Figure 5. Flow curves fitted the Carreau model for the thickeners used, dissolved in water and milk.

All the flow curves fitted the Carreau model. Zero-shear viscosity values for Nutilis pastes in water are lower than for Resource pastes.

However, shear thinning slope is similar in both of them. Important changes in milk are observed for the lowest concentration of Nutilis thickener, as shear thinning index and zero-shear viscosity decreased significantly.

Therefore, composition of the dispersing medium should be taken into consideration when using these thickeners for dysphagia patients. It is clear that viscosity of pastes depends on the interaction of their components with food matrix. In this case, gums included in Nutilis thickener modify behaviour of the thickener when dissolved in milk [2-3].

## References

1. Pelletier, C.A., (1997). A comparison of consistency and taste of five commercial thickeners. *Dysphagia*, 12, 74-78.
2. Cho, H.M., Yoo, W. and Yoo, B. (2012). Steady and dynamic rheological properties of thickened beverages used for dysphagia diets. *Food Sci. Biotech*, 21, 1775-1779.
3. Sopade, P.A., Halley, P.J., Cichero, JAY., Ward, L.C., Hui L.S., Teo K.H. (2008). Rheological characterisation of food thickeners marketed in Australia in various media for the management of dysphagia. II: Milk as a dispersing medium. *J. Food Eng.* 84, 553-562.
4. Sopade, P.A., Halley, P.J., Cichero, JAY. Ward, L.C. (2007). Rheological characterisation of food thickeners marketed in Australia in various media for the management of dysphagia. I: Water and cordial. *J Food Eng.* 79, 69-82.

## Perspectives in Fundamental and Applied Rheology

### *Contact Address:*

*amtemota@alumni.uv.es; M.Jesus.Hernandez@uv.es*  
*Department de Física de la Terra i Termodinàmica*  
*Facultat de Física*  
*Universitat de València*  
*46100 Burjassot, València*  
*Tel: 0034963544902*

## CHAPTER 21

# Flow behaviour of citrus flavoured soy desserts. Influence of interaction between protein and starch

*C. Arancibia, S. Bayarri and E. Costell*

*Instituto de Agroquímica y Tecnología de Alimentos. CSIC. Avenida Profesor Agustín Escardino 7, 46980, Paterna, Valencia (Spain)*

### Introduction

The growing interest in soy-based product consumption as an alternative to dairy products has attracted much attention recently. Health benefits of soy foods have shown that consumption of soy proteins, as part of the regular diet, provide multiple benefits for atherosclerosis, menopausal symptoms and osteoporosis as well as risk reduction of coronary heart disease and of breast and prostate cancers. The main problems facing the acceptance of these products are related to their flavour, commonly being referred to as “beany”, certain astringency and bitter taste, as well as some undesirable textural characteristics [1]. Some authors have described the texture of soy-based products as chalky, dry or oily [2, 3] and they have proposed the use of different stabilizers to improve this attribute. In any case, the sensory problems of soy-based products are also related with soy protein content. Most of the actual commercial soy products are formulated with soy protein contents (less than 3g/100g), that are lower than that recommended by the Food and Drug Administration (6.25 g/serving of soy protein to state a health claim on its label). This study aims to obtain information about effect of interaction between soy protein and starch on flow behaviour of citric flavoured high protein soy desserts.

## Experimental

### *Samples preparation and composition*

Samples were prepared from soy protein isolate (90% protein) (SPI) (PROSOL 90-GF NT, Cargill, Spain), medium crosslinked modified tapioca starch (C\* Creamtex 75720, Cargill Ibérica SL, Spain), deionised water, citrus flavour (Naranja 15904A, Lucta S.A., Spain) and yellow colorant (T-PT8-WS, CHR Hansen S.A., Spain).

Different formulations were prepared varying SPI content (6 and 8% w/w, that corresponded to 6.75 and 7.9 g protein/125 g product) and starch concentration (2, 2.5 and 3% w/w). Two more samples without starch added were prepared as control samples. The amounts of sugar (4% w/w), citrus flavour (0.01% w/w) and colorant (0.026%) remained fixed. Identification of samples is given in Table 1.

*Table 1. Composition of citrus flavoured soy desserts*

Sample Code	SPI concentration (%)	Starch concentration (%)
A	6	0
B	6	2
C	6	2.5
D	6	3
E	8	0
G	8	2
H	8	2.5
K	8	3

Starch samples were prepared in batches of 800 g as follows: soy protein, starch, sugar and colorant were mixed with the help of a propeller stirrer in a flask for 10 min at room temperature. The flask was placed in a water bath at  $90\pm 1^\circ\text{C}$  and stirred constantly. After 15 min the product temperature reached  $85 \pm 1^\circ\text{C}$  and heating was continued at this temperature for 10 min. The sample was cooled in a water bath at  $10^\circ\text{C}$ . Aroma was added and the sample was stirred for 5 min. All samples were transferred to a closed flask and stored ( $4\pm 1^\circ\text{C}$ ; 24 h) prior to rheological measurements.

### *Rheological measurements*

Rheological measurements were carried out in a controlled stress rheometer RS1 (Thermo Haake, Germany), using a parallel plate geometry (60 mm diameter; 1mm gap). At least, two batches of each composition were measured in duplicate at a controlled temperature of  $10\pm 1^\circ\text{C}$ . Samples were allowed to rest for 10 min before measurement and a fresh sample was loaded for each measurement.

The flow behaviour of each sample was measured and shear stress values were recorded up and down between shear rates 1- 200s<sup>-1</sup> over a 60-s period. Experimental data of descending flow curve of control sample (without starch) was fitted to Ostwald-de Waale model ( $\sigma = K \dot{\gamma}^n$ ), and flow curves of samples with starch were fitted to Herschel-Bulkley model ( $\sigma = \sigma_0 + K \dot{\gamma}^n$ ). Yield stress ( $\sigma_0$ ), consistency index (K), flow index (n), apparent viscosity at 1s<sup>-1</sup> ( $\eta_1$ ) and percentage of relative hysteresis area ( $A_R$ ) values, were calculated. Since parameter K units depend on n values, apparent viscosity values at 1s<sup>-1</sup> were used instead of K to compare samples viscosity. Finally, apparent viscosity at 50s<sup>-1</sup> ( $\eta_{50}$ ) and the Kokini oral shear stress index (OSS) were calculated as physical indices of sensory thickness perceived. Wood [4] suggested that apparent viscosity at a shear rate of 50s<sup>-1</sup> represents the in-mouth shear rate and Kokini et al. [5] proposed a thickness physical index based on the change of in-mouth shear stress during product ingestion.

#### *Statistical analysis*

Two-way analysis of variance with interactions, considering SPI and starch concentrations as factors, was applied. Minimum significant differences were determined by the Tukey's test ( $\alpha=0.05$ ) (XLSTAT-Pro software v.2007, Adinsoft, Paris, France).

### **Results and Discussion**

Figure 1 shows the flow curves for soy-based desserts with different SPI and starch concentrations. All samples presented hysteresis loops when they were sheared during a complete cycle, indicating that the sample flow was time-dependent. This thixotropic behaviour increased with starch concentration.

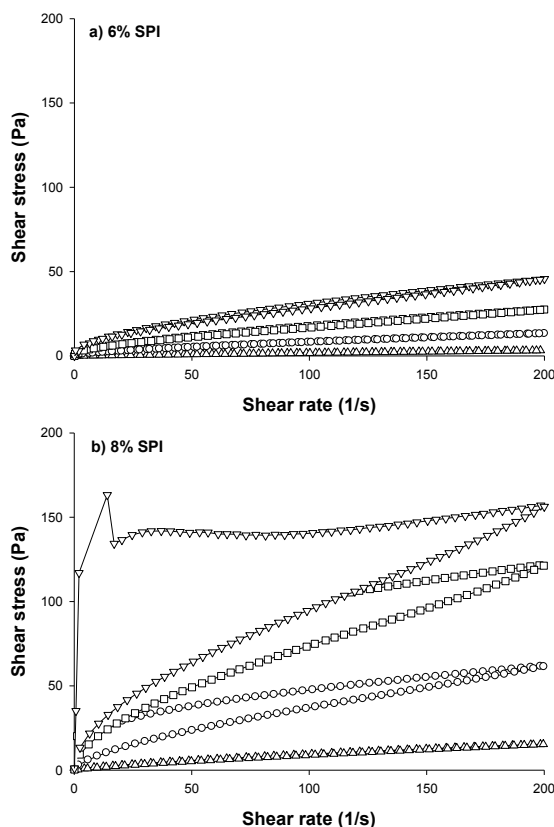


Figure 1. Flow curves of citrus flavoured soy desserts containing 6% (a) or 8% (b) of soy protein isolate (SPI) and different starch concentrations ( $\Delta$ : 0%,  $\circ$ : 2%,  $\square$ : 2.5% and  $\nabla$ : 3%)

Minor difference in both the form and magnitude of the hysteresis loops were observed in samples with 6% SPI (Figure 1a), whereas greater differences were noticed in samples with the highest SPI concentration (Figure 1b). This seems indicate that this time-dependent behaviour is influenced by both starch and SPI concentrations. Samples with starch and with the highest SPI content showed an evident overshoot in the stress-rate curves indicating a more structured system, which partially broke down with increasing shearing time (Figure 1b). A similar fact was detected by Lizarraga *et al.* [39] when the flow of whey protein concentrate and  $\lambda$ -carrageenan aqueous mixtures, was studied. They interpreted that the overshoot in flow curves at low shear rates, when WPC concentration increases, was due to the effect of interactions between the two biopolymers. The maximum in the stress represents the yielding transition since the continuous network changes to a discontinuous state at this point [7]. At the lowest SPI concentration,

it can be seen that the samples were relatively deformable by shearing and the flow curves do not show any overshoot. In general, the most of samples showed a non-Newtonian shear-thinning flow with an initial resistance to flow, that was consistent with Herschel-Bulkley model ( $R^2 > 0.99$ ). Control samples flow did not show yield stress and it fitted well to the Ostwald-de Waele model ( $0.98 < R^2 < 0.99$ ).

A two-way ANOVA with interactions was done to analyse how starch and protein concentration influenced flow parameters. ANOVA results showed a significant effect ( $p < 0.05$ ) of interaction between SPI and starch concentration on flow parameters (Table 2). This interaction indicated that the effect of starch concentration differed, depending on the SPI content. As expected,  $\sigma_0$  and  $\eta_1$  values increased significantly with starch concentration, being this variation greater in samples prepared with 8%SPI (Table 3). Except for sample A ( $n=0.90$ ) the flow index values varied between 0.70 and 0.78, indicating a clear shear-thinning behaviour. At the intermediate starch concentrations, samples with 6% (samples B and C) and its counterparts prepared with 8% SPI (samples G and H) did not show significant differences in shear-thinning (Table 3).

*Table 2. Two-way ANOVA of rheological parameters of citrus flavoured soy desserts containing different soy protein isolate (SPI) and starch concentrations. F and P values*

Flow parameters	Main effects				Interactions	
	A: SPI concentration		B: Starch concentration		A × B	
	F-value	p-value	F-value	p-value	F-value	p-value
$\sigma_0$ (Pa)	749.43	<0.01	915.27	<0.01	175.94	<0.01
n	492.70	<0.01	482.61	<0.01	110.70	<0.01
$\eta_1$ (Pa s)	1244.0	<0.01	1328.1	<0.01	347.34	<0.01
Ar (%)	1049.1	<0.01	144.59	<0.01	76.08	<0.01
$\eta_{50}$ (Pa s)	6113.5	<0.01	2803.4	<0.01	983.43	<0.01
OSS	13908	<0.01	5369.6	<0.01	1085.3	<0.01

$\sigma_0$  = yield stress, n = flow index,  $\eta_1$  = apparent viscosity at  $1\text{s}^{-1}$ , Ar = relative hysteresis area,  $\eta_{50}$  = apparent viscosity at  $50\text{s}^{-1}$  and OSS = Kokini oral shear stress index.

Regarding Ar value, it was observed that the effect of SPI content was more evident than the starch concentration, as reflected by the corresponding F values (Table 2). Samples with 8% SPI show significantly higher Ar values, and an increase in the starch content only had a significant effect at the lowest starch concentrations (2 and 2.5%) (Table 3).

Table 3. Mean values and significant differences of flow parameters of citrus flavoured soy desserts containing different soy protein isolate (SPI) and starch concentrations.

Sample Code*	$\sigma_0$ (Pa)	$n$	$\eta_1$ (Pa s)	Ar (%)	$\eta_{50}$ (Pa s)	OSS
A	-	0.90 <sup>a</sup>	0.03 <sup>a</sup>	1.29 <sup>e</sup>	0.02 <sup>a</sup>	2.67 <sup>g</sup>
B	0.61 <sup>d</sup>	0.74 <sup>c</sup>	0.98 <sup>e</sup>	1.29 <sup>e</sup>	0.11 <sup>f</sup>	6.49 <sup>f</sup>
C	2.04 <sup>c</sup>	0.74 <sup>c</sup>	2.62 <sup>d</sup>	3.78 <sup>cd</sup>	0.21 <sup>e</sup>	9.14 <sup>e</sup>
D	4.82 <sup>b</sup>	0.76 <sup>b</sup>	5.30 <sup>c</sup>	6.98 <sup>c</sup>	0.37 <sup>d</sup>	11.93 <sup>d</sup>
E	-	0.78 <sup>b</sup>	0.24 <sup>a</sup>	5.35 <sup>cd</sup>	0.10 <sup>f</sup>	6.76 <sup>f</sup>
G	1.87 <sup>c</sup>	0.72 <sup>c</sup>	3.19 <sup>d</sup>	22.82 <sup>b</sup>	0.48 <sup>c</sup>	16.24 <sup>c</sup>
H	5.01 <sup>b</sup>	0.72 <sup>c</sup>	7.14 <sup>b</sup>	30.39 <sup>a</sup>	0.81 <sup>b</sup>	21.64 <sup>b</sup>
K	12.53 <sup>a</sup>	0.70 <sup>d</sup>	16.58 <sup>a</sup>	32.25 <sup>a</sup>	1.48 <sup>a</sup>	31.43 <sup>a</sup>

$\sigma_0$  = yield stress,  $n$  = flow index,  $\eta_1$  = apparent viscosity at 1 s<sup>-1</sup>, Ar = relative hysteresis area,  $\eta_{50}$  = apparent viscosity at 50 s<sup>-1</sup> and OSS = Kokini oral shear stress index.

\* Descending flow curves data of samples A and E were fitted to Ostwald-de Waele model and flow curves of the rest of samples were fitted to Herschel-Bulkley model.

By comparing the two thickness indices values, apparent viscosity at 50s<sup>-1</sup> ( $\eta_{50}$ ) and the Kokini oral shear stress index (OSS) (Table 3), the same information was obtained. Both indices increased with starch concentration and SPI content had the greater effect. This result confirms the practical utility of these instrumental measurements to predict perceived consistency or thickness in this type of products although, as commented by Cook *et al.* [8], the OSS index has a real meaning in a sensory sense. It is not only based on one shear rate value, it accounts for the shear-thinning flow of product over a range of shear rates.

### Acknowledgements

To Sistema Bicentenario Becas Chile for the fellowship awarded to author Arancibia and to Fondo Social Europeo for financing the contract of author Bayarri (I3P program, CSIC).

### References

1. Da Silva, J., Prudencio, S., Carrão-Panizzi, M., Gregorut, C., Fonseca, F., and Mattoso L. (2012). *Int J Food Sci Tech.* 47, 1630-1638.
2. Deshpande, R.P., Chinnan, M.S., and McWatters, K.H. (2005). *J Sensory Stud.* 20,130-46.

## Part II: Food, Cosmetics and Pharmaceutical Products

3. Potter, R.M., Dougherty, M.P., Halteman, W.A, and Camire, M.E. (2007). *Lwt-Food Sci Technol.* 40, 807-814.
4. Wood, F.W. (1968). *Rheology and texture of foodstuff.* Society of Chemical Industry, London, U.K.
5. Kokini, J.L., Kadane, J.B., and Cussler, E.L. (1977). *J Texture Stud.* 8, 195–218.
6. Lizarraga, M.S., Vicin, D.D., Gonzalez, R., and Rubiolo A. (2006). *Food Hydrocolloid.* 20, 740-748
7. Arancibia, C., Bayarri, E., and Costell, E. (2013). *Food Biophys.* 8, 122-136.
8. Cook, D.J., Hollowood, T.A., Linfoth, R.S.T and Taylor, A.J. (2003). *Chem. Senses* 28, 11-23.

### *Contact Address:*

*C. Arancibia (carancibia@iata.csic.es)*

*Instituto de Agroquímica y Tecnología de Alimentos (CSIC). Avda. Agustín Escardino 7, 46980, Paterna, Valencia, Spain.*

*Tel.:+34 963900022; Fax:+34 963636301*



## CHAPTER 22

# Rheological and microstructural study on food emulsions stabilized by tuna proteins: effect of emulsion pH

Ruiz D<sup>1</sup>., Romero A.<sup>2</sup>, Franco JM<sup>1</sup>., Partal P.<sup>1</sup>, Gallegos, C.<sup>1</sup>

<sup>1</sup> Departamento de Ingeniería Química. Centro de Investigación en Tecnología de Productos y Procesos Químicos (Pro<sup>2</sup>TecS). Universidad de Huelva. Campus del Carmen, 21071, Huelva. Spain. Spain.

<sup>2</sup> Departamento de Ingeniería Química. Facultad de Química. Universidad de Sevilla. 41012, Sevilla Spain.

### Introduction

Emulsions are thermodynamically unstable systems with respect to water and oil phase separation. Many factors (e.g. pH, electrolytes, emulsifying agents, co-additives, and storage conditions) can influence emulsion stability, resulting in a wide variety of physicochemical phenomena such as phase separation, flocculation, creaming, droplet coalescence, or even chemical hydrolysis [1].

Stability, structural parameters, such as droplet size distribution and the nature and strength of interdroplet interactions, and the rheological behaviour of emulsions are closely related, all of them being influenced by the processing conditions and emulsion formulation [2].

Among emulsifiers, proteins have been widely used in the food industry, providing stability against phase separation in different food products, such as dairy products, baked food, ice creams, and mayonnaise. In food emulsions, such as mayonnaise and salad dressings, egg yolk is the most widely used emulsifier.

Nowadays, there is an increasing interest in the study of fish by-products to encourage its utilisation as a raw material in the food industry [3]. Marine by-products contain valuable proteins and lipids, as well as some vitamins and minerals. Fish by-products are mainly used for feed production as fish meal and oil; however its profitability is rather low. Better profits can be obtained by making products for industrial use and human consumption, such as biopolymers for the pharmaceutical and biotechnological industries, extraction and purification of enzymes and bioactive peptides.

Thus, different authors have used alternative proteins such as fish proteins, for example, Cofrades et al. [4] showed that acto-myosin from hake had higher

emulsifying activity and stability than acto-myosin from chicken and pork. On the other hand, Petursson et al. [5] used protein fractions extracted from cod as emulsifiers, yielding fairly stable emulsions. This work explores the feasibility of using proteins extracted from tuna as emulsifiers for novel o/w food products.

### Experimental Methods

#### *Materials*

Commercial sunflower oil was purchased from a local supermarket and used without further treatment. Tuna (Yellowfin, *Thunnus Albacares*) was kindly donated by Unión Solazonera Isleña, S.A. (USISA, España).

Protein isolates were basically obtained by following a procedure for extracting edible protein from animal muscle. At a temperature below 10°C, tuna muscle was milled and dispersed in a 0.1 mM citric acid solution, using a 1:9 weight ratio (g tuna muscle/ g citric acid solution). This dispersion, at pH between 4.0 and 4.3, was then centrifuged at 4200 rpm, for 5 min, leading to a protein precipitate and a solubilised protein fraction. The latter, with an average protein content of 2.82 wt. %  $\pm$  0.13, was collected and stored at -30°C.

#### *Emulsion preparation*

The solubilised protein fraction was used as emulsifier. Protein concentration in the emulsion was 0.50 wt% and 70 wt. % oil. Distilled and deionised water was used to prepare all solutions and o/w emulsions.

Lab-scale manufacture of emulsions was accomplished by means of an homogenizer Ultra Turrax T-50 (Ika, Steufen, Germany), at 7600 r.p.m for 5 min. Sunflower oil was slowly added to the aqueous phase (containing the remaining ingredients) at room temperature (always below 30°C). Emulsions were stored at 4°C for, at least, 24 h and, then, at 25°C, for 1 h, before testing. These samples were visually observed during storage and their stability related to the appearance of an oil-aqueous phase interface.

#### *Rheological tests*

The rheological characterization, at 25°C, was carried out in a controlled-stress rheometer RS150 (HAAKE, Germany). Small amplitude oscillatory shear (SAOS) tests, within the linear viscoelasticity region, were carried out in a frequency range comprised between 0.06 and 70 rad/s, using a cone-and-plate geometry (35 mm diameter, 1° angle). Stress sweep tests, at the frequency of 6.28 rad/s, were previously performed on each sample to determine the linear viscoelasticity region.

### Emulsion microstructure

Optical microscopy was used to study the morphology of emulsions. A drop of sample was placed between microscope slides. Emulsions were observed, at room temperature, in an optical microscope BX51 from Olympus Optical (Japan).

### Results and Discussion

Figure 1 shows stress sweep tests conducted on emulsions formulated with 70% oil, 0.5% protein and different pH value. As may be seen, the critical stress for the onset of the non-linear viscoelastic behaviour,  $\tau_c$ , decreases as pH does. Similarly, modulus values of both viscoelasticity functions become lower with as pH is more acid. However, such a decrease turns out to be more apparent between pH 3 and 2.5.

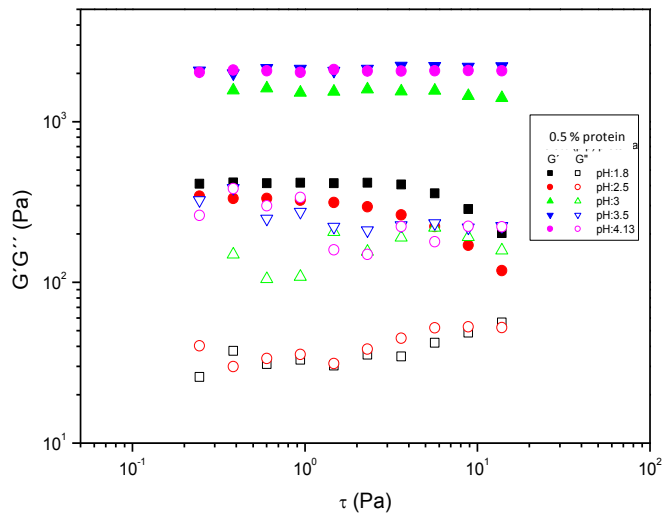


Figure 1. Stress sweep tests performed on emulsion having different pH: Storage  $G'$  and loss  $G''$  moduli.

Once the linear viscoelastic region was determined, frequency sweep tests in oscillatory shear were carried out, at constant stress, within the linear viscoelastic region. The evolution of the storage,  $G'$ , and loss,  $G''$ , moduli with frequency is shown in Figure 2.

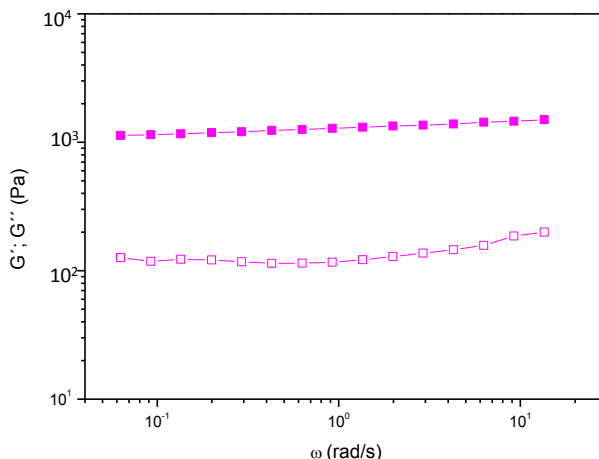


Figure 2. Evolution of moduli  $G'$  y  $G''$  with frequency: 0.5% protein, 70% oil, pH=4.13.

The storage modulus is always higher than the loss modulus within the experimental frequency range studied. Hence, these emulsions present a predominantly elastic response. Moreover,  $G'$  values show a slight and power-law dependence on frequency (Figure 2). This behaviour has been usually found in highly concentrated emulsions, such as commercial or model mayonnaises and salad dressings.

Furthermore, such a rheological response is typical of the plateau region of the mechanical spectrum and may be related to the formation of an elastic structural network due to interactions among the emulsifier molecules. Thus, the appearance of a plateau region in the mechanical spectra of emulsions has been related to an extensive flocculation process, due to interactions among the emulsifier molecules. In this case, proteins lead to the formation of an extensive three-dimensional network, due to entanglements among protein segments adsorbed at the oil-water interface.

Concerning emulsions stabilized by tuna proteins, the nature and strength of such interactions among droplets seem to give rise to different viscoelastic modulus values which depend on the selected pH.

Figure 3 shows micrographs taken from emulsions formulated at two pHs. From them, droplet size distribution can be deduced. The two selected emulsions show smaller droplets as pH is lower. It is worth noting that both a high flocculation degree and the low mean particle diameter would contribute to an increase in the viscoelastic moduli.

However, even though smaller droplets are obtained by lowering pH, the resulting emulsion exhibits a weakening (i.e. lower moduli) of its microstructure suggesting a reduced entanglement density for the most acid emulsion.

These results suggest that the effect of pH on the elastic network of these emulsions may be mainly explained in terms of the modification in the density of entanglements among droplets.

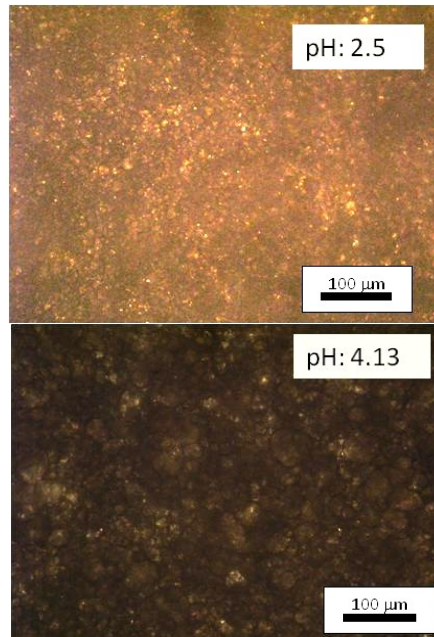


*Figure 3. Micrographs of emulsions at pH 2.5 and 4.13*

### **Concluding Remarks**

The observed viscoelastic behaviour is typical of highly structured systems and has been usually found in highly concentrated emulsions, such as commercial or model mayonnaises and salad dressings.

However, these emulsions may exhibit a weakening in its microstructure at low pH, suggesting a reduced entanglement density under acidic conditions.

As a result, proteins from the bulk and from the o/w interface participate in this process, leading to highly structured systems in which the viscoelastic response, under oscillatory shear, would be mainly controlled by such a connective protein network, particularly at pH values close to the protein isoelectric point (located at about pH=5.5).

### References

1. Heurtault, B., Saulnier, P., Pech, B., Venier-Julienne, M., Proust, J., Phan-Tan-Luu, R., Benoit, J. (2003). *Eur. J. Pharm. Sci.* 18: 55-61.
2. Gallegos, C. and Franco, J.M. (1999). Rheology of food Emulsions in *Advances in the Flow and Rheology of Non-Newtonian Fluids*, edited by D. Siginer, D. De Kee, and R.P. Chhabra, Elsevier, Amsterdam 87-118
3. García-Sifuentes, C., Pacheco-Aguilar, R., Lugo-Sánchez, M., García-Sánchez, G., Ramírez-Suárez J.C., García-Carreño, F. (2009). *Food Chem.* 114: 197–203.
4. Cofrades, S., Carballo, J., Careche, M., & Colmenero, F. J. (1996). *Food Science and Technology-Lebensmittel-Wissenschaft Technologi.* 29: 379–383.
5. Petursson, S., Decker, E. A., & McClements, D. J. (2004). *Journal of Agricultural and Food Chemistry* 52: 3996–4001.

### Contact Address:

*D. Ruiz (dolores@uhu.es)*

*Department: Ingeniería Química*

*Faculty/School of Engineering: Facultad de Ciencias Experimentales*

*University: 21071. Huelva*

*Address: Campus del Carmen*

*Tel: 34 959 21 82 04; Fax: 34 959 21 99 83*

## **PART III**

# **Formulation and Product Engineering**



## CHAPTER 1

# Influence of homogenization rate of O/W emulsions containing a mixture of green solvents and a polyoxyethylene glycerol ester.

*J. Santos, L.A. Trujillo, M.C. García, J. Muñoz and N. Calero.*

*Departamento de Ingeniería Química. Facultad de Química. Universidad de Sevilla c/ P. García González, 1, E41012, Sevilla, Spain.*

### Introduction

The role of green solvents in the chemical and pharmaceutical industries is becoming more and more important. Thus, many of the classical solvents used in agrochemical formulations are being gradually withdrawn from the market in developed countries and replaced by solvents derived from renewable raw materials. Fatty acid dimethylamides are green solvents which may find applications in different fields [1]. We report in this chapter information on the development of emulsions containing a fatty acid dimethylamide and in addition D-Limonene. The latter can be derived from lemon peel and find applications in cosmetics, detergency and food stuffs. Ethoxylated glycerine esters are eco-friendly and nontoxic surfactants [2], hence they can be tested as emulsifiers. Emulsions are unstable from a thermodynamic point of view, although they can exhibit a high kinetic stability. Most applications of emulsions rely on a long physical stability. Rheological tests conducted under linear conditions are sensitive to the microstructure of emulsions. However, they must be interpreted with caution when monitoring the physical stability of emulsions. This is especially challenging if two destabilization mechanisms are taking place simultaneously [3]. In addition, studying the flow behaviour of emulsions is vital to assess their applications. The microstructure of emulsions must stand the flow fields required for their applications. Bearing all the factors analysed in mind we have designed

an experimental set up not only based on rheometry but also on laser diffraction and multiple light scattering.

The main objective of this work was to study the influence of the homogenization rate on both the rheology and physical stability of slightly concentrated O/W emulsions formulated with a mixture of a fatty acid dimethylamide and D-limonene as green solvents.

### Experimental

The fatty acid dimethylamide used was namely N,N-dimethyldecanamide (DMA-10) kindly provided by BASF. D-limonene was purchased from Sigma-Aldrich. A polyoxyethylene glycerol ester, Levenol C-201<sup>®</sup>, (HLB: 13) provided by KAO as a gift, was used as emulsifier.

The preparation of O/W emulsions studied was carried out using a rotor-stator homogenizer (Silverson L5M), equipped with a mesh screen, at different homogenization rates (7000, 6000, 5000, 4000 and 3000 rpm) for an operation time of one minute. The composition of emulsions was as follows. 30 wt% mixture of green solvents (mass ratio: 75% DMA-10/25% D-Limonene); 3 wt% polyoxyethylene glycerol ester; 0.1 wt% antifoam emulsion (Dow Chemical).

The droplet size distribution (DSD) measurements of emulsions were performed with a laser diffraction particle size analyzer (Mastersizer X, Malvern). DSD measurements were conducted as a function of aging time after 3, 13, 21, and 40 days of preparation.

Rheological experiments were done with a Haake MARS controlled-stress rheometer, equipped with a sand-blasted Z-20 coaxial cylinder (Thermo-Scientific, IFI). Sand blasting prevents significant wall-depletion phenomena from occurring under shear flow. Steady shear flow tests were carried out from 0.05 to 1Pa, at 20°C and different aging times (3, 13, 21 and 40 days). Special attention was paid to sampling strategy in order to avoid experimental artefacts.

Multiple light scattering (MLS) measurements were carried out with a Turbiscan Lab-Expert analyzer (Formulaction) at room temperature.

## Results and Discussion

Table 1 shows the Sauter mean diameter ( $D_{32}$ ) of oil droplets for the emulsions studied as a function of homogenization rate.  $D_{32}$  decreased with homogenization rate, levelling off between 6000 - 7000 rpm. However, the rheology and physical stability of emulsions against creaming may be conditioned not only by the size of droplets but also by the polydispersity of size distribution. The polydispersity of emulsions was determined on the basis of the uniformity. This increased by 22% when the homogenization rate increased from 6000 rpm to 7000 rpm. Thus, although the  $D_{32}$  was slightly smaller, a marked increase of polydispersity occurred for the emulsion processed at 7000 rpm (data not shown). In fact the DSD shifted from monomodal to bimodal when the homogenization rate increased from 4000 rpm to 5000 rpm. At the latter rate and above over-processing yielded some coalescence.

Table 1. Sauter diameters for the emulsions processed at different homogenization rates.

	Homogenization rate (rpm)				
	7000	6000	5000	4000	3000
$D(3,2)$ ( $\mu\text{m}$ )	0.33	0.35	0.47	0.73	1.07

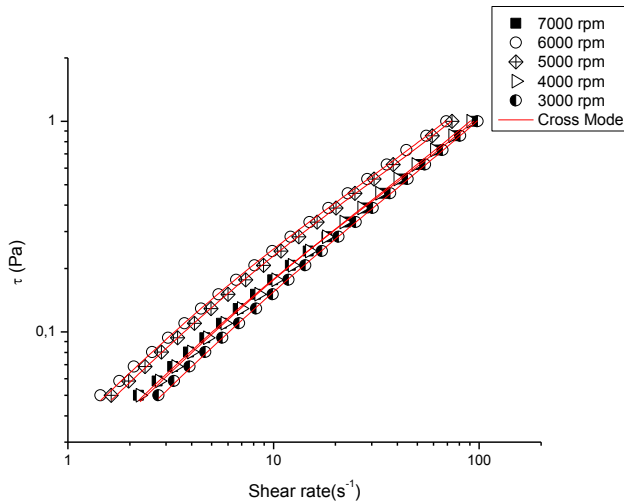


Figure 1. Flow curves for all the emulsions studied at different homogenization rates.  
 $T^a=20^\circ\text{C}$ .

Figure 1 shows the flow curves of all emulsions formulated at different homogenization rates, fitted to the Cross model, neglecting the infinite-shear rate Newtonian viscosity. The zero shear viscosity increased with homogenization rate in the 3000-6000 rpm range, while both the critical shear rate for the onset of shear thinning response and the flow index decreased. The zero-shear viscosity exhibited a peak of 70 mPa·s for the emulsion processed at 6000 rpm, which also showed the lowest  $D(v, 0.9)$ . This supports the maximum viscosity may be ascribed to an increase in the effective disperse phase concentration [4]. Interestingly, the emulsion processed at 7000 rpm showed values of Newtonian viscosity; flow index and critical shear rate that ranged between those of the emulsions processed at 3000 rpm and 4000 rpm regardless of its low  $D_{32}$  value. This emphasizes the important effect of the high volume fraction of the bimodal DSD. The effect of recoalescence induced by over processing probably was more important than the low  $D_{32}$  values achieved. Conversely the contrary seems to be true for the emulsion prepared at 6000 rpm.

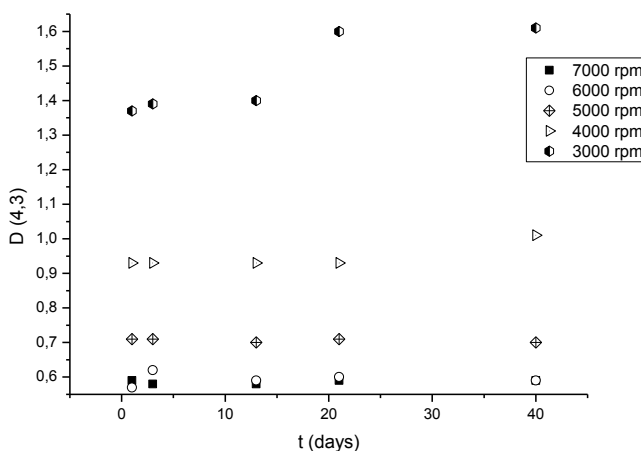


Figure 2. Volume mean diameter as a function of aging time for all the emulsions studied at different homogenization rates.

Figure 2 shows the volume mean diameters for all emulsions monitored at different aging times. No significant changes in volume mean diameters were observed for any of the emulsions studied except for the emulsion processed at 3000 rpm. In this case, the volume mean diameter increased from day 13 to day 40, indicating the occurrence of some coalescence.

Figure 3 illustrates the effects of aging time on the flow behaviour of the emulsion processed at 5000 rpm. Flow curves fitted the Cross model. Table 2 shows that the zero-shear viscosity increased with aging time for all the emulsions studied, except for that processed at 3000 rpm from day 21 onwards. This fact supports the result obtained by laser diffraction, which indicated the existence of some coalescence. This was induced by a previous creaming process. Increasing zero-shear viscosity values with aging are consistent with the occurrence of a destabilization mechanism based on creaming.

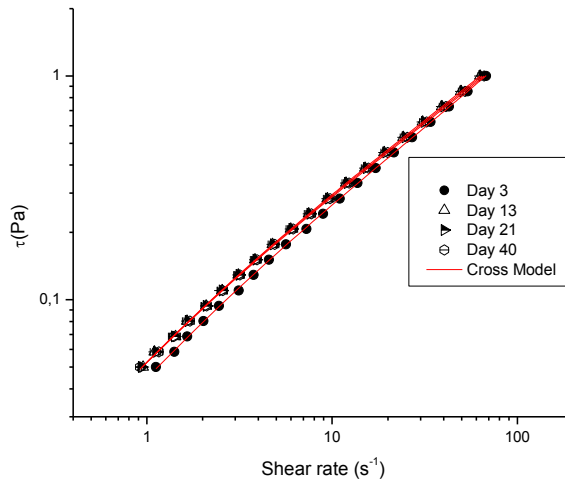


Figure 3. Influence of aging time on the flow curves for the emulsion processed at 5000 rpm. Continuous lines illustrate data fitting to the Cross model.

Table 2. Influence of aging time on the Newtonian viscosity for the emulsions processed at different homogenization rates

$\eta_0$ (mPa·s)	Homogenization rate (rpm)				
Aging time	7000	6000	5000	4000	3000
3 days	42	70	61	46	29
13 days	44	74	75	57	38
21 days	51	81	75	59	33
40 days	51	81	76	61	30

Figure 4 shows MLS results for the emulsion processed at 5000 rpm. All emulsions showed a decrease of backscattering (BS) in the lower part of the vial. This confirms that a creaming process is taking place. The delay time for the onset of creaming was detected at shorter aging time for emulsions processed below 5000 rpm. The best MLS results were exhibited by the emulsion prepared at 6000 rpm.

### Concluding Remarks

We may conclude that the emulsion processed at 6000 rpm showed the best results related to its physical stability, possessing the minimum value for  $D(v, 0.9)$  and the maximum value of  $\eta_0$ . Furthermore, the variation of  $\eta_0$  for this emulsion was less pronounced with aging time than for the rest of the emulsions studied. This work demonstrates that the use of the combination of rheological measurements, laser diffraction and multiple light scattering techniques is a powerful tool for the detection of physical destabilization mechanisms of emulsions.

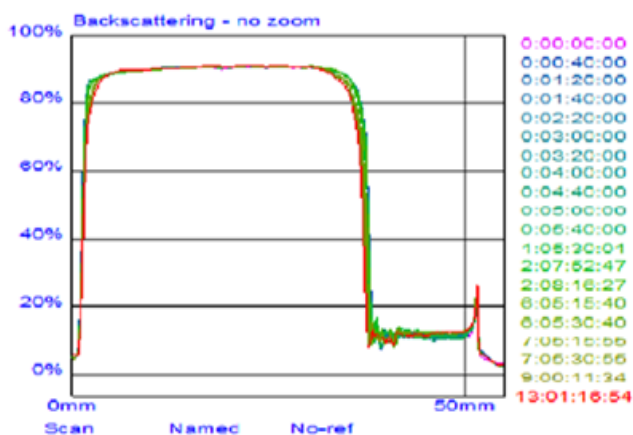


Figure 4. Influence of the aging time on the backscattering in the emulsion processed at 5000 rpm.

### Acknowledgments

The financial support received (Project CTQ2011-27371) from the Spanish MINECO and from the European Commission (FEDER Programme) is kindly acknowledged.

## References

1. Bigorra, J. (2010). Innovative solvents based on renewable raw materials. Proceedings of 40th Annual Meeting of CED. Barcelona, Spain.
2. Castán, P., González, X. (2003). Skin properties of glycerine polyethoxylene esters. Proceedings of 40th Annual Meeting of CED. 33, 325-338.
3. Tadros, Th.F. (2010). Rheology of Dispersions. Principles and Applications. Wiley-VCH. Weinheim, Germany.
4. Barnes, H.A. (1989) A introduction to rheology. Elsevier science publishers b.v. Amsterdam, The Netherlands.

### *Contact Address:*

*N. Calero (nuriacalero@us.es)*

*Departamento de Ingeniería Química.*

*Facultad de Química. Universidad de Sevilla.*

*c/ P. García González, 1, E41012, Sevilla, Spain. Telf.:+34 954 557179; Fax:+34 954556447*



## CHAPTER 2

# Rheological behaviour and microstructure of NCO-terminated castor oil bituminous products

A.A. Cuadri, M. García-Morales, F.J. Navarro, P. Partal

*Departamento de Ingeniería Química, Centro de Investigación en Tecnología de Productos y Procesos Químicos (Pro<sup>2</sup>TecS), Campus de 'El Carmen', Universidad de Huelva, 21071, Huelva (Spain).*

### Introduction

Bitumen, by-product from crude oil fractionation, has shown to be the most suitable material as a binder in paving [1]. Unfortunately, road pavements deteriorate over time under the combined effects of traffic loading and weathering. Common road distresses are: a) rutting or permanent deformation of the pavement at the hottest climates; and b) thermal cracking, also referred to as thermal fracture, due to pavement lack of flexibility at low temperatures [2].

Hence, bitumen performance has traditionally been improved through the addition of either “passive” virgin polymers (SBS, SBR, EVA, etc.) or waste polymers (plastics from agriculture crumb tyre rubber, etc.). These polymers are just physically mixed with bitumen. As an alternative, “active” polymers are able to form chemical bonds with some bitumen fractions, which prevent the resulting blend from phase separation during its storage at high temperature in absence of stirring [3]. In this category, the most common are the MDI-derived prepolymers [4] which consist of a “soft or flexible segment” represented by polyols (PEG, PPG, etc.), and a “hard or stiff segment” constituted by diisocyanates (MDI, HDI, etc.). Recently, the utilization of renewable resources in the formulation of MDI-derived prepolymers results of increasing interest as a substitute for petro-chemical derivatives [5].

On this ground, a NCO-terminated prepolymer derived from castor oil has been used as modifier in asphaltic binders with improved rheological properties.

### Experimental Methods

#### *Materials*

Bitumen with a penetration of 114 dmm and R&B softening temperature of 40 °C, according to ASTM D5 and ASTM D36, respectively, was used as base material for the polymer modification.

Two different types of polymers, which represent “active” and “passive” categories, respectively, have been considered:

- a) On the one hand, castor oil (with hydroxyl index of 125 mg KOH/g) was functionalised with isocyanate groups, by its reaction with polymeric 4,4'-diphenylmethane diisocyanate (with free -NCO content of 31 wt.%). This reaction was carried out at 60 °C, for 48 h, under agitation and with N<sub>2</sub> blanketing. A molar ratio -NCO/-OH of 8:1 was selected, assuring an excess of non-reacted MDI molecules in the product (referred to as MDI-CO). This polymer is expected to bring about "chemical" modification of bitumen, via -NCO groups.
- b) On the other hand, for the sake of comparison, the commercially available SBS triblock copolymer "Kraton D-1101" was selected for "physical" modification, through its mere physical dispersion in bitumen.

#### *Samples Preparation*

In relation to “chemical” modification, blends of bitumen and 2 wt. % of MDI-CO prepolymer were prepared, at 90 °C and for 1 h, in a cylindrical vessel with a four-bladed turbine rotating at 1200 rpm. Subsequently, the resulting binder was divided into three parts: i) one was tested as such (“non-cured” binder); ii) another one was further mixed with 2 wt.% water, at 90 °C and for 45 min (“water-modified” binder); and iii) the third part was poured onto aluminium foil, forming a thin layer which was exposed for up to 6 months to the ambient, under free access of air/moisture (“ambient- cured” binder).

In addition, “physical” modification was carried out by adding 3 wt. % SBS to the base bitumen (formulation typically used in the paving industry). This blend was processed at 180 °C and for 2 h, in a high shear mixing device.

#### *Testing procedures*

Viscous flow measurements, at 60 °C, were conducted in a controlled-stress rheometer Physica MCR-301 (Anton Paar, Austria). Serrated plate-and-plate geometry (25 mm diameter and 1 mm gap) was always used.

Modulated Differential Scanning Calorimetry (MDSC) was performed with a TA Q-100 (TA Instruments, USA). Samples of 5-10 mg were always subjected to the following testing procedure: temperature range from -40 to 85°C; heating rate of 5 °C/min; amplitude of modulation of 0.5 °C; a period of 60 s; and N<sub>2</sub> as purge gas, with a flow rate of 50 mL/min. In order to provide the same recent thermal history,

all the samples were placed into hermetic aluminium pans for 24 h before measurement.

## Results and Discussion

Figure 1 displays the viscous flow curves, at 60 °C, for neat bitumen, SBS-reference and MDI-CO modified binders. A nearly Newtonian behaviour in the whole interval of shear rates tested is shown by the neat bitumen. On the contrary, MDI-CO modified binders present a different viscous flow behaviour, with a constant viscosity,  $\eta_0$ , at the lowest shear rates, followed by a shear-thinning region above a “critical” shear rate value,  $\dot{\gamma}_c$ .

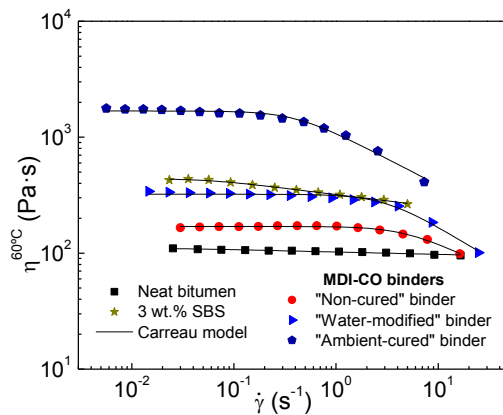


Figure 1. Viscous flow curves, at 60 °C, for neat bitumen, SBS-reference binder and MDI-CO modified binders.

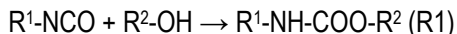
This behaviour can be described by the Carreau’s model fairly well:

$$\frac{\eta}{\eta_0} = \frac{1}{\left[1 + (\lambda \cdot \dot{\gamma})^2\right]^s} \quad (1)$$

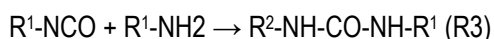
where  $\eta_0$  (Pa·s) is the zero-shear viscosity,  $\lambda$  (s) is a time constant whose inverse approximately matches the threshold shear rate mentioned above, and “s” is a parameter related to the slope of the shear-thinning region. Table 1 gathers Carreau’s model parameters calculated for the different modified bitumen samples prepared.

As can be observed in Figure 1, the “non-cured” binder presents a clearly higher value of viscosity than the neat bitumen. Thus, during the bitumen-prepolymer blending for 1 h, a part of the free -NCO is known to react with certain pendant groups, mainly -OH, present in the asphaltene molecules. This provokes an

increase in the binder viscosity, due to the formation of urethane linkages according the following reaction [6]:



However, a much higher degree of modification was observed when the binder was subjected to a further curing stage of up to 6 months at room temperature (see “ambient-cured” binder in Fig.1). With this regard, some water from the ambient is expected to slowly diffuse into the modified binder, promoting the two following series reactions [6]:



A significant increase in the binder viscosity derived from the development of a more complex microstructure is achieved [4]. On the other hand, 2 wt. % water was added to the modified binder after its processing, in an attempt to spare the time required for its maturing. However, it was not possible to obtain a material equivalent to the 6 months-cured binder by mere addition of water. These observations confirm that the slow diffusion of water into previously MDI-CO binder results is a more efficient method of bitumen chemical modification, if compared to the direct water addition. Thus, reactions R1, R2 and R3 would be occurring simultaneously during the curing stage. On the contrary, direct addition of water would compete with the bitumen for the free –NCO sites available and reaction R1 would be hampered, which limits the resulting degree of modification.

In addition, the Carreau’s model parameters (see Table 1) reveal the development of a more complex microstructure for the “ambient-cured” binder, as demonstrated by a higher value of viscosity, along with a lower  $\dot{\gamma}_c$ , which denotes a higher level of susceptibility to shearing [4].

*Table 1. Carreau’s model parameters for neat bitumen, SBS-reference sample and MDI-CO modified binders.*

	$\eta_0$ (Pa·s)	$\lambda$ (s)	s
Neat bitumen	110	--	0.01
3 wt. SBS	438	16.67	0.05
“Non-cured” binder	170	0.22	0.20
“Water-modified” binder	322	0.33	0.26
“Ambient- cured” binder	1683	2.51	0.22

The above-mentioned enhancements in the binders rheological behaviour suggest significant changes in their microstructure, which can be detected by means of the non-reversing component of the heat flow curve obtained by modulated DSC.

The analysis of the “fourth” thermal event, as reported by Masson and Polomark [7], may provide an approximate idea on changes occurred at a microstructural level. In fact, that event (endotherm at 50 °C) relates to the diffusion of relatively large structures with high molecular weight, as those found in resins and asphaltenes, to form independent domains. Thus, the enthalpy values associated to this event,  $\Delta H_{4th}$ , are clearly seen to increase after MDI-CO/modification and water addition (“water-modified” binder), and, mainly, through ambient curing for 6 months (“ambient-cured” binder), with values of 2.55 and 6.82 J/g, respectively. This fact demonstrates a larger rearrangement of domains composed by high molecular weight structures, with melting temperatures between 40 and 80 °C, and provides an explanation to the previous viscous flow curves.

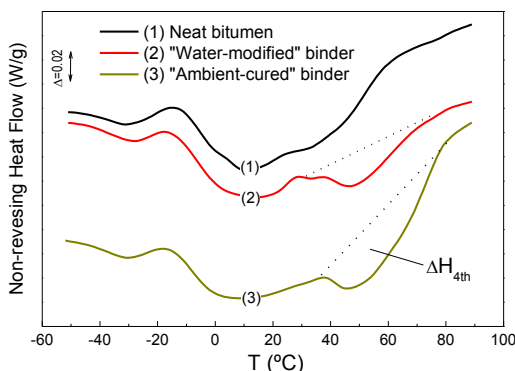


Figure 2. Non-reversing heat flow curves for neat bitumen, “water-modified” and “ambient-cured” binders.

### Concluding Remarks

In this work, the bitumen modification based on NCO-terminated PU prepolymers has been evaluated. Thus, castor oil was used as an alternative polyol in its synthesis. Two different routes were identified: a) first one, which takes place during the blending of prepolymer/bitumen; and b) second one, which develops during the binder ambient curing, or after addition of water. Interestingly, a viscosity increase of more than one decade was observed after 6 months of ambient curing, which represents a more efficient way of modification than water addition itself.

The results evidence the adequacy of castor oil in the synthesis of NCO-functionalized prepolymers for chemically modified bituminous binders, and may constitute a step forward in the use of polyols derived from this and other renewable sources.

### References

1. Read, J., Whiteoak, D. (1967). The Shell Bitumen Handbook, fifth ed., Surrey, U.K.
2. Cuadri, A.A., Partal, P., Navarro, F.J., García-Morales, M., Gallegos, C. (2011). Fuel 90, 2294-2300.
3. Pérez-Lepe, A., Martínez Boza, F.J., Attané, P., Gallegos, C. (2006). J. Apply. Polym. Sci. 100, 260-267.
4. Martín-Alfonso, M.J., Partal, P., Navarro, F.J., García-Morales, M., Gallegos, C. (2008). Eur. Polym. J. 44, 1451–1461.
5. Swamy, B.K.K., Siddaramaiah, Somashekar, R. (2003). J. Mater. Sci. 38, 451-460.
6. Singh, B., Tarannum, H., Gupta, M. (2003). J. Appl. Polym. Sci. 90, 1365–1377.
7. Masson, J.F., Polomark, G.M. (2001). Thermochem. Acta 374, 105-114.

### Contact Address:

Antonio Cuadri ([antonio.cuadri@diq.uhu.es](mailto:antonio.cuadri@diq.uhu.es))

*Departamento de Ingeniería Química*

*Centro de Investigación en Tecnología de Productos y Procesos Químicos (Pro<sup>2</sup>TecS), Campus de 'El Carmen' • Universidad de Huelva*

*Huelva, 21071,(Spain).*

## CHAPTER 3

# Rheological Characterization of $\alpha$ -pinene multiple emulsions formulated with two amphiphilic copolymers with different HLB and gellan gum.

M.C. García<sup>1</sup>, M.C. Alfaro<sup>1</sup>, J. A. Carmona<sup>1</sup>, P. Cox<sup>2</sup>, J. Muñoz<sup>1</sup>

*1 Departamento de Ingeniería Química. Facultad de Química. Universidad de Sevilla.*

*2 Department of Chemical Engineering. University of Birmingham.*

### Introduction

There is an increasing interest in finding alternative solvents to those classically used that pose safety, health and environmental (SHE) hazards. Alpha-pinene is a terpenic solvent which can be classified as renewable and green solvent.

The formulation of multiple emulsions requires at least an oil phase, an aqueous phase and two emulsifiers. One of them must be mainly hydrophobic, while the other mainly hydrophilic [1]. Apart from emulsifying properties, amphiphilic copolymers provide steric stabilization not only due to their high molecular weight but also to their tailored chemical structure [2].

Multiple emulsions are formed by large and polydispersed droplets which are thermodynamically unstable. In addition to the classic destabilization processes (coalescence, flocculation and creaming), a) water drops may coalesce with others inside oil droplets or b) the multiple drops may lose their internal droplets. Water permeation by diffusion through the oil membrane may cause swelling or shrinking of droplets [3], [4], [5].

Polysaccharides are currently used as thickening agents and stabilizers of emulsions. Gellan gum is a polysaccharidic biopolymer which is commercially manufactured by microbial fermentation. It must be noted that gellan gum exhibits excellent gelling properties at very low gum concentrations hence it is used in foods. However its applications as stabilizer of emulsions have scarcely been studied.

The goal of this study was to analyze the effect of a change in the mass ratio of copolymers on the properties of  $\alpha$ -pinene multiple emulsions prepared by means

of a protocol in series based on rotor-stator, high-pressure valve and rotor-stator homogenizations.

### Experimental

Low-acyl gellan gum (Kelcogel-F) was kindly provided by CP Kelco-San Diego and was used at 0.4 wt % concentration. Sodium azide (0.1 wt%) was used as preservative. A blend of polydimethylsiloxane and modified starch (Rhodia) was used as defoaming agent at 0.05 wt%. The oil phase was  $\alpha$ -pinene Leavo 95 provided by Destilaciones Bordas- Chinchurreta. AB hydrophilic nonionic polyakylene oxide (EO-PO) block copolymer Atlas G-5000™ (HLB 16.9) and ABA hydrophobic block copolymer Atlox 4912™ (HLB: 5-6), obtained by esterification of poly(12-hydroxystearic acid), PHSA (A) with poly alkylene glycols (B), were kindly provided by Croda.

Emulsions were prepared as follows. Atlas G-5000™ and Atlox 4912™ were separately dissolved in deionized water and  $\alpha$ -pinene, respectively. This was achieved with a magnetic rod Hotplate stirrer [SB162-3], Stuart, Scientific Laboratory Supplies. A primary emulsion was prepared using a Silverson L4RT rotor-stator homogenizer selecting a rotational speed of 10600 rpm and an operation time of 150 s. Subsequently the primary emulsion was submitted to 3-passes under high-pressure valve homogenization (FT9 Homogeniser, Armfield) at 6894 kPa (68 atm). The last step consisted of mixing the resulting emulsion with a concentrated gellan gum aqueous solution for 60 s, using the Silverson homogenizer.

Note: E30/X/Y stands for emulsions containing 30 wt%  $\alpha$ -pinene, X wt% Atlas G-5000™ and Y wt% Atlox 4912™.

Emulsions aged for two days were characterized by rheology at 20°C, laser diffraction and confocal scanning laser microscopy (CSLM) at room temperature.

Mechanical spectra were determined by small amplitude oscillatory shear (SAOS) from 3 to 0.01Hz, allowing an equilibration time of 600s. These tests were carried out with a TA Instruments AR-1000 CS-rheometer, using a cone & plate geometry (60mm diameter and 10° angle). Flow curves were run using the same rheometer with a 40mm diameter serrated parallel plate geometry, using a controlled-stress protocol.

The droplet size distributions (DSDs) of multiple emulsions were determined by laser diffraction with a Malvern Mastersizer Hydro2000 analyser.

A SPE Leica confocal scanning laser microscope was used with a 60X oil immersion objective.

## Results and Discussion

### *Mechanical spectra*

Mechanical spectra exhibited  $G'$  values higher than those of  $G''$  in the whole frequency range studied, indicating that the elastic component was dominant on the viscous one in these emulsions. Figure 1 illustrates the results obtained as a log-log plot of the complex viscosity against angular frequency. Complex viscosity values increased with the Atlas G-5000™/Atlox 4912™ mass ratio, MR, in emulsions formulated with both copolymers. With regards to emulsions formulated with just one of the copolymers, the emulsion containing Atlox 4912™ exhibited the lowest complex viscosity values, while the emulsion formulated with Atlas G-5000™ showed values which were not significantly different to those of the emulsion with a MR value of 2. A deeper analysis of results plotted in Figure 1 reveals that two groups of emulsions can be identified. The higher complex viscosity values were found for emulsions with  $MR \geq 2$ , i.e. for emulsions with a high content in Atlas G-5000™. On the other hand, emulsions with  $MR \leq 1.0$  showed significantly lower complex viscosity values. In fact, these values progressively went down as MR values decreased. In addition a clear change in the frequency dependence of the loss tangent took place for  $MR \leq 0.2$ .

### *Flow curves*

Figure 2 shows the flow curve results. All the emulsions studied exhibited shear thinning behaviour under steady shear. The highest viscosity values at the lowest shear stresses are shown by emulsions with a high Atlas G-5000™/Atlox 4912™ mass ratio, accordingly to the viscoelastic results obtained (Figure 2). Differences in viscosity dampened with increasing shear stress such that they were not significant above roughly 10 Pa or  $1 \text{ s}^{-1}$ .

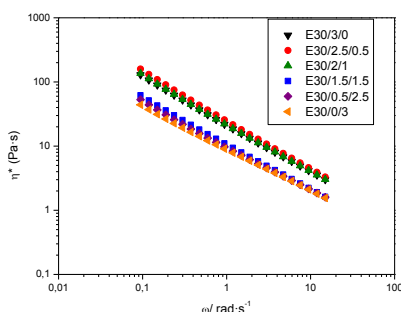


Figure 1. Influence of Atlas G-5000/ Atlox 4912 mass ratio on the frequency dependence of complex viscosity in 30 wt%  $\alpha$ -pinene multiple emulsions.  $T=20^{\circ} \text{ C}$ .

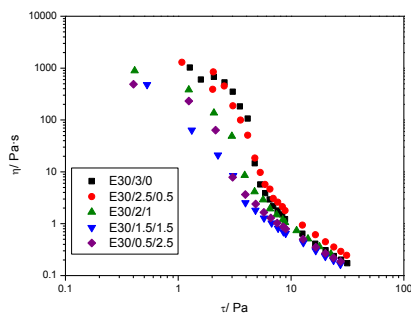


Figure 2. Influence of Atlas G-5000/ Atlox 4912 mass ratio on flow curves of 30 wt%  $\alpha$ -pinene multiple emulsions.  $T=20^{\circ}$  C.

### CSLM micrographs

Figure 3 shows, as an example, the CSLM results obtained for an emulsion formulated with Atlas G-5000™ as unique emulsifier. Oil droplets formed a network of entangled flocs which were trapped in the viscous continuous phase formed by gellan gum. This guaranteed a long physical stability. A reduction of the MR parameter to 1 resulted in a loss of connectivity among oil flocs and a slight increase of Sauter and volumen mean diameters (coalescence) (parameters in Table 1). The lack of Atlas G-5000™ in the formulation was catastrophic for the microstructure of these emulsions since extensive coalescence could be clearly observed. The micrographs support the rheological and droplet size distribution results obtained.

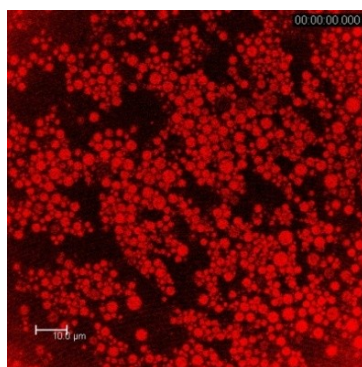


Figure 3. CSLM micrograph of E30/3/0 (prepared with Atlas G-5000™ as emulsifier)  $\alpha$ -pinene multiple emulsion aged for 2 days

Table 1. Sauter's mean diameter, volume mean diameter and span of 30 wt%  $\alpha$ -pinene emulsions aged for 2 days.

	D [3,2] ( $\mu\text{m}$ )	D [4,3] ( $\mu\text{m}$ )	Span
E30/3/0	2.59	3.12	1.20
E30/2.5/0.5	2.66	3.24	1.23
E30/2/1	2.38	3.11	1.36
E30/1.5/1.5	2.52	3.46	1.43
E30/0.5/2.5	2.72	4.00	1.73
E30/0/3	12.11	29.20	1.16

## Conclusions

Alpha-pinene in W/O/W emulsions can be prepared using an AB hydrophilic non-ionic block copolymer, Atlas G-5000™ or using additionally an ABA hydrophobic block copolymer Atlox 4912™. The presence of gellan gum in the continuous phase guarantees a long-term physical stability.

Slightly concentrated (30 wt%)  $\alpha$ -pinene multiple emulsions prepared with 3 wt% copolymer and 0.4 wt% gellan gum showed viscoelastic properties with the elastic component being dominant over the viscous one. Under steady shear these emulsions exhibited shear thinning flow properties.

The microstructure of these emulsions consists of  $\alpha$ -pinene droplets containing water droplets inside, which are trapped in a continuous phase controlled by a concentrated gellan gum solution. The best results, according to rheological, droplet size distribution and microstructural information, were obtained when a ratio of 2.5 wt% Atlas G-5000™ to 0.5 wt% Atlox 4912™ was used as emulsifier.

## Acknowledgements

The financial support received (Project CTQ2011-27371) from the Spanish Ministerio de Economía y Competitividad and from the European Commission (FEDER Programme) is kindly acknowledged. The authors are also grateful to the following companies for providing materials for this research, Croda, CP Kelco and Destilaciones Bordas-Chinchurreta.

### References

1. Opawale, F. O., and Burgess, D. J. *J Pharm Pharmacol* 50 (1998) 965-973.
2. Reekmans, S., Novel surfactants and adjuvants for agrochemicals. In: *Chemistry and Technology of Agrochemical Formulations*. Ed. D. A. Knowles. Kluwer Academic Publishers. The Netherlands (1998).
3. Mastsumoto, S., Inoue, T., Kohda, M., Ohta, T., An attempt to Estimate Stability of the oil layer in W/O/W emulsions by means of viscosimetry. *J. Interface Sci.* 77, (1980) pp 564-565.
4. Florence, A. T., Whitehill, D., *Int. J. Pharm*, 11 (1982) 277-308.
5. Sugiura, S., Nakajima, M., Yamamoto, K., Iwamoto, S., Oda, T., Satake, M., Seki, M. *Journal of Colloid and Interface Science* 270 (2004) 221-228.

### Contact Address:

*M.C. García (mccgarcia@us.es)*

*Dpto. Ingeniería Química,*

*Facultad de Química,*

*Universidad de Sevilla, C/ P. García González s/n, 41012, Sevilla (Spain)*

*Tel.:+34 954 557179 // Fax:+34 954 556447.*

## CHAPTER 4

# Modification of PVC plasticizers using ionic liquids

*S. Marceneiro<sup>1,2</sup>, Q. Hu<sup>1</sup>, A.M.A. Dias<sup>1</sup>, I. Lobo<sup>2</sup>, E. Pinho<sup>2</sup>, H.C. de Sousa<sup>1</sup>, M. G. Rasteiro<sup>1</sup>*

<sup>1</sup>*CIEPQPF, Chemical Engineering Department, FCTUC, University of Coimbra, Rua Sílvio Lima, Pólo II – Pinhal de Marrocos, 3030-790 Coimbra, Portugal*

<sup>2</sup>*TMG Automotive, S. Cosme do Vale, Apartado 14, 4761-912 Vila Nova de Famalicão, Portugal*

### Introduction

Plasticized poly(vinyl chloride), PVC, is a rubbery material which is obtained from plastisols [1]. The major plasticized PVC applications are usually flexible consumer products, such as wires, isolation cables, flooring, and packaging materials, as well as medical and automotive applications [2]. Plasticizers can weak the intermolecular bonds between polymer chains, improving its workability, toughness and flexibility [3]. In industrial processing, PVC particles are firstly swollen by the plasticizer and the final flexible product is later obtained by the gelation (with temperature) of the swelled particles [4,5]. The plasticizing efficiency largely depends on the type and concentration of employed plasticizers, which have also a direct influence on the plastisols rheological, thermal and mechanical properties of the processed polymers [6]. Depending on the target application, the rheological behaviour of PVC plastisols, mainly their aging behaviour (increase of the viscosity with time) is one of the most important properties to take into account [7,8]. The most commonly used PVC plasticizers are alkyl esters of phthalic acids, such as Di-isononyl phthalate (DINP). However, phthalates present a relatively high volatility which leads to plasticizer exudation, migration and diffusion from the matrix with the consequent effects on the chemical/physical properties of the polymer and, eventually, health risks issues [9].

Several bio-based plasticizers (presenting lower toxicity risks) have been proposed as alternatives to phthalate-based plasticizers (eg. Citrates) [10]. Recent intensive research on the physico-chemical properties of ionic liquids (ILs) indicates that these compounds may present several advantageous properties to be used as new, safer and efficient plasticizers for PVC. Among others properties ILs present high thermal stability, low non-flammability and a negligible volatility [11].

The aim of this work is to study the influence of phosphonium-based ionic liquids (PhILs) namely trihexyl(tetradecyl)phosphonium dicyanamide ( $[P_{6,6,6,14}][dca]$ ) and trihexyl(tetradecyl)phosphoniumbis(trifluoromethylsulfonyl)imide ( $[P_{6,6,6,14}][Tf_2N]$ ), on the aggregates size distribution and rheological behaviour of emulsion PVC (E-PVC) plastisols when mixed either with Di-isononyl Phthalate (DINP) or acetyltri-2-ethylhexyl citrate (CITROFOL® AHII).

### Experimental

#### *Materials*

Di-isononyl phthalate (DINP) and emulsion PVC powder (VICIR E 1970P,  $M_w=85.8 \text{ kg}\cdot\text{mol}^{-1}$ , apparent density= $1.16 \text{ g}\cdot\text{cm}^{-3}$ , K-value=70) were supplied by Companhia Industrial de Resinas Sintéticas, CIREs, S.A., Portugal. Acetyltri-2-ethylhexyl citrate (CITROFOL® AHII) was supplied by Jungbunzlauer Inc, Switzerland. The employed PhILs ( $[P_{6,6,6,14}][dca]$  and  $[P_{6,6,6,14}][Tf_2N]$ ) were obtained from Cytec Industries, France, with purities >98%. *n*-Heptane (purity >99%) was obtained from José M. Vaz Pereira S.A., Portugal.

#### *Preparation of the plastisol formulations*

Plastisol samples were prepared at room temperature by mechanical stirring (Janke & Kunkel, Germany) of all the components (150 parts of total plasticizer amount per 100 parts of polymer). The total plasticizer amount considers the use of conventional plasticizer alone or its mixture with PhILs, at different substitution amounts of 0 and 15% (w/w). The specific compositions are shown in Table 1. After mechanical stirring, at 25 rpm for 2.5 hours, the obtained suspension was vacuumed for one hour at 1 mbar to reduce the presence of air bubbles. Plastisols aging was studied by several characterization techniques at different time intervals and up to 14 days.

#### *Rheological measurements*

Rheological properties, including viscoelastic properties, were measured using a controlled stress rheometer (Model RS1, Haake, Germany) with a cylindrical sensor system Z34 DIN connected to a thermo controller recirculation bath (Thermo Haake C35P, Germany). Temperature was set constant at  $\pm 23^\circ\text{C}$ . Flow tests were performed for different aging times (0, 0.2, 1, 2, 7 and 14 days). The rheometer worked in controlled stress mode and the shear rate was varied between  $0.5$  and  $30 \text{ s}^{-1}$ . 50 ml of plastisol were used in each test. Results are the average of, at least, three measurements for each sample.

### *Particle size and zeta potential measurements*

The average surface charge (zeta potential) of dry PVC powder and the particle size distribution of the PVC powder and pastes were measured by electrophoretic light scattering and Laser Diffraction spectroscopy (LDS), respectively (Zetasizer Nano ZS and Mastersizer 2000, Malvern Instruments, UK). For all the tests performed, plastisol samples were dispersed in at 1% (w/v) in *n*-heptane according to an already published procedure [4]. Particle size measurements were carried out before/after submitting samples to ultrasounds (displacement=5 kHz /time=15s). LDS results are the average of at least three measurements for each sample.

## **Results and Discussion**

### *E-PVC powder properties*

Due to its particular properties VICIR E 1970P is one of the most suitable PVCs for the manufacture of highly flexible foams and is widely used for applications in the automotive industry. According to the results obtained in this work its zeta potential is around -43.5 mV. It also presents a broad particle size distribution with  $d_{50}$  of approximately 20.3  $\mu\text{m}$ .

### *Plastisols Aging*

This work aimed to evaluate the influence of the plasticizer type and composition on the viscosity of each plastisol system. Moreover it was intended to conclude about the influence of each mixture on the aging process of the plastisols. These results will permit to infer how those mixtures affect the swelling of the E-PVC particles which is a crucial step to latter guarantee good gelation of the plastisol and good properties of the final product (films/foams). The results obtained for the PSD evolution are shown in Table 1.

These results can be directly related with the flow test measurements which are presented in Figure 1. As can be seen progressive aging is observed for all the prepared plastisols. According to data presented in Table 1 the size of the particles increase during aging meaning that particles are being swelled by the plasticizer or plasticizer mixtures. This was observed for all the formulations except when CITROFOL® AHII is mixed with  $[P_{6,6,6,14}][dca]$ .

Table 1. Particle size distributions ( $d_{50}$ =particle diameter corresponding to 50% cumulative) for the E-PVC plastisols. For each plasticizer the upper and bottom lines represent mixtures measured without and with ultrasounds, respectively.

Plasticizer	$d_{50}$ ( $\mu\text{m}$ )	
	0 days	14 days
DINP	10.8±0.1	36.1±6.6
DINP	10.9±0.1	22.4±0.9
DINP	31.1±0.5	75.4±1.6
[P <sub>6,6,6,14</sub> ][dca]	60.5±0.5	68.4±1.3
DINP	21.0±1.1	38.5±6.0
[P <sub>6,6,6,14</sub> ][Tf <sub>2</sub> N]	19.5±0.5	21.5±1.1
CITROFOL	8.7±0.3	13.9±0.9
CITROFOL	11.5±1.0	16.6±0.9
CITROFOL	1379.8±0.3	118.3±4.6
[P <sub>6,6,6,14</sub> ][dca]	1377.3±1.0	95.6±2.4
CITROFOL	12.4±1.1	15.1±1.3
[P <sub>6,6,6,14</sub> ][Tf <sub>2</sub> N]	9.1±0.1	11.2±0.2

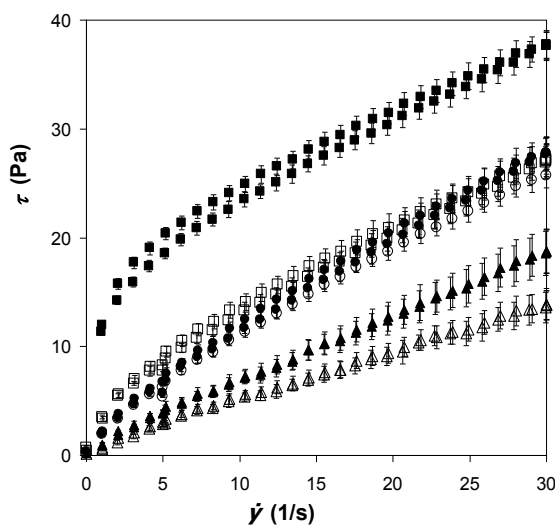


Figure 1. Flow tests of fresh plastisol samples using the following plasticizers: DINP alone (■); DINP with 15% (w/w) [P<sub>6,6,6,14</sub>][dca] (▲), DINP with 15% (w/w) [P<sub>6,6,6,14</sub>][Tf<sub>2</sub>N] (●) and CITROFOL® AHII alone (□), CITROFOL® AHII with 15% (w/w) [P<sub>6,6,6,14</sub>][dca] (Δ) and CITROFOL® AHII with 15% (w/w) [P<sub>6,6,6,14</sub>][Tf<sub>2</sub>N] (○).

This can be justified by the observed incompatibility of this plasticizer mixture. During solvation, it was also observed that larger aggregates were broken since  $d_{90}$  values decreased.

Pastes that were prepared using DINP as plasticizer showed higher viscosities than the ones obtained with CITROFOL® AHII. This behaviour was also observed for higher plasticizer amounts (data not shown). The flow tests indicate that DINP takes longer to incorporate in the E-PVC granules which results in a more pronounced aging behaviour. The plastisol prepared only with DINP present more pronounced plastic flow behaviour. On the contrary, plastisols based on CITROFOL® AHII are less sensitive to aging and present faster solvation and swelling of the PVC particles. This results in plastisols that are more stable during time.

The incorporation of PhILs into the plasticizer mixture induces a Newtonian behaviour to the plastisols opposing to the pseudo-plastic behaviour observed for the same plastisols prepared without PhIL. Moreover, it is observed that aging is more pronounced for plastisols prepared without ionic liquid. When comparing both PhILs it can be seen that  $[P_{6,6,6,14}][Tf_2N]$  needs more time to swell the E-PVC particles than  $[P_{6,6,6,14}][dca]$  most probably due to the higher molar volume of the first.

The ultrasound effect in the particle size measurements of E-PVC plastisols was also evaluated to infer about the resistance of the aggregates with time. In general terms the effect of ultrasounds is more evident after 14 days aging, agreeing with the fact that aggregates are more swollen after 14 days of age. As can be seen in Table 1 ultrasounds have more effect on the plastisols prepared without ionic indicating that particles swelled with PhILs are more stable. Based on the preliminary results reported in this work, it is possible to conclude that PhILs can indeed be used as alternatives or at least as enhancers for the commonly used phthalate-based plasticizers with a significant improvement of the rheological properties of E-PVC plastisols.

## References

1. Howick, C. (1995). *Plast., Rubber Comp. Process. Appl.* 23, 53-60.
2. Howick, C. (2007). *Green Chem.* 9, 243-246.
3. Daniels, P.H. (2009) *J. Vinyl Addit. Technol.* 15, 219-223.
4. Rasteiro, M.G., Antunes, E. (2005) *Part. Sci. Technol.* 23, 361-375.
5. Rasteiro, M.G., Tomás, A., Ferreira, L., Figueiredo, S. (2009) *J. Appl. Polym. Sci.* 112, 2809-2821.
6. Garcia, J.C., Marcilla, A. (1998) *Polymer* 39, 3507-3514.
7. Marcilla, A., Garcia, J.C., Beltran, M. (1997) *Eur. Polym. J.* 33, 753-759.
8. Nakajima, N., Harrell, E.R. (2005) *J. Appl. Polym. Sci.* 95, 448-464.

## Perspectives in Fundamental and Applied Rheology

9. Heudorf, U., Mersch-Sundermann, V., Angerer, J. (2007) *Int. J. Environ. Health* 210, 623-634.
10. Gil, N., Negulescu, I., Saska, M. (2006) *J. Appl. Polym. Sci.* 102, 1366-1373.
11. Dias, A.M.A., Marceneiro, S., Braga, M.E.M., Coelho, J.F.J., Ferreira, A.G.M., Simões, P.N., Veiga H.I.M., Tomé, L.C., Marrucho, I.M., Esperança, J.M.S.S., Matias, A.A., Duarte, C.M.M., Rebelo, L.P.N., de Sousa, H.C. (2012) *Acta Biomaterialia* 8,1366-1379.

### *Contact Address:*

*M.G. Rasteiro (mgr@eq.uc.pt)*  
*Chemical Engineering Department,*  
*Faculty of Science and Technology*  
*University of Coimbra*  
*Rua Silvío Lima, Polo II, Coimbra, 3030-790*  
*Portugal*  
*Tel.: 351239798700; Fax: 351239798703*

## CHAPTER 5

# Rheological characterization of lubricating greases based on vegetable oil-derived basestocks containing biodegradable and traditional thickeners agents

L.A. García-Zapateiro<sup>1,2</sup>, J.M. Franco<sup>2,3</sup>, C. Valencia<sup>2,3</sup>, M.A. Delgado<sup>2,3</sup>, C. Gallegos<sup>2,3</sup>

<sup>1</sup> *Departamento de Operaciones Unitarias. Facultad de Ingeniería. Grupo de Investigación Ingeniería de Fluidos Complejos y Reología de Alimentos (IFCRA). Universidad de Cartagena. 130015 Cartagena de Indias. Colombia.*

<sup>2</sup> *Departamento de Ingeniería Química. Campus de "El Carmen". Universidad de Huelva. 21071 Huelva. Spain. Campus de Excelencia Internacional Agroalimentario, ceiA3.*

<sup>3</sup> *Pro<sup>2</sup>TecS – Chemical Process and Product Technology Research Center. Universidad de Huelva. 21071 Huelva. Spain*

### Introduction

New technologies aimed at the development of products from renewable sources have emerged during the last decade, due to increased concerns over the use of petroleum-based products caused by the progressive depletion of the world reserves of fossil fuels, and also owing to concerns on their environmental impact [1]. Lubricating greases basically consist of a thickener agent, generally a metal soap, dispersed in mineral or synthetic oil, forming a colloidal suspension. Particularly, lithium 12-hydroxystearate soap is the most widely used thickening agent. The thickener forms an entanglement network, which traps the oil and confers the appropriate rheological and tribological behaviour to the grease [2]. However, vegetable oils constitute a suitable alternative for replacing 'mineral oils', as they are wholly biodegradable and non-toxic. On the other hand, the use of residual acid oils and ricinoleic acid-derived estolides as base materials for the manufacturing of lubricating greases may have additional benefits, mainly from an environmental point of view. This work deals with the rheological and thermogravimetric characterization of a variety of lubricating greases based on vegetable oil-derived basestocks containing biodegradable and traditional thickeners agents.

### Experimental

#### *Materials*

12-hydroxystearic acid, anhydrous lithium hydroxide (Verkol Lubricantes S.A.), castor oil (211 cSt at 40 °C, Guinama, Spain), acid oil (33.90 cSt at 40°C, Coreysa, Spain) resulting from the refining treatment of high-oleic sunflower oil and estolides (581.56 cSt at 40 °C, Mw=1832 g/mol) obtained from ricinoleic acid [3] were used to prepare traditional lithium lubricating greases. Chitosan (average molecular weight:  $2.29 \times 10^5$  g/mol, degree of deacetylation: 86.3%, Qingdao Fraken, China), Kraft cellulose pulp from *Pinus radiata* produced in the laboratory and ethyl cellulose (Mn=66,000 g/mol, 49% ethoxy content, Sigma-Aldrich) were used as biodegradable thickener agents.

#### *Manufacturing of lubricating greases*

Lithium lubricating grease (C1) processed with castor oil as base oil was prepared according to details and procedure described elsewhere [2]. Lithium soap concentration was fixed at 14% w/w in the final product.

Lubricating greases manufactured with acid oil (O1) and ricinoleic acid-derived estolides (E1) were obtained as follows. The process was performed in a stirred batch reactor (600 g) using an anchor impeller geometry applying a rotational speed of 60 rpm. In a first step, 55% of the total amount acid oil or ricinoleic acid-derived estolides was charged into an open vessel. This was pre-heated up to 90 °C and lithium hydroxide 3.5% w/w was then slowly added in the form of aqueous solution. Once neutralization was completed, part of the remaining base oil (15%) was added and a heating profile up to a maximum temperature of 180 °C was imposed, in order to induce both the phase transition of the crystallites into a waxy phase and the evaporation of the water. Then the mixture was maintained at the maximum temperature for one hour and added a third batch of base oil (15%). Thereafter, fourth batch of base oil (15%) at 120 °C was added. Finally, a homogenization treatment (rotational speed: 8800 rpm) during 15 min was applied using a rotor-stator turbine (Ultra Turrax T-25, Ika, Staufen, Germany).

The processing of cellulose derivatives and chitosan-based gel-like dispersions was carried out according to previous studies [4, 5]. Kraft cellulose pulp (3%)/ethyl cellulose (4%) and chitosan (32%) were used as biodegradable thickeners. Castor oil, ricinoleic acid-derived estolides and acid oil were used as biodegradable base oils.

#### *Rheological Measurements*

Rheological measurements were carried out in controlled-stress (Haake MARS-Rheostress Thermo Scientific, Germany), using serrated plate-plate geometry (35 mm diameter, 1 mm gap). Small-amplitude oscillatory shear (SAOS)

measurements, inside the linear viscoelasticity regime, were performed in a frequency range between  $10^{-2}$  and  $10^2$  rad/s, at 25°C. Stress sweep tests, at a frequency of 1 Hz, were first performed on each sample to determine the linear viscoelasticity region.

#### *Thermogravimetric analysis (TGA)*

Measurements of mass losses versus temperature were performed using a Thermogravimetric analyzer, model Q-50 (TA Instrument Waters, USA), under N<sub>2</sub> purge. Typically, 5–10mg of sample were placed on a Pt pan, and heated from 30 °C to 600°C, at 10 °C/min.

## **Results and Discussion**

### *Rheological characterization*

Figure 1 shows the evolution of the linear viscoelasticity functions with frequency, at 25°C, for lithium lubricating greases, processed using different biodegradable basestocks: castor oil (C1), ricinoleic acid-derived estolides (E1) and acid oil (O1). As can be observed, the so called “plateau” region of the mechanical spectrum is always noticed and the linear viscoelasticity response is qualitatively similar for all the samples studied and also similar to that found with other standard lubricating greases [2]. As can be seen in Figure 1, higher values of the SAOS functions were obtained when the ricinoleic acid-derived estolide was used in the formulation, as a consequence of the higher molecular weight and viscosity. Figure 2 and 3 show the mechanical spectra, obtained from SAOS measurements inside the linear viscoelastic range, for chitosan and kraft cellulose pulp/ethyl cellulose-based gel-like dispersions, respectively. As can be observed, the values of the SAOS functions for chitosan-based gel like dispersions (Figure 2) are more than two decades higher than lithium greases. Furthermore, contrary to the tendency previously discussed, a significant decrease in  $G'$  and  $G''$  values were found when castor oil was replaced by a more viscous base oil, such as ricinoleic acid-derived estolide, which may be attributed to a lower affinity of the estolide by the chitosan, as a consequence of the reduced polarity induced by the esterification reaction [6]. However, a very thin layer of separated oil can be detected after several months of ageing due to a certain degree of particles sedimentation. For Kraft cellulose pulp/ethyl cellulose gel-like dispersions (Figure 3), ethyl cellulose was added as rheology modifier of the base oil thus avoiding oil phase separation (oil bleeding) by forming a soft gel. The values of  $G''$  are similar for all base oils studied as a consequence of oil modification with ethyl cellulose. However, slightly lower  $G'$  values were found when *ricinoleic acid-derived* estolide was used as base oil. Moreover, a different evolution of the SAOS functions with frequency was observed for these gel-like dispersions, showing a tendency to a crossover between  $G'$  and  $G''$  at high frequency.

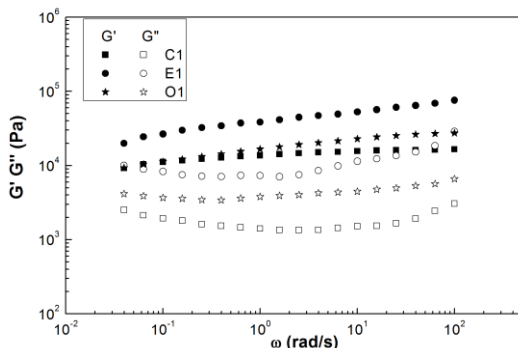


Figure 1. Evolution of the storage modulus ( $G'$ ) and loss modulus ( $G''$ ) with frequency, for lithium lubricating greases manufactured with castor oil (C1), ricinoleic acid derived-estolides (E1) and acid oil (O1).

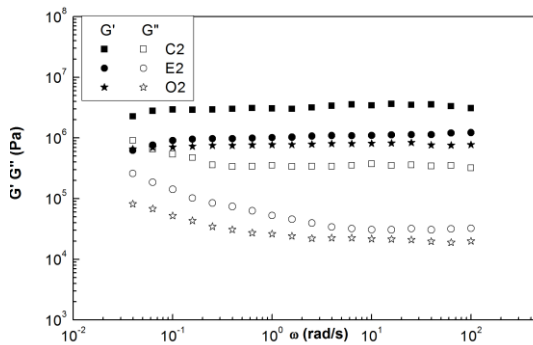


Figure 2. Evolution of the storage modulus ( $G'$ ) and loss modulus ( $G''$ ) with frequency, for gel-like dispersions processed with Chitosan and castor oil (C2), ricinoleic acid derived-estolides (E2) and acid oil (O2).

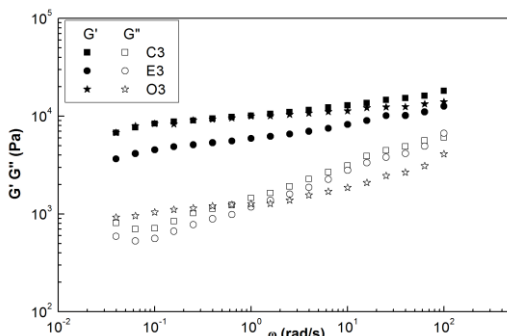


Figure 3. Evolution of the storage modulus ( $G'$ ) and loss modulus ( $G''$ ) with frequency, for gel-like dispersions processed with Kraft cellulose pulp (3%)/ethyl cellulose (4%) and castor oil (C3), ricinoleic acid derived-estolides (E3) and acid oil (O3).

*Thermogravimetric analysis.*

In addition to the rheological behaviour previously discussed, the thermal resistance of these lithium lubricating greases and gel-like dispersions, potentially applicable as biolubricating greases, has been studied by means of thermogravimetric analysis, which provides information on the thermal decomposition of this type of materials. Table 1 gathers the temperature for the onset of thermal decomposition ( $T_{\text{onset}}$ ), the temperature at which decomposition rate is maximum ( $T_{\text{max}}$ ) and the percentage of non-degraded residue of the samples studied. As can be observed, in general, the thermal decomposition takes place in two stages. Sample containing kraft cellulose pulp/ethyl cellulose and acid oil as base oil display a lower thermal stability (lower  $T_{\text{onset}}$ ), being its maximum decomposition rate reached at lower temperature ( $T_{\text{max}}$ ), whereas lithium thickeners generally provided higher thermal resistance. Moreover, some of these lubricating greases show much higher  $T_{\text{onset}}$  and  $T_{\text{max}}$  values than a standard lubricating grease prepared with naphthenic oil ( $T_{\text{onset}}= 223\text{ }^{\circ}\text{C}$  and  $T_{\text{max}}=296^{\circ}\text{C}$ ).

*Table 1. TGA characteristic parameters for samples studied.*

<b>SAMPLE</b>	<b><math>T_{\text{onset}}</math> (<math>^{\circ}\text{C}</math>)</b>	<b><math>T_{\text{max}}</math> (<math>^{\circ}\text{C}</math>)</b>	<b>Residue(%)</b>
C1	353/454	395/494	2.68
E1	330/446	380/496	0.25
O1	383/431	392/471	2.35
C2	302/385	324/421	9.50
E2	299/350/437	322/384/467	10.19
O2	273/390	323/438	5.78
C3	377	421	5.88
E3	332/450	382/475	1.08
O3	232/396	293/446	0.71

**Acknowledgements**

This work is part of a research project (CTQ2010–15338) sponsored by a MEC-FEDER Programme. The authors gratefully acknowledge the financial support.

### References

1. Campella, A. Rustoy, E., Baldessari, A. and Baltanás M.A. (2010). *Bioresource Technol.* 101, 245-254.
2. Martín-Alfonso, J.E. Valencia, C., Sánchez, M.C. Franco, J.M, Gallegos, C. (2011). *Mat. Chem. Phys.* 128, 530–538.
3. García-Zapateiro, L.A., Franco, JM. Valencia, C. Delgado, M.A., and Gallegos, C. (2013). *J. Ind. Eng. Chem.* 19, 1289–1298.
4. Nuñez N., Martín-Alfonso, J. E. Eugenio, M. E Valencia, C. Díaz, M. J. and Franco J. M (2011). *Ind. Eng. Chem. Res.*, 50, 5618–5627
5. Sánchez, R. Stringari, G.B. Franco J.M., Valencia, C. Gallegos C. (2011). *Carbohydrate Polymers* 85 705–714.
6. Salimon, J. Nallathamby, N. Salih, N. Mudhaffar, B.A. (2011). *J. Anal. Methods Chem.* 263624. doi:10.1155/2011/263624.

### Contact Address:

C. Valencia ([barragan@uhu.es](mailto:barragan@uhu.es))  
Dpto de Ingeniería Química. Facultad de Ciencias Experimentales. Universidad de Huelva.  
Campus del Carmen, 21071, Huelva (Spain).  
Telf.:+34 959218201; Fax:+34 959219984

## CHAPTER 6

# Preparation, Rheology and Physical Stability of O/W emulsions formulated with a mixture of green solvents

*Trujillo, L.A. , Ramírez, P, Pérez-Mosqueda, L.M. , Alfaro, M.C. , Muñoz, J.*

*Dpto. Ingeniería Química, Facultad de Química, Universidad de Sevilla (Spain)*

### Introduction

Droplet size distribution (DSD) is perhaps the most important factor in determining properties like consistency, rheology or shelf life stability of emulsions. In general, emulsions with smaller droplet size result in greater stability. Current equipment used for emulsion preparation includes rotor-stator devices, membranes, colloid mills, sonicators or high pressure homogenizers.

The dimethyl amides of fatty acids are solvents that meet the requirements to be considered green solvents that can be used in agrochemicals [1]. The  $\alpha$ -pinene is also a renewable solvent, which may be obtained from pine resins or distillation.

Polyoxyethylene glycerol esters derived from cocoa oil (Levenol) are non-ionic surfactants which fulfil the environmental and toxicological requirements to be used as emulsifiers in order to design eco-friendly products.

Rheology, laser diffraction and multiple light scattering measurements are powerful tools to cooperatively assess the success of formulations and processing methods when preparing emulsions.

The goal of this work was to investigate the influence of emulsification method on the rheological properties, (DSD) and physical stability of O/W eco-friendly emulsions formulated with a mixture of green solvents ( $\alpha$ -pinene and N,N-Dimethyl decan-1-amide) as oil phase and a glycereth-17 cocoate (Levenol C201<sup>®</sup>) as emulsifier.

### Experimental

30 wt% oil-in-water emulsions with a total surfactant (glycereth-17 cocoate, Levenol C201) concentration of 3 wt % were prepared using a mixture of green solvents, N,N-dimethylamide (DMA-10) and  $\alpha$ -pinene, as oil phase.

Emulsions with a 75/25 mass ratio of solvents (DMA10/ $\alpha$ -pinene) were prepared using four different emulsification methods based on two rotor-stator devices and two high-pressure (HP) homogenizers, respectively. Namely, an Ultra-Turrax T50 equipped with a G45F dispersing unit, a Silverson L5M equipped with an emulsor mesh screen, a high pressure valve homogenizer (HPvH), Avestin EmulsiFlex-C5 and a Microfluidizer, M110P based on microchannel technology were used.

The effect of changing the values of a) homogenization speed in rotor-stator devices and b) number of passes and/or pressure in HP homogenizers on the rheology and stability of emulsions has been studied.

The rheological measurements were carried out with a CS Haake-MARS rheometer (Thermo), using a sandblasted Z20 coaxial cylinder geometry to avoid slip-effects. Temperature was kept constant at 20°C.

DSD measurements were performed by laser diffraction with a Mastersizer X (Malvern) for about 60 days.

Multiple light scattering (MLS) scans were carried out with a Turbiscan Lab-expert (Formulaction) for about 75-100 days at 25°C, which provided information on the destabilization kinetics and the main mechanism involved.

### Results and Discussion

#### *Droplet size distributions*

Figure 1 shows the volume mean diameter ( $d_{4,3}$ ) of emulsions aged for 24 hours as a function of the homogenization speed used in rotor-stator devices. The emulsions prepared with an Ultra-Turrax T50/G45F exhibited a decrease of diameter with the increase of homogenization speed. By contrast, the  $d_{4,3}$  of emulsions prepared with Silverson L5M levelled off between 6000 and 8000 rpm. Interestingly, the  $d_{4,3}$  values were always lower than those obtained with Ultra-Turrax T50/G45F at the same homogenization speeds. All emulsions exhibited monomodal DSDs and submicron  $d_{3,2}$  and  $d_{4,3}$  mean diameters, which is favourable to slow down the creaming destabilization process.

Figure 2 illustrates that 2-passes through HP-homogenizers resulted in worse results, i.e. greater  $d_{4,3}$  values. This is due to the occurrence of recoalescence as a consequence of some over-processing [2]. This means that the extremely high

energy per unit volume provided by HP homogenizers must be optimized in order not to break the O/W interface formed by glycereth-17 cocoate surfactant.

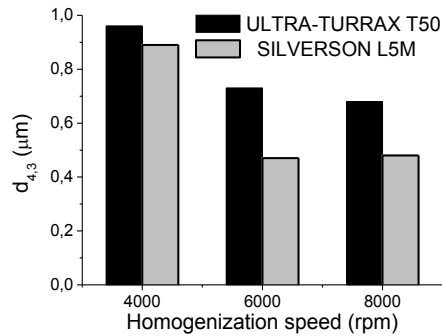


Figure 1. Volume mean diameter for emulsions processed with rotor/stator devices at different homogenization speeds. Aging time of emulsions: 24 h.

All emulsions prepared with HP homogenizers exhibited bimodal DSDs, although the secondary maximum turned out to be always quite small. The appearance of a second peak was a clear manifestation of over-processing even after 1-pass. Emulsions obtained after 1-pass through the Microfluidics homogenizer at the lower pressure showed better  $d_{4,3}$  values than those obtained using the HP-valve homogenizer.

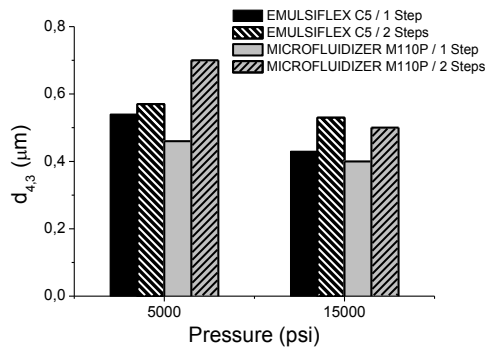


Figure 2. Volume mean diameter at 24h for emulsions processed with a high-pressure valve homogenizer and a Microfluidizer at different pressures and passes

Figure 3 shows the DSDs of emulsions prepared with the processing variables that yielded the lowest  $d_{4,3}$  value for each emulsification method used. The Silverson L5M equipped with the emulsor mesh screen provided similar  $d_{4,3}$  values to those of high pressure devices but different DSDs. This was due by some recoalescence induced by HP homogenizers. However, both the

Microfluidizer M110P and the Avestin EmulsiFlex C5 provided a markedly higher fraction of droplets with smaller diameters.

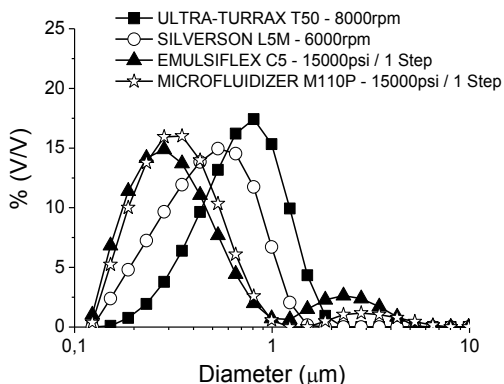


Figure 3. Droplet size distributions at 24h for the emulsions with lowest volume mean diameter for each emulsification method

### Rheological measurements

Figure 4 shows a comparison of flow curves of emulsions prepared with different processing conditions. All emulsions exhibited shear thinning behaviour which fitted the power-law equation within given shear rate ranges. Emulsions prepared with rotor-stator devices showed similar viscosity values to each other and their flow indexes ( $n$ ) ranged from 0.87 to 0.94. It must be noted that their apparent viscosities were significantly lower than those of emulsions prepared with HP homogenizers. The latter emulsions showed more marked shear thinning properties as demonstrated by the flow index ( $n$ ) values, which ranged from 0.53 to 0.68.

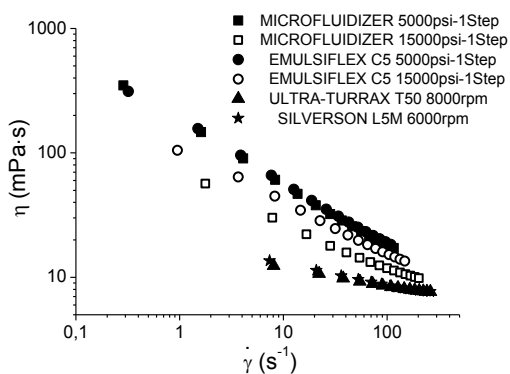


Figure 4. Flow curves of emulsions prepared with different homogenizers and processing variables.  $T=20^{\circ}\text{C}$ .

### Physical stability

The emulsions processed at 5000 psi with 1-pass exhibited the lowest flow index and the highest apparent viscosities, regardless of the HP homogenizer used. None of the emulsions showed linear viscoelastic properties.

Figure 5A and 5B provide examples of MLS results. Figure 5A (Ultra-Turrax T50/G45F at 4000rpm) showed a slight decrease of backscattering (BS) at the bottom of the measuring cell. This was consistent with the onset of a creaming destabilization process, which could not be visually observed. No evidence of droplet flocculation or coalescence could be detected as demonstrated by the essentially constant BS values at the middle of the measuring cell. The creaming rate was slower for those emulsions prepared in rotor-stator homogenizers which exhibited the lower  $d_{3,2}$  and  $d_{4,3}$  values, the most stable emulsion being that obtained with Silverson L5M at 6000 rpm. Figure 5B shows that BS for the emulsion prepared with the Microfluidizer M110P at 5000 psi and 1-pass increased with aging time along the full measuring cell, indicating the occurrence of flocculation and/or coalescence). The influence of aging time on the DSD demonstrated that the MLS was consistent with a flocculation process. Emulsions prepared with HP homogenizers at 1-pass exhibited enhanced stability. In fact, the most stable emulsion was that prepared with the Microfluidizer M110P at 15000 psi.

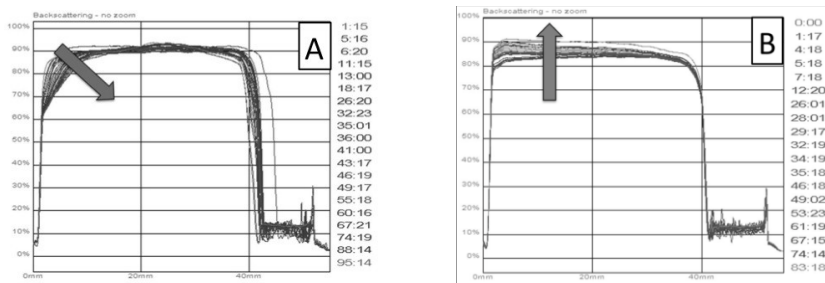


Figure 5. Influence of the ageing time on the backscattering in the emulsion processed with (A) Ultra-Turrax T50 at 4000 rpm and (B) Microfluidizer M110P at 5000 psi / 1 step.

### Concluding remarks

Regardless of the emulsification method used, all samples showed submicron volume mean droplet diameters. The higher fraction of smaller droplets was achieved by both high pressure homogenizers. Flow curves of all emulsions exhibited shear thinning behaviour. None of the emulsions exhibited linear

viscoelastic properties. The emulsions obtained by high pressure homogenizers showed higher apparent viscosity and more marked shear thinning properties (lower flow index values) than those prepared with rotor-stator homogenizers. MLS demonstrated that the emulsions with smaller droplet sizes exhibited enhanced stability against creaming.

### **Acknowledgments**

The financial support received (Project CTQ2011-27371) from the Spanish MINECO and from the European Commission (FEDER Programme) is kindly acknowledged.

### **References**

1. Hoefler, R., Bigorra, J. *Green Chemistry* 9, 203-212 (2007).
2. Håkansson, A. et al. *Food Hydrocolloid*, 23, 1177-1183 (2009).

### *Contact Address:*

*M. Carmen Alfaro Rodríguez (alfaro@us.es)  
Dpto. Ingeniería Química, Facultad de Química, Universidad de Sevilla,  
C/ Prof. García González, 1, 41012 Sevilla, Spain  
Phone:+34 954557179*

## CHAPTER 7

# Influence of the presence of sodium bicarbonate on thermal and mechanical properties of soy-based plastics processed through injection moulding

*Fernández-Espada, L. , Bengoechea, C. , Ruiz M.; Guerrero, A.*

*Departamento de Ingeniería Química, Universidad de Sevilla, Facultad de Química. Calle Profesor García González 1, 41012 Sevilla Spain*

### Introduction

Plastic materials are ubiquitous in the everyday life, especially in the food market (e.g. packaging). In order to diminish the environmental impact produced by crude oil based products as well as the dependence on non-renewable raw materials, industry has been increasingly developing bioplastics based on natural polymers, as proteins. The present work focuses on the study of the influence of the presence of sodium bicarbonate on some thermal and mechanical properties of soy-based (soy protein isolate, SPI) plastics using glycerol (GL) as plasticiser. Soy proteins have already been used in the manufacture of bioplastics as they are low-cost readily available raw materials [1]. Bioplastics were obtained through injection moulding after an adequate mixing of the ingredients. The gradual release of carbon dioxide from the bioplastic onto the headspace of the packing, as a result of sodium bicarbonate decomposition, would provide some benefits related to its well-known antimicrobial activity [2].

Thus, the eventual goal of the present work has been to evaluate the potential use of sodium bicarbonate in bioplastics formulations for future MAP (Modified Atmosphere Packaging) applications.

### Experimental

#### *Materials*

Soy protein isolate (SPI, min. 90% protein content, SUPRO 500E) was obtained from Protein Technologies International, Inc. (USA). Glycerol, from Panreac

## Perspectives in Fundamental and Applied Rheology

Quimica S.L.U. (Spain), was used as plasticiser, and sodium bicarbonate from Sigma Aldrich (Spain) was included in some probes.

The SPI/GL blends (50/50), with and without sodium bicarbonate (1%), were achieved using a Brabender Plastograph PL3s (Brabender® GmbH & Co. KG, Germany), which can be used in batch processing operations and which provides the required agitation. The angular velocity of the slower blade was 50 rpm, and the blending process took 10 minutes. The blend was produced at room temperature, under adiabatic conditions, following the same protocol as in previous papers [3]. Samples were frozen in sealed plastic bags prior to its injection. Injection moulding procedure was carried out in a Haake Minijet II (Thermo Scientific, Germany) at different conditions (injection chamber temperature: 40°C; mould temperature: 60, 70, 80, 90°C; injection pressure: 500 bars).

### *Thermogravimetry*

Thermogravimetric analyses were carried out on selected samples by using a SDT Q-600 device (TA Instruments, USA) under N<sub>2</sub> purge. Approximately, 5-10 mg of each sample were placed on a Pt pan, and heated from 30 up to 600 °C, at 10 °C/min.

### *Tensile Tests*

Tensile tests were performed on dumb-bell shaped type IV samples with a MTS Insight 10 kN (USA), according to ASTM D638 (2003), with an extension rate of 1 mm/min, at room temperature. An extensometer was used in order to accurately register the sample elongation.

### *Water uptake*

Water absorption tests, according to UNE-EN ISO 62:2008, were carried out on circular probes (25×1.5 mm<sup>2</sup>) immersed into distilled water for 24 h, and the water absorption percentage calculated as:

$$\text{water absorption} = \frac{\text{wet wt.} - \text{reconditioned wt.}}{\text{conditioned wt.}} \times 100$$

Where conditioned weight is the initial weight of the probe; wet weight refers to the weight of the probe just after 24 h of water immersion; reconditioned weight is the final weight of the wet sample after 24 h of drying in an oven at 50°C.

### *Carbon dioxide estimation*

Carbon dioxide emission from selected probes was evaluated by placing a circular probe (0.74 cm<sup>3</sup>) into a sealed container. The level of carbon dioxide in the headspace of the container (54.30 cm<sup>3</sup>) was measured using a PBI Dansensor CheckPoint (Dansensor AS, Denmark) after 24 h.

## **Results and Discussion**

### *Thermal Gravimetry*

Thermal Gravimetric Analysis (TGA) was performed both on raw materials (sodium bicarbonate, SPI, Figure 1A) and on mixtures (SPI+GL+ 0/1% sodium bicarbonate, Figure 1B) prior to its injection. From Figure 1A, it may be deduced that, under the conditions used, thermal decomposition of sodium bicarbonate into carbon dioxide and water takes place from 105 to 190°C approximately. Between those temperatures, a peak in the derivative of the weight loss along heating may be observed at 150°C. On the other hand, SPI decomposes along a wide range of temperatures, showing a maximum around 310°C. When studying the mixtures to be used in the injection-moulding device (Figure 1B), it is possible to distinguish several peaks related to the different formulation ingredients. Thus, for both blends (50/50 SPI/GL blends, with and without bicarbonate), besides the peak associated to the protein, another maximum, related to the presence of glycerol, appears around 200°C, which is in agreement with some data previously reported in the literature [4]. TGA results shown in Figure 1B may be used to evaluate the sodium bicarbonate decomposition along thermal treatment of different blends, as a slight difference in the derivative weight vs. temperature profile may be observed, even at the low concentration studied (1%). This effect becomes more apparent when a blend having 10% sodium bicarbonate was studied. It seems that the thermal conditions to be used in the injection moulding stage should be moderate, in order to minimize the bicarbonate loss along processing (lower than 90°C if possible). Anyway, the influence of different pressure conditions should not be disregarded.

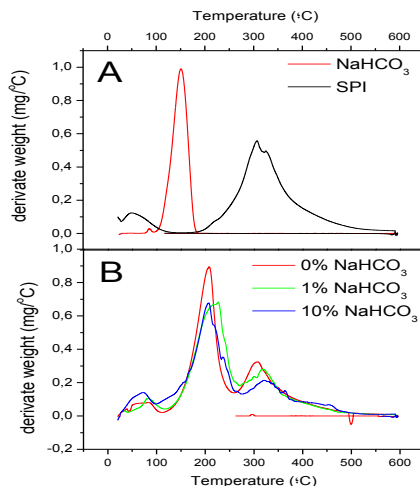


Figure 1. Derivative of the weight loss along heating from 30 to 600°C for sodium bicarbonate and soy protein isolate (SPI) (A); and for SPI+glycerol+ 0/1/10% sodium bicarbonate blends

Tensile Tests

Figure 2 shows representative parameters from tensile tests performed on probes prepared at different mould temperatures (E (Young’s Modulus),  $\epsilon_{\text{breaking}}$  (breaking strain) and  $\sigma_{\text{breaking}}$  (breaking strength)). An increase from 60 to 90°C leads to an increase in material resistance, yielding higher E,  $\epsilon_{\text{breaking}}$  and  $\sigma_{\text{breaking}}$  values. This figure also shows how the presence of sodium bicarbonate generally affects the mechanical properties of these samples. Thus, the blend with sodium bicarbonate generally possesses lower E, and higher  $\epsilon_{\text{breaking}}$  and  $\sigma_{\text{breaking}}$ . These results point out the importance of the balance between the higher mechanical properties obtained when processing at high temperatures and the consequent greater losses of sodium bicarbonate. The selection of an optimal temperature is a key parameter for bioplastic processing.

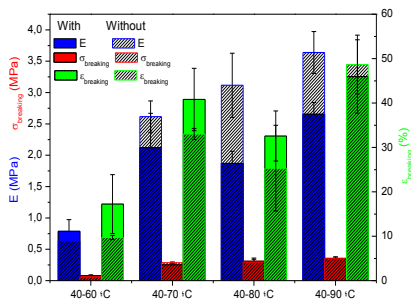


Figure 2. Tensile strength parameters for SPI+glycerol+ 0/1% sodium bicarbonate blends

### Water Uptake

In Figure 3, the percentages of water uptake by the SPI/GL bioplastic probes, with and without sodium bicarbonate, processed at different mould temperatures after 24 h of water immersion, are displayed, as well as the amount of material lost by solubilisation after that time. The addition of sodium bicarbonate always yielded a remarkable increase in water uptake (i.e. addition to probes moulded at 130°C duplicates water uptake). No large differences were found in the percentage of material loss by solubilisation between both samples, though, in both cases, it was around 50%, which may be associated to glycerol losses.

### CO<sub>2</sub> emissions

Gas measurements in the headspace of a sealed Petri dish show a slight increase of  $0.163 \pm 0.07$  % in the level of CO<sub>2</sub>, when at least one SPI+GL+1% sodium bicarbonate probe was included.

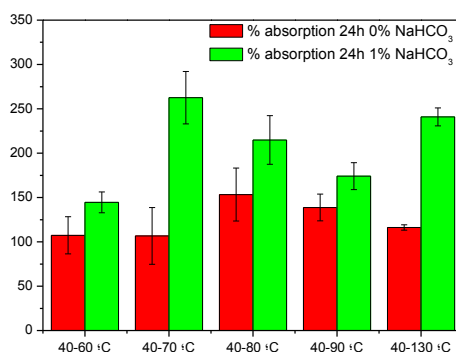


Figure 3. Water uptake and material loss after 24 h for SPI+glycerol+ 0/1% sodium bicarbonate probes

It should be taken into account the low concentration of sodium bicarbonate in the probes (1%). Future research will focus on the optimisation of CO<sub>2</sub> emissions, considering different processing parameters and formulations (e.g. sodium bicarbonate concentration).

### Concluding remarks

According to TGA tests, sodium bicarbonate remains unaltered when processing at 90°C or below.

## Perspectives in Fundamental and Applied Rheology

A reduction in the moulding temperature leads to a progressive impairment of mechanical properties. In contrast, there is not any apparent relationship with water uptake

Adding sodium bicarbonate to injection moulded SPI/glycerol probes also deteriorates their mechanical properties, but has proven to be a good strategy to increase water adsorption, which may be relevant for a variety of applications (i.e. in the manufacture of biodegradable superabsorbent materials).

An effective method of processing SPI-based bioplastics, containing unaltered sodium bicarbonate, by mixing and injection moulding and using a moderate moulding temperature (i.e. 70°C) has been developed. Preliminary results using these bioplastic probes are fairly promising, since they have shown to release carbon dioxide to a significant level. However, further studies have to be carried out in order to optimize both formulation and processing, in terms of maximizing carbon dioxide release for modified atmosphere packaging applications.

### References

1. Mungara, P., Zhang, J., Zhang, S., and Jane, J.L., (2002). In Protein-Based Films and Coatings (Gennadios, A., ed.), pp. 621-639. CRC Press, Florida.
2. Kerry, J.P., O'Grady, M.N., and Hogan, S.A. (2006). Meat Science, 74, 113-130.
3. Zárate, L., Martínez, I., Romero, A., Partal, P., and Guerrero, A. (2011). Journal of the Science of Food and Agriculture, 91 (4), 625-635.
4. Yunos, M.Z.B., and Wan Abdul Rahman, W. A. (2011). Journal of Applied Sciences, 11 (13), 2456-2459.

### Acknowledgements

Authors acknowledge financial support of this work by the Ministerio de Economía y Competitividad through the project MAT2011-29275-C02-02

### Contact Address:

*C. Bengoechea (cbengoechea@us.es)  
Departamento de Ingeniería Química  
Facultad de Química, Universidad de Sevilla  
C/Profesor García González, 1, 41012  
Telf.: +34954 557 179*

## CHAPTER 8

# Relationship between protein stabilized emulsions properties and controlled emulsification process by a mixer type rheometer

A. Romero<sup>1</sup>, P. Marchal<sup>2</sup>, L. Choplin<sup>2</sup>, A. Guerrero<sup>1</sup>

<sup>1</sup> *Departamento de Ingeniería Química, Facultad de Química. Universidad de Sevilla (Spain)*

<sup>2</sup> *GEMICO, ENSIC, Nancy-Université (France)*

### Introduction

Proteins are widely used as emulsifier for O/W emulsions since they facilitate breakage of oil drops (by lowering the interfacial tension) and prevent droplets coalescence over emulsification and storage [1]. In addition, the emulsification process plays an essential role in the final emulsion [2].

Mixer-type rheometers, which belong to the category of process rheometers, allow the possibility to extract rheological information directly from a batch or semi-batch process during and after the preparation of complex products such as emulsions. The so-called Couette analogy may be used in order to transform the torque-rotor speed data into shear stress-shear rate curve [3].

The objective of this research is to characterize the emulsion, stabilized by different protein concentrates, over and after processing by a mixer-type rheometer in order to put forward the utility of this rheometer as a valuable tool for understanding and controlling the emulsification process. In addition, a further objective of this work is to find a relationship between viscosity values of emulsions reached during emulsification and its stability.

### Experimental

#### *Materials*

Albumin protein (ca. 85 wt%), potato protein (c.a. 80 wt%), rice protein (79 wt% protein) and crayfish protein isolate (ca. 91 wt%) were obtained from Proanda

(Barcelona, Spain), Protastar (Barcelona, Spain), Remy Industries (Leuven, Belgium) and Alfocan S.A. (Seville, Spain), respectively. Sunflower oil was purchased in a local market. Glycerol, used for calibration, was purchased from Sigma-Aldrich (France).

### *Methods*

#### *Emulsification Process*

The mixer-type rheometer consists of a cylindrical vessel equipped with a double helical ribbon impeller installed in a RS150 controlled stress rheometer [4]. Different o/w emulsions are prepared into the mixer-type rheometer (rotating at 5 rad/s) with an Ultra Turrax T-25 homogenizer from IKA. Emulsion were prepared at 15,000 rpm, 65 wt% oil, 3 wt% protein content by using different protein concentrates (Rice, Potato, Crayfish and Albumin proteins) as emulsifiers. The detailed emulsifying process consists of 30 s with only Ultra Turrax (UT) homogenization, 420 s. with UT homogenization and oil addition, followed by 60 s. with UT homogenization and the last 290 s. without UT homogenization in order to stabilize the viscosity value.

#### *Characterization of emulsions*

Steady state shear flow tests were carried out at 25°C using plate and plate geometry (dia. 25) with a rough surface and a gap between plates of 1mm. Measurements of droplet size distribution (DSD) were performed in a laser light scattering apparatus (Malvern Mastersizer 2000, U.K.). For this purpose 0.5 mL of emulsion was taken and diluted in 11.5 mL of 0,05 M, pH Tris-HCL buffer with 1% SDS, in order to facilitate disruption of flocs prior to any DSD measurements [5].

In addition, steady shear flow and DSD properties were carried out along time (1 and 30 days after emulsification) in order to study emulsion stability. Emulsions were stored at 5°C, being subjected to the same thermo-rheological history before performing any test. In order to evaluate the emulsion stability, the coalescence index (CI) was calculated as a function of Sauter diameter ( $d_{3,2}$ ), as follows:

$$CI = \left[ 1 - \frac{d_{3,2}(0)}{d_{3,2}(t)} \right] \quad (1)$$

where  $d_{3,2}(0)$  and  $d_{3,2}(t)$  are the Sauter diameters after 1 and 30 days, respectively.

## **Results and Discussion**

### *Calibration of the mixer-type rheometer*

According to previous studies [1] constants related to the torque ( $K_\tau$ ) and shear rate ( $K_\dot{\gamma}$ ) can be determined through a calibration procedure that makes use of a

Newtonian fluid ( $n=1$ ) of known viscosity. Therefore, these constants are calculated in relation of volume occupied by sample in the vessel of the mixer-type rheometer) taking into account the addition rate of sample.

Figure 1 shows the constant values calculated as a function of the volume occupied by the sample in the measuring vessel (mixer type rheometer). In addition, a very good agreement between the viscosity results obtained with the cylindrical vessel (mixer-type rheometer) equipped with a double helical ribbon impeller and a conventional geometry, such as parallel plates may be observed in Figure 2 for either of the two fluids at the same experimental conditions (shear rate and temperature).

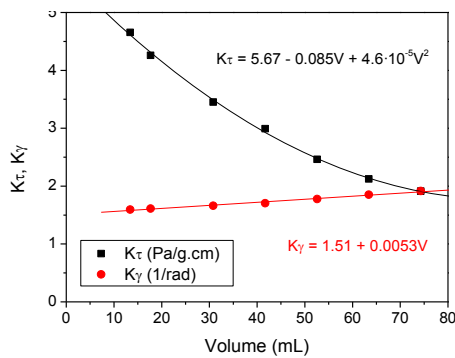


Figure 1. Evolution of constant values: related to the torque ( $K_{\tau}$ ) and shear rate ( $K_{\gamma}$ ); in relation to the volume occupied by sample.

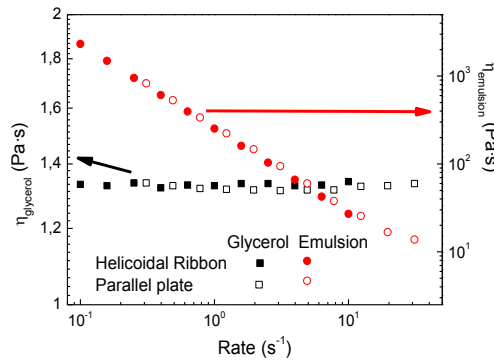


Figure 2. Viscosity values obtained with helicoidal ribbon (mixer-type rheometer) and parallel plate (conventional geometry) of glycerol (Newtonian fluid) and a reference emulsion (Non-newtonian fluid).

These results confirm the validity of the method used in order to control the real viscosity of emulsions.

*Emulsifying process*

Figure 3 shows the evolution of viscosity at 5 rad/s along the emulsifying time for different protein concentrates according to the previously described emulsification method. The constant values related to the torque ( $K_\tau$ ) and shear rate ( $K_\gamma$ ) were selected according to the volume occupied by sample.

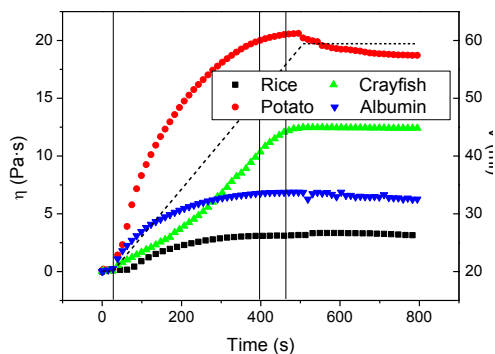


Figure 3. Evolution of viscosity at 5 rad/s over the emulsifying time for emulsions stabilized with different protein systems. Volume occupied by sample (dash line)

The evolution is similar in all cases showing a remarkable increase in viscosity during the second period that corresponds to oil addition, followed by constant values in emulsion viscosity once oil addition was finished. This stabilization in viscosity value is more clearly observed in the case of rice and albumin since it takes place from the end of the second stage. It is interesting to point out the marked differences of the final viscosity for the four emulsions. Thus, the viscosity of emulsions stabilized with albumin, crayfish and potato protein are around twice, four and six times the value of the rice-based emulsion viscosity, respectively.

*Characterization of emulsions*

Figure 4 shows the flow properties for emulsions stabilized by different protein concentrates as a function of the storage time (day 1 and 30).

Emulsions exhibit a decrease in viscosity (shear thinning behavior) following the same sequence in viscosity values as that one shown in figure 3. In addition, a significant decrease along time can be noticed, especially significant for rice and crayfish protein stabilized emulsions. These differences between different protein stabilized emulsions can be attributed to the different interfacial properties of the studied protein concentrates (interfacial tension and rheological properties of the O/W interfacial films)(cita).

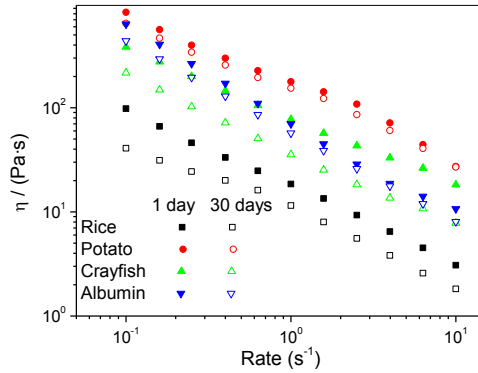


Figure 4. Steady shear flow curves of emulsions processed at the selected conditions and containing 65 wt% oil and 3 wt% protein concentrates for different protein concentrates as a function of the storage time.

Figure 5 shows the evolution of DSD profiles for emulsions stabilized by different protein concentrates as a function of the storage time (day 1 and 30). As may be observed, all DSD profiles exhibit unimodal distributions.

Albumin and Crayfish-based emulsions show a clear evolution over storage time that evidences occurrence of coalescence phenomena (CI are 0.01, 0.01, 0.03 and 0,02 for Rice, Potato, Crayfish and Albumin, respectively).

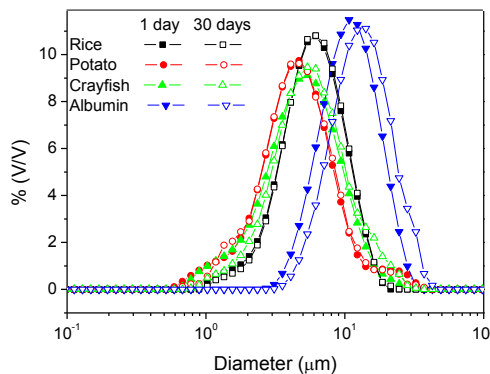


Figure 5. Evolution of droplet size distribution for emulsions processed at the selected conditions and containing 65 wt% oil and 3 wt% protein concentrates for different protein concentrates as a function of the storage time.

On the other hand, storage time does not yield any significant difference on DSD profiles of Potato and Rice-based emulsions. This is consistent with the results of flow properties of Potato-based system but is not for Rice-based emulsions. Thus, the difference found in apparent viscosity when using rice has to be attributed to impairment in the emulsion network structure over time.

### Concluding Remarks

Results put forward the importance of controlling the emulsification process in order to optimize DSD and rheological properties of the final emulsion. In addition, an excellent agreement has been found between in situ and off-line measurements obtained in mixer-type and conventional rheometers, respectively.

Most of flow properties and DSD results may be explained in terms of interfacial properties. Thus, potato exhibits the lowest interfacial tension and the best interfacial rheological properties, leading to the highest stability, whereas destabilization by coalescence is detected for albumin and crayfish. On the other hand, although no evolution of DSD is found for rice, storage time leads to a weakening of the emulsion that eventually might produce emulsion destabilization.

### Acknowledgements

Authors gratefully acknowledge financial support of this work by the Andalusian Government (project TEP-6134-2010) and by “Ministerio de Educación” from Spanish Government (JC2010-0117).

### References

1. Tcholakova, S., Denkov, N.D., Ivanov, I., and Campbell, B. (2006) *Adv. Colloid. Interfac. Sci.* 123-126, 259-293.
2. McClements, D.J. (2005) *Food Emulsions Principles, Practice and Technique*, CRC Press, Boca Raton, Florida.
3. Ait-Kadi, A., Marchal, P., Chrissetment, A.S., Choplin, L., and Bousmina, M. (2002) *Can. J. Chem. Eng.* 80, 1166-1174.
4. Nzihou, A., Bournonville, B., Marchal, P. and Choplin, L. (2004) *Chem. Eng. Res. Des.* 82, 637-641.
5. Nzihou, A., Bournonville, B., Marchal, P. and Choplin, L. (2004) *Food Hydrocolloid.* 82, 637-641.

*Contact Address:*

*A. Guerrero (aguerrero@us.es)*

*Dpto. Ingeniería Química, Facultad de Química, Universidad de Sevilla,*

*C/ Profesor Garcia Gonzalez, 1-41012 Sevilla, Spain*

*Tel.:+34 954 557179; Fax:+34 954 556447*



## CHAPTER 9

# Effects of Nanoclay/MDI Modification on Bitumen Properties

*F.J. Ortega<sup>1</sup>, F.J. Navarro<sup>1</sup>, M. García-Morales<sup>1</sup>, T. McNally<sup>2</sup>*

*<sup>1</sup>Department of Chemical Engineering  
Research Centre for Product and Chemical Process Technology (Pro2TecS)  
Campus "El Carmen", University of Huelva, Huelva, 21071, Spain*

*<sup>2</sup>Polymer Processing Research Centre (PPRC)  
School of Mechanical & Aerospace Engineering Queen's University Belfast  
BT9 5AH, UK*

### Introduction

Bitumen, residue from crude oil distillation, is a complex mixture of different organic molecules, comprising predominantly hydrocarbons with a small amount of structurally analogous heterocyclic species and functional groups containing sulphur, nitrogen and oxygen atoms [1, 2]. Because of its good viscoelastic properties, bitumen is widely used as a binder in road construction. However, vehicle loads and environmental factors may affect its properties, leading to problems like high-temperature rutting or low-temperature cracking. The addition of polymers has shown to improve its performance. With this purpose, a variety of polymers have been used (SBS, SBR, EVA, etc) [3]. In this sense, the present work deals with the flow viscous behaviour of MDI and MDI/nanoclay modified bituminous binders.

### Experimental

Bitumen with a penetration grade within the interval 160/220 (EN 1426) was used as the base bitumen for the modification. Polymeric MDI (4,4'-diphenylmethane diisocyanate) and Bentone™ 128 nanoclay were employed as modifiers.

Modified bitumens were prepared by melt blending, with a 4-blade turbine. Two different procedures were followed: a) Nanoclay/MDI modification: bitumen was first heated at 150°C, after which 10 wt.% Bentone™ 128 nanoclay was added and preblended for 10 min. Then, an Ultraturrax™ high shear mixer was used for 20 min to ensure the adequate dispersion of the Bentone™ 128. Finally, 2 wt.% polymeric MDI was added and blended for up to 24h; b) MDI modification: bitumen was first heated at 150°C and 2 wt.% polymeric MDI was added and blended for up to 24h. In both procedures, samples were taken at 1h and 24h, and

stored in a freezer for subsequent studies. Blanks of neat bitumen without additives were also prepared in order to evaluate the effect of temperature and agitation.

Steady-state viscous flow tests at 60°C were carried out in controlled-stress mode on a Physica MCR-301 rheometer (Anton Paar, Austria).

### Results and Discussion

According to Figure 1, neat bitumen and its 1h blank can be described as Newtonian fluids, as viscosity remains nearly constant in the entire range of shear rates applied. Furthermore, both of them show similar values of viscosity. On the contrary, the 24h blank presents, due to oxidation, a much higher value of Newtonian viscosity. Also, a critical shear rate establishes the onset of a shear-thinning region, at which viscosity significantly decreases.

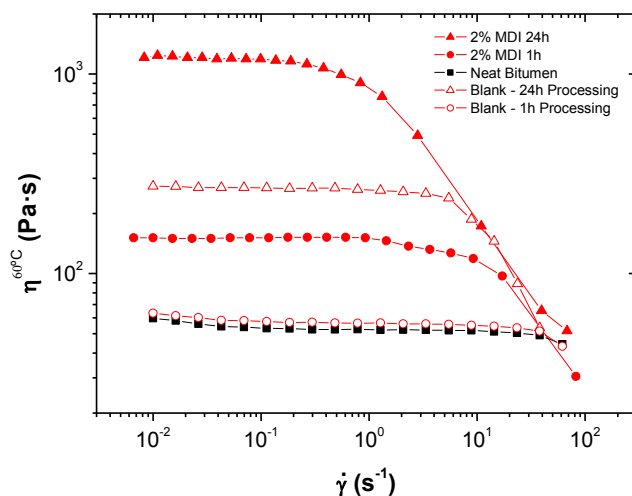


Figure 1. Viscosity curves, at 60°C, for the neat bitumen and 2 wt.% MDI modified binders.

Addition of 2 wt.% MDI leads to important changes in the flow viscous behaviour, if compared to their respective blanks. On the one hand, a significant increase in viscosity can be observed, mainly for the 24h-sample. On the other hand, the above mentioned critical value of shear rate for the onset of the shear-thinning region becomes lower. New complex structures originated after reaction of –NCO groups in MDI and bitumen (formation of urethane bonds [4]) yield an increase in the material viscosity, which remains constant until the so-called critical shear rate. At this point and above, the structure is altered because of the imposed shear stress, exhibiting reduced resistance to shearing. If compared with the 1h system,

the extended 24h blending time reveals a noticeable increase in viscosity of nearly one order of magnitude, as a consequence of: a) a larger extent of the above reaction b) possible side reactions involving –NCO groups, air, moisture, etc.; c) bitumen primary ageing, due to oxidation during the 24h processing at high temperature.

Figure 2 provides graphical description of the flow behaviour for the neat bitumen and its corresponding nanoclay and nanoclay/MDI modified binders.

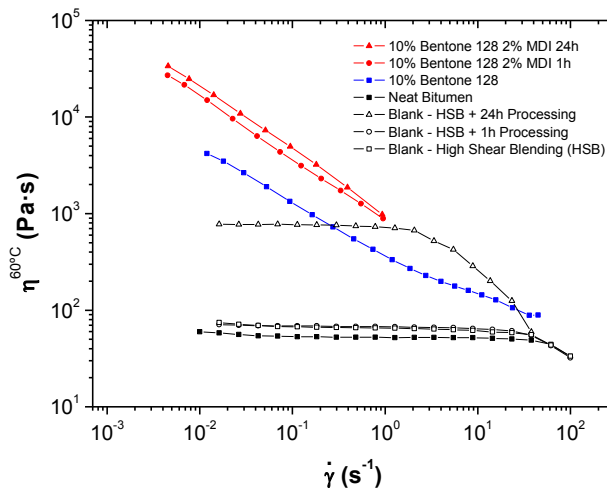


Figure 2. Viscosity curves, at 60°C, for the neat bitumen its corresponding nanoclay and nanoclay/MDI modified binders.

If compared to the MDI modified binders, the nanoclay modified binder shows a very different flow viscous behaviour. This material behaves as a shear-thinning fluid in the whole range of shear rates applied. No zero-shear viscosity is observed at the lowest values of shear rates. This shear-thinning behaviour is probably the result of the intercalation or exfoliation experienced by the nanoclay particles during its high shear blending with bitumen. At low shear rates, the possibly intercalated or exfoliated nanoclay particles may offer high resistance to flow, leading to higher values of viscosity. As the shear rate is increased, viscosity values decrease, most probably caused by the progressive orientation of the nanoclay particles in the nanoclay modified binder. This tendency is maintained up to the highest values of shear rates studied ( $50 \text{ s}^{-1}$ ), at which viscosity is not much higher than that of the neat bitumen. In the case of nanoclay/MDI modification, a similar degree of shear-thinning is observed. Hence, the slopes of the viscosity curves are approximately the same as before. However, the

presence of 2 wt.% MDI in the nanoclay/MDI modified binders markedly increases their viscosity with respect to the nanoclay modified binder.

These results may be attributed to the combined effect of the aforementioned intercalated or exfoliated nanoclay particles, along with chemical changes involving the –NCO groups. Both effects lead to higher resistance to flow and the consequent increase in the viscosity values. As the combination of nanoclay particles and isocyanate-terminated prepolymer led to a higher degree of modification than the mere sum of their single contributions, we may assume the existence of synergy between both. Thus, the combined addition of nanoclay and MDI plays a significant role on enhancing the viscosity of the blend, through further reactions which occur between –OH pendant groups on the nanoclay surface and -NCO in the prepolymer. These reactions yield a much more complex structure and so, different rheological behaviour, if compared to the binders in Figure 2. The effect of blending duration was also considered. Figure reveals the low influence of extending the blending (from 1h up to 24h) on the viscous flow response.

### Conclusions

This work studied the effect of nanoclay/MDI modification on the viscous flow properties of bituminous binders. The addition of 2 wt.% polymeric MDI led to a significant increase in viscosity, mainly after 24h of blending. This result is a consequence of reactions involving –NCO and bitumen, and influenced by –NCO side reactions and oxidation at high temperature under agitation. The addition of 10 wt.% Bentone™ 128 nanoclay produced a shear-thinning bituminous binder, for which no zero-shear viscosity was observed, together with a considerable increase in viscosity. The combined addition of 2 wt.% polymeric MDI and 10 wt.% Bentone™ 128 nanoclay resulted in a notable increase in viscosity (probably due to the synergistic interaction of the modifiers), while maintaining the same shear-thinning behaviour. A prolonged blending time of 24h had low influence on the viscous flow response of these binders. In order to shed some light on this issue, further research on the synergistic interaction between nanoclay, polymeric MDI and bitumen is to be conducted.

### Acknowledgements

This work is part of a research project sponsored by “Junta de Andalucía” (TEP-6689). The authors gratefully acknowledge their financial support.

## References

1. Claudy, P., Letoffe, J.F., King, G.N., Brule, B., Planche, J.P. (1991). Fuel Sci Technol Int, Vol. 9, pp. 71-92.
2. Morgen, P., Mulder, A. (1995). The Shell Bitumen Industrial Handbook. Shell Bitumen Publications, London (UK).
3. García-Morales, M., Partal, P., Navarro, F.J., Martínez-Boza, F., Gallegos, C., González, N. et al. (2004). Fuel, Vol. 1, pp. 31-38.
4. Martín-Alfonso, M.J., Partal, P., Navarro, F.J., García-Morales, M., Bordado, J.C.M., Diogo, A.C. (2009). Fuel Process Technol, Vol. 90, pp. 525-530.

## Contact Address:

*Francisco José Ortega Bravo (francisco.ortega@diq.uhu.es)*  
*Department of Chemical Engineering*  
*Research Centre for Product and Chemical Process Technology (Pro2TecS)*  
*Faculty of Experimental Sciences*  
*University of Huelva*  
*Huelva, 21071, Spain, Telf.: 959219998*



## CHAPTER 10

# Rheology, microstructure and physical stability of limonene in water emulsions stabilized by PE9400 and rosin gum. Influence of surfactant concentration

Ramírez, P.<sup>1</sup>, Pérez-Mosqueda, L.M.<sup>1</sup>, Trujillo, L.A.<sup>1</sup>, Santos, J.<sup>1</sup>, Alfaro, M.C.<sup>1</sup>, Muñoz, J.<sup>1</sup>

<sup>1</sup> Dpto. Ingeniería Química, Facultad de Química, Universidad de Sevilla (Spain)

### Introduction

D-Limonene is an organic compound obtained from the peel of citrus fruit. It is an interesting bio-derived solvent which has been used in food [1] and pharmaceutical applications. Furthermore, this bio-solvent is an interesting candidate for replacing more polluting solvents such as hexane or xylene in agrochemical formulations.

Pluronics are non-ionic triblock copolymers used as stabilizers for suspensions, emulsions and foams, which are present in many industrial applications, such as cosmetics, foods, pharmaceuticals, agrochemicals, paints [2]. Recently, the interfacial properties of the Pluronic PE9400 adsorbed onto the limonene-water interface have been reported [3].

Recent results obtained by our research group have demonstrated that concentrated limonene-in-water emulsions,  $\phi = 50\%$ , stabilized by Pluronic PE9400, are destabilized by both, creaming and Ostwald ripening. These destabilization processes are suppressed by adding a lipophilic gum (rosin gum). Addition of rosin gum leads to lower droplet size and also acts as a weighting agent, diminishing the difference of density between the oil and the continuous phase.

Rosin is a natural occurring gum, also called colophony, obtained mainly from pine resin.

In the present study, the influence of Pluronic PE9400 concentration (ranging from 1 to 8 wt%) on the rheology, microstructure and physical stability of limonene in water emulsions containing 30 wt% of rosin gum has been studied.

### Experimental

50 wt% oil-in-water emulsions were prepared using a 30 wt% dispersion of rosin gum in D-Limonene as oil phase. Surfactant concentration (Pluronic PE9400) ranged from 1 to 8 wt%. Concentrated emulsions were prepared with a rotor-stator homogenizer (Ultraturrax T-25) at 17500 rpm for a minute.

Flow curves were carried out with a Haake MARS rheometer (Thermo), using a sandblasted Z20 coaxial cylinder geometry. Temperature was kept at 20°C. Small amplitude oscillatory shear (SAOS) measurements were carried out with a CS AR-2000 rheometer (TA-Instruments), using a serrated plate & plate geometry (diameter: 40mm; measuring gap: 1mm). Temperature was kept at 20°C by a Peltier system.

Laser diffraction measurements were performed with a Mastersizer X (Malvern) particle size analyzer to determine the droplet

size distribution (DSD) and mean droplet diameters of the emulsions studied.

Multiple light scattering scans (Turbiscan Lab-expert) provided information on the destabilization kinetics and the main mechanism involved.

Furthermore, optical micrographs were used to show the microstructure of these emulsions.

### Results and Discussion

#### *Droplet size distributions (DSDs)*

All the emulsions prepared showed a monomodal droplet size distribution, which shifted towards lower droplet sizes with increasing surfactant concentrations.

Figure 1 shows the Sauter's mean diameter ( $d_{3,2}$ ) of emulsions aged for 24 hours (black bars) and 30 days (grey bars) as a function of Pluronic PE9400 concentration. The initial Sauter's mean diameter decreased from 1.02  $\mu\text{m}$  to 0.35  $\mu\text{m}$  with increasing surfactant concentrations. The minimum mean diameter ( $\sim 0.35 \mu\text{m}$ ) was achieved at a concentration of 6% (w/w). Further increase in surfactant concentration did not result in smaller ( $d_{3,2}$ ). These experimental results obtained by means of laser diffraction measurements were confirmed by optical micrographs of emulsions (figure not shown). It is noteworthy that stable submicron emulsions were obtained at surfactant concentrations within the 3-7 wt% (range). The increase in the ( $d_{3,2}$ ) values of the emulsions with less surfactant (1 and 2 wt%) can be ascribed to the occurrence of coalescence, enhanced by creaming of the bigger droplets of these emulsions. A slight increase in the ( $d_{3,2}$ ) value was observed for the most concentrated (8 wt%) emulsion studied after

aging for 30 days. This increase is likely to be related to a depletion flocculation process due to an excess of surfactant micelles in solution, which eventually enhanced the coalescence of emulsion droplets.

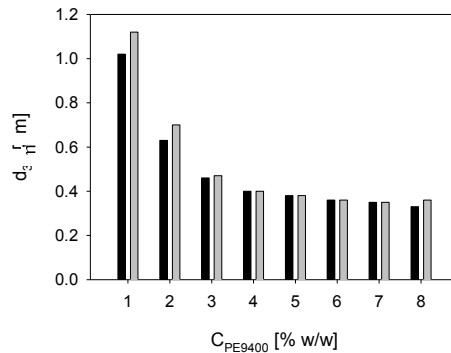


Figure 1. Sauter's mean diameter at 24h (black bars) and at 30 days (grey bars) for emulsions processed with ultraturrax-T25 at different Pluronic concentrations.

### Stability curves

In order to gain a deeper insight into the destabilization mechanism of these emulsions, multiple light scattering (MLS) measurements were carried out. Figure 2 show the evolution of backscattering (BS) profiles for 30 days, as a function of the sample height,  $H$ , at the bottom of the measuring cell. The detection of a decrease in the BS at the bottom of a measuring cell is related to the onset of a creaming destabilization process. A marked decrease of the BS was detected for the 1 wt% (Figure 2A) and 8 wt% (Figure 2C) emulsions. Moreover, a visual inspection of both emulsions at 30 days confirmed the appearance of gravitational separation (creaming) in these emulsions. No experimental evidence of creaming was detected for the rest of emulsions as shown for the 4 wt% emulsion (Figure 2B). Moreover, no evidence of droplet flocculation or coalescence could be detected as demonstrated by the essentially constant BS values at the middle of the measuring cell.

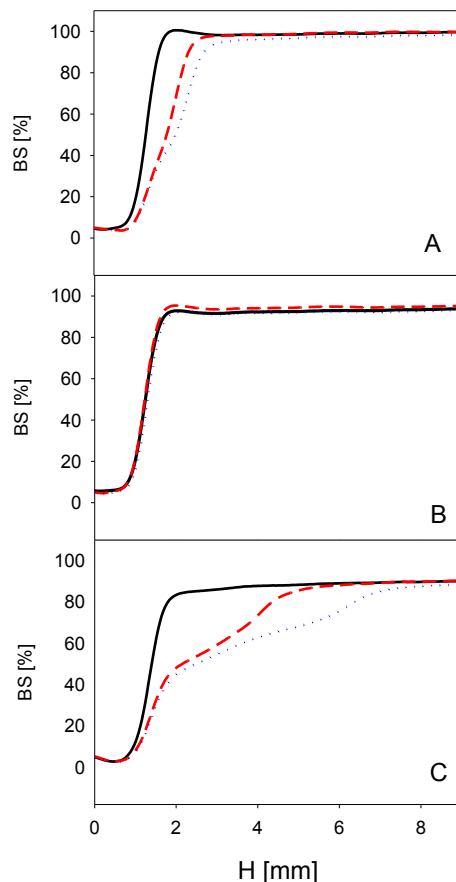


Figure 2. Evolution with aging-time of the stability curves for emulsions at different Pluronic PE9400 concentrations: 1 wt% (A), 4 wt% (B) and 8 wt% (C). Black-solid lines (1day), red-dashed lines (14 days) and dotted-blue lines (30 days)

### Rheology measurements

Figure 3 show three representative flow curves of emulsions, containing 1 wt%, 4 wt% and 8 wt% PE9400. The experimental data fitted the Cross model and the fitting parameters are shown in Table 1. All emulsions exhibited shear-thinning behaviour, which was more marked with increasing surfactant concentration as confirmed by the decreasing values of the flow index,  $n$  (Table 1). It must be emphasized the two-order of magnitude increase in the  $\eta_0$  value when increasing surfactant concentration from 4 wt% to 8 wt%. Interestingly, the flow curves at the higher shear rates showed a clear trend to converge on each other. These facts

are consistent with the occurrence of depletion flocculation, which could explain the creaming of the emulsion containing 8 wt% PE9400.

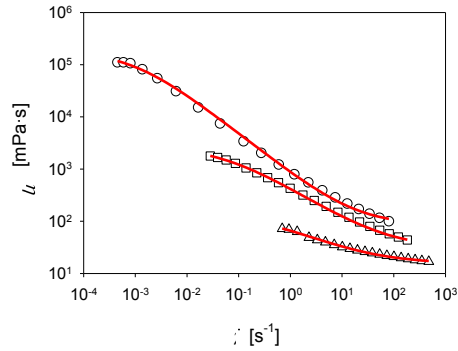


Figure 3. Flow curves for the emulsions at different PE9400 concentrations: 1 wt% (triangles), 4 wt% (squares) and 8 wt% (circles). The lines are the best fit to the Cross model.  $T=20^{\circ}\text{C}$ .

$$\eta = \eta_{\infty} + \frac{\eta_0 - \eta_{\infty}}{1 + \left(\frac{\dot{\gamma}}{\dot{\gamma}_c}\right)^{(1-n)}} \quad (1)$$

Table 1. Fitting parameters for the Cross model.

C [wt%]	$\eta_0$ [mPa·s]	$\eta_{\infty}$ [mPa·s]	$\dot{\gamma}_c$ [s <sup>-1</sup> ]	$n$
1	150	15	0.43	0.40
4	2852	30	0.06	0.34
8	183938	85	9.4E-04	0.22

Only did the emulsion containing 8 wt% PE9400 showed linear viscoelastic properties, with  $G'$  over  $G''$  throughout all the frequency range (20-0.05 rad<sup>-1</sup>) (data not shown). Figure 4 illustrates the increase in  $G^*$  and loss tangent with aging time. This indicates that the increase of  $G''$  with aging time was more marked than the increase of  $G'$  when flocculation enhancing coalescence takes place.

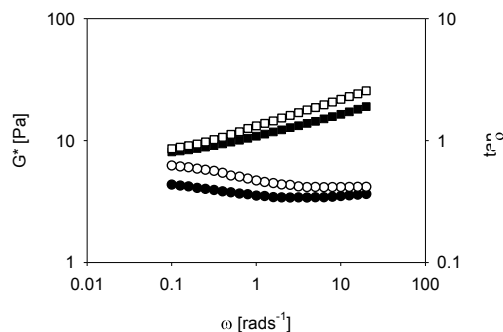


Figure 4. Frequency sweeps (20-0.05 rad/s) of emulsion containing 8 wt% Pluronic PE9400 at 24 hours (filled symbols) and at 30 days (open symbols).  $G^*$  (squares) and  $\tan(\delta)$  (circles).  $T = 20^\circ\text{C}$

### Concluding remarks

Stable submicron concentrated ( $\phi = 50$  wt%) emulsions containing a disperse phase of 30 wt% rosin gum in d-limonene can be obtained in the 3-7 wt% range with Pluronic PE9400.

Below 3 wt% PE9400, emulsions have higher droplet sizes and are prone to undergo creaming and eventually coalescence.

An excess of surfactant concentration leads to a fast destabilization by depletion flocculation, as inferred from the rheological results obtained.

### Acknowledgments

The financial support received (Project CTQ2011-27371) from the Spanish MINECO and from the European Commission (FEDER Programme) is kindly acknowledged.

### References

1. S.M. Jafari, S.M., Beheshti, P. Assadpoor, E. (2012) J. Food Eng., 109, 1.
2. Tadros, T. F. (2005) Applied Surfactants. Principles and Applications, Wiley-VCH, Weinheim.
3. Pérez-Mosqueda, L. M., Maldonado-Valderrama, J., Ramírez, P., Cabrerizo-Vílchez, M.A., Muñoz, J. (2013) Colloids Surf. B. Accepted Manuscript. doi: 10.1016/j.colsurfb.2013.05.029

*Contact Address:*

*Pablo Ramírez del Amo (pramirez@us.es)*

*Dpto. Ingeniería Química, Facultad de Química, Universidad de Sevilla, C/ Prof. García González, 1,  
41012 Sevilla, Spain*

*Tel.:+34 954557179*



**PART IV**  
**Multiphasic Systems, Composites,**  
**Polymers and Liquid Crystals**



## CHAPTER 1

# Influence of the calcium sulfate source on the rheological behaviour of calcium sulfoaluminate cement pastes

*Isabel Santacruz<sup>1</sup>, Marta García-Maté<sup>1</sup>, Miguel A.G. Aranda<sup>1,2</sup>, Ángeles G. De la Torre<sup>1</sup>*

<sup>1</sup> *Departamento de Química Inorgánica, Cristalografía y Mineralogía, Universidad de Málaga, 29071-Málaga, Spain*

<sup>2</sup> *CELLS-Alba synchrotron, Carretera BP 1413, Km. 3.3, E-08290 Cerdanyola, Barcelona, Spain*

### Introduction

Calcium sulfoaluminate (CSA) cements are receiving increasing attention since their manufacture produces much less CO<sub>2</sub> than ordinary Portland cement (OPC) [1]. In addition, they show interesting properties such as high early-age strengths, short setting times, impermeability and sulfate and chloride corrosion resistance. CSA cements may show variable compositions, but all of them contain Klein's salt (Ca<sub>4</sub>Al<sub>6</sub>SO<sub>16</sub>). They are prepared by mixing the clinker with different amounts of a calcium sulfate set regulator. The early hydration of the CSA cements is mainly governed by the amount and reactivity of the calcium sulfate source with Klein's salt in presence of water [2]. It gives as main crystalline phase ettringite also named as AFt and an amorphous aluminium hydroxide [3]. The control of the rheological behaviour [4] of cement pastes is a key point [5,6] to improve the workability of concrete to obtain more homogeneous mixtures and hence, improved mechanical properties in general and compressive strengths in particular.

The objective of this work is to understand the effect of the amount and type of calcium sulfate, added to a commercial CSA clinker, on the rheological behaviour of fresh cement pastes, setting time, phase assemblage, and hence, compressive strength of the corresponding mortars.

### Experimental

A commercial CSA clinker (BELITH S.P.R.L., Belgium) was used as raw material. CSA cements were prepared by mixing clinker with commercial micron natural gypsum (G) (BELITH S.P.R.L., Belgium) or anhydrite (A) or bassanite (B).

Hereafter G<sub>x</sub>, A<sub>x</sub> and B<sub>x</sub>, respectively, where x stands for the amount of sulfate source (10-30 wt%). Anhydrite and bassanite were prepared by heating the commercial gypsum at 700°C/1h and 90°C/48h, respectively.

Cement pastes were prepared with distilled water at w/CSA ratios of 0.4 and 0.5. A commercial polycarboxylate-based superplasticizer (SP), Floadis 1623 (Adex Polymer S.L., Spain), with a 25 wt% of active matter, was added when appropriate. The added amount is given as the percentage of active matter in the SP on a dry solid basis. The pastes were mechanically stirred with helices according to the EN196-3:2005 standard procedure. The initial setting time of pastes was measured using the Vicat test method according to UNE-EN 196-3.

Rheological measurements of pastes were carried out using a viscometer (Model VT550, Thermo Haake, Karlsruhe, Germany) with a serrated coaxial cylinder sensor, SV2P, provided with a solvent trap to reduce evaporation. Flow curves were obtained with controlled rate (CR) measurements. Ramp times of 6 s were recorded in the shear rate range between 2 and 100 s<sup>-1</sup>, for a total of 12 ramps. A further decrease from 100 to 2 s<sup>-1</sup> shear rate was performed by following the same ramp times. Before starting the rheological measurement, the pastes were pre-sheared for 30 s at 100 s<sup>-1</sup> and held at 0 s<sup>-1</sup> for 5 s.

LXRPD studies were performed on grounded anhydrous materials and pastes (after stopping hydration) at 1 and 3 hydration days. Patterns were recorded on an X'Pert MPD PRO diffractometer (PANalytical) using strictly monochromatic CuK $\alpha_1$  radiation ( $\lambda=1.54059\text{\AA}$ ) [Ge(111) primary monochromator] as detailed in [7]. Rietveld quantitative phase analyses (RQPA) were performed as reported elsewhere [7]. Standard mortars were prepared with a water/CSA/sand ratio of 0.5/1/3 and mechanically homogenized according to EN196-1. Cubic samples of 30×30×30 mm were cast in a jolting table (Model UTCM-0012, 3R, Montauban, France) with a total of 120 knocks. Compressive strengths of mortars were measured at 1 and 3 hydration days (Model Autotest 200/10 W, Ibertest, Spain).

### Results and Discussion

The effect of the gypsum content (10, 20 and 30 wt%) on the rheological behaviour of fresh concentrated pastes (w/CSA=0.4) has been studied. The flow curves of those pastes, Figure 1, show that the gypsum content has a negligible effect on their rheological behaviour, which can be extrapolated to more dilute pastes (e.g. w/c=0.50). Contrarily, the gypsum content has a very important effect in the hydration chemistry [4]; LXRPD studies reveal that ettringite is the main crystalline hydration product together with amorphous aluminium hydroxide. If gypsum is depleted, as it is the case for G10 pastes, then layered calcium aluminium monosulfate is formed. In the case of G30 and G20 pastes, Klein's salt and gypsum contents decreased but they were not depleted within the first hydration days. This will affect mechanical strengths of the corresponding mortars.

For example, mortars with a w/CSA ratio of 0.5 after 3 hydration days show compressive strength values of 33, 45 and 43 MPa, for those with 10, 20 and 30 wt % of gypsum, respectively. It must be highlighted that G20 and G30 mortars show similar strengths than OPC mortars, but less CO<sub>2</sub> is released during their productions.

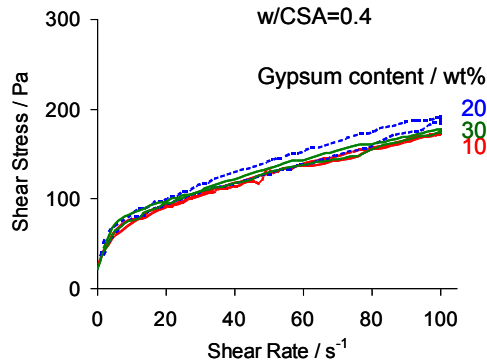


Figure 1. Flow curve of G10, G20 and G30 pastes.

Further studies were performed on pastes with a w/CSA ratio of 0.5, and 25 wt% of G, A and B. The type of calcium sulfate present in the cement modifies the setting time, e.g. initial setting times are 190, 320 and 20 min, respectively meanwhile final values are 210, 720 and 60 min, respectively. The latter, being enormously sensitive for the mortars' homogenisation. This is likely due to the rehydration of bassanite to form gypsum. Furthermore, this sulfate source has an important effect on the rheological behaviour of the pastes, as can be observed in Figure 2. All the pastes show shear thinning behaviour and a rheopectic cycle (-700, -171 and -13650 Pa·s<sup>-1</sup> for G25, A25 and B25 pastes, respectively). Bassanite paste shows both the highest viscosity and the largest rheopectic cycle. Since our objective is to compare both the effect of the calcium sulfate during hydration and mortars mechanical strengths, similar viscosity values are required for all the pastes. In order to achieve that, different amounts of SP were added to B25 pastes, with the consequent reduction in viscosity.

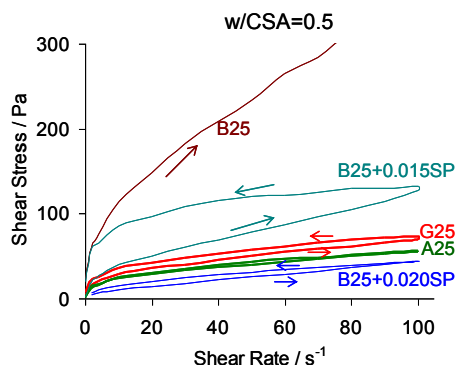


Figure 2. Flow curves of G25, A25, B25 and B25 with 0.012 and 0.020 wt% of superplasticizer.

After the addition of 0.020 wt% of SP, the rheological behaviour of B25 paste was quite similar to those of G25 and A25, showing slightly lower viscosity values (e.g. G25, A25 and B25 pastes showed viscosity values of 0.4, 0.7 and 0.55 Pa·s at 100 s<sup>-1</sup>, respectively), and a small rheopectic cycle (-440 Pa·s<sup>-1</sup>).

The mineralogical changes of the cement pastes with hydration time were quantified by LXRPD. Table 1 reports RQPA results for G25 and A25 cement pastes including the amorphous and non-quantified crystalline contents (ACn) and free water (FW).

Table 1. RQPA (including ACn and FW) for G25 and A25 pastes after 1 and 3 hydration days.

Phase	G25		A25	
	1d	3d	1d	3d
Klein's salt	5.9(2)	3.5(2)	7.3(2)	5.1(2)
Gypsum	2.7(2)	2.4(2)	-	-
Anhydrite	-	-	6.6(2)	5.2(2)
Ettringite	25.6(2)	29.8(2)	20.4(2)	29.9(2)
β-belite	8.3(4)	8.5(4)	7.5(4)	8.7(3)
Minor phases	7.1(3)	6.8(3)	4.2(2)	5.0(2)
ACn	42.0(7)	43.0(7)	42.0(6)	41.6(5)
FW	8.4	6.0	12.0	4.5

Table 2. Compressive strength values for G25, A25, B25 and B25 with 0.020 wt% SP.

Name	Compressive Strength (MPa)	
	1d	3d
G25	41 ± 2	59 ± 1
A25	21 ± 1	64 ± 1
B25	2.1 ± 0.3	5 ± 1
B25+0.020 wt% SP	11 ± 2	18 ± 2

Within the first hydration day, the formation of ettringite occurred at a greater extent for G25, which shows lower Klein's salt and higher ettringite contents than A25. Hence, G25 mortars show higher mechanical strengths at 1 day, Table 2. On the other hand, after 3 days, similar ettringite contents were observed for both pastes. However, the setting time for A25 was much longer than that of G25, presenting a higher plasticity which can better accommodate the precipitation of ettringite. G25 and A25 mortars show similar compressive strengths, being slightly higher for A25, likely due to the plasticity. Compressive values for B25 and B25 with 0.020 wt% of SP are also shown in Table 2. The low strength values for B25 at 1 and 3 days are related with the high viscosity (low workability) of the pastes which causes heterogeneous mortars. In addition, B25 mortars with SP show higher strengths than B25 due to the lower viscosity, however, the short setting times still produces heterogeneous mortars with uncontrolled porosity.

## Conclusions

The effect of three calcium sulfate sources (gypsum, anhydrite and bassanite) on the rheological behaviour of fresh CSA cement pastes, setting time, chemical behaviour during hydration and compressive strengths of the corresponding mortars has been studied. The rheological behaviour is not affected by the addition of different gypsum contents. Furthermore, the addition of bassanite increases the viscosity at very early hydration ages, and considerably reduces the setting time. The chemistry developments in these pastes affect the compressive strengths of the corresponding mortars.

## References

- [1] Aranda, M.A.G., and De la Torre, A.G. (2013). In Eco-efficient concrete (Pacheco-Torgal, F., Jalali, S., Labrincha, J., and John, V.M. eds.), pp. 488-522, Woodhead Publishing Limited, Cambridge.
- [2] Sahu, S., Havlica, J., Tomková, V., and Majling, J. (1991). *Thermochim.* 175, 45-52.
- [3] Winnefeld, F., and Lothenbach, B. (2010). *Cem. Concr. Res.* 40, 1239-1247.

## Perspectives in Fundamental and Applied Rheology

- [4] García-Maté, M., Santacruz, I., De la Torre, A.G., León-Reina, L., and Aranda, M.A.G. (2012) *Cem. Concr. Comp.* 34, 684–91.
- [5] García-Maté, M., De la Torre, A.G., León-Reina, L., Aranda, M.A.G., and Santacruz, I. *Cem. Concr. Res.*, In Press.
- [6] Champenois, J.B., Dit Coumes, C.C., Poulesquen, A., Le Bescop, P., and Damidot, D. (2013) *Rheol. Acta* 52, 177-187.
- [7] Álvarez-Pinazo, G., Cuesta, A., García-Maté, M., Santacruz, I., Losilla, E.R., De la Torre, A.G., León-Reina, L., and Aranda, M.A.G. (2012) *Cem. Concr. Res.* 42, 960–71.

### *Contact Address:*

*Isabel Santacruz (isantacruz@uma.es)  
Departamento de Química Inorgánica, Cristalografía y Mineralogía  
Facultad de Ciencias, Universidad de Málaga,  
29071-Málaga, Spain  
Tel.: +34952131992; Fax: +34952131870*

## CHAPTER 2

# Rheological behavior of LDPE/montmorillonite nanoclays

*Tiago Brehm<sup>1</sup>, Johnson C. P. Santos<sup>1,2</sup>, João Paulo Borges<sup>1</sup> and Maria Teresa Cidade<sup>1</sup>*

*<sup>1</sup>Cenimat/I3N, Departamento de Ciência dos Materiais, Faculdade de Ciências e Tecnologia, FCT, Universidade Nova de Lisboa, 2829-516 Caparica, Portugal*

*<sup>2</sup>Departamento de Tecnologia de Alimentos, Universidade Federal de Viçosa, Av. P. H. Rolfs s/n, Campus Universitário, 36570-000 Viçosa, Minas Gerais, Brasil*

### Introduction

In the last two decades polymer clay nanocomposites have attracted a great interest from both academia and industry, due to the fact that they have shown to present improved mechanical, thermal, barrier and fire properties when compared to the neat polymers, like polystyrene polyethylene-tereftalate and polyester, just to mention a few [1,2].

Different polymers have been employed as matrices in the preparation of polymer/clay nanocomposites, among which, one of the most used is the polyethylene (PE), due to its low weight, low cost and good processability. The polymer/clay nanocomposites display, in general, good optical, electrical and barrier properties and also reduced flammability [3,4].

The work now presented is part of a larger research work that has the objective of developing nanocomposite films, made of montmorillonite dispersed in a low density polyethylene (LDPE), and evaluate their efficiency related to the mechanical, barrier and thermal properties, for applications as packaging.

### Experimental

The low density polyethylene used in this study was kindly provided by the company REPSOL (Sines, Portugal); it is characterized by a melt flow index of approximately 0.71 g/10 min and a density of 920 kg/m<sup>3</sup>.

Two types of montmorillonite (MMT) were used: Cloisite 20A and Cloisite 93A, supplied by Southern Clay Products, Inc., Clay Rockwood Additives GmbH (Moosburg, Germany).

Nanocomposites LDPE/MMT films were prepared in two steps: mixing and extrusion.

Incorporation of the MMT into the polymer was performed in a HAAKE PolyLab OS RheoDrive, model PTW 16 mixer. The mixture obtained after 15 minutes at a temperature of 190 °C and 80 rpm, was then compressed in order to facilitate the cut into small pieces used in the following step.

Composite films were produced by extrusion at 190 °C and 20 rpm, using a single screw extruder, BARBENDER OHG DUISBURG 2000, PLASTIC-CORDER. The contents of both cloisite 20A and 93A were, 0, 0.5, 1.0, 1.5, 2.5, 3.5 and 4.5 wt %.

Composite films were characterized by SEM (SEM-FIB, Zeiss Auriga). Before being examined by SEM the samples were cryogenically fractured and coated with gold.

The rheological properties of the composites were evaluated in a Bohlin Gemini HR<sup>NANO</sup> rotational rheometer. The geometry used was parallel plates with a diameter of 25mm, and a gap of 700 μm. Oscillatory and steady state measurements were performed at a constant temperature of 200°C.

## Results and Discussion

### *Morphological Characterization*

SEM images, presented in figure 1, reveal the presence of some agglomerates indicative of a poor dispersion of the nanoclays in the composite. Typical lamellar structures characteristic of Montmorillonite (MMT) aggregates are observed in Figure 1 (c).

### *Rheological Characterization*

The characterization started with oscillatory measurements in the linear viscoelastic region (strain of 10%). The elastic modulus ( $G'$ ) and the viscous modulus ( $G''$ ) were obtained as function of the angular frequency ( $\omega$ ) in the range 1 – 100 rad/s. In steady state mode, the samples were subjected to a pre-condition stage, with a pre-shear of 5s<sup>-1</sup> during 60s and an equilibration time of 180s. After pre-shear the apparent viscosity ( $\eta$ ) of the composite was obtained as function of the shear rate ( $\dot{\gamma}$ ) in the range 0.1 – 100 s<sup>-1</sup>. These characterization tests were done to analyse the influence of the content and type of nanoclay in the rheological properties of the composites. In figures 2 and 3 we may see the angular frequency dependence of elastic modulus of the samples, which increases, as expected, with the angular frequency.

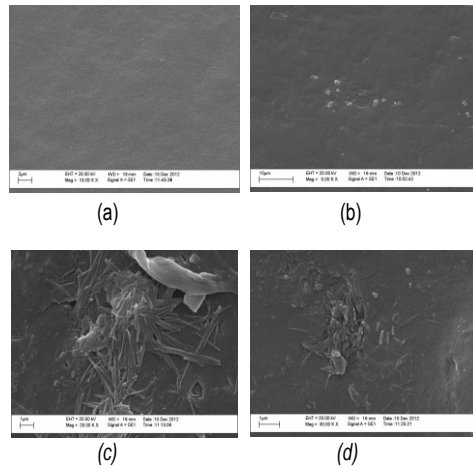


Figure 1. SEM images of polyethylene (PE) (a) and: PE-MMT (1,5 % Cloisite 20A) (b); PE-MMT (2,5 % Cloisite 20A) (c); PE-MMT (3,5 % Cloisite 20A) (d).

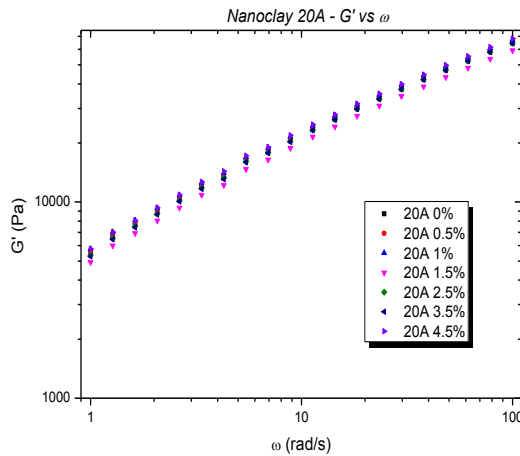


Figure 2. Elastic modulus ( $G'$ ) v angular frequency ( $\omega$ ) for LMWPE/20A

It is possible to observe that the curves remain basically unaltered with the variation of the content of nanoclay. The small variations in the curves are due to a certain lack of reproducibility. It is also possible to observe, by comparing figure 2 and figure 3, that even for different nanoclay the properties remain unchanged.

Figures 4 and 5 show the angular frequency dependence of the viscous modulus, for both clays. Once again, the different curves are roughly the same.

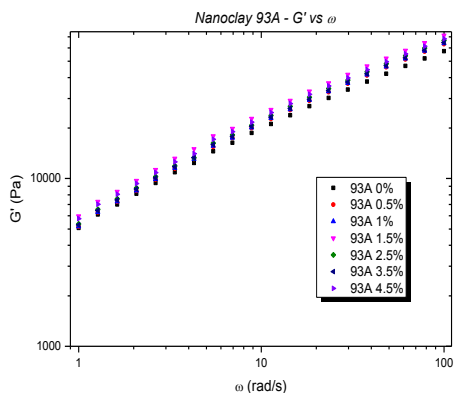


Figure 3. Elastic Modulus ( $G'$ ) vs angular frequency ( $\omega$ ) for LMWPE/93A

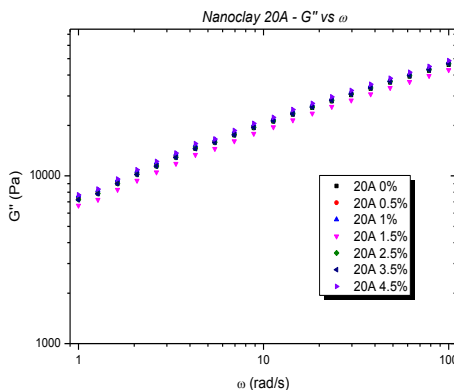


Figure 4. Viscous modulus ( $G''$ ) vs angular frequency ( $\omega$ ) for LMWPE/20A

So, we can state that data obtained in oscillatory mode corresponds, basically, to the polymer matrix. Steady state measurements were also performed to evaluate the influence of the content of both nanoclays in the apparent viscosity of the composites. These results are shown in figures 6 and 7, for nanoclay 20A and 93A, respectively. In both cases it is possible to observe that the apparent viscosity decreases with the applied shear rate, meaning that the samples present a shear-thinning behaviour. Despite the different nanoclay content and even the type of nanoclay, it is impossible to find a dependence of the apparent viscosity with these two parameters. As mentioned before, also in this case, the values

obtained correspond basically to the LDPE matrix. The differences among different curves may only be explained based on low reproducibility.

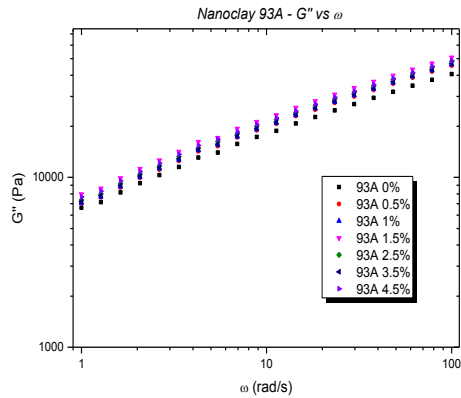


Figure 5. Viscous modulus ( $G''$ ) vs angular frequency ( $\omega$ ) for LMWPE/93A

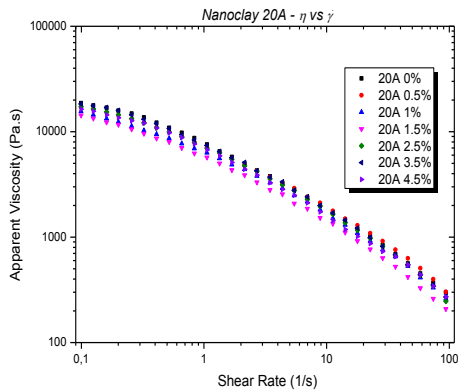


Figure 6. Apparent viscosity ( $\eta$ ) vs shear rate ( $\dot{\gamma}$ ) for LMWPE/20<sup>a</sup>

Considering all rheological tests performed, it is possible to state that the addition of nanoclays seems not to change the rheological properties of the matrix. This happens even for the higher contents of nanoclay studied and for different types of nanoclays.

This conclusion is most probably due to the low content of nanoclay, and to the low adhesion between the matrix and the nanoclay. In fact, Ali Durmus *et al* [5] studied the effect of different compatibilizers and different contents of nanoclay 20A in linear low density polyethylene (LLDPE) based nanocomposites, concluding that there are no significant effects for contents until 5% (wt) of nanoclay or without compatibilization. The absence of a compatibilizer is

responsible for the very weak, or even lack, of interactions between continuous and disperse phases, which results in poor adhesion between the nanoclay and the polymer matrix.

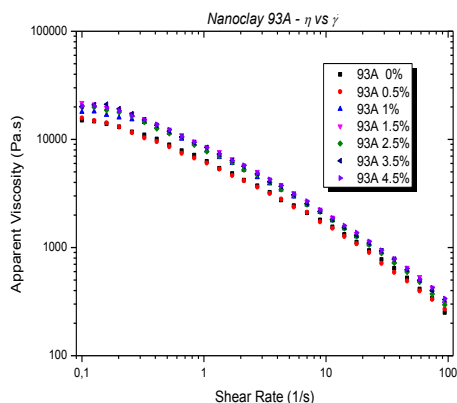


Figure 7. Apparent viscosity ( $\eta$ ) vs shear rate ( $\dot{\gamma}$ ) for LMWPE/93A

Further research will be performed with compatibilized and non-compatibilized nanocomposites for a higher range of nanoclay contents, in order to improve the mechanical properties of these nanocomposites.

### References

1. Okamoto, M, Morita, S., Taguchi, H., Kim, Y.H., Kotato, T and Tateyamo, H. (2000). *Polymer* 41, 3887.
2. Lee, S.R. Park, H.M.; Lim, H., Kang, T; Li, X; Cho, W.J.; Ha, C.S., *Polymer*, 2002, 43, 2495.
3. Araújo, E; Melo, T. J. A.; Oliveira, A. D.; Araujo, H. L. D.; Araujo, K. D.; Barbosa, R. *Polímeros: Ciência e Tecnologia*, 6, n° 1, p. 38 (2006).
4. Wang, K.H.,Choi, M.H., Koo, C.M., Choi, Y.S. and Chung, I.J. (2001). *Polymer* 42, 9819.
5. Durmus A., Kasgoz A. and Macosko, C.W. (2007). *Polymer* 48,4492.

### Contact Address:

Maria Teresa Cidade (mtc@fct.unl.pt)

Dep. Ciência dos Materiais, Faculdade de Ciências e Tecnologia da Universidade Nova de Lisboa

2829-516 Caparica Portugal

Telf.: 351 212948584

Fax: 351 212957810

## CHAPTER 3

# Taking advance of dynamic viscoelastic measurements to investigate polyurethane/graphene nanocomposites

*Leire Sangroniz, Jorge Canales, M<sup>a</sup> Eugenia Muñoz and Antxon Santamaria*

*Department of Polymer Science and Technology and POLYMAT Institute  
The University of the Basque Country (UPV/EHU)*

### Introduction

Graphene is an atomically thick, two dimensional sheet, composed of sp<sup>2</sup> carbon atoms arranged in a honeycomb structure, with extraordinary physical properties.

Graphene can be dispersed in polymer matrices, giving rise to nanocomposites that open the door to new materials with excellent expected properties. These nanocomposites have attracted great interest [1], notwithstanding important aspects, such as their rheological behaviour, have been practically ignored, so far.

In this work the viscoelastic response of polyurethane (PUR) /graphenes nanocomposites is investigated with the aim of disclosing basic and applied issues of these materials. One potential application of these nanocomposites is their use as electrically conductive adhesives. In particular, dynamic viscoelastic results in the terminal zone are contemplated, covering the following aspects: a) Aspect ratio of graphene dispersed in PUR, as evaluated using the complex viscosity b) Percolation threshold compared with PUR/MWCNT (Multiwalled Carbon Nanotube) nanocomposites c) Crystallization process, favoured by graphene, studied analysing the evolution of viscoelastic functions.

### Experimental

A commercial semicrystalline polyurethane PB121 (Merquinsa), which contains polycaprolactone and 1,4- butanediol (BD) and 4,4'-Diphenylmethane diisocyanate MDI was employed as the polymer matrix. Its glass transition

temperature is,  $T_g = -40^\circ\text{C}$  and its melting temperature,  $T_m = 54^\circ\text{C}$ . This polymer is used as a hot-melt adhesive, because it melts at a relatively low temperature and becomes semi-crystalline at room temperature, fixing permanent welding.

Commercial graphene, Avangraphene® (Avanzare, Spain), was dispersed in the polyurethane to obtain the nanocomposites. The dispersion was reached by melt mixing method in a Haake Mini-Lab twin screw extruder (Thermo Electron Corp.).

The dynamic viscoelastic behaviour of compression moulded samples was investigated using a Thermo-Haake Rheostress viscoelastometer with parallel-plate geometry. Small amplitude oscillatory flow measurements in the linear regime were conducted at a temperature of  $T = 100^\circ\text{C}$ ; frequency sweep tests were carried out. Also, sweep experiments at a frequency of 1 Hz, at  $T = 50^\circ\text{C}$  were performed, to investigate the isothermal crystallization.

### Results and Discussion

The following dynamic viscoelastic functions were analysed in frequency sweep experiments in the molten state, and as a function of time at  $T = 50^\circ\text{C}$ : a) Elastic modulus,  $G'$  b) Viscous modulus,  $G''$  c) Complex viscosity,  $\eta^*$ , which is derived from the latter.

The plots of the complex viscosity as a function of graphene concentration (not shown) indicate an increase of the viscosity typical of suspensions. Actually, the results were well fitted to the Maron Pierce equation [2], which was developed for suspensions:

$$\frac{\eta^*}{\eta_{PU}^*} = \left(1 - \frac{\phi}{\phi_m}\right)^{-2} \quad (1)$$

Where  $\eta^*$  and  $\eta_{PU}^*$  are the respective complex viscosities of the nanocomposite and PUR, taken at a frequency of 0.1Hz,  $\phi$  is the volume fraction and  $\phi_m$  is the maximum packing fraction.

It has been observed that  $\phi_m$  decreases as the morphology of the particles deviates from a spherical shape. Based on studies about square sheets, it is shown [3-4] that the maximum packing fraction is correlated with the aspect ratio,  $p$ , through the equation:

$$\phi_m = \frac{3.55}{p} \quad (2)$$

In our case, the value obtained from Maron-Pierce equation is  $\phi_m = 0.19$ , which gives an aspect ratio value of  $p=18.7$ . This value is very small for graphene, and rather approaches to the value of graphite. Since the value given by equation 2 is an average, we assume that the commercial graphene contains considerable amounts of graphite. In fact, similar studies carried out in our laboratory with a home made graphene [4] give an aspect ratio of  $p=177$ .

The low exfoliation level of the particles, disclosed by rheological measurements, leads to doubt about their capacity to bring about a percolation network. In Figure 1, the  $G'$  and  $G''$  results obtained for PUR/Graphene and PUR/MWCNT nanocomposites are shown.

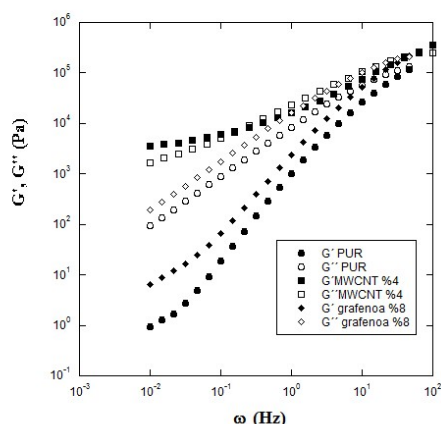


Figure 1. Elastic and viscous moduli as a function of frequency for PUR/8wt % Graphene and PUR/4wt % MWCNT nanocomposites

The percolation network is based on polymer-nanoparticle-polymer bridging, that causes a suppression of flow at low frequencies. This gives rise to  $G' > G''$  when the frequency tends to zero, for nanocomposites above the percolation threshold. In Figure 1 it is seen that this requirement is fulfilled for PUR/4%MWCNT nanocomposite, but not for the PUR/Graphene nanocomposite, even at the highest graphene concentration, 8wt %, considered in this work. Therefore, higher graphene concentrations would be necessary to reach the percolation threshold. This result announces that the drastic increase of the electrical conductivity, which is observed at the percolation threshold, should be reached at a considerable high graphene concentration. This limits the possibilities of elaborating electrically conductive hot-melt adhesives using the graphene of this work.

In hot-melt adhesives, such as the polyurethane we contemplate in this work, tackiness is necessary to reach an initial or immediate adhesion. But, permanent adhesion is only reached when a network formed by crystal junctions is developed. A rapid crystallization process ensures reaching permanent adhesion in a short

time, which is always suitable. This real fact leads to consider the effect of graphene on the crystallization of polyurethane matrix. The nucleating effect of other nanoparticles, like nanoclays and carbon nanotubes, has been investigated at a great extent, but studies on graphene are scarce. For comparison purposes, the isothermal crystallization of pure polyurethane and the nanocomposites at  $T=50^{\circ}\text{C}$  is investigated. The crystallization process can be monitored measuring the dynamic viscoelastic functions as a function of time. The change from a molten liquid state to a semi crystalline solid state gives rise to dramatic changes in the elastic and loss moduli. In Figure 2 the evolution of  $G'$  with time, at a constant frequency of 1Hz and  $T=50^{\circ}\text{C}$ , is displayed.

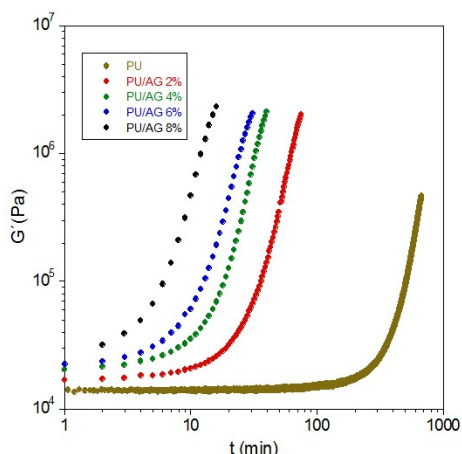


Figure 2. Evolution of the elastic modulus with time during isothermal crystallization at  $T=50^{\circ}\text{C}$ . From right to left the concentration of graphene increases.

The sudden  $G'$  increase after a certain induction time is due to crystallization. It is clearly seen that increasing graphene concentration accelerates the process, so favouring crystallization. A characteristic time for the onset of the crystallization process,  $t_c$ , can be estimated drawing two tangent lines to the  $G'$ - $t$  curves. The values of this characteristic crystallization time are presented in Table 1.

As can be deduced from the results of Figure 2 and Table 1, the presence of graphene shortens very considerably the crystallization time of polyurethane. This is an interesting result from a practical point of view, because reducing the time for permanent adhesion (crystallization) is a valuable contribution in the field of adhesives.

Nowwithstanding the graphene of this work does not promise a significant electrical conductivity increase, it clearly favours the crystallization process of polyurethane.

Table 1. Characteristic crystallization time (see text) for pure polyurethane and the nanocomposites.

Tc (minutes)	wt% graphene
240	0 (neat PUR)
21	2
13	4
10	6
6	8

## References

1. Kim, H., Abdala, A.A., and Macosko, C.V. (2010). *Macromolecules*, Vol. 43, pp. 6515–6530.
2. Maron, S.H. and Pierce, P.E. (1956). *J. Colloid Sci.* 11, 80-95
3. Sangroniz, L. and Santamaria, A. submitted for publication in *Ekaia*
4. Jorge Canales, Ph.D. Thesis in progress (UPV/EHU)

## Acknowledgements

This work has been done under the auspices of the UFI 11/56 of the UPV/EHU. Financial support is acknowledged from GIC IT-441-10 (Basque Government) and MAT 2010-16171 (Spanish Government). J.C. acknowledges a Thesis grant from Basque Government.

## Contact Address:

Jorge Canales ([jorge.canales@ehu.es](mailto:jorge.canales@ehu.es))

Polymer Science and Technology Department and POLYMAT Institute  
University of The Basque Country  
Centro Joxe Mari Korta  
Avenida Tolosa 72, 20018 Donostia-San Sebastián, Spain  
Phone 943 018494, Fax number 943 01 7065



## CHAPTER 4

# The rheological behavior of concrete equivalent mortars when electric arc furnace slag is used as fine aggregated

*F. Contreras-de Villar<sup>1</sup>, F.J. Rubio-Hernández<sup>2</sup>, M.D. Rubio-Cintas<sup>1</sup>*

*<sup>1</sup> Department of Industrial and Civil Engineering, University of Cádiz (Spain)*

*<sup>2</sup> Department of Applied Physics II, University of Málaga (Spain)*

### Introduction

The environmental impact of some wastes is exacerbated by its contaminant effects. An example of these undesirable by-products is the electric arc furnace slag because it contains several heavy metals in its composition. The steel industry annually produces large quantities of this waste; however its use in civil engineering applications is only interesting if there are no environmental effects caused by the substitution of concrete aggregates with the wastes. It has been proved that the leaching products of the electric arc furnace slag (EAFS) are not a problem [1]. Despite several investigations have been conducted on the possibility of electric arc furnace being used satisfactorily in concrete [2-6], the rheological behavior of the concrete formulation resulting from the partial substitution of aggregated by an specific electric arc furnace slag has not been properly made yet.

### Experimental

This study was made on the concrete equivalent mortars [7]. This model basically results from the substitution of aggregates by 0/1 sand, but maintaining constant the specific area occupied by the material that has been substituted. Details of the process to get the concrete equivalent mortar can be found in [7]. In this research part of the 0/1 sand has been substituted by electric arc furnace slag of the same particle size.

A Gemini150 CS rheometer (Malvern Inst.) has been used. This rheometer is equipped with a control temperature Peltier system. Each experiment was conducted on a fresh sample at  $(25.0 \pm 0.1)$  °C.

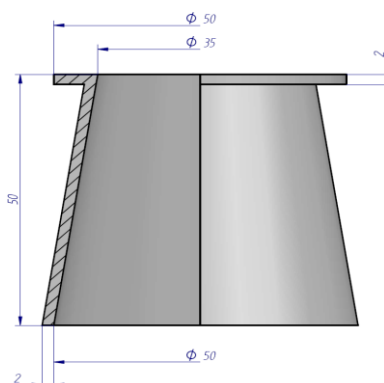


Figure 1. Mini-cone geometry.

Table 1. Characteristics of the cement used in this study.

<b>Chemical characteristics</b>	<b>Value</b>	<b>Especificacion AENOR</b>
Lost by calcination %	2.45	Max. 5
Insoluble residue	1.31	Max. 5
SO <sub>3</sub>	3.33	Max. 4
Chlorides	0.035	Max 0.10
<b>Physical Properties</b>	<b>Value</b>	<b>Especificacion AENOR</b>
Le Chatelier	0.2	Max. 10
Initiation Cure	2h 37 m	Min. 45 Minutes
End Cure	3h 20 m	
<b>Mechanical Properties</b>	<b>Value</b>	<b>Especificacion AENOR</b>
2 Days	42.1	Min. 30
28 Days	63	Min. 52.5

The spread flow was measured using a mini-cone test. Its dimensions are given in Figure 1. It is a smaller version of the Abrams cone for cement pastes and grouts. The tested volume was 0.287 l. The final spread is measured on two perpendicular diameters 1 min after cone lifting. Due to the fact that mini cone tests supplied large slump values, which is an indication of low yield stress values, four serrated vane geometry was used for the measurement of the rheological parameters with the rheometer. The diameter of the rotor was  $25.0 \pm 0.1$  mm, which was introduced in a cup (stator) with an inner diameter of  $37.0 \pm 0.1$  mm. The advantage of using this geometry with cementitious materials has been extensively justified (see for example [8]). The rheometer was calibrated before use with calibration oil (190104) which is supplied by the fabricant.

Some characteristics of the cement (CEM I 52.5R) are shown in Table 1. The additive here used was Glenium AC324 (BASF).

### Results and Discussion

The steady flow curve of the conventional concrete equivalent mortar (CCM) is shown in Figure 2.

The experimental points have been fitting with the modified Bingham model,

$$\tau = \tau_0 + \eta_p \dot{\gamma} + c \dot{\gamma}^2; \quad \tau \geq \tau_0 \quad (1)$$

As can be seen, the second order coefficient ( $c$ ) is virtually zero, which confirms that the CC is a Bingham fluid. The yield stress is relatively high  $\tau_0=(110\pm 3)$  Pa and the plastic viscosity is relatively low  $\eta_p=(3.50\pm 0.13)$  Pa·s.

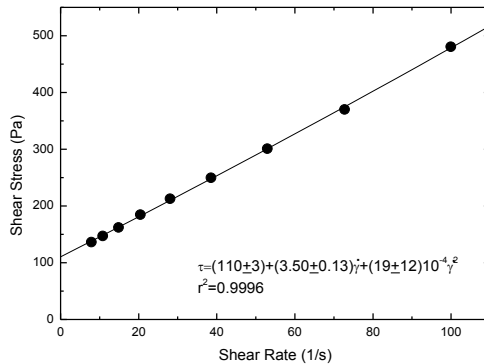


Figure 2. Steady flow curve of the CCM.

The steady flow curve by the equivalent mortar to the self-compacting concrete (SCC) is shown in Figure 3.

As can be seen the second order coefficient is positive ( $c=(0.012\pm 0.001)$  Pa·s<sup>2</sup>) which reflects the characteristic shear-thickening behaviour of the SCC [9-10]. On the other hand, the yield stress is comparatively low  $\tau_0=(26\pm 1)$  Pa, which corresponds to a system that easily flows; and the plastic viscosity is twice the corresponding to the CCM ( $\eta_p=(6.8\pm 0.1)$  Pa·s), which manifests itself as a non segregating material. The sands (0/2 and 0/4) of CC and SCC have been substituted by EAFS, maintaining constant the grading curve composition. The quantity of water added to the concretes with EAFS was higher than that used with the original concretes because the absorption coefficients of the slag are much higher. However the w/c ratio was maintained constant.

For the calculation of the equivalent mortars composition the sands have been substituted by EAFS 0/1 and the gravel by sand 0/1. See tables 2 and 3.

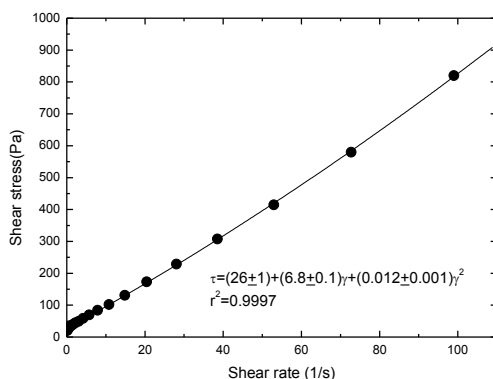


Figure 3. Steady flow curve of the SCCM.

Table 2. Composition of the concretes.

Material	CC	SCC	CCS	SCCS
<b>Cement (kg)</b>	325	350	325	350
<b>W/C</b>	0.50	0.55	0.50	0.55
<b>Additive (%)*</b>	1.1	2.2	3.4	4.5
<b>Sand 0/2 (kg)</b>	289	610	---	---
<b>Sand 0/4 (kg)</b>	673	573	---	---
<b>Gravel 4/16 (kg)</b>	962	666	1215	820
<b>EAFS 0/1 (kg)</b>	---	---	208	406
<b>EAFS 0/2 (kg)</b>	---	---	523	713

\*Calculated respect to the cement weight

Table 3. Composition of the equivalent mortars.

Material	CCM	SCCM	CCSM	SCCSM
<b>Cement (g)</b>	130	140	130	140
<b>W/C</b>	0.50	0.55	0.50	0.55
<b>Additive (%)*</b>	1.1	2.2	3.4	4.5
<b>Sand 0/1 (0/2) (g)</b>	92.48	195.20	---	---
<b>Sand 0/1 (0/4) (g)</b>	94.22	80.22	---	---
<b>Sand 0/1 (4/16) (g)</b>	22.02	22.22	8.58	10.25
<b>EAFS 0/1 (0/1) (g)</b>	---	---	72.38	141.29
<b>EAFS 0/1 (0/2) (g)</b>	---	---	198.74	270.94

\*Calculated respect to the cement weight

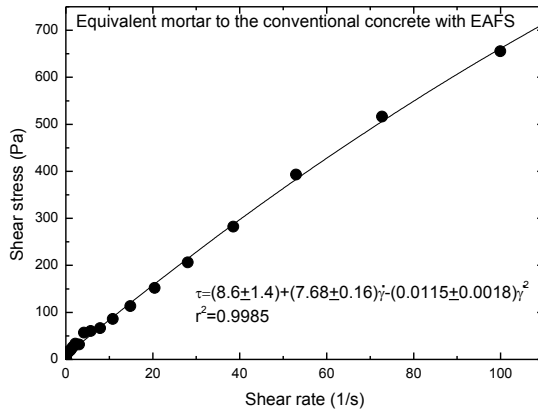


Figure 4. Steady flow curve of the CCSM.

As can be seen in Table 4, with the experimental error the higher the slump value the lower the yield stress is. On the other hand, the substitution of sand by EAFS modifies the behaviour of the CCM to a self-compacting material. This sentence is supported by the fact that the yield stress of CCSM reduces to small values and the plastic viscosity increases, which is an indication of non-segregating behaviour. Moreover, the SCCM improvement this behaviour when the sand is substituted by EASF.

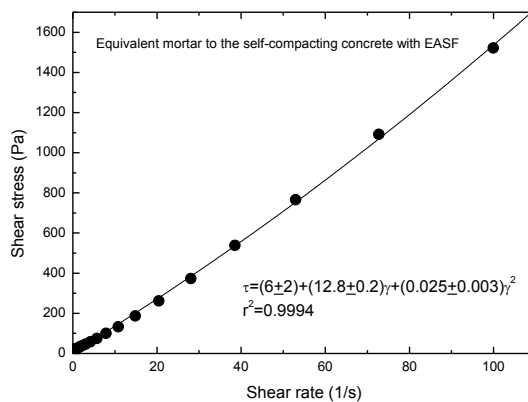


Figure 5. Steady flow curve of the SCCSM.

Table 4. Correlation between the slumps and the rheological parameters.

Material	CCM	SCCM	CCSM	SCCSM
Slump (mm)	120	180	173	183
Yield stress (Pa)	110	26	8.6	6
Plastic Viscosity (Pa·s)	3.5	6.8	7.7	12.8

## Concluding Remark

Despite the fact that the grading of both sands and EASF types are not the same, the substitution of sand by EASF gives the equivalent mortars a self-compacting behaviour when the original mortar is conventional, and enhances the behaviour when the original mortar correspond to a self-compacting formulation.

## References

1. Bäverman, C., and Aran-Aran, F. (1997). *Studies in Environmental Science* 71, 373-376.
2. Manso J.M., Polanco J.A., Losañez M., and González J.J. (2006). *Cement and Concrete Composites* 28, 528–34.
3. Maslehuddin M., Sharif A.M., Shameem M., Ibrahim M., and Barry M.S. (2003). *Construction and Building Materials* 17,105–112.
4. Pellegrino C., and Gaddo V. (2009). *Cement and Concrete Composites* 31, 663–671.
5. Beshr H., Almusallam A.A., and Maslehuddin M. (2003). *Construction and Building Materials* 17, 97–103.
6. Abu-Eishah, S.I., El-Dieb, A.S., and Bedir, M.S. (2012). *Construction and Building Materials* 34, 249–256.
7. Rubio-Hernández, F.J., Velázquez-Navarro, J.F., and Fernández-Ordóñez, L.M. (2013). *Materials and Structures* 46, 587-605.
8. Estellé, P., and Lanos, C. (2008). *Chemical Engineering and Science* 63, 5887–5890.
9. Feys, D., Verhoeven, R., and De Schutter G. (2008). *Cement and Concrete Research* 38, 920-929.
10. Feys, D., Verhoeven, R., and De Schutter G. (2009). *Cement and Concrete Research* 39, 510-523.

## Contact Address:

F. Contreras de Villar ([francisco.contreras@uca.es](mailto:francisco.contreras@uca.es))  
 Department of Industrial and Civil Engineering  
 Escuela Politécnica Superior de Algeciras  
 University of Cádiz (Spain)

## CHAPTER 5

# When Liquid Crystalline Cellulose Flows and Relaxes

*Paulo Teixeira<sup>1</sup>, Susete N. Fernandes<sup>2,3</sup>, João Canejo<sup>2,3</sup>, Maria Helena Godinho<sup>2,3</sup>,  
Catarina Leal<sup>2,4</sup>, Loic Hilliou<sup>1</sup>*

<sup>1</sup>*IPC – Instituto de Polímeros e Compósitos, Departamento de Engenharia de Polímeros,  
Universidade do Minho, Guimarães, Portugal*

<sup>2</sup>*CENIMAT/I3N, Faculdade Ciências e Tecnologia, Universidade Nova de Lisboa, Caparica,  
Portugal.*

<sup>3</sup>*Departamento de Ciência dos Materiais, Faculdade de Ciências e Tecnologia, Universidade Nova  
de Lisboa, Caparica, Portugal.*

<sup>4</sup>*ISEL – Instituto Superior de Engenharia de Lisboa, Área Departamental de Física, Lisboa, Portugal.*

### Introduction

Cellulose-based liquid crystalline materials can generate stimuli-responsive fibers and films [1,2]. Changes in orientational order, which can be affected by variation of temperature and UV irradiation as well as by the presence of solvent vapours, give rise to stresses, which result in strains and modifications in sample shape. The processing conditions of the liquid crystalline material are crucial for fibers and films characteristics. One of the most simple cellulose derivatives that can generate liquid crystalline phases in a wide temperature range is Acetoxypolypropylcellulose (APC). This behavior enables extrusion in a molten state. Here we characterize, for the first time, the rheological behavior of APC, using slit die rheometry, over a wide range of shear rates, thus extending previous reports where rotational rheometry was employed [3] and thus avoiding possible experimental pitfalls associated with free surface defects. Real-time polarized optical microscopy (Rt-POM) was also applied during measurements. The evolution of APC textures was performed during steady-state and after cessation of shear. The combination of slit die rheometry with Rt-POM has provided crucial information in the understanding of the rich viscoelastic liquid crystalline behavior presented by APC. Both stress relaxation and band texture evolutions are

presented and discussed in light of earlier studies carried out at much smaller shear rates [3,4].

### Experimental

#### *Samples*

To a three-neck reactor with mechanical stirring and 300 mL of glacial acetic anhydride, 100 g of (hydroxypropyl)cellulose (HPC) (nominal  $M_w=100000$ , molar substitution = 3.5 determined by  $^1H$  NMR) were added. To the resulting solution, 27,5 mL of acetic acid, a catalyst for nucleophilic and esterification reactions, was finally added. During eight days the solution was heated and stirred at 60 °C for periods of 4 hours per day. After this time the reaction was quenched with the addition of distilled water, and the crude product was washed several times against distilled water until neutral pH. APC was further purified by dissolution in acetone, followed by precipitation in water. The polymer, a whitish viscous solid, was dried during several days under reduced pressure at 60 °C until constant weight and a final yield of circa 80 % was obtained. The number of acetyl groups per residue, evaluated by  $^1H$  NMR, was 2.2. [5,6]

#### *Experimental Procedures*

Slit die rheometry, was performed in a Rosand RH10 Advanced Capillary Rheometer, equipped with a home-made slit with dimensions 60mmx10mmx1mm, where a transparent quartz cell was mounted allowing optical observations during flow. Details about the set-up can be found elsewhere [7].

The tests were carried out over a wide range of shear rates: 2 – 1000  $s^{-1}$ , at 90°.

Real-time polarized optical microscopy (Rt-POM) was applied during measurements.

### Results and Discussion

The viscosity was found to have a shear-thinning behaviour in all the probed shear-rate range. The experimental data were fit to a power law and a shear thinning exponent  $n = -0.57 \pm 0.02$  was found as can be seen in Fig. 1. The stress relaxation after shear cessation relates to the formation of a band texture for shear rates larger than a critical value.

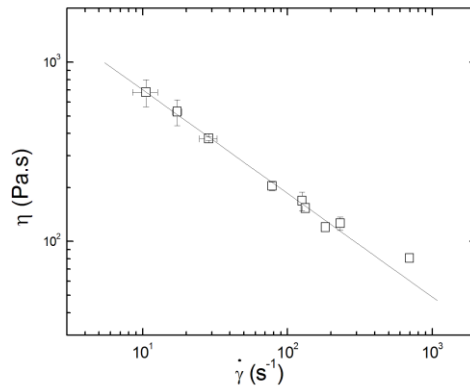


Figure 1. Viscosity as a function of shear rate, for APC at 90°C; line represents is a power law fit to the data with exponent  $-0.57 \pm 0.02$ .

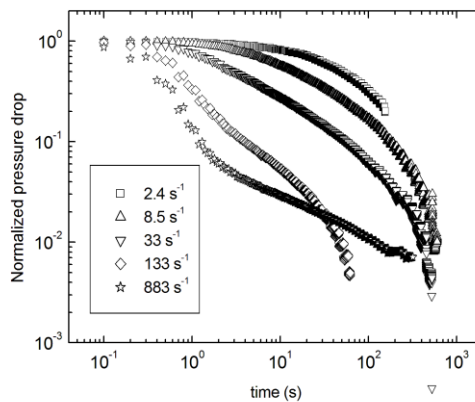


Figure 2. Normalized pressure drop as a function of time, during the relaxation process, after the imposition of several shear rates in the range:  $2 - 1000 \text{ s}^{-1}$ , for APC at 90°C.

The stress relaxation after cessation of shear is depending on the flow history. There is a critical shear rate value above which the stress relaxation appears to be faster for the shorter time range, i.e., at the beginning of the relaxation process. After some time of relaxation the process follows the same behaviour as the one observed for lower shear rate values, see Fig. 2. The relaxation process can be characterized by two characteristic times; when flow in excess of the critical shear rate is applied, see Fig. 3. Rheological measurements are in good agreement with the results obtained from optical characterization with Rt-POM. Illustrative images are included in Fig. 4.

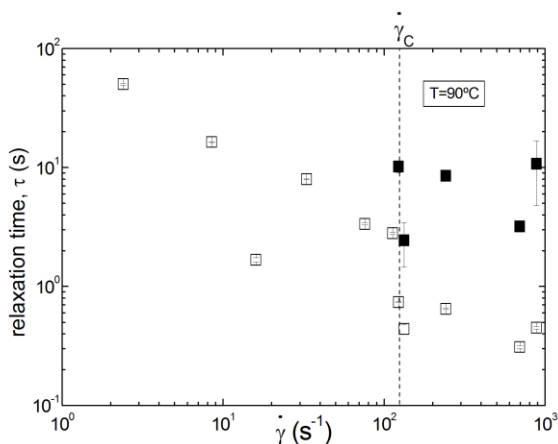


Figure 3. Relaxation time as a function of shear rate, for APC at 90°C.

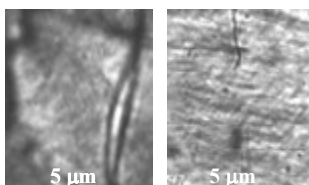


Figure 4. Textures developed during the relaxation process: a) for the shear rates  $8,5s^{-1}$  (left) and  $242s^{-1}$  (right), after 10 s of relaxation, for APC at 90°C.

With this study it is proved that APC follows a shear thinning behaviour with an exponent close to 0.6, for a wide shear rate range that reaches high shear rate values, never probed before. The relaxation mechanism developed after cessation of shear involves two distinct relaxation times above a critical shear rate value.

Taking into account the results obtained it seems that new horizons were open in order to produce cellulosic fibres and films, with enhanced mechanical properties, from liquid crystalline melts.

#### Acknowledgements:

This work was partially supported by the Portuguese Science and Technology Foundation grant and projects, PTDC/CTM/099595/2008, PTDC/CTM/101776/2008, PTDC/CTM-POL/1484/2012 and PEst-C/CTM/LA0025/2011 (Strategic Project - LA 25 - 2011-2012). S.N. Fernandes acknowledge FCT for grant SFRH/BPD/78430/2011.

## References

1. M.H. Godinho, J.P. Canejo, G. Feio, E.M. Terentjev. (2010) *Soft Matter*, 6(23), 5965.
2. Yong Geng, Pedro L. Almeida<sup>1</sup>, Susete N. Fernandes, Cheng Cheng, Peter Palffy-Muhoray & Maria H. Godinho., *Scientific Reports (Nature publish group)*, (2013) DOI: 10.1038/srep01028).
3. Cidade, M. T., Leal, C. R., Godinho, M. H., Navard, P., & Martins, A. F., (1995). *Mol. Cryst. Liq. Cryst.*, 261, 617-625.
4. Harrison, P., Navard, P., & Cidade, M. T. *Rheol. Acta*, 38, 594 (1999).1. Gill, S. R., et. al., (2005). *J. Bacteriol.* 187, 2426-38.
5. Costa I, Filip D, Figueirinhas JL, Godinho MH, (2007) *Carbohydr Polym.*, 6, 159–165.
6. Godinho MH, Filip D, Costa I, Carvalho A-L, Figueirinhas JL, Terentjev EM, (2009) *Cellulose*, 16, 199–205.
7. P.F. Teixeira, L. Hilliou, J.A. Covas and J.M. Maia, (2013). *Rheologica Acta.*, in print DOI 10.1007/s00397-013-0695-5.

## Contact Address:

*Catarina R. Leal (cleal@adf.isel.pt)*  
*Área Departamental de Física,*  
*ISEL – Instituto Superior de Engenharia de Lisboa*  
*Rua Conselheiro Emídio Navarro, 1, 1949-014 Lisboa, Portugal.*  
*Telf.:+351218317135; Fax:+351218317138*



## **PART V**

# **Non-Newtonian Fluid Mechanics**



# CHAPTER 1

## Numerical simulations of the flow through blood vessels with stenosis

S. Murillo-González<sup>1</sup>, J Ortega-Casanova<sup>1</sup>, F.J. Rubio-Hernández<sup>2</sup>

<sup>1</sup> Department of Mechanical Engineering and Fluid Mechanics, University of Málaga (Spain)

<sup>2</sup> Department of Applied Physics II, University of Málaga (Spain)

### Introduction

The blood is basically a suspension of red cells (around 99% of the suspended phase) in plasma. When the blood is at rest, the red blood cells form a more or less strong structure. When it flows this structure breaks down due to the predominance of the hydrodynamic forces on the interactions between red blood cells. These forces erode the structure when the shear increases giving place to the well known shear-thinning behaviour of the blood [1]. The red blood cells are deformable. This fact joined to the elasticity of plasma [2] makes the blood a viscoelastic fluid [3]. Therefore a comprehensive study on the behaviour of the blood flow should consider a constitutive equation which provides for the elastic and viscous components of the stress tensor.

The purpose of this work has been simulating the human blood flow through a vessel with a stenosis. Firstly, it has been assumed only viscous behaviour. After this, the viscoelasticity of the blood has been considered in order to establish the usefulness of both methods.

### Experimental

#### *Materials and methods*

Human blood stabilized with sodium citrate has been used. The rheological measurements were performed with a controlled stress rheometer Gemini150 (Malvern Inst.). Double gap cylinder geometry was used (DG 24/27). An increasing shear rate ramp from  $10^{-3}$  to  $10^2 \text{ s}^{-1}$  was applied to each sample to obtain the steady shear flow curve. The linear viscoelastic limit was determined with an amplitude sweep test. A stress relaxation test was conducted to determine the contribution of the relaxation times of the material to their linear viscoelastic behavior following the Generalized Viscoelastic Maxwell Model. The temperature was controlled with a Peltier system and maintained constant at  $36.5 \pm 0.1 \text{ }^\circ\text{C}$ .

*Code validation*

To get the numerical results of the blood flowing through a vessel, several numerical simulations have been conducted with the open source code openFoam. In order to validate the numerical code used to obtain the numerical results, some preliminary test were carried out. They consist in solving the fully developed Poiseuille flow, driven by a constant pressure gradient ( $p_l$ ) of a incompressible viscoelastic fluid flowing between two infinite parallel plates, separated a known distance ( $2h$ ) considering initially the fluid at rest. The equations governing the motion of the fluid are:

$$\nabla \cdot \vec{v} = 0 \quad (1)$$

$$\rho \frac{\partial \vec{v}}{\partial t} + \rho \vec{v} \nabla \cdot \vec{v} = -\nabla p + \eta_s \nabla^2 \vec{v} + \nabla \cdot \tau_p \quad (2)$$

$$\lambda_k \frac{\partial \tau_{pk}}{\partial t} + \tau_{pk} = 2\eta_{pk} D \quad (3)$$

$$D = \frac{1}{2} (\nabla \cdot \vec{v} + \nabla \cdot \vec{v}^T); \tau_p = \sum_{k=1}^N \tau_{pk}$$

where  $\eta_s$  is the solvent viscosity and  $\eta_p$  is the extra elastic viscosity contribution corresponding to the polymeric part of the fluid, and  $\lambda$  is the relaxation time.

The governing parameters of the problem are

$$Wi = \frac{\lambda U}{h}, Re = \frac{\rho U h}{\eta_0}, E = \frac{Wi}{Re} = \frac{\lambda \eta_0}{\rho h^2} \quad (4)$$

with  $\eta_0 = \eta_s + \eta_p$ ,  $Wi$  is the Weissenberg number,  $Re$  is the Reynolds number and  $E$  is the elasticity number. The simulations were carried out with the parameters  $Re = 5$ ,  $Wi = (1,2,2.5,3)$ ,  $E = (0.2,0.4,0.5,0.6)$ , which correspond to  $\lambda = (0.5,1.0,1.25,1.5)$  s.

The analytical time evolution of the velocity for a fully developed flow was derived [4] and it has been used to validate the numerical code used in the simulations. In particular, the time evolution of the x-velocity in a point in the middle of the channel has been compared, and shown in Figure 1. As one can see, the agreement is quite good and the numerical code used is able to capture the viscoelastic behavior of a fluid.

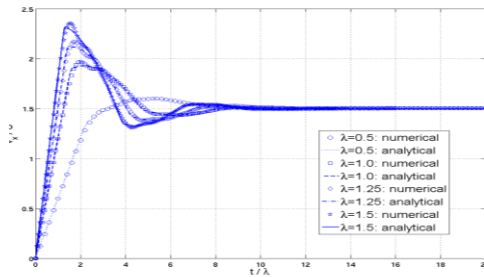


Figure 1. Numerical and analytical temporal evolution of the  $x$ -velocity at the middle of the channel for the relaxation times indicated in the legend.

## Results and Discussion

### Viscous behaviour

The experimental steady viscosity curve shown in Figure 2 is the average of three measurements made with the blood of each one of the donors. As can be seen the blood is a shear-thinning fluid between  $10^{-3}$  and  $1 \text{ s}^{-1}$ . At higher shear rates this system reaches a Newtonian plateau ( $5 \pm 2 \text{ mPa} \cdot \text{s}$ ). The constitutive equation of the Generalized Newtonian Fluid (GNF) with Sisko’s model [5] for the shear rate dependence of the viscosity,

$$\bar{\tau} = \eta(\dot{\gamma})\dot{\gamma} = (5 + 4.2\dot{\gamma}^{-0.83}) \cdot 10^{-3}\dot{\gamma} \quad (5)$$

has been proposed to perform simulations of blood flow when presumably dominates the viscous behaviour.

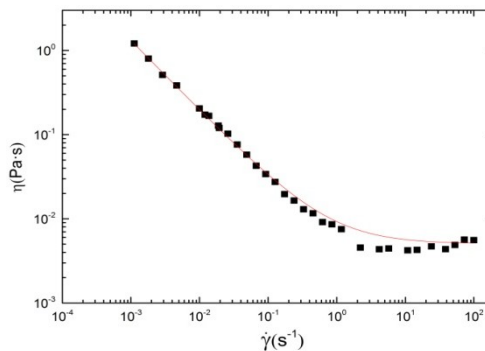


Figure 2. Steady viscosity curve of the blood at  $36.5^\circ\text{C}$ . Sisko’s model has been fitted to the experimental data.

Once the viscosity of the blood has been characterized and fitted with Sisko's model, it has been used to carry out numerical simulations in a stenosed vessel to compare the results with those obtained with the Newtonian behaviour of the

blood under the same conditions. The vessel has been considered as an axisymmetric cylindrical pipe of diameter  $D$  and length  $L = 30D$  with the flow driven by a constant pressure gradient, which correspond to  $Re \approx 410$  when a Newtonian fluid flowing through a uniform pipe. The stenosis has been located in the middle of the tube with a minimum radius of  $0.5D$ . At the steady state, Newtonian and Sisko's flows are different as can be seen in Figure 3.

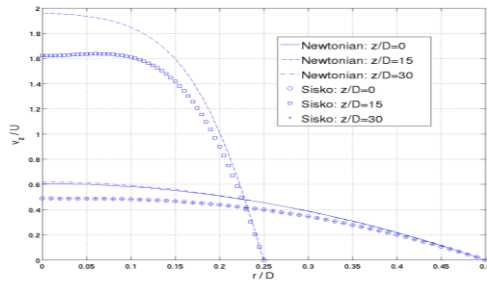


Figure 3. Radial comparison of the axial velocity at the axial coordinates and viscous behaviours indicated

On the one hand, with respect to the uniform tube, the losses due to the stenosis reduce the flow rate. In particular, at the axis  $v_z/U = 2$  when the tube is uniform, whereas the stenosis reduce this ratio to 0.6 and 0.5 when the fluid is Newtonian and non-Newtonian, respectively, far away from the stenosis. On the other hand, focusing our attention on the stenosed vessel, if one takes into account the non-Newtonian behaviour of the blood, by means of Sisko's model, the flow has lower velocities around the axis of the vessel than the Newtonian fluid, which is associated with higher values of viscosity in that region due to lower values of the shear rate. Therefore, it is clear that, at least at moderate Reynolds numbers, the shear-thinning behaviour of the blood will give different conclusions than the Newtonian behaviour when a stenosis problem is analysed.

### Viscoelastic behaviour

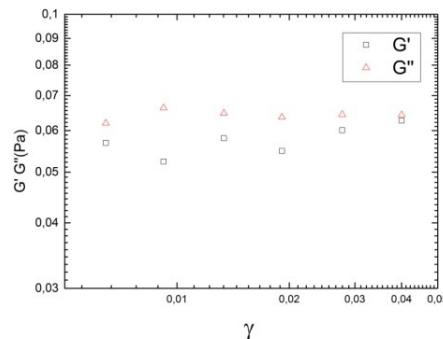


Figure 4. Amplitude sweep of the blood at  $36.5\text{ }^{\circ}\text{C}$ .  $f = 1\text{ Hz}$ .

The results of the amplitude sweep are shown in Figure 4. As can be seen the linear viscoelastic (LVE) region extend until  $\gamma = 0.04$ . Therefore, due to the fact that our interest limits to the LVE behaviour, the stress relaxation test has been obtained by applying a constant deformation into this region (Figure 5). A good fit has been obtained using three terms of the Generalized Maxwell model,

$$G(t) = \sum_{i=1}^3 G_i \exp\left(-\frac{t}{\lambda_i}\right) \quad (6)$$

The characteristic relaxation time of the blood has been calculated as,

$$\lambda = \frac{\sum_{i=1}^3 \lambda_i G_i}{\sum_{i=1}^3 G_i} = 0.38 \text{ s} \quad (7)$$

Therefore, the constitutive equation of the Generalized Linear Viscoelastic Fluid with the GLVE function given by the Generalized Maxwell model [6],

$$\bar{\tau}(t) = \int_{-\infty}^t \sum_{i=1}^3 G_i \exp\left(-\frac{t-t'}{\lambda_i}\right) \bar{\gamma}(t') dt' \quad (8)$$

has been proposed to perform simulations of blood flow when its elastic component should be taken into account.

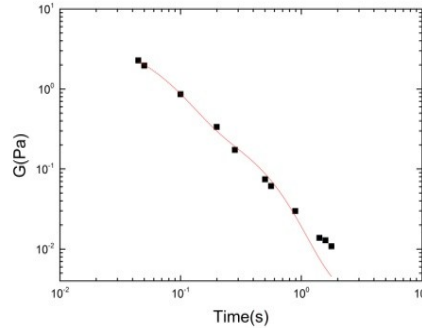


Figure 5. Stress relaxation of the blood at 36.5 °C.  $\gamma_0 = 0.03$ . Generalized Maxwell's model has been fitted.

With the viscoelastic behaviour of the blood characterized and fitted by the Generalized Maxwell model, different numerical simulations were carried out in order to identify the main differences with respect to the Newtonian model. The comparison is shown in Figure 6, where the temporal evolution of the axial velocity on the axis at three different locations (just below the stenosed zone,  $z/D = 15$ , upstream,  $z/D = 10$ , and downstream,  $z/D = 20$ , of it) is shown. As expected, at the steady state, the solution given by both models is the same, whereas the temporal evolution is different depending on the location along the vessel. Upstream and just under the stenosed zone, the temporal evolutions are quite similar, being different the evolution of the motion downstream the contraction.

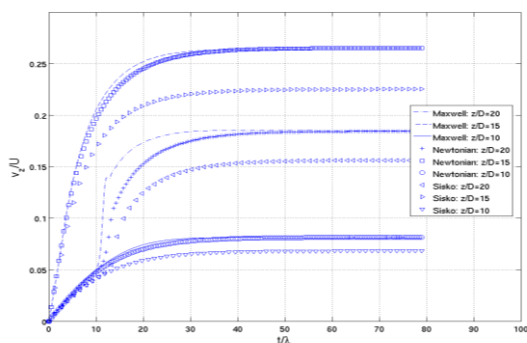


Figure 6. Temporal evolution of the axial velocity at  $r=0$  and the axial locations and models indicated in the legend.

## Conclusions

In this work, the viscous and viscoelastic behaviours of human blood have been characterized and fitted to Sisko and Generalized Maxwell models to get some numerical simulations of the flow of blood through a stenosed vessel driven by a constant pressure gradient. It has been shown that the solutions are different depending on the model used, so one has to take care when neglect the elastic component of blood. Different values of the pressure gradient, both constant and pulsating, are being studied numerically. Moreover the influence of the stenosis size will be also considered. All these studies will be the content of a future work.

## References

1. Cokelet, G.R. (1987). The rheology of tube flow of blood. *Handbook of bioengineering*, 14, 14-1.
2. Brust, M., Schaefer, C., Doerr, R., Pan, L., Garcia, M., Arratia, P. E., & Wagner, C. (2013). Rheology of human blood plasma: Viscoelastic versus Newtonian behavior. *Physical Review Letters*, 110(7), 078305.
3. Thurston, G. B. (1972). Viscoelasticity of human blood. *Biophysical Journal*, 12(9), 1205-1217.
4. Waters, N. D. and King, M. M. (1970). Unsteady flow of an elasto-viscous liquid. *Rheologica Acta*, 9(3), 345-355.
5. Sisko, A. W. (1958). The flow of lubricating greases. *Industrial & Engineering Chemistry*, 50(12), 1789-1792.
6. Morrison, F.A. (2001). *Understanding Rheology*, Oxford University Press, New York.

## Contact Address:

J Ortega-Casanova (jortega@uma.es)  
 Departamento de Ingeniería Mecánica y Mecánica de Fluidos  
 E.T.S Ingenieros Industriales, Universidad de Málaga (Spain)

## CHAPTER 2

# Velocity overshoots in rectangular rectilinear microchannels

*F.J. Galindo-Rosales, S.J. Haward, M.A. Alves*

*CEFT - Department of Chemical Engineering, Faculty of Engineering, University of Porto, Rua Dr. Roberto Frias s/n, 4200-465 Porto, Portugal*

### Introduction

Wormlike micelles (WLM) are formed by the self-assembly of amphiphilic surfactant molecules in solution above a critical micellar concentration [1]. They are sometimes referred to as “living” or “equilibrium” polymer solutions, because the highly deformable WLM shares many of the characteristics of a high molecular weight polymer molecule, but with the important difference that the micelle can break and reform dynamically. This ability confers unique rheological properties to these fluids that make them extremely useful in many applications and processes ranging from inkjet printing to enhanced oil recovery and as working fluids in district heating/cooling systems or as rheology modifiers for consumer products like paints, detergents and shampoos [2, 3]. In semi-dilute or concentrated WLM systems, the linear rheology obeys almost ideal Maxwellian behaviour and can be well described by a single-mode Maxwell-Debye relaxation mechanism [4]. However, in any real application in which the fluid may be used, i.e. in the non-linear regime, their behaviour is usually far from simple and a wide range of poorly-understood phenomena can be found, including shear banding [5], flow-induced structure formation [6], and elastic and interfacial instabilities [7].

In this work, we report flow velocimetry measurements with a WLM solution in a rectilinear microchannel of rectangular cross section with high aspect ratio. Such a fundamental experiment is of course relevant to almost any flow-related industrial process involving WLM as well as to lab-on-a-chip applications and microfluidic rheometry. The flow fields in shear-banding and non-shear banding WLM solutions have been studied previously in similar planar geometric configurations [8-10]. These investigations revealed a pseudo-Newtonian parabolic velocity profile across the width of the channel at low flow rates, which evolves towards a plug-like profile at higher flow rates due to shear-thinning (or shear-banding). Such plug-like velocity profiles can be readily predicted using simple generalized Newtonian fluid (GNF) models that describe shear-thinning fluid rheology, e.g.

Carreau-Yasuda or Ellis models [11]. Most studies using high aspect ratio microchannels have focused on the mid-plane of the channel, assuming that the flow is quasi-two-dimensional. One important exception was the study of Nghe et al. [12] where measurements were made over the channel cross-section, but the authors did not reach all the way to the channel end-walls and focussed on elucidating the details of interfacial instability between shear bands in the microchannel [12]. Additionally, results were only presented for a single imposed pressure gradient corresponding to the stress-plateau region of the flow curve.

In this work, we report measurements of the fully-developed velocity field across the channel width and at various depths ranging from the end-wall up to the channel mid-plane. Thus, the velocity field is mapped over the entire channel cross section for a wide range of imposed volume flow rates. At low volume flow rates, we report intriguing non-monotonic velocity profiles through the channel depth that are not predicted by the models most commonly used to fit the non-linear rheology of WLM solutions.

### Materials and Methods

We use a well-studied WLM solution composed of 30mM cetylmethylammonium bromide(CTAB) and 240mM sodium salicylate (NaSal). As shown in Figure 1, the fluid is strongly shear thinning, but does not exhibit a stress plateau in the flow curve, which is characteristic of shear-banding systems.

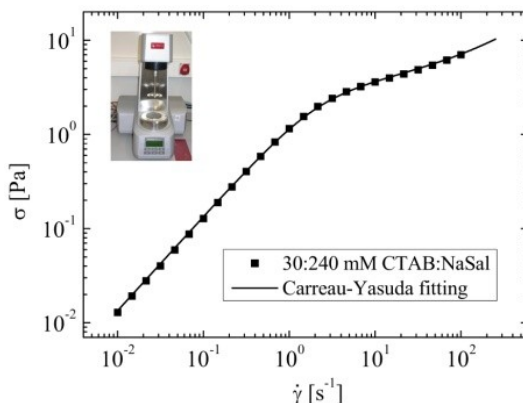


Figure 1. Experimental flow curve of the 30:240mM CTAB:NaSal and fitting curve to the Carreau-Yasuda model.

We perform flow velocimetry experiments under fully-developed flow conditions in a simple rectangular rectilinear microchannel of high aspect ratio  $\alpha=H/w=12.92$ :  $w = 120 \mu\text{m}$ ,  $H = 1550 \mu\text{m}$  (see Figure 2).

A syringe pump (neMESYS, Cetoni GmbH) is used to inject the fluid at constant flow rate in the microchannel. This syringe pump guarantees a high precision and minimizes pulsation in the generated fluid streams. Hamilton syringes with different volumes are used according to the desired flow rate.

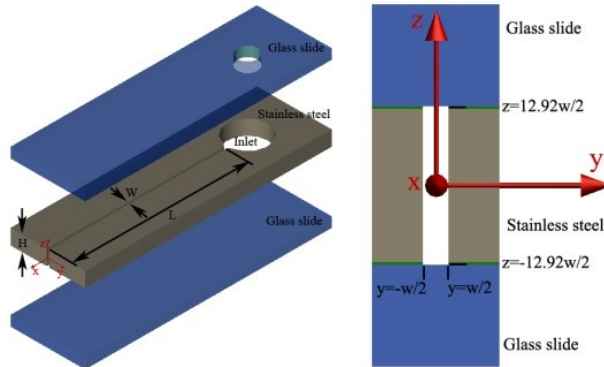


Figure 2. On the left an exploded schematic illustration of the flow-cell showing the glass covers and the stainless-steel microchannel. On the right a cross section of the straight microchannel, bonded with epoxy resin.

Micro-particle image velocimetry ( $\mu$ -PIV) is performed on test fluid seeded with  $0.5 \mu\text{m}$  diameter fluorescent tracer particles (Nile Red, Molecular Probes, Invitrogen; Ex/Em: 535/575 nm; cp 0.002 wt.%). A  $20\times 0.25\text{NA}$  objective is used to focus on  $xy$ -planes between the bottom-wall and the mid-plane of the straight microchannel at  $z$ -steps of  $50\mu\text{m}$ . The resulting measurement depth ( $\delta z_m$ ) over which microparticles contribute to the determination of the velocity field is  $\delta z_m \approx 14\mu\text{m}$ , or  $\sim 1\%$  of the depth of the flow cell. The  $\mu$ -PIV technique is described in more detail in ref. [7].

We map the flow field across the full  $yz$  cross section of the microchannel, from one of the end-walls ( $2z/w = -12.92$ ) into the channel mid-plane ( $2z/w = 0$ ) by means of  $50 \mu\text{m}$  steps, over a wide range of imposed flow rates (from  $0.075 \text{ ml/h}$  to  $10 \text{ ml/h}$ ). In order to ensure steady flow, each flow rate is imposed and maintained for at least  $40\text{min}$  prior to the beginning of  $\mu$ -PIV measurements (one hour at the lowest flow rates). Measurements are made at a distance  $L = 3.5 \text{ mm}$  ( $L/w = 29.17$ ) from the inlet of the rectilinear microchannel to avoid entry effects.

## Results and Discussion

At low flow rates, we find that the velocity field varies in an entirely unexpected way through the channel depth, with the highest flow velocities observed close to

the channel end-walls, as shown in the left-hand side of Figure 3a. In order to obtain the shear rate contours shown in the right-hand side of Figures 3a,b, we have derived the velocity profiles after having fitted them in y-direction to a 15<sup>th</sup> order polynomial function and in the z-direction to an overdamped harmonic oscillator with the form given in Eq. (1):

$$u(z) = Ae^{(-z/Z_1)} + Be^{(-z/Z_2)} + C \quad (1)$$

The shear rate is calculated as in Eq. (2):

$$\dot{\gamma} = \sqrt{\left(\frac{du}{dy}\right)^2 + \left(\frac{du}{dz}\right)^2} \quad (2)$$

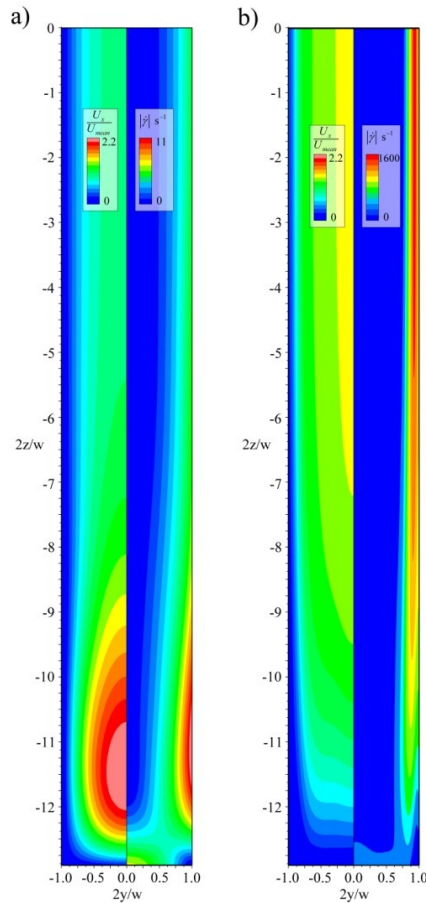


Figure 3. Velocity and shear rate contour plots in the microchannel for (a)  $Q = 0.075\text{ml/h}$  and (b)  $Q = 10\text{ml/h}$ .

As the flow rate is increased, the magnitude of the velocity overshoot near the end-wall diminishes and shifts towards the channel mid-plane. Eventually, at high flow rates the velocity profile in the  $yz$ -plane adopts a more plug-like form, as normally expected for shear-thinning fluids [8], see Fig. 3b and Fig. 4. The non-monotonic, fully-developed velocity profiles observed at low flow rates have been observed by previous investigators [13]. Such profiles are not predicted by the GNF or Johnson-Segalman models, which are the most commonly used constitutive equations to simulate flows of wormlike micellar fluids and should be accounted for in order to improve and optimize applications involving flows of such fluids.

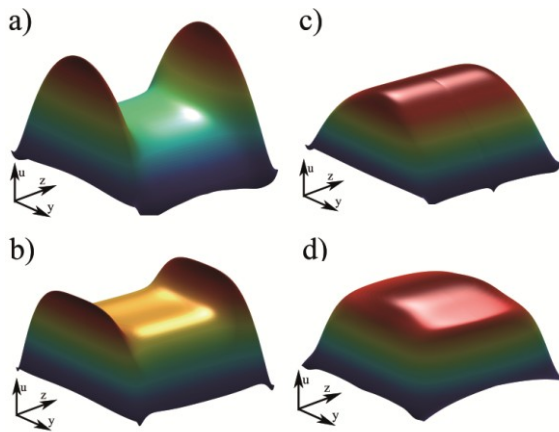


Figure 4. Velocity profiles for (a)  $Q=0.075\text{ml/h}$ , (b)  $Q=0.15\text{ml/h}$ , (c)  $Q=1\text{ml/h}$  and (d)  $Q=10\text{ml/h}$ .

Experimental results for laminar flow of high molecular weight flexible polymer solution through a symmetrical plane sudden expansion preceded by a gradual contraction from a square duct also showed spanwise<sup>1</sup> profiles of the streamwise velocity exhibiting extreme velocity overshoot with very strong gradients near the side-walls, known as “cat’s ears” due to their appearance [14]. However this phenomenon is due to the combined effect of the contraction-expansion geometry and the elasticity of the fluid, and has been reproduced numerically under creeping-flow conditions [15]. The current experimental results are obtained in a rectilinear channel under fully developed conditions. Therefore, they are the result of a distinct physical mechanism than the previously reported “cat’s ears” flow profiles. The results here reported stand as a challenge to be reproduced by theorists and those who simulate viscoelastic flows.

<sup>1</sup>As in [14], we use the terms spanwise for the  $z$ -direction and streamwise for the flow in  $x$ -direction.

## Acknowledgements

Authors acknowledge financial support from Fundação para a Ciência e a Tecnologia and FEDER through the project PTDC/EME-MFE/114322/2009 and scholarship SFRH/BPD/69663/2010, and European Commission Marie Curie action FP7-PEOPLE-2011-IIF grant 298220.

## References

1. Larson, R.G. (1990) The structure and rheology of complex fluids, Oxford University Press, U.K.
2. Rothstein, J. (2008). In Rheology Reviews (Binding, D.M. and Walters, K., eds.), Vol. 6, pp. 1-46, The British Society of Rheology, U.K.
3. Anderson, V.J., Pearson, J.R.A. and Boek, E.S. (2006). In Rheology Reviews (Binding, D.M. and Walters, K., eds.), Vol. 4, pp. 217-253, The British Society of Rheology, U.K.
4. Spenley, N.A., Cates, M.E. and McLeish, T.C.B. (1993). Phys. Rev. Lett. 71, 253-258.
5. Lerouge, S. and Berret, J.F. (2009). In Advances and Polymer Science (Dusek, K. and Joanny, J-F, eds.), Springer, Germany.
6. Vasudevan, M., Buse, E., Lu, D.L., Krishna, H., Kalyanaraman, R., Shen, Q., Khomami, B. and Sureshkumar, R. (2010). Nature Materials 9, 436-441.
7. Haward, S.J., Ober, T.J., Oliveira, M.S.N., Alves, M.A. and McKinley, G.H. (2012). Soft Matter 8, 536-555.
8. Ober, T.J., Soulages, J. and McKinley, G.H. (2011). J. Rheology 55, 1127-1159.
9. Masselon, C., Salmon, J.B. and Colin, A. (2008) Phys. Rev. Lett., 100, 038301.
10. Nghe, P., Degré, G., Tabeling, P. and Ajdari, A. (2008) Appl. Phys. Lett. 93, 204102.
11. Bird, R.B., Armstrong, R.C. and Hassager, O. (1987) Dynamics of Polymeric Liquids, John Wiley and Sons, U.S.
12. Nghe, P., Fielding, S.M., Tabeling, P. and Ajdari, A. (2010). Phys. Rev. Lett. 104, 248303.
13. Ober, T.J., personal communication (2012).
14. Poole, R.J., Escudier, M.P. and Oliveira, P.J. (2005). Proc. R. Soc. A 461, 3827-3845.
15. Poole, R.J. and Alves, M.A. (2009) J. Non-Newt. Fluid Mech., 160, 47-54.

## Contact Address:

*F.J. Galindo-Rosales (galindo@fe.up.pt), S.J. Haward (shaward@fe.up.pt) and M.A. Alves (mmalves@fe.up.pt)*  
*Dpto de Engenharia Química. Faculdade de Engenharia da Universidade do Porto*  
*Rua Dr. Roberto Frias s/n, 4200-465, Porto (Portugal).*  
*Tel.:+351 224081079; Fax:+351 224081440*

## CHAPTER 3

# Torque measurements in Newtonian and non-Newtonian fluids in Couette-Taylor flow

*Borja Martínez-Arias, Jorge Peixinho, Olivier Crumeyrolle and Innocent Mutabazi*

*LOMC, CNRS-University of Le Havre, France*

### Introduction

Couette-Taylor flow, i.e. the flow between concentric cylinders has served as a case study for transition to turbulence since Taylor's 1923 experiments. Most of the previous works deal with Newtonian fluid flow although several studies were conducted with non-Newtonian fluids such as polymer solutions. The challenge of the non-Newtonian problem is the increase of dimensionality of the parameter space, including parameters depending on the rheology.

The present work deals with the measurement of the flux of angular velocity from the inner cylinder to the outer cylinder, closely connected to the torque. Our objective was to carry out a consistent and comprehensive study of the flow patterns and the torque scaling law for different rotation speed.

A brief description of the experimental setup and the working fluids is given. Then, the results consist in flow visualization photographs and associated torque measurements. The effect of polymer additives on the flow patterns and the torque scaling are discussed.

### Experimental setup

The Couette-Taylor geometry used here is fitted on a rheometer (Physica MCR 501 from Anton Paar). The radii of the inner and outer cylinder are  $r_i = 50 \pm 0.01$  mm and  $r_o = 55 \pm 0.01$  mm, respectively. The gap between cylinders is  $d = r_o - r_i = 5 \pm 0.01$  mm. The length of the inner cylinder is  $L = 150 \pm 0.5$  mm. Thereby, the dimensionless parameters for the geometry are the radius ratio  $\eta = r_i / r_o = 0.909$  and the aspect ratio  $\Gamma = L / d = 30$ . There is a gap between the base of the inner cylinder and the bottom of the outer cylinder of  $0.5 \pm 0.001$  mm. It creates a space, which accommodates an air bubble. The top part of the gap between both cylinders is closed with a PVC cover and the outer cylinder is made of glass. The

performed experiments aimed to study the relationship between the rotational speed of the inner cylinder ( $\Omega$ ) and the torque it exerts in the fluid ( $T$ ). A schematic diagram of the geometry is shown in figure 1.

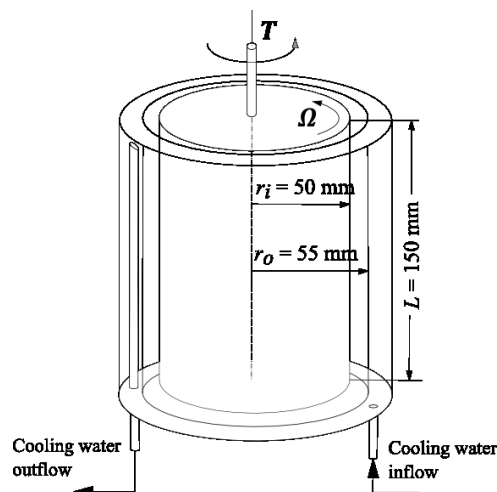


Figure 1. Schematic diagram of the Couette-Taylor apparatus

The rotational speed is made dimensionless using the Reynolds number,  $Re = \Omega r_i d / \nu$ , where  $\nu$  is the kinematic viscosity of the working fluid. Alternatively, several authors [1] used the Taylor number defined as  $Ta = Re (d / r_i)^2$  (here  $d / r_i = 0.1$ ). The torque is made dimensionless using the dimensionless torque,  $G = T / \rho \nu^2 L$ , where  $\rho$  is the density of the working fluid.

Both Newtonian fluids and polymeric solutions are investigated. For the experiments with Newtonian fluids, mixtures of water and glycerine in different concentrations were used (50%<sub>wt</sub> water + 50%<sub>wt</sub> glycerine, and 30%<sub>wt</sub> water + 70%<sub>wt</sub> glycerine). For the non-Newtonian fluids, 75 ppm of polyethylene oxide (PEO) was added to a viscous Newtonian solvent (a mixture of water and polyethylene glycol (PEG) ). The polymers were obtained from Sigma Aldrich and their quoted relative molar mass is 8 000 000 and 20 000 g.mol<sup>-1</sup> for PEO and PEG, respectively. All working fluids are transparent, for the flow visualization kalliroscope is added (2%<sub>wt</sub> of the total amount). A cooling system allows keeping the temperature of the fluid at  $22 \pm 0.01^\circ\text{C}$ .

A cone-plane geometry was used to measure the shear viscosity of the polymer solutions. The shear viscosity was almost constant for the shear rate range of interest. The values obtained are presented in table 1. Each property was obtained as a statistical average of three measurements.  $\mu_{\text{solvent}}$  is the shear viscosity before adding the polymer.  $\mu_{\text{solution}}$  is the shear viscosity of the solution after the addition of the polymer. The first normal stress difference,  $N_1$ , can be

obtained from the cone-plane test and can be used to quantify the magnitude of the elastic stresses in the polymer solution. The Weissenberg number compares the elastic stresses to the viscous stresses.

Table 1. Properties of the polymer solution

Fluid composition	$\rho$ (kg/m <sup>3</sup> )	$\mu_{\text{solvent}}$ (mPa.s)	$\mu_{\text{solution}}$ (mPa.s)
Water 85 % PEG 15 % PEO 75 ppm	1024±1	29.6±0.4	30.7±0.2

### Experimental protocol

Different procedures were followed to measure the torque and speed in the Newtonian and the viscoelastic fluid. For the first case, it was imposed a constant torque during a sufficiently long time, while measuring the speed. Then, all the speed data were averaged to get one resulting point. For the case of the viscoelastic solution only one experiment was run after filling the gap between both cylinders with fluid, in order to avoid the polymer degradation [2]. It was imposed a constant acceleration, using a speed control protocol, while measuring the torque with small sampling times. The ramping rate, i.e., the dimensionless acceleration, was  $dRe/d\tau = 0.07$ .  $\tau$  is the dimensionless time, which is the ratio between the time  $t$  and the radial viscous diffusion time,  $d^2/\nu$ .

## Results and Discussion

### Newtonian fluid

It is well known that several centrifugal instabilities appear in the Couette-Taylor flow when increasing the  $Re$ , giving rise to different structures. Flow visualization photographs of these structures, showed in figure 2, have been taken using short exposure times. Figure 2(a) is a photograph of the Couette laminar flow, where all the fluid particles move on axisymmetric azimuthal trajectories. Figure 2(b) corresponds to Taylor vortex flow (TVF), a flow pattern characterised by time-independent, axisymmetric and toroidal vortices. Figure 2(c) corresponds to wavy vortex flow (WVF), a flow pattern that consists of time-dependent, non-axisymmetric vortices characterised by a single axial wavenumber and an azimuthal wavenumber.

In both figures 2(b) and 2(c) the number of vortices equals 30, the aspect ratio of the gap. This means that each vortex has an aspect ratio of one. Clearly each flow

pattern corresponds to a specific mode of energy dissipation. Hence, the associated torque should have special properties.

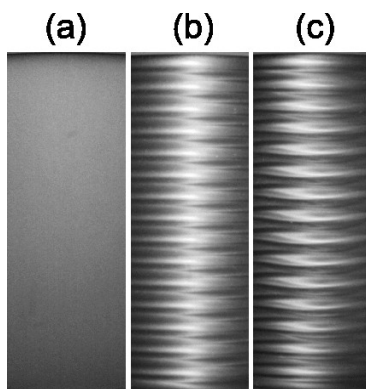


Figure 2. Flow visualization photographs of the Newtonian flow taken at different  $Re$ : (a) Laminar flow, (b) Taylor vortex flow (TVF) at  $Re = 146$  and (c) Wavy vortex flow (WVF) at  $Re = 178$

The results of the torque-speed measurements are presented in figure 3(a). The evolution of the relationship between  $G$  and  $Re$  can be described in three stages. For  $Re < 139$  (black dots), the slope is linear and corresponds to laminar flow. Actually, the critical  $Re$  associated to the onset of TVF for the present geometry is  $Re_c = 139$  [4], represented as a green vertical line in figure 3(a). For  $139 < Re < 155$  (blue squares), TVF (see figure 2(b)) is observed. For  $155 < Re < 200$  (red triangles), WVF (see figure 2(c)) is observed.

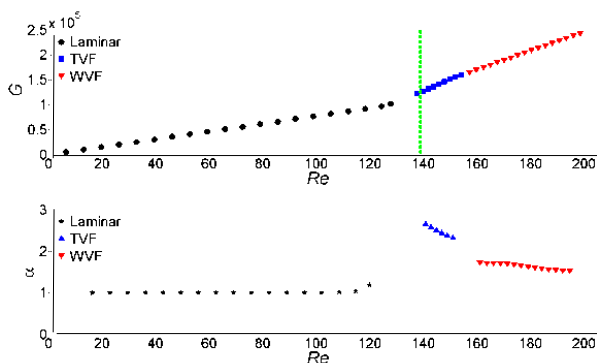


Figure 3. (a) Variation of the dimensionless torque ( $G$ ) as a function of  $Re$  for the Newtonian fluid, (b) Variation of the exponent ( $\alpha$ ) of the power-law scaling as a function of  $Re$

The transport of angular momentum through the gap between the cylinders can be estimated via the torque applied by the fluid to the rotating cylinder. Its dependence on the  $Re$  can be described through a power-law scaling of the form:

$$G \propto Re^\alpha \quad (1)$$

High precision data of the torque data enables to quantify the exponent, which varies with the flow regime. Figure 3(b) shows the variation of the exponent ( $\alpha$ ) of the power scaling law as a function of  $Re$ .  $\alpha$  is obtained from a least square fitting, based on three points, of the local torque versus  $Re$  data. The exponent for the laminar flow is exactly one. When the vortices appear in the fluid the exponent increases abruptly. Then as  $Re$  becomes larger, the exponent decreases moderately. Eventually, the exponent decreases abruptly when the WVF starts to develop.

#### *Viscoelastic polymer solution*

Previous studies have revealed that the addition of polymer in a Couette-Taylor flow [1,2,3] lead to new flow patterns corresponding to elastic instabilities. Examples of such patterns are presented in figure 4.

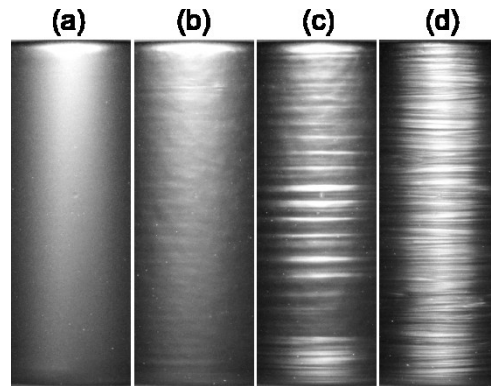


Figure 4. Flow visualization photographs of the 75 ppm POE ( $8 \text{ Mg.mol}^{-1}$ ) in the PEG-water solvent at different rotation rates. (a)  $Re = 14$ , (b)  $Re = 23$ , (c)  $Re = 28$  and (d)  $Re = 36$

The first instability that has been discerned manifests as a time-dependent rough pattern. It is shown in figure 4(b). This first instability appears at a lower  $Re$  than for the Newtonian case. By increasing the  $Re$  the TVF seems to transiently appear, as shown in figure 4(c). As the  $Re$  is increased further, the vortices are replaced by time-dependant fine entwined structures, which appear and disappear rapidly. They are shown in figure 4(d).

The associated torque evolution is presented in figure 5. Again, the torque measurement is very sensitive to the flow pattern. The analysis of the power-law exponent is sensitive enough to detect the rough pattern range.

Another interesting finding is that the exponent is larger, although fluctuating, for polymer solutions than for Newtonian fluids [5]. This seems to be in agreement with the idea that elastic instabilities are more dissipative than centrifugal instabilities.

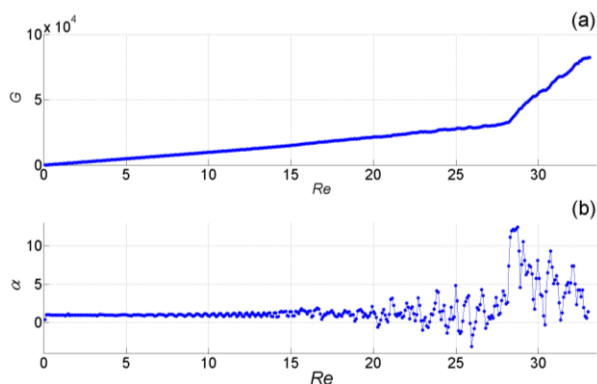


Figure 5. (a) Variation of the dimensionless torque ( $G$ ) as a function of the  $Re$  for the 75 ppm POE ( $8 \text{ Mg}\cdot\text{mol}^{-1}$ ) in a PEG-water solvent, (b) Variation of the exponent ( $\alpha$ ) of the power-law as a function of  $Re$

### Acknowledgments

The authors acknowledge the financial support of the french Agence Nationale de la Recherche (ANR), through the program "Investissement d'Avenir" (ANR-10-LABX-09-01), LabEx EMC<sup>3</sup>.

### References

1. Crumeyrolle, O., Mutabazi, I., and Grisel, M. (2002) *Phys. Fluids*, 14(5), 1681-1688.
2. Dutcher, C.S., and Muller, S.J. (2013) *J. Rheol.*, 57(3), 791.
3. Muller, S.J., Larson, R.G., and Shaqfeh, E.S.G. (1989) *Rheol. Acta*, 28(6), 499
4. Esser, A, and Grossmann, S. (1996) *Phys. Fluids*
5. Yi, M.-K., and Kim, C. (1997) *J. Non-Newtonian Fluid Mech.*, 72, 113-139.

### Contact Address:

Borja Martínez ([borja.martinez-arias@doct.univ-lehavre.fr](mailto:borja.martinez-arias@doct.univ-lehavre.fr))  
LOMC, CNRS-University of Le Havre  
Address: 53, Rue de Prony. 76600 Le Havre, France  
Telf.: +33 2 35 21 71 33

## CHAPTER 4

# Numerical Investigation of Viscoelastic Instabilities in Taylor-Couette Flow with Counter-Rotating Cylinders

*Mohammadali Masoudian, Laura Campo-Deaño and Fernando T. Pinho*

*Department of Mechanical Engineering, Faculty of Engineering, University of Porto, Porto, Portugal*

### Introduction

The flow between concentric rotating cylinders, also called Taylor–Couette flow (TC), is a fundamental flow to understand the dynamics of Newtonian and non-Newtonian fluids. Over the years it has been the subject of studies of hydrodynamic stability with Newtonian and more specifically with non-Newtonian liquids due to its quasi-controllable nature and importance for polymer processing, rheological testing and the fundamental understanding of the mechanisms of flow instability [1].

For Newtonian fluids, the Taylor-Couette flow with inner cylinder rotation has been extensively investigated whereas the case with cylinders rotating in opposite directions (counter-rotating cylinders) has received less attention. In this latter case the flow is unstable in the region between the inner cylinder and the radial position of zero velocity [2]. Andereck et al [3] performed some flow visualizations and spectral studies of flow between concentric cylinders and they observed different flow states depending on the independent rotation of the cylinders. On the other hand, in the case of non-Newtonian fluids, some experimental works were also carried out to study pure elastic instabilities of dilute polymer solutions [4] and critical reviews focused on the understanding of physical mechanisms and principles governing these instabilities [5]. As for Newtonian fluids, few works involving the rotation of both the inner and the outer cylinders were developed [6–10]. These experimental works were performed using either shear-thinning fluids or Boger like fluids. Boger fluids are more appropriate to separate elastic from viscous effects due to their constant shear viscosity, in contrast with shear-

thinning viscoelastic fluids where both effects become increasingly relevant with shear-rate. In regard to numerical simulations, which allow for very refined studies of transition, many studies focused on the understanding of the effects of rheological parameters upon the transitions for purely elastic and inertial elastic flows [9,11]. However, very few computational studies have dealt with viscoelastic instabilities driven by the outer cylinder in a counter-rotating TC setup.

In this work we numerically investigate instabilities in counter-rotating Taylor-Couette flows at a constant elasticity number, represented here by the  $El$  number ( $El = Wi/Re = \lambda \nu/d^2$ ), in order to observe the pattern of elastic instabilities. To this end, Boger fluids were used here described by the Oldroyd-B model.

## Theory

### Governing Equations

The governing equations for complex fluid flow are the continuity equation and the momentum equation:

$$\nabla \cdot \vec{u} = 0 \quad (1)$$

$$\rho \left[ \frac{\partial \vec{u}}{\partial t} + \nabla \cdot \vec{uu} \right] = -\nabla P + \eta_s \nabla \cdot \nabla u + \nabla \cdot \tau \quad (2)$$

where the fluid total extra stress ( $\tau_t$ ) is determined by the Oldroyd-B model, which describes the viscoelastic fluid as the sum of an incompressible Newtonian solvent of constant viscosity  $\eta_s$ , with a polymeric stress contribution  $\tau_p$  also of constant viscosity  $\eta_p$

$$\tau_t = 2\eta_s D + \tau_p \quad (3)$$

and

$$D = \frac{1}{2} (\nabla u + \nabla u^T) \quad (4)$$

where  $D$  is the rate deformation tensor. The constitutive equation for the Oldroyd-B model is:

$$\tau + \lambda \left( \frac{D\tau}{Dt} - [\tau \cdot \nabla u] - [\tau \cdot \nabla u]^T \right) = 2\eta_p D \quad (5)$$

### Dimensionless numbers

Some dimensionless numbers are involved in the analysis of viscoelastic instabilities in a Taylor-Couette flow. In this work, as we consider counter-rotating cylinders where  $R_i$  is the inner radius and  $R_o$  is the outer radius, the relevant dimensionless numbers are: the Reynolds number ( $Re$ ) defined as  $Re = |\Omega_o - \Omega_i| R_i d / \nu$  where  $d = R_o - R_i$  and which represents the ratio between inertial and viscous forces; the viscosity ratio  $\beta$ , defined as  $\beta = \eta_s / \eta_0$  with the zero shear viscosity defined as  $\eta_0 = \eta_s + \eta_p$ ; the Weissenberg number ( $Wi$ ) given by  $Wi = \lambda |\Omega_o - \Omega_i| R_i / d$  which represents the product of the relaxation time of the fluid by a characteristic rate of strain; and the Elasticity number ( $El$ ), which is the ratio between elastic and inertial forces,  $El = Wi / Re = \lambda \nu / d^2$ . The values of  $Re$ ,  $El$  and  $\beta$  used are listed in Table 1.

Table 1.  $Re$ ,  $El$  and  $\beta$  for current work

$Re_i$	275
$Re_o$	-100
$El$	0.0115
$\beta$	0.11

### Geometry and Boundary Conditions

In order to avoid the bottom and upper walls effect in flow patterns geometrical conditions are chosen according to [6],  $R_i = 0.06946$  m,  $R_o = 0.07615$  m, and  $h = 0.406$  m, corresponding to a radius ratio of 0.912 and an aspect ratio  $\Gamma = h / (R_o - R_i) = 60.7$ .

### Results and Discussion

Results for the Taylor-Couette flow with counter-rotating cylinders of Table 1 are presented and discussed. Figure 1 represents the flow patterns corresponding to low ( $El = 0.0001$ ), and high ( $El = 0.0115$ ) elasticity numbers, showing a destabilized flow as a consequence of the enhanced elastic instabilities as the Elasticity number increases at the constant  $Re$  number in Table 1.

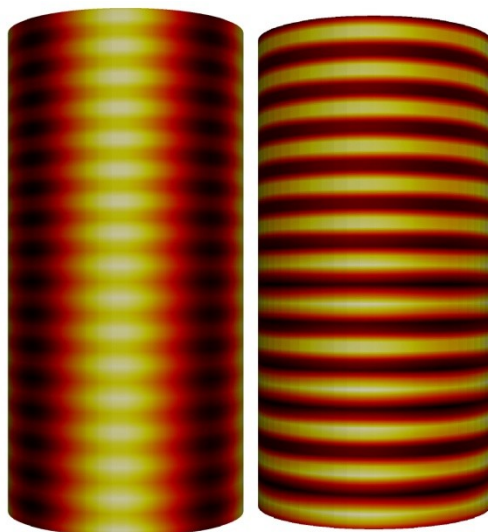


Figure 1. flow pattern right: low elasticity number,  $EI=0.0001$ , and left: high elasticity number,  $EI=0.0115$ .

At low  $EI$  numbers when the instability appears there are only flow variations in space, but not in time. However, due to the oscillatory nature of instabilities both in space and time at higher  $EI$  numbers ( $EI=0.0115$ ), time averaging was performed over all statistics. For instance, Figure 2a shows the temporal averaged velocity magnitude normalized with inner wall velocity, along the cylinders.

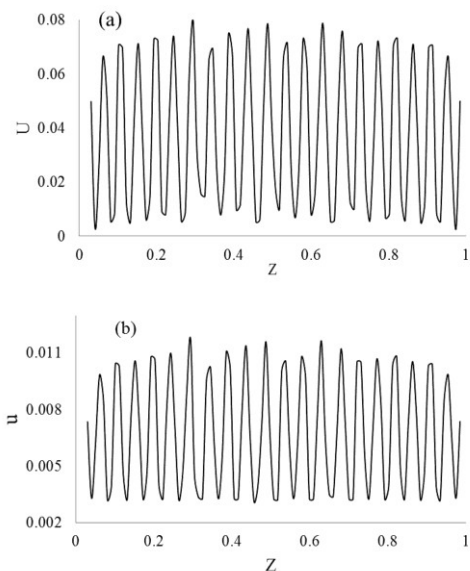


Figure 2. Velocity profiles a) Time-averaged velocity, b) standard deviation  $EI=0.0115$ .

In order to show how much variation or dispersion exists from the average velocity the standard deviation (Figure 2b) was calculated. Note that this velocity is also normalized by the inner wall velocity.

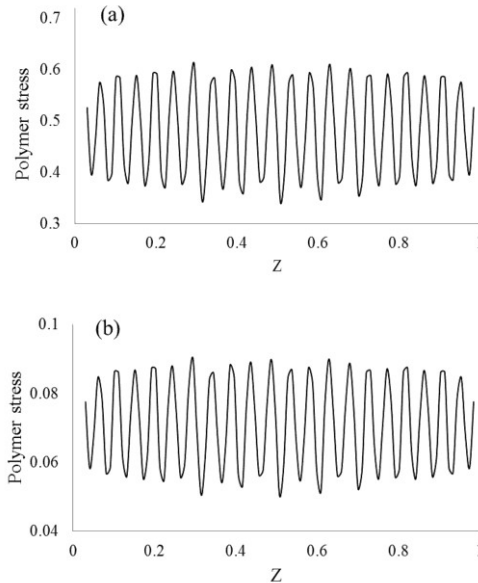


Figure 3. Profiles of the spatial variation of the polymer stresses a) time-averaged polymer stress, b) standard deviation  $El=0.0115$

In addition, the polymeric contribution to the stress is also presented. Figure 3a shows the time-averaged polymer stress magnitude normalized with inner wall stress, along the cylinders, and Figure 3b shows the standard deviation calculated for the polymer stress magnitude.

## Conclusions

In this paper numerical simulations aimed at computing viscoelastic instabilities in a Taylor-Couette flow with counter-rotating cylinders were performed at constant  $Re$  and  $El$  numbers. Future works involves a complete study of the different flow states in order to map the elastic instabilities with counter-rotating cylinders increasing the  $El$  number. For that end, different complex fluids will be modelled namely shear-thinning and Boger fluids described by the simplified PTT model with a linear stress function and the Oldroyd-B model, respectively.

## Acknowledgements

Authors acknowledge funding from FCT, COMPETE and FEDER through projects PTDC/EME-MFE/99109/2008, PTDC/EME-MFE/113589/2009 and scholarship SFRH/BPD/69664/2010.

## References

1. Groisman, A. and Steinberg, V. (1998). *Physics of Fluids*, 10, 2451-2463.
2. van Hout, R. and Katz, J. (2012). *Physics of Fluids*, 23, 105102.
3. Andereck, C. D., Liu, S. S. and Swinney, H. L. (1986). *J. Fluid Mech.*, 164, 155-183.
4. Larson, R. G., Shaqfeh, E. S. G. and Muller, S. J. (1990). *J. Fluid Mech.*, 218, 573-600.
5. Shaqfeh, E. S. G (1996). *Annu. Rev. Fluid Mech.*, 28, 129-185.
6. Baumert, B. M. and Muller, S. J. (1995). *Rheol. Acta*, 34, 147-159.
7. Baumert, B. M. and Muller, S. J. (1997). *Phys. Fluids*, 9, 566-586.
8. Baumert, B. M. and Muller, S. J. (1999). *J. Non-Newtonian Fluid Mech*, 83, 33-69.
9. Dutcher, C. S. and Muller, S. J. (2011). *Journal of Rheology*, 55, 1271.
10. Dutcher, C. S. and Muller, S. J. (2013). *Journal of Rheology*, 57, 791.
11. Muller, S. J. (2008). *Korea-Aust. Rheol. J.* 20 (3), 117-125.

## Contact Address:

*M. Masoudian (mmasoudian@fe.up.pt)*  
*L. Campo-Deaño (campo@fe.up.pt)*  
*F. T. Pinho (fpinho@fe.up.pt)*  
*Department of Mechanical Engineering,*  
*Faculty of Engineering*  
*University of Porto*  
*Rua Dr. Roberto Frias s/n 4200-465, Porto, Portugal*  
*Tel.: +351 22 508 15 97; Fax: +351 22 508 14 40*

## CHAPTER 5

### Flow of Red Blood Cells in Microchannel Networks: *in vitro* studies

Diana Cidre<sup>1</sup>, Raquel O. Rodrigues<sup>1</sup>, Vera Faustino<sup>1,2</sup>, Elmano Pinto<sup>1,2</sup>, Diana Pinho<sup>2</sup>, David Bento<sup>2</sup>, Carla S. Fernandes<sup>1</sup>, Ricardo Dias<sup>1,2</sup>, Rui Lima<sup>1,2</sup>

<sup>1</sup> ESTiG/IPB, Polytechnic Institute of Bragança, Bragança (Portugal)

<sup>2</sup> CEFT, Faculty of Engineering, University of Porto (Portugal)

#### Introduction

Human blood is a multiphase biofluid primarily composed by the deformable red blood cells (RBCs) suspended in plasma. Because the complex structure of RBCs, blood exhibits unique flow characteristics on micro-scale level, due to their complex biochemical mechanisms and their response to both shear and extensional flow, which influence the rheological properties and flow behaviour of blood [1,2].

In the past years *in vitro* blood studies have been extensively performed and some important physiological phenomena, such as Fahraeus and Fahraeus-Lindqvist effect, were revealed [1,3]. This pioneer studies performed by Fahraeus and Fahraeus-Lindqvist in straight glass microchannels [4] revealed that for narrow tubes (diameter < 300  $\mu\text{m}$ ), the apparent viscosity of blood declines with decreasing diameter. More recently, due to the developments in microscopy, computers and image analysis techniques, several researchers have used new measuring methods to obtain deeper quantitative understanding of the blood flow dynamics, *in vitro* [5-8] and *in vivo* experiments [9-10]. The increasing interest by the microfluidic and biomedical communities has also played a key role in several recent developments of lab-on-chip devices for blood sampling, analysis and cell culturing, aimed in a near future, the development of blood diagnostic devices, as an alternative tool to the traditional diagnostic strategies.

However, the blood flow in microvascular networks phenomena remains incompletely understood. Thus, it is important to investigate in detail the behaviour of RBCs flow occurring in a microchannel network, such as, with divergent and convergent bifurcations, which mimics the irregular vessel segments linked by numerous diverging and converging bifurcations.

Previously, we made *in vitro* studies in microchannels with a simple divergent and convergent bifurcation, that showed a pronounced cell-free layer (CFL)

immediately downstream of the apex of the convergent bifurcation [1,4]. This interesting result led us to the present work, where the CFL in a microchannel network is investigated by using a high-speed video microscopy system in order to further understand the blood flow behaviour in microvessels networks.

### **Experimental Work**

#### *Microchannel fabrication and geometry*

The microchannels fabricated for the assays have been produced in PDMS by photolithography from a photo-resist mould. The mould was fabricated by photolithographic technique on a silicon (Si) wafer with an ultra-thick photoresist (SU-8). In this process, a layer of SU-8 photoresist was spin-coated onto the Si wafer and patterned by UV exposure through a photomask. After various curing steps, a SU-8 developer was then used to obtain the final mould master containing the inverse of the desired microchannels.

Proceed to the silanization of templates for later replicate them in PDMS. The silanization process consists in a petri dish, place a drop of trichlorosilane and place it next to the SU-8 mould for 20 minutes in a flow chamber. The trichlorosilane will leave a thin film in the mould in order to protect them and help in the removal of PDMS.

The PDMS was prepared by mixing a base and curing agent at a weight ratio of 10:1 for the channels, and 20:1 for the glass slide. After removing the bubbles created during the mixing steps, the mixture was poured over the mould master and baked in the oven for about 20 min at 80°C. The PDMS is then removed from the mould, cooled to room temperature and the input/output ports were made with an appropriate punching.

Finally, the PDMS microchannel structure was sealed with a glass slide previously spin-coated with PDMS and baked in the oven for 20 min at 80°C. After this procedure the microfluidic device returns to the oven for further 24 hours for a strong seal.

The geometry used is complex, containing several bifurcations and confluences (see Fig. 1). Figure 1 illustrates the configuration and the most relevant dimensions of the geometry used in the study.

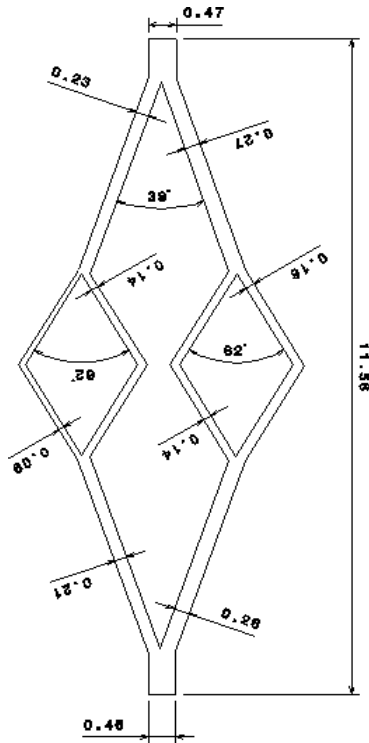


Figure 1. Geometry and dimensions of the microchannel in mm.

### Experimental Set-up

The blood samples used were collected from a healthy adult sheep, and ethylenediaminetetraacetic acid (EDTA) was added to prevent coagulation. The RBCs were separated from the blood by centrifugation and washed twice with physiological saline (PS). The washed RBCs were suspended in Dextran 40 (Dx 40) to make up the required RBCs concentration by volume. All blood samples were stored hermetically at 4°C until the experiment was performed at an ambient temperature of about 22°C.

The high-speed video microscopy system used in the present study consists of an inverted microscope (IX71, Olympus) combined with a high-speed camera (i-SPEED LT, Olympus) (see Fig. 2). The PDMS microchannel was placed on the stage of the microscope where the flow rate of the working fluids was kept constant by means of a syringe pump (PHD ULTRA) with a 1 ml syringe (TERUMO® SYRING).

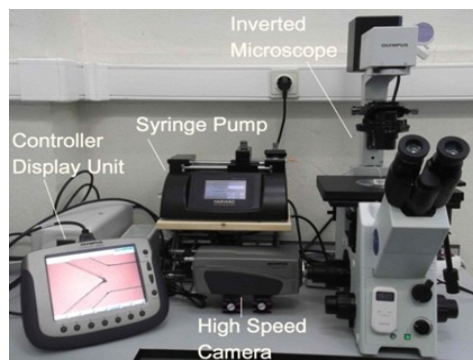


Figure 2. Experimental Set-up.

The assays were conducted with 5  $\mu\text{l}/\text{min}$  of flow rate and a haematocrit level of 10% (10% Htc).

All images were recorded at the centre plane of the microchannels using a rate of 60 frames/second. The recorded images were transferred to a computer and then processed and analyzed using an image processing program (Image J, 1.46r).

### Results and Discussion

The results were taken in several sections of the microchannel, however the last confluence was analysed in more detail for being the last apex of the microchannel network.

The recorded videos were treated by “Z Project” function, which is implemented in *ImageJ* software. Consecutive frames were added to each other using average intensity. Finally, a treatment of the image was made to convert it in a binary image (see Fig. 3). Figure 3 shows the existence of a CFL around the apex of the three confluences and its propagation in a straight line in the region after it.

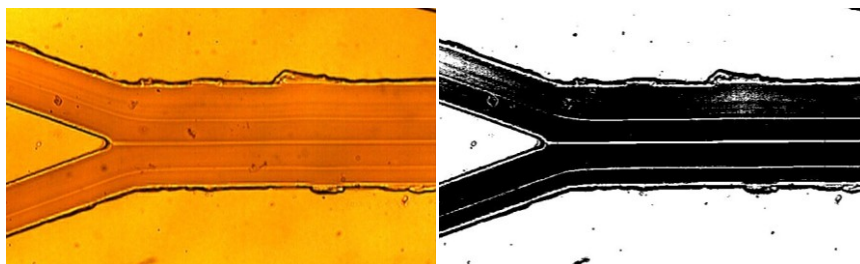


Figure 3. Image of the confluence obtained after “Z Project” using average intensity function (UP) and image results from the binarization (DOWN).

Figure 4 graphically represents the coordinates of the three CFLs obtained in the final confluence of the microchannel network, using the binary image and the “wand tracing” tool of *ImageJ* software.

The graphical outcome of Figure 4 shows a higher CFL in the middle zone that was resulting from the final confluence, and two slightest CFLs resulting from the other upstream confluences.

These preliminary results appear to indicate that these variances in the CFLs are derived from the differences in the confluences geometries that influences the RBCs velocities and trajectories profiles, as was shown by preview studies made by Leble and coworkers [1].

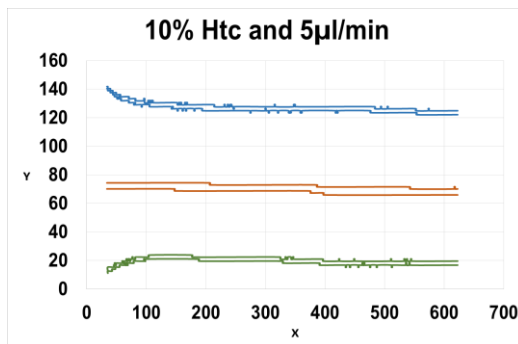


Figure 4. Coordinates of the cell-free layer (CFL) formed in the confluences.

## Conclusions

In the present work, we reported an assay on microchannel network with several divergent and convergent bifurcations using a constant flow rate of red blood cells. At the last convergent bifurcation we report a total of three cell-free layers (CFLs) resulting from the complex microchannel network geometry, where the middle streamline formed around the last apex is more pronounced than the ones formed upstream.

The early results appear to indicate that this variance in the CFLs derives from the differences in the confluences geometries that influences the RBCs velocities and trajectories profiles.

## Acknowledgments

The authors acknowledge the financial support provided by: PTDC/SAU-BEB/108728/2008, PTDC/SAU-BEB/105650/2008, PTDC/EME-MFE/099109/2008 and PTDC/SAU-ENB/116929/2010 from FCT (Science and Technology Foundation), COMPETE, QREN and European Union (FEDER).

### References

1. Leble, V., Lima, R., Dias, R., and Fernandes, C. (2011). *Biomicrofluidics* 5, 044120
2. Wan, J., Forsyth, A. M., and Stone, H. A. (2011), *Integr. Biol.* 3, pp.972-981
3. Lima, R., Ishikawa, T., Imai, Y. and Yamaguchi, T. (2012)., Single and two-phase flows on Chemical and Biomedical Engineering, (Dias, R., Martins, A., Lima, R., and Mata, T. eds.) pp.513-547, Bentham Science Publishers
4. Fahraeus, R., Lindqvist, T. (1931). *Am. J. Physiol.* 96, pp.562
5. Goldsmith, H., and Turitto, V. (1986). *J. Thromb. Haemost.* 55, pp.415
6. Chien, S., Usami, S., Skalak, R. (1984). In *Handbook of Physiology – The cardiovascular system IV* (Renkin, E. M., and Michel, C.C. eds), pp.217, American Physiological Society, Bethesda
7. Abkarian, M., Faivre, M., Horton, R., Smistrup, K., Best-Popescu, C.A., and Stone, H.A. (2008). *Biomed. Mater.* 3, 034011
8. Lima, R., Wada, S., Tsubota, K., and Yamaguchi, T. (2006). *Meas. Sci. Technol.* 17, pp.797
9. Jeong, J.H., Sugii, T., Minamiyama, M., Takeuchi, H., and Okamoto, K. (2006). *Microvasc. Res.* 73, pp.39
10. Sugii, Y., Nishio, S., Okamoto, K. (2002). *Physiol. Meas.* 23, pp.403

## CHAPTER 7

# Visualization of the cell-free layer (CFL) in a PDMS microchannel with a micro-stenosis

*Diana Pinho<sup>1,2</sup>, Tomoko Yaginuma<sup>2</sup>, Vera Faustino<sup>1,2</sup>, Elmano Pinto<sup>1,2</sup>, Raquel O. Rodrigues<sup>2</sup>, Diana Cidre<sup>2</sup>, Ana I. Pereira<sup>2,3</sup>, Rui Lima<sup>1,2</sup>*

<sup>1</sup>CEFT, Faculdade de Engenharia da Universidade do Porto (FEUP), Portugal

<sup>2</sup>ESTiG, Polytechnic Institute of Bragança, Portugal

<sup>3</sup>Algoritmi, Universidade do Minho, Portugal

### Introduction

Red blood cells (RBCs) are responsible for the supply of oxygen and nutrients to the body and removal of carbon dioxide and metabolic wastes from tissues. The blood flow behaviour in microcirculation depends on several combined effects such as cell deformability, flow shear rates and geometry of the microvessel, as well as biochemical and biophysical factors which may also affect the rheological characteristics of blood [1-5].

This study presents a microfluidic device for partial extraction of RBCs by means of a micro-stenosis. RBCs have a tendency to undergo axial migration due to the parabolic velocity profile which results in a high shear stress around wall that forces the RBC to move towards the center induced by the tank treading motion of the RBC membrane [1, 2]. As a result there is a formation of cell-free layer (CFL) with extremely low concentration of cells [1-5]. Based on this phenomenon several works have proposed microfluidic designs to separate the suspending physiological fluid from whole in vitro blood [6, 7]. However, most of these studies have the aim of the complete extraction of cells from plasma which is not the case of the present study. The biomedical device that is present in this work aims to obtain a CFL with a low enough RBC concentration to perform cell deformability measurements downstream the micro-stenosis. The main purpose of this work is to use polydimethylsiloxane (PDMS) microchannels having different micro-stenosis (50% and 75%), and explore their effect on the thickness of the CFL. For this propose a combination of image analysis techniques able to measure automatically the CFL thickness before and after micro-stenosis is used.

This paper is organized as follows. The section Experimental consists of Working fluids and microchannel geometry, Experimental Set-Up and Image Analysis. In the section Results and Discussion, it is presented and discussed the results.

## Experimental

### *Working fluids and microchannel geometry*

The fluid used in this study was dextran 40 (Dx40) containing about 9% (i.e. Hematocrit, Hct = 9) by volume of human RBCs. The samples of blood were collected from a healthy adult volunteer and heparin was added in order to prevent coagulation. The RBCs were washed twice with a physiological saline (PS) solution and diluted with Dx40 to make up the required RBC concentration. All blood samples were stored hermetically at 4°C until the experiments were performed at controlled temperature of approximately 37°C. All procedures in this work were carried out in compliance with the Ethics Committee on Clinical Investigation of Tohoku University.

The microchannels tested in this study were fabricated using common soft-lithography techniques and consist in a straight channels with 100  $\mu\text{m}$  of wide and with a micro-stenosis regions of 25  $\mu\text{m}$  and 50  $\mu\text{m}$  of wide ( $W_1$ ), Figure 1.

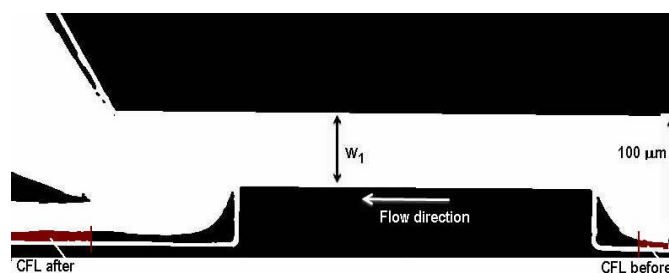


Figure 1. Schematic view to represent the areas where the data was taken, before and after the artificial micro-stenosis.

### *Experimental set-up*

The high-speed video microscopy system used consists of an inverted microscope (IX71, Olympus, Japan) combined with a high-speed camera (Phantom v7.1) (Figure 2). A syringe pump (KD Scientific Inc.) was used to push the working fluids through the microfluidic devices combined with a 500  $\mu\text{L}$  syringe (Hamilton). The flow rate used in our experiments was 1, 5 and 10  $\mu\text{L}/\text{min}$ . A thermo plate controller (Tokai Hit) was set to 37°C.

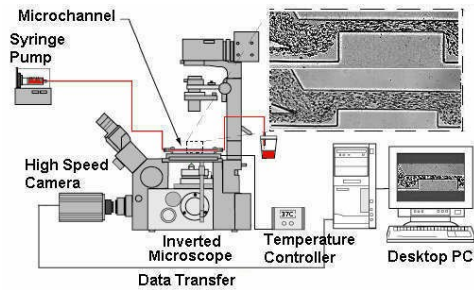


Figure 2. High-speed video microscopy system.

### Image analysis

The image sequence were captured at the centerplane of the microchannels with a resolution of  $800 \times 304$  pixels, at a rate of 8000 frames/s and an exposure time of 0.125 ms, then all videos were transferred to the computer and evaluated in Image J (NIH) [6].

First, the captured videos were converted to a sequence of static images (stack) and then, for each pixel, the maximum intensity of all the images in the stack was selected using the “Z project”, a function from ImageJ.

The results image has a region of RBCs core brighter than the background. To obtain the data it is necessary to apply a level of threshold to convert the grey scale images into binary images. An example of a binary image obtained after image processing is presented in Figure 3 b).

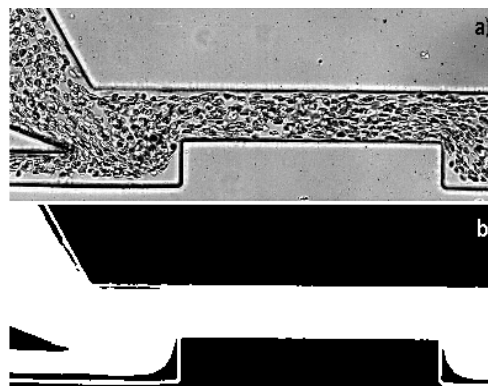


Figure 3. a) Original Image; b) Binary Image obtained after the image processing steps.

### Results and Discussion

In this section the results of flow visualizations are presented and discussed and the effect of a micro-stenosis on the CFL thickness is evaluated.

In Figure 4 it is possible to observe the data obtained using the image analysis techniques already described in the section Image analysis.

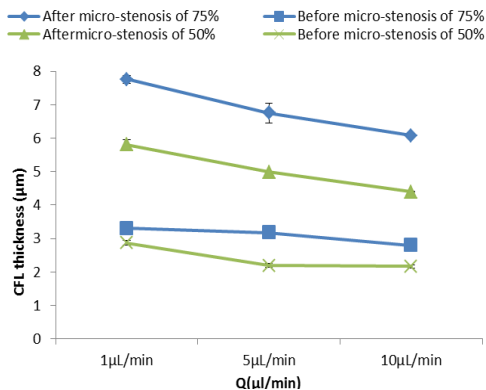


Figure 4. CFL thickness before and after the micro-stenosis for different flow rates.

Figure 4 shows visibly that for both micro-stenosis, 75% and 50%, the CFL thicknesses are enhanced. Moreover, it is also clear that the enhancement is more pronounced for the channel with a contraction of 75% than that for the micro-stenosis of 50%. In the next figure it is possible to observe better this conclusion.

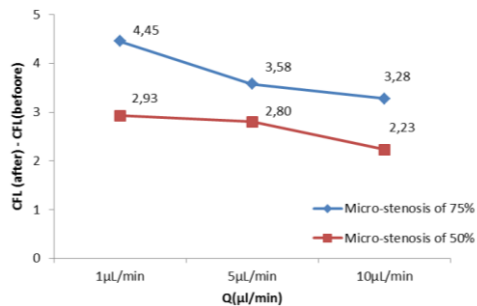


Figure 5. Difference of the CFL thickness after and before for the two geometrie.

Figure 5 represents the difference between the CFL thickness after and before,  $CFL(\text{after})-CFL(\text{before})$ , for the both geometries studied in this work. As seen in the previous figure, the biggest contraction leads to a bigger difference between after and before CFL thickness.

The results suggest that the CFL thickness increases for larger contraction ratio. This way we expect to deeply understand the effect of the constrictions on the CFL thickness and consequently use these results to design and optimize a biochip able to perform in one single channel both cell separation and deformation measurement.

### Acknowledgments

The authors acknowledge the financial support provided by: PTDC/SAU-BEB/108728/2008, PTDC/SAU-BEB/105650/2008, PTDC/EME-MFE/099109/2008 and PTDC/SAU-ENB/116929/2010 from FCT (Science and Technology Foundation), COMPETE, QREN and European Union (FEDER).

### References

1. Caro, C., Pedley, T., Schroter, R. and Seed, W. (1978). Oxford University Press.
2. Lima, R., Ishikawa, T., Imai, Y. and Yamaguchi, T. (2012). In Single and two-Phase Flows on Chemical and Biomedical Engineering, (Dias et al. Eds.), pp. 513-547, Bentham Science.
3. Lima, R., Ishikawa, T., Imai, Y., Takeda, M., Wada, S. and Yamaguchi, T. (2009). *Annals of Biomedical Engineering*. 37, 1546-59.
4. Fujiwara, H., Ishikawa, T., Lima, R., Matsuki, N., Imai, Y., Kaji, H., Nishizawa, M. and Yamaguchi, T. (2009). *Journal of Biomechanics* 42, 838-843.
5. Lima, R., Oliveira, M.S.N., Ishikawa, T., Kaji, H., Tanaka, S., Nishizawa, M. and Yamaguchi, T., (2009) *Biofabrication*, 1, 1-7.
6. Faivre, M., Abkarian, M., Bickraj, K. and Stone, H. (2006). *Biorheology* 43, 147-159.
7. Sollier, E., Cubizolles, M., Fouillet, Y. and Achard, J. (2010). *Biomedical Microdevices*, 12, 485-97.

### Contact Address:

*Diana Pnho (diana@ipb.pt)*

*Department: Mechanical Technology*

*Faculty/School of Engineering: ESTiG*

*University: Polytechnic Institute of Bragança (IPB)*

*Address: Campus de Santa Apolónia - Apartado 134 - 5301-857 Bragança - Portugal*



## **PART VI**

# **Rheometry and Experimental Methods**



## CHAPTER 1

### New trends in Rheology and accesories.

*D. Davila, C. del Rio, C. Gracia-Fernández*

*TA Instruments Spain (Waters Chromatography)*

#### Introduction

The Discovery Hybrid Rheometer (DHR) features powerful new technologies from the world leader in rheological measurements. Our new hybrid technology combines a patented magnetic bearing, drag cup motor, force rebalance transducer (FRT), new patent-pending optical encoder dual-reader, and True Position Sensor (TPS) into a single-head rheometer.

The DHR has improved every performance specification and delivers strain, strain rate, stress control, and normal force accuracy.

#### INNOVATIONS

##### *Optical Encoder Dual-Reader*

All DHR systems feature optical encoders for high resolution displacement measurements. The HR-3 features a patent-pending optical encoder with dual reader. This new technology provides ultra high displacement resolution of two nanoradians, reduces noise, and enhances phase angle measurements. The benefit is better data and higher sensitivity when running challenging materials over a broad range of conditions, or even extreme conditions.

##### *New True Position Sensor (TPS)*

The DHR includes a patent-pending True Position Sensor (TPS) for true gap accuracy. The TPS is a high resolution linear position sensor that ensures the most accurate data, by measuring and compensating for the effects of thermal

## Perspectives in Fundamental and Applied Rheology

expansion, in real time. Unlike competitive devices, the TPS eliminates thermal expansion errors without the need for special high inertia iron core geometries and environmental systems.

The TPS works with all Smart Swap™ geometries and Smart Swap™ environmental systems.

### *Normal Force Rebalance Transducer (FRT):*

The TA Instruments ARES-G2 force rebalance technology has long been the industry standard for normal force measurements. This FRT technology is now part of the Discovery Hybrid Rheometer.

### *Second Generation Magnetic Thrust Bearing:*

The DHR is the only commercial rheometer with a magnetic thrust bearing and our second generation patented design offers improved low torque performance and mapping stability. The low-end torque performance of any rheometer depends on bearing friction which results in residual torques.

### *Interfacial Rheology*

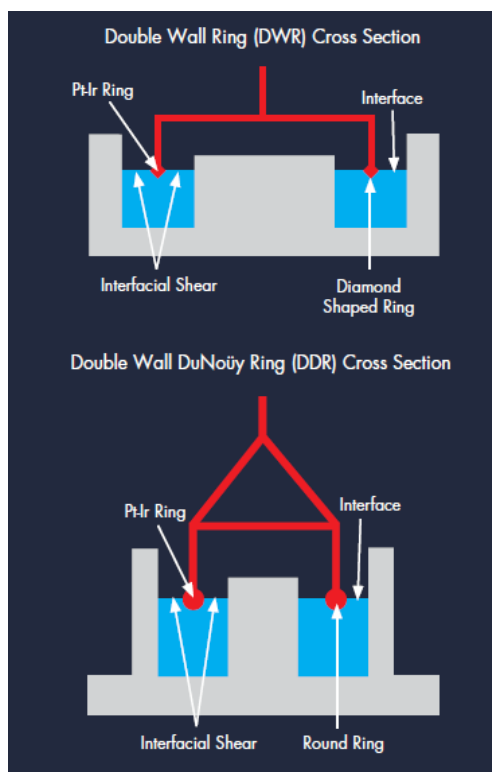
In all TA Instruments interfacial rheology systems, the sample is contained in a Delrin® trough complete with fluid level monitoring windows and injection ports. The measuring rings of the Double Wall Ring (DWR) and Double Wall Du Nouy Ring (DDR) geometries are made of platinum-iridium. These materials are selected for their inert chemistry and ease of cleaning.

TA Instruments is the only supplier offering patented double wall geometry configurations that provide interfacial shear planes on both sides of the geometry surface for higher sensitivity to the monolayer viscoelastic response.

Only the DWR is capable of truly quantitative viscoelastic parameters because the interface is “pinned” to the diamond shaped cross-section of the geometry ring. This patented ultra-low inertia ring(1) has a diameter of 60 mm and was designed for ease-of-use and maximum sensitivity. Surface viscosity measurements can be conducted on surface viscosities as low as  $10^{-5}$  Pa.s.m without complicated sub-phase corrections. And, oscillation measurements are possible over the widest frequency range of any interfacial system. The du Nouy ring geometry of the DDR is an industry standard device used for surface tension measurements. The round cross-section allows for meniscus formation between the interface and geometry,

creating a slight error in the absolute data. With a much smaller diameter of 20 mm, this system is ideal for testing interfacial properties of samples that are available in very limited quantities, such as biological or pharmaceutical materials.

The Bicone is a double conical stainless steel geometry with a sharp edge that reproducibly pins the interface. Because of the large drag created by the surface of the cone submerged within the sub-phase, large corrections are required to obtain quantitative parameters. the geometry's large moment of inertia limits measurement capability to interfacial viscosity in steady shear mode, precluding valuable measurements of quiescent structure and elasticity.



### *Small Angle Light Scattering*

The SALS accessory consists of upper and lower assemblies and quartz plate geometry. The lower assembly includes an integrated Class 2 laser (with 0.95 mW diode and wavelength  $\lambda = 635$  nm) situated below a patented(1) Peltier Plate with a 5 mm diameter quartz window. The Peltier Plate surface is stainless steel with a

## Perspectives in Fundamental and Applied Rheology

temperature range of 5 to 95°C. The upper assembly consists of a set of lenses and a camera. The

scattered light is focused through a lens pair mounted within a height-adjustable cap to focus at varying sample depth. The light is then focused through a second lens and sent through an adjustable polarizer for both polarized and depolarized measurements. Finally, the scattering is collected through a pinhole and recorded by the camera. The upper geometry is a 50 mm diameter, 2 mm thick optical quartz disk. To comply with the single-point correction for the parallel plates, the laser is set at 0.76 times the plate radius which is 19 mm from the axis of rotation of the

plate. This arrangement keeps the SALS system compact, while allowing for quick and reproducible positioning and focusing. A set of neutral density filters is available as an option to reduce laser intensity.

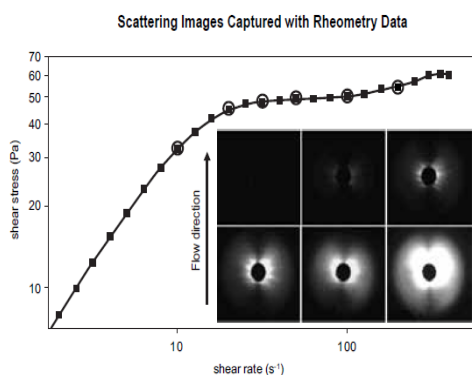


Figure 1. Shear induced structure.

## UV CURING ACCESSORY

UV-curable materials are widely used for coatings, adhesives, and inks. When these materials are exposed to UV radiation, a fast cross-linking reaction occurs, typically within less than a second to a few minutes. Two Smart Swap™ accessories for rheological characterization of these materials are available for the DHR-3 and DHR-2 rheometers. One accessory uses a light guide and reflecting mirror assembly to transfer UV radiation from a high-pressure mercury light source. The second accessory uses self-contained light emitting diodes (LED) arrays to deliver light to the sample. Accessories include 20 mm quartz plate, UV light shield, and nitrogen purge cover. Optional temperature control to a maximum

of 150°C is available using the Electrically Heated Plates (EHP) option. Disposable plates are available for hard UV coatings, which cannot be removed from the plates once cured.

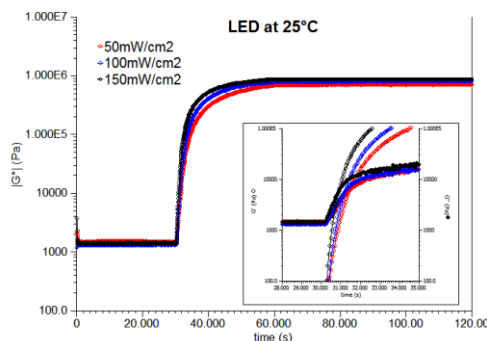


Figure 2 : UV curing at different intensities using the LED accessory.

## Dielectric Accessory

The DETA (Dielectric Thermal Analyzer)

is an accessory which expands the testing capabilities of the ARES strain controlled rheometer to include investigations of the dielectric response of materials. The DHR dielectric accessory uses a material characterization technique similar to dynamic mechanical analysis, except that an oscillating electrical field (AC field) is used (as opposed to a mechanical force [stress]), and the oscillating strain is a stored charge (Q) in the sample. Dielectric analysis is a very powerful technique for characterizing polar materials such as PVC, PVDF, PMMA, and PVA. It is also very powerful for monitoring curing kinetics of materials such as epoxy and urethane systems. The wide range of frequencies available in dielectric analysis (20 Hz to 1 MHz and higher depending on the LCR Meter also extends the measurement range over traditional dynamic mechanical analysis (typically below 100 Hz).

In dielectric analysis, the sample basically behaves like a capacitor. Q is measured as its derivative  $dQ/dt = AC$  current. When the oscillating electric field is applied to a material, random dipoles in the material orient with the field (as shown in figure below). The dielectric accessory measures the degree to which the sample is storing a charge (capacitance) or passing the charge (conductance) through its bulk.

## Perspectives in Fundamental and Applied Rheology

The combination of the Dielectric Accessory with a high-precision DHR rheometer allows for the simultaneous collection of rheological and dielectric information. In addition, dielectric measurements can be run independently of rheological measurements and still benefit from the instrument test platform. This is because dielectric measurements are conducted on a material sandwiched between parallel plates (with some axial force applied to ensure good surface contact) and surrounded by some type of temperature control. Gap temperature compensation keeps the gap constant, allowing for consistent capacitive measurements.

### **Electrorheology**

Electrorheological (ER) fluids are suspensions of extremely fine non-conducting particles in an electrically insulating fluid which show dramatic and reversible rheological changes when an electric field is applied. These changes in apparent viscosity can be up to five decades in magnitude. For example, a typical ER fluid can go from the consistency of a liquid to that of a solid, and back, with response times on the order of milliseconds. The change in rheological properties depends on the applied electric field, i.e. the potential divided by the distance between the plates. Another way to think of the effect is as an electric field dependent shear yield stress. When activated, an ER fluid behaves as a Bingham plastic (a type of viscoelastic material), with a yield point that is determined by the electric field strength. After the yield point is reached, the incremental shear stress is proportional to the rate of shear (in a “Newtonian fluid” there is no yield point and stress is directly proportional to shear). Hence, the resistance to motion of the fluid can be controlled by adjusting the applied electric field. ER fluids were discovered around 1940, and today we can see significant improvements in performance and reliability of these materials. Additionally, we see a great deal of interest in characterizing ER fluids, as they have found more potential applications (damping devices, clutches, braking devices, actuators, optical devices, and polishing devices, to name a few).

*Contact Address:*

*C. Gracia-Fernández (cgracia@tainstruments.com)*

*Department,: Rheology Application support*

*Telf.,Fax: 902 254 254*

## CHAPTER 2

# Blood flow in microchannels manufactured by a low cost technique: xurography

*Elmano Pinto<sup>1,2</sup>, Bruna Taboada<sup>1,2</sup>, Vera Faustino<sup>1,2</sup>, Diana Cidre<sup>1</sup>, Raquel Rodrigues<sup>1</sup>, João Miranda<sup>2</sup>, Valdemar Garcia<sup>1</sup>, Ricardo Dias<sup>1,2</sup>, Rui Lima<sup>1,2</sup>.*

*<sup>1</sup> Mechanical Technology, ESTiG, Polytechnic Institute of Bragança (IPB), Portugal.*

*<sup>2</sup> Department of Chemistry, CEFT, Faculdade de Engenharia da Universidade do Porto (FEUP), Portugal.*

### Introduction

The xurography is a technique that has been used to make molds to produce microchannels. In contrast to soft lithography [1, 2], xurography uses equipments and materials commonly used in the printing industry, such as cutting plotters, vinyl and other materials. The main advantage of this technique is to fabricate microchannels at a reduced cost [3, 4].

The Fahraeus-Lindqvist effect is a well know phenomenon that happens in microcirculation, where red blood cells (RBCs) have tendency to migrate toward the centre of the microtube resulting in a marginal cell-free layer (CFL) at regions adjacent to the wall [5]. Recently several studies showed strong evidence that the formation of the CFL is affected by the geometry of the microchannel [1, 6, 7] and the physiological conditions of the working fluid, such as the hematocrit (Hct) [2, 8].

The main objective of the present work is to fabricate polydimethylsiloxane (PDMS) microchannels by using a soft xurography technique to perform blood flow studies. Additionally, a high-speed video microscopy system is used to measure the CFL thickness in two different geometries, i. e., bifurcations and confluences.

### Experimental

Microchannels were initially developed with a CAD software, the geometries were selected taking into account a previous study about the blood flowing through microchannels with bifurcations and confluences fabricated by a soft lithography technique [9]. The parent microchannel has 500  $\mu\text{m}$  in width and the two branches of the bifurcation and confluence corresponds to 50% of the width of parent channel [3]. Figure 1 shows the geometry and dimensions used in this study.

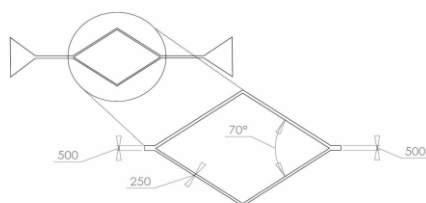


Figure 1. Schematic diagram of the geometry with the main channel of 500  $\mu\text{m}$  and 250  $\mu\text{m}$  ramifications.

This geometry was used to fabricate the molds by using a cutting plotter Jaguar II and vinyl HEXIS. The mold was used for the production of PDMS microchannels. The PDMS was obtained by mixing curing agent (10:1 ratio) with PDMS deposited in the mold. The glass side was prepared with PDMS (20:1 ratio) and dispersed by means of a spin coater. The PDMS was cured in an oven at 80 °C for 20 minutes. Then by using a blade the microchannels were cut off and the inlet/outlet holes of the fluid were done by using a fluid dispensing tip. Finally, to have a strong adhesion of the materials, the device was placed in the oven at 80 °C for 24 hours.

The fabricated microchannels were used to study blood flow with a hematocrit (Hct) of 5% and different flow rates. The suspending fluid was a dextran 40 solution and the flow rates tested were 5 and 15 ml/min.

The blood samples were taken from a healthy ovine and were washed twice with physiological saline using a centrifuge at a speed of 2000 rpm for 15 min at 4 °C. After washing, a separate test tube with 25  $\mu\text{l}$  of RBCs was added to dextran 40 until fill a 5 ml sample.

We used a syringe pump (*Harvard Apparatus PHD ULTRA™*) to control the flow of the fluids. To visualize and measure the flow we have used an inverted microscope (*IX71, Olympus*) combined with a high speed camera (*i-SPEED LT*). Figure 2 shows the experimental apparatus used to control the flow and to visualize the flow in microchannels.

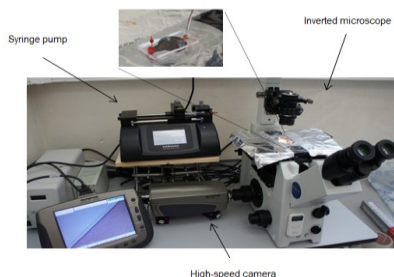
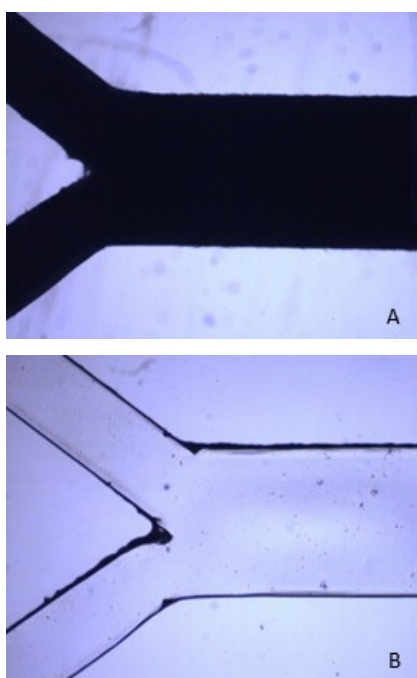


Figure 2. Experimental apparatus to control and visualize the flow in microchannels produced by xurography.

A manual tracking plugin (MTrackJ), of the image analysis software Image J, was used to track individual RBC flowing around the boundary of the RBCs core. By using MTrackJ plugin, the centroid of the selected RBC was automatically computed [6]. After obtaining x and y coordinates, the data were exported for the determination of each individual RBC trajectory and consequently the CFL thickness [7].

## Results and Discussion

Figure 3 shows the vinyl mold master and the correspondent PDMS microchannel.



*Figure 3. Images obtained using an inverted microscope with a 4x objective lens: A - The vinyl mold master fabricated by a cutting plotter; B - PDMS microchannel of the confluence.*

Overall, by using our cutting plotter it was possible to obtain good enough quality master molds and correspondent PDMS microchannels to study blood flow phenomena at microscale level. However, detailed analysis of the geometries has shown that the quality of the microchannel tend to decreases as it size decreases. This is mainly related to the limitation of our cutting plotter to cut precisely geometries with dimensions smaller than 500  $\mu\text{m}$  [3].

## Perspectives in Fundamental and Applied Rheology

To evaluate the geometrical quality of the mold masters and correspondent microchannels several microscopic images were obtained along the device. Figure 4 shows a schematic representation of the sections where the microscopic images were taken.

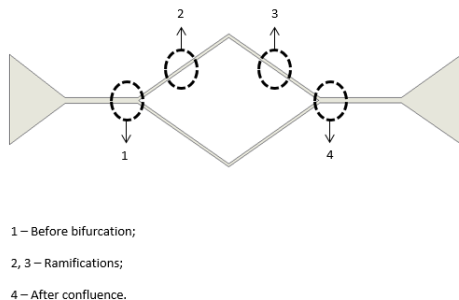


Figure 4. Schematic representation of the microchannel geometry and location of the sections where the images were collected to evaluate the geometrical quality.

Figure 5 shows the width measurements of both mold masters and PDMS replica with microchannels.

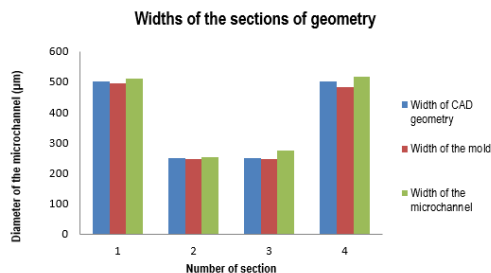


Figure 5. Comparison between the theoretical values obtained from AutoCAD, vinyl master molds and PDMS replica.

The mold masters and the microchannels have dimensions close to the theoretical values. Detailed microscopic visualizations have shown that the decrease in the size of the geometry resulted in an increase in the percentage error in the manufacturing process of the master molds.

Throughout the experimental tests performed with different flow rates we found that in the zone around the branching the CFL thickness was independent of the flow rate. Therefore, we have decided to analyse the variation of the CFL preferably in the area before bifurcation and immediately after the confluence (Figures 6 and 7 respectively).

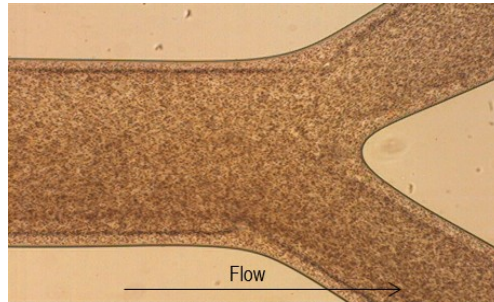


Figure 6. Blood flowing around the bifurcation with 5% Hct and a flow rate of 10  $\mu\text{l}/\text{min}$ .

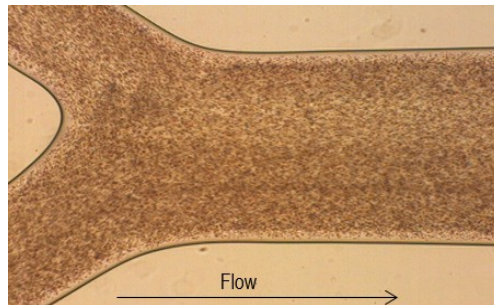


Figure 7. Blood flowing around the confluence with 5% Hct and a flow rate of 10  $\mu\text{l}/\text{min}$ .

In the zone after the confluence, the CFL thickness is slightly bigger when compared with the other sections of the microchannel. In Figure 7 is possible to observe the CFL thickness through the full length of the microchannel. Our preliminary results indicate a slight increase of the CFL downstream the confluence.

The quality of the images and the analysis methodology may have caused the observed variations. Detailed studies are currently under way and will be published in due time.

Our results corroborate the work of Leble et al [9], that found a formation of a CFL in the region of the confluence apex. This phenomenon was observed in a microchannel three times smaller than the one used in the current study as they used a soft lithography technique to fabricate the microchannels. However, at higher dimensions the current work has shown evidence of a CFL around the apex of the confluence. Hence, by using xurography it is also possible to study several blood flow phenomena happening in microcirculation.

## Acknowledgments

The authors acknowledge the financial support provided by: PTDC/SAU-BEB/108728/2008, PTDC/SAU-BEB/105650/2008, PTDC/EME-MFE/099109/2008 and PTDC/SAU-ENB/116929/2010 from FCT (Science and Technology Foundation), COMPETE, QREN and European Union (FEDER).

## References

1. Lima, R., Wada, S., Tanaka S., Takeda M., et al. *Biomedical Microdevices*, vol.10(2), pp.153-167, 2008.
2. Garcia V., Dias R., Lima R.. *InTech* vol.17, pp. 394-416, 2012.
3. Pinto, E., Pinho, D., Bento, D., et al. 5th Portuguese Congress on Biomechanics, pp. 301-306, 2013
4. Gojo, R., Morimoto, Y., Takeuchi, S. International Conference on Miniaturized Systems for Chemistry and Life Sciences. October, 2008, San Diego, California, USA.
5. Caro, C., Pedley, T., Schroter R., Seed, W.. *The mechanics of the circulation*, Cambridge University Press, 1978.
6. Pinho, D.. Master Thesis in Biomedical Technology, Polytechnic Institute of Bragança, Portugal, 2011.
7. Lima, R., Ishikawa, T., Imai, Y., et al. *Journal of Biomechanics* 41, pp. 2188-2197, 2008.
8. Fujiwara, H., Ishikawa, T., Lima, R., et al. *Journal of Biomechanics* 42, pp. 838-843, 2009.
9. Leble, V., Lima, R., Dias, R., et al. *Biomicrofluidics* 5, 044120, 2011.

## Contact Address:

*Elmano Pinto (elmano@ipb.pt)*

*Department: Mechanical Technology*

*Faculty/School of Engineering: ESTiG*

*University: Polytechnic Institute of Bragança (IPB)*

*Address: Campus de Santa Apolónia - Apartado 134 - 5301-857 Bragança - Portugal*

## CHAPTER 3

# Synthesis and rheological characterization of magnetic fluids: influence of the stabilizer agents

*L. Irazu<sup>1</sup>, J. Berasategui<sup>1</sup>, M.J. Elejabarrieta<sup>1</sup>, M.M. Bou-Ali<sup>1</sup>, M. Moral<sup>2</sup>, I. Alejandre<sup>3</sup>, M. T. López-López<sup>2</sup>, J.D.G. Durán<sup>2</sup>*

*<sup>1</sup> Mechanical and Industrial Production Department, Mondragon Unibertsitatea (Spain).*

*<sup>2</sup> Department of Applied Physics, Faculty of Sciences, Campus de Fuentenueva, University of Granada (Spain)*

*<sup>3</sup> Fagor Hometek, Mondragón (Spain)*

### Introduction

Magnetorheological fluids (MRF) are suspensions of micron size ferro- or ferrimagnetic particles dispersed in a carrier fluid which can be aqueous or not [1]. These particles due to their size have a magnetic multidomain. When an external magnetic field is applied the dipole moments are oriented in the field direction and sense and the particle acquires a net dipole moment different from zero. As a consequence the particles are aligned forming chains which generate a change in the rheological properties of the fluid [2], making it an intelligent material with a growing industrial interest.

One of the biggest issues of these fluids is the sedimentation of the magnetic particles. Due to this phase separation the fluid behavior is unpredictable and therefore is not useful for any application. The improvement in the MRF stability by using additives broadens both the operating conditions of the fluid, as the potential industrial applications.

In this study has been synthesized and characterized different magnetorheological fluids. The aim of this work is to analyze the influence of different stabilizing additives on the sedimentation of MRF and on the rheological effect using viscometry tests at different magnetic fields and temperatures.

### Experimental techniques

The characterization of the MRFs has been carried out by sedimentation tests and a magnetorheological analysis based on viscometry tests at different magnetic fields and temperatures [3].

The sedimentation tests involve the time evolution of the suspensions of each fluid, measuring the height of the sediment,  $h_s$ , and the total height of the fluid,  $h_0$ , at set times, Figure 1.

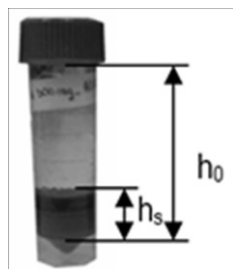


Figure 1. Total height,  $h_0$ , and the height of the sediment,  $h_s$ .

For the magnetorheological characterization a rotational rheometer of stress control Anton Paar Physica MRC-501 has been used. The MRFs have been characterized at different magnetic fields in the MRD-70/1T cell using the configuration of parallel plates of 20mm (PP20-MRD). In order to measure the magnetic field applied to the sample gaussmeter GH-55 has been used. The two temperatures at which the samples have been analyzed, 25°C and 60°C, have remained constant through a water bath Julabo F25. All formulations have been characterized following the same procedure. Viscometry results have been obtained by applying a logarithmic ramp of speed in 80 points for 3s.

In the magnetorheological characterization to convert the mechanical parameters, moment and rotational speed, to rheological parameters, stress and strain rate, the conversion of Rabinowitsch [4-6] has been applied. The yield stress values have been obtained according to Bingham model [3].

### Synthesis and formulation of MRF

In all the formulations the same mineral oil as carrier liquid, solid phase and surfactant, both in type and concentration have been used. The mineral oil is from Repsol YPF. The spherical magnetic particles, CIP (Carbonyl Iron Powder) have been provided by BASF and the concentration of it in the MRFs is 10% in volume, which is 3.825 g. The surfactant used has been the aluminium stearate (AlSt) and

the MRFs contain 0.025 g of it [7]. As stabilizing additives Lubrizol ® 3702, Clay and PMMA have been used, [8-10].

To formulate all the MRFs the same synthesis procedure has been followed and mechanical and ultrasonic agitations have been combined.

In Table 1, the different components used to formulate the MRFs analyzed in this study and their geometrical and physical properties at 25°C can be seen.

Table 1. Geometric and physical properties at 25°C of the components of the MRFs.

		Size [ $\mu\text{m}$ ]	Density [ $\text{g}/\text{cm}^3$ ]	Viscosity [ $\text{mPa}\cdot\text{s}$ ]
Carrier liquid	Mineral Oil	--	$0.845 \pm 0.017$	$13.8 \pm 1.4$
Magnetic particles	CIP	Diameter $1.28 \pm 0.54$	7.65	--
Surfactant	AlSt	--	0.25	--
Additives	Lubrizol ® 3702	--	$0.954 \pm 0.022$	$4510 \pm 345$
	Clay	Diameter $8.0 \pm 3.3$ Thickness [11]: $0.12 \pm 0.06$	0.416	--
	PMMA	6	1.18	--

Table 2. Mass of the components of MRFs.

	Carrier Liquid ( $\pm 0.001$ g)	Additives ( $\pm 0.001$ g)		
	Mineral oil	Lubrizol	Clay	PMMA
<b>MRF_LZ</b>	3.422	0.645	--	--
<b>MRF_Clay_10g/l</b>	3.8025	--	0.050	--
<b>MRF_Clay_40g/l</b>	3.570	--	0.200	--
<b>MRF_PMMA_1.5g</b>	2.729	--	--	1.500
<b>MRF_PMMA_2g</b>	2.370	--	--	2.000

As a summary, Table 2 shows the mass of the magnetorheological fluids synthesized in this work. The nomenclature used is the following: MRF refers to magnetorheological fluid and then it is mentioned the type and concentration of the additive used.

**Results**

For applications of MRFs interest the fluid to present good stability, with a slow sedimentation and easy re-dispersion, and high magnetorheological effect.

In order to analyze the stability of the fluid, the sedimentation velocity and the existence of aggregates depending on the type and amount of stabilizing additive used have been observed.

In Figure 2, as a summary, the sedimentation curves of the most stable fluids of each formulation can be seen.

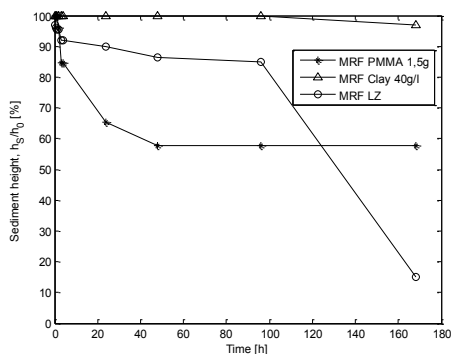


Figure 2. Sedimentation comparative of fluids containing Clay, PMMA and Lubrizol.

The MRF with PMMA deposits first and moreover the elevated height of the sediment indicates that aggregates are generated. Comparing the fluid containing Clay and Lubrizol can be seen that the fluid formulated with Clay is the one which presents the best stability.

The viscometry tests without applying a magnetic field at 25°C and 60°C have been done. The fluid MRF\_Clay\_10g/l presents the lowest viscosity, therefore is the most appropriate one to obtain high magnetorheological effect.

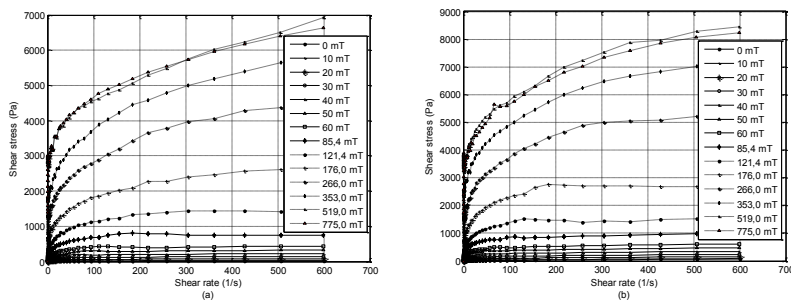


Figure 3. Rheograms of (a) MRF\_Clay\_10g/l and (b) MRF\_Clay\_40g/l MRF for magnetic field between 0 and 775mT at 25 °C.

In Figure 3 and in Figure 4, the rheograms of the MRFs containing Clay at different magnetic fields and at 25°C and 60°C can be seen.

Increasing the temperature the yield stresses decrease for the two concentrations of clay. This tendency is more remarkable for the 40g/l concentration of clay. Moreover, it can be seen that the concentration of clay at high strain rate affects more at low temperatures than at high temperatures and the MRF\_Clay\_40g/l is the formulation that presents the maximum stress at the most intense magnetic field.

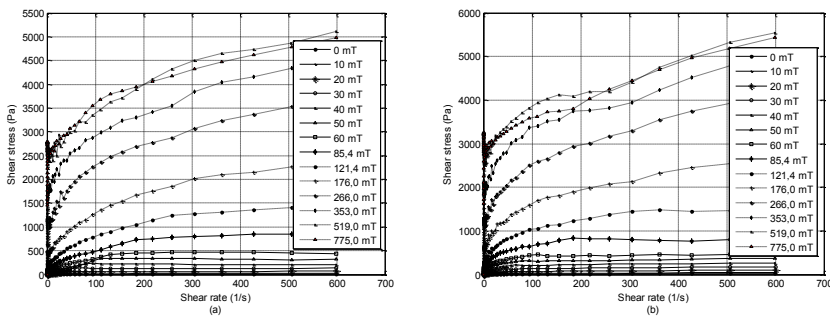


Figure 4. Rheograms of (a) MRF\_Clay\_10g/l and (b) MRF\_Clay\_40g/l MRF for magnetic field between 0 and 775mT at 60°C.

In Figure 5 the yield stresses at different magnetic field for the fluids containing PMMA and Lubrizol at 25°C and 60°C can be seen [8].

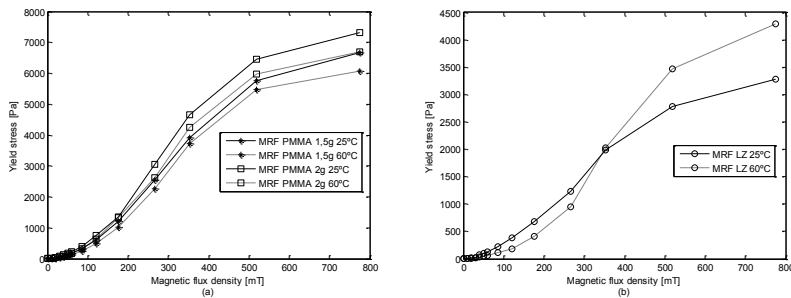


Figure 5. Yield stresses of MRFs containing (a) PMMA and (b) Lubrizol at 25° and 60°C.

The yield stresses increase with PMMA concentration and decrease with the temperature for all the magnetic fields, Figure 5 (a). In the MRFs containing Lubrizol, Figure 5 (b), increasing the temperature the yield stresses increase for bigger magnetic fields than 350mT.

### Conclusions

The sedimentation tests show that fluids containing PMMA deposit faster than those containing Clay or Lubrizol. From the sedimentation point of view the most appropriate formulation is MRF\_Clay\_40g/l.

In the viscometry tests it has been observed that the formulations containing PMMA are the ones with the highest yield stresses, but, they present an unstable behavior. Comparing the formulations containing Clay and Lubrizol is seen that the ones containing Clay have higher yield stresses at 25°C, but, are more sensitive to temperature increase.

Therefore, taking into account the results obtained in sedimentation tests and viscometry tests to work at 25°C the fluid MRF\_Clay\_40g/l is the most appropriate one, because, at this temperature presents higher yield stress than the MRF containing Lubrizol.

In applications in which the fluid works at higher temperatures, equilibrium between sedimentation and yield stress has to be found. At elevated temperatures the fluid with Lubrizol presents higher yield stresses.

### Acknowledgement

The present study has been partially supported by ACTIMAT project, UE2013-09, MAGNETO (INNFACTO-020000-2010-006) and AVISUINT (DPI 2012-36366) projects.

### References

1. Galindo González, C. (2008). *Tesis doctoral, Universidad de Granada*, pp. 9-11.
2. Bossis, G., Lacis, S., Meuniera, A., Volkovaa, O. (2002). *Journal of Magnetism and Magnetic Materials* 252, pp. 224–228.
3. Zubieta, M., Elejabarrieta, M. J., Bou-Ali, M. M. (2009). *Smart materials and structures*, Vol. 18, pp. 1-6.
4. *Deutsches Institute für Normung* (1976). DIN 53 018-1.
5. Zubieta, M., Elejabarrieta, M. J., Bou-Ali, M. M. (2009). *Rheol Acta*, Vol 48, pp. 89-95.
6. Soskey, P.R., Winter, H.H. (1984). *J. Rheol* Vol. 28, pp. 625-645.
7. López-López, M.T., Zugaldia, A., Gómez-Ramirez, A., González-Caballero, F., Durán, J.D.G. (2008). *Journal of Rheology*, Vol. 52, n 4, pp 901-912.
8. Duran, J.D.G., González-Caballero, F., Delgado- Mora, A.V., Ramón-Iglesias, G., López-López, M.T., Jiménez-Olivares, M.L., Fernández, L., Insa, J., Romero, E. (2008). *Patente Española ES 2 301 390 A1*.

## Part VI: Rheometry and Experimental Methods

9. Hato, M.J., Hyoung Jin Choi, Hyung Hoon Sim, Byung Oh Park, Ray, S.S. (2011). *Colloids and Surfaces A: Physicochemical and Engineering Aspects*, Vol. 377, pp.103-109.
10. Jae Lim You (2008). *IEEE Transactions on Magnetics*, Vol. 44, pp. 3867--3870.
11. Gómez Ramirez, A.M. (2011). *Tesis doctoral, Universidad de Granada*, pp. 21.

### Contact Address:

Leire Irazu (leireirazu@msn.com)  
Mechanical and Industrial Production Department,  
Mondragon Goi Eskola Politeknikoa  
Mondragon Unibertsitatea  
Loramendi 4, 20500 Mondragón  
Telf.: 943794700; Fax: 943791536



## CHAPTER 4

# Assessment of wall-depletion phenomena in dilute multiple emulsions

M.C. García<sup>1</sup>, J. Muñoz<sup>1</sup>, M.C. Alfaro<sup>1</sup>, J.M. Franco<sup>2</sup>

<sup>1</sup> Departamento de Ingeniería Química, Facultad de Química, Universidad de Sevilla (Spain).

<sup>2</sup> Departamento de Ingeniería Química, Facultad de Ciencias Experimentales. Universidad de Huelva (Spain).

### Introduction

The occurrence of wall slip poses dramatic problems when conducting some rheological experiments. Different materials such as microgel dispersions, emulsions, foams and suspensions are prone to undergo wall-depletion phenomena under shear. This is due to the occurrence of a significant velocity gradient in a thin layer of lower viscosity adjacent to the surface of sensor systems and pipes. In other words, wall-depletion phenomena take place during the flow of multiphase systems due to the displacement of the disperse phase away from solid boundaries [1]. This fact results in a thin liquid film of continuous phase in contact with the wall of the measuring geometry, which is responsible for underestimated bulk viscosity values [2]. In order to reduce slip, the use of sensor systems with modified surfaces is becoming more and more popular.

This phenomenon has been previously studied for concentrated emulsions and it has been reported that the wall slip effects depend on the type of emulsions and composition. Thus, wall slip is more important in emulsions which have large droplets or are weakly flocculated and flocs behave as individual large droplets under action of gravity [3].

The occurrence of slippage is currently checked by comparing non-linear shear flow results obtained at different gap sizes in parallel plate and coaxial cylinder geometries [1]. In addition slip may be detected by comparing the shear flow results obtained with cone & plate geometries of different angles. Goshawk et al [4] and Citerne et al [5] suggested that slip effects can influence the mechanical spectra of concentrated emulsions. However, their conclusion was not clearly supported by results reported.

The goal of this work was to assess the possible occurrence of wall-depletion phenomena in dilute multiple emulsions.

Dilute emulsions are currently associated to a disperse volume fraction below 0.2. The rheology of dilute emulsions must be essentially governed by droplet-continuous phase hydrodynamics. This means, droplet-droplet interactions must be negligible.

Multiple emulsions like W/O/W consist of aqueous dispersions of oil globules which, in turn, contain smaller aqueous droplets.

Generally, two surfactants of opposite solubility are needed to prepare multiple emulsions. While an oil-soluble emulsifier (HLB < 10) is required to form the interface surrounding the inner water droplets, a water soluble emulsifier (HLB > 10) must be adsorbed onto the oil interface [6]. The lipophilic and hydrophilic surfactants must be dissolved into the organic and aqueous continuous phase, respectively.

Block copolymers can find interesting applications in the formulation of emulsions since they can simultaneously play the roles of emulsifier and stabilizer. This is due to their ability to decrease the interfacial tension as well as to their high molecular weight.

### Experimental Methods

The organic phase used (15 wt%) was 2-ethylhexyl lactate, a green solvent kindly supplied by BASF. Its density (20°C) is 940 Kg/m<sup>3</sup>, its melting point is -23°C and its boiling point is around 246°C.

Two amphiphilic copolymers manufactured by Croda were used as emulsifiers. Atlas G-5000™ is a hydrophilic AB block copolymer of HLB 16.9, whose hydrophobic chains, pHSAs (A = poly 12-hydroxystearic acid) act as anchoring groups into the organic phase and the central hydrophilic chain, PEG (B = polyethylene glycol) provides stability to the external aqueous phase. The other copolymer used was Atlox 4912™ (HLB 5.5). It is an ABA block copolymer based on poly 12-hydroxystearic acid and PEG. Both surfactants were kindly supplied by Comercial Química Massó. The concentration of copolymers used was 1.5 wt %.

In addition, a MD10 defoaming agent (Dow Corning) was used.

Emulsions were prepared by a primary homogenization step with an Ultraturrax T-50/G45F rotor-stator device, followed by a high-pressure homogenization step (secondary homogenization) based on microchannel emulsification (Microfluidizer® M110L). ECH(1)15-1.5-1.5 stands for the final emulsion.

The possible occurrence of wall-depletion phenomena when determining the flow properties of emulsion ECH(1)15-1.5-1.5 was assessed by comparing the results obtained with several geometries and rheometers. Two controlled-stress rheometers; namely a Haake-MARS (Thermo) and a Physica MCR-501 (Anton Paar) and one controlled-strain ARES (TA-Instruments) rheometer were used.

Results provided by several conventional geometries with surfaces of different nature (smooth, serrated, sandblasted) and mixing geometries were obtained. In addition a Hoesppler viscometer was also used for further comparison of viscosity values.

Transmitted light and phase contrast optical microscopies (Axio Scope A1, Carl Zeiss with a 63X objective) were used to gain a deeper insight into emulsion's microstructure. Droplet size distribution (DSD) measurements were carried out by laser diffraction with a Mastersizer Hydro2000 MU (Malvern).

### Results and Discussion

The emulsion studied exhibited Newtonian behaviour at 25°C, regardless of the rheometer, geometry or surface characteristics of sensor systems used. Table 1 shows the different viscosity values determined for the emulsion ECH(1)15-1.5-1.5 at 25°C. The viscosity values obtained in the University of Huelva with the Physica MCR-501 using a serrated-surface and a smooth-surface coaxial cylinder and those calculated from flow curves ran with the ARES were not significantly different to each other. With regards to results obtained in the University of Seville, we must emphasize that the values of viscosity obtained with the MARS rheometer when high surface coaxial cylinders were used turned out to be quite similar, regardless of their surface characteristics. This can be checked by comparing the results obtained with the Z38 and Z40 coaxial cylinders. The former has a serrated surface, while the latter has a smooth one. In addition these values were not significantly different to that calculated from a falling ball Hoesppler viscometer.

All results analysed so far support that slip effects in the dilute W/O/W emulsion studied were not significant.

The slight differences (around 10%) observed between the average viscosity values calculated with the facilities of the Universities of Huelva and Seville (2.11 vs 2.56) point to differences between the temperature-control systems used in the two laboratories involved in this project.

A further point to discuss is the higher values provided by the double helix-shaped mixing geometry used with the ARES and the sandblasted Z20 coaxial cylinder used with the MARS. These results may be ascribed to their relatively low measuring surface, which challenged their accuracy for the low viscosity of the emulsion studied.

The low viscosity shown by the multiple emulsion studied in this research may be ascribed to a) its low oil content and b) its DSD. The facts that the emulsion studied can be classified as a dilute one and that the concentration of copolymers was not great enough to form a concentrated micellar system in the continuous phase were responsible for the limited increase in viscosity if compared with the continuous phase.

Table 1. Values of viscosity as a function of geometry, surface characteristics and rheometers used.  $T = 25^{\circ}\text{C}$ .

Measuring set-up	$\eta$ (mPa·s)	Standard deviation
Smooth cylinder, Physica MCR-501	2.06	0.01
Serrated cylinder, Physica MCR-501	2.10	0.03
Smooth cylinder, ARES	2.16	0.05
Mixing geometric, ARES	3.15	0.13
Sandblasted cylinder Z20, MARS	2.70	0.01
Serrated cylinder Z38, MARS	2.54	0.04
Smooth cylinder Z40, MARS	2.58	0.03
Hoeppler viscometer	2.55	0.01

Thus, the concentration gradient throughout the thin lubricating layer formed by the measuring surface must be rather low. This may prevent significant wall depletion phenomena from occurring.

Figure 1 illustrates the DSD of emulsion ECH(1)15-1.5-1.5 and the values of the mean  $d_{4,3}$ ;  $d_{3,2}$  diameters and span are shown in the inset.

The volumetric DSD obtained was clearly multimodal. The higher volume fraction of droplet diameter did not enhance the emulsion viscosity since their contribution to the specific surface was rather low. The first peak of the DSD did correspond to a droplet size as low as 550nm and its height was similar to that of the second peak, which was located around 5.75  $\mu\text{m}$ . This is a clear indication of the great number of submicron droplets formed. If the volumetric DSD were re-plotted as a function of the droplet number percentage, it could be observed that 18% of submicron droplets were obtained. The droplet number percentage corresponding to higher diameters was negligible in practice.

These results were supported by optical microscopy micrographs, which were consistent with the lack of either significant droplet-droplet interactions or jamming effects. In addition they demonstrated these emulsions could be described as multiple.

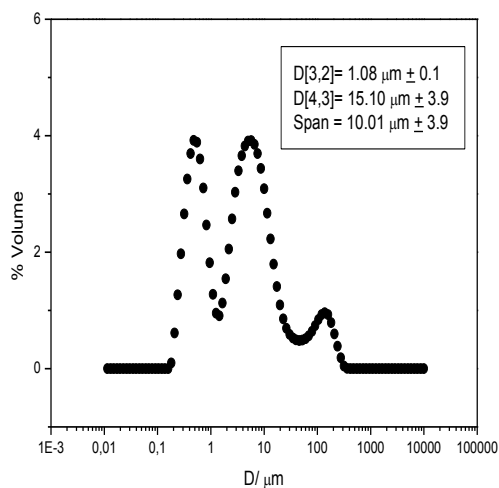


Figure 1. Droplet size distribution of 15 wt% emulsion ECH(1)15-1.5-1.5 (●) Temperature: 20°C

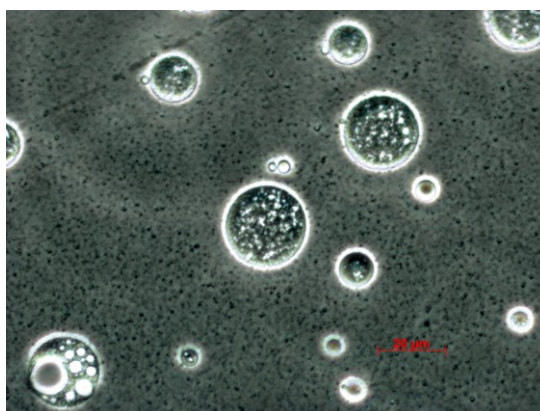


Figure 2. Micrograph of emulsion ECH(1)15-1.5-1.5 obtained by optical microscopy.

### Concluding remarks

We can conclude that the dilute multiple emulsion studied exhibited a polydisperse droplet size distribution, Newtonian behaviour and the lack of slip effects under shear.

### Acknowledgements

The financial support received (Project CTQ2011-27371) from the Spanish MINECO and from the European Commission (FEDER Programme) is kindly acknowledged. Dr. García is also grateful to MINECO for awarding her a fellowship during her stay at the University of Huelva.

### References

1. Barnes, H. A., *J. Non-Newtonian Fluid Mech.* 56, (1995) 221.
2. Yoshimura, A. S., and Proud'Homme, R. K. *Journal of Rheology*, 32 (1988) 575-584.
3. Franco, J.M., Gallegos, C., and Barnes, H.A., *J. Food Eng.* 36 (1998) 89-102.
4. Goshawk, J.A., Binding, D.M., Kell, D.S., Goodacre, R. *J. Rheol.* (1998) 42, 1537-1553.
5. Citerne, G.P., Carreaur, P. J., Moan, M., *Rheol Acta*, 40 (2001) 86-96.
6. Pays, K., Giermanska-Kahn, J., Pouligny, B., Bibette, J., Leal-Calderon, F. *Journal of Controlled Release* 79 (2002) 193–205.

### Contact Address:

*J. Muñoz (jmunoz@us.es)*

*Dpto. Ingeniería Química, Facultad de Química, Universidad de Sevilla,*

*C/ P. García González s/n, 41012, Sevilla (Spain)*

*Tel.:+34 954 557179 // Fax:+34 954 556447.*

## CHAPTER 5

# Simultaneous Rheometry and FT-IR Spectroscopy or Polarization Light Microscopy

*Fabian Meyer and Fritz Soergel*

*Thermo Fisher Scientific, Karlsruhe, Germany*

### Introduction

In polymers e.g. the stretching of macromolecules under shear, cross-linking kinetics [1] as well as crystallization and melting of crystals [2] are of interest. Emulsions and microemulsions play an important role in pharmaceutical, cosmetics and many other areas. During the emulsification process it is desired to achieve a defined droplet size distribution. In the further processing of emulsions as well as in their application, the material is subject to mechanical stresses, which can lead to breaking [3] or coalescence (Figure 3) and other unwanted effects causing a change in morphology and particle size distribution. Furthermore, the stability achieved by proper formulation and processing, can be negatively affected by inappropriate storage conditions. Using a technique that simulates and measures the effects of all these influences, enables designers and manufactures to optimize formulations and processing as well as product performance.

### Experimental

For a deeper understanding of structure-properties relationships, usually more than one analytical technique is required. However, when samples are tested on two separate analytical instruments, the comparability and reproducibility of the results have certain limitations. Only when exactly the same material is subject to a simultaneous investigation, these limitations can be overcome.

Rheometry delivers an integral mechanical response of the investigated sample (bulk properties) under stress or deformation. The mechanical properties, however, are directly related to the molecular structure and its changes [4]. Combining rheometry with other analytical techniques allows for a comprehensive investigation and provides a more complete picture of the sample characteristics.

## Perspectives in Fundamental and Applied Rheology

The comparability of all data sets is guaranteed and reproducibility is improved. Efficiency is higher, sample consumption and lab space requirements are minimized.

Finding the right complementary technique is a key factor for maximizing the information gained. Optical as well as spectroscopic methods provide structural information beyond the dynamic-mechanical response and are therefore predestinated for simultaneous application with rheometry.

### Simultaneous Rheometry and FT-IR Spectroscopy

When combining Rheometry with FT-IT spectroscopy, the rheometer can be used on the one hand to provide well-defined stress, deformation and temperature profiles - the simultaneously recorded spectra then reveal the induced molecular changes, e.g. stretching, orientation or shear-induced breaking of emulsions [3]. On the other hand, physical and chemical processes like formation of hydrogen bridge bonds, UV-induced or chemical cross-linking or curing reactions can be investigated. The area under the relevant peaks in the FT-IT spectra can be determined and plotted together with the simultaneously acquired rheological data as a function of time or temperature, revealing for example the reaction kinetics [1].

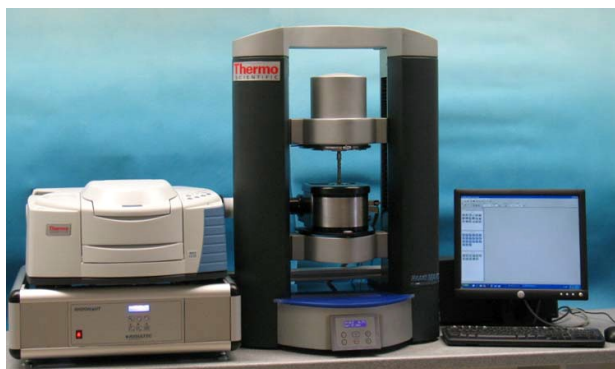


*Figure 1. Setup for simultaneous Rheometry and FT-IR Spectroscopy with Thermo Scientific Nicolet iS10 FT-IR Spectrometer and HAAKE MARS Rheometer with Rheonaut module*

The Rheonaut module (Resultec analytic equipment, Illerkirchberg, Germany) is an accessory for the HAAKE MARS rheometer combining rheometry with FT-IR spectroscopy. The module comprises components for IR spectroscopy as well as for temperature control (0 to 100 °C or ambient to 400 °C). The complete setup is shown in Figure 1 including a standard FT-IR spectrometer with side port.

The stationary plate of the rheometer features a monolithic diamond element that serves as the ATR (attenuated total reflection) probe, offering a single internal reflection. It has an excellent inertness to chemicals and abrasion. Compared to standard infrared transmission spectroscopy or specular reflection spectroscopy

techniques, the sample thickness can thus be adjusted to the rheological needs and is independent of the IR requirements.

Rheological data and IR spectra are fully correlated and thus allow for simultaneous investigation of changes on the molecular level and the mechanical bulk properties [1, 3].

### Simultaneous Rheometry and Light Microscopy

The combination of rheometry with light microscopy (with or without polarization filters), allows to study not only the change of a material's structure and properties under shear deformation (e.g. emulsification, coagulation, aggregation and disaggregation) but furthermore temperature dependent changes like crystallization [2, 4]. Particle size and particle size distribution can be determined – even at high shear rates (up to 45,000 1/s) using a stroboscope instead of a cold light source. For emulsions with low optical contrast, the quality of the images can be improved by introducing a half circle diaphragm in the lighting tube [5].

The HAAKE RheoScope module is a compact accessory for the HAAKE MARS rheometer, integrating an optical microscope, a video camera and a temperature control unit (-5 °C to 300 °C). The combination of the HAAKE MARS and the HAAKE RheoScope module enables the operator to measure the rheological properties and to observe and record the microscopic structure of the tested sample simultaneously.

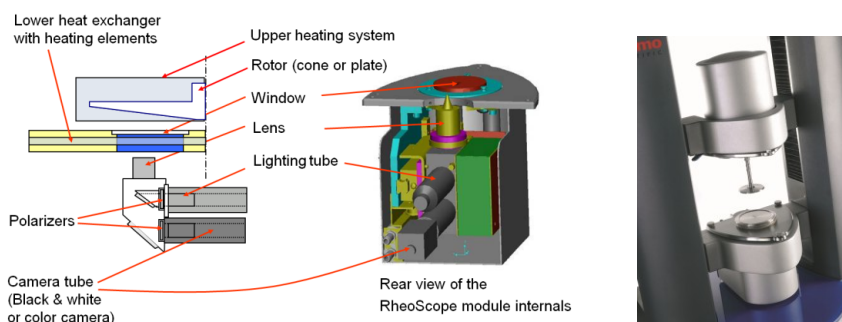


Figure 2. HAAKE RheoScope module: Schematic drawing (left: side view, center: rear view) and mounted in the HAAKE MARS rheometer (right)

The complete control of the optical components is fully integrated in the measuring software, including radial positioning of the lens and focus adjustment. Both polarization filters can be moved into and removed out of the optical paths as shown in Fig. 2. Additionally, the polarization can be crossed by angular adjustment. Contrast, brightness, gamma value and (auto) exposure time of the camera can be set. Rheological data and microscopic images are fully correlated and can be viewed during measurement and analysis of the results.

## Perspectives in Fundamental and Applied Rheology

Coalescence can occur for example in a salad dressing even at lower shear rates and within a short time (Fig. 3). First a constant shear rate of 500 1/s was applied in CR mode, followed by a shear stress of 0 Pa for 10 s, finally twice the initial shear rate was applied (1000 1/s). The HAAKE RheoScope module was equipped with a x 20 lens, delivering together with the selected resolution of the camera an images size of 640 x 480  $\mu\text{m}$ . A C60/1° Ti rotor with polished surface was used [5].

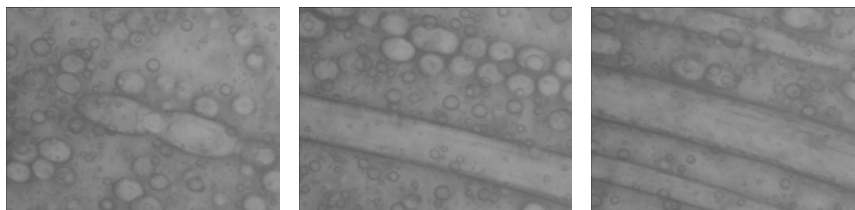


Figure 3. Coalescence: at 500 1/s applied for 0.3 s (left) and for 5.4 s (center) as well as at 1000 1/s for 4.8 s (right)

### References

1. Feustel, M., Küchenmeister, C., and Plog, J. (2010) Detailed analysis of curing reactions of polyurethane resins using the Rheonaut technology for simultaneous rheometry and FT-IR spectroscopy. Thermo Scientific Application Note V-247.
2. Soergel, F., Hauch, D., Jährling, M., Paulsen, K., Weber-Kleemann, A., Cech, T., Gryczke, A., Schmolzer, S., and Zecevic, D. (2013) Investigation of pharmaceutical hot-melts via simultaneous rheometry and polarization microscopy. Thermo Scientific Application Note V-262.
3. Sugimoto, K., Soergel, F., and Feustel, M. (2012) Monitoring emulsions morphology under shear via simultaneous rheometry and in-situ FT-IR spectroscopy. Thermo Scientific Application Note V-257.
4. Oldörp, K. (2009) What happens when rheological properties change? Looking into rheological properties with simultaneous collection of microscopic images. Thermo Scientific Application Note V-228.
5. Soergel, F., Meyer, F., Sierro, P., and Küchenmeister-Lehrheuer, C. (2013). Image acquisition with the HAAKE RheoScope module at high shear rates using a stroboscope light source and contrast enhancing illumination. Thermo Scientific Application Note V-265.

### Contact Address:

Fabian Meyer ([fabian.meyer@thermofisher.com](mailto:fabian.meyer@thermofisher.com))  
Thermo Fisher Scientific,  
Dieselstr. 4, 76227 Karlsruhe, Germany  
Telf.: +49-721-4094-327; Fax: +49-721-4094-300

## CHAPTER 6

# Flow visualizations in a rotating vane rheometer

*E. Gutiérrez-Barranco<sup>1</sup>, L. Parras<sup>1</sup>, C. del Pino<sup>1</sup>, F. J. Rubio-Hernandez<sup>2</sup>*

*<sup>1</sup> Mecánica de Fluidos, E.T.S. Ingenieros Industriales, Universidad de Málaga (Spain)*

*<sup>2</sup> Física Aplicada II, E.T.S. Ingenieros Industriales, Universidad de Málaga (Spain)*

### Introduction

The use of vane rheometers (i.e., when the vane geometry is used) to measure the flow properties of non-Newtonian fluids has been increasingly popular in the last years. It measures the torque of a rotating element that consists in a tiny thin blade introduced into the sample producing a minimum amount of disturbance in the flow. It is suitable for materials as clays, muds or gels, where the micro structure should not break before each measurement. Additional advantages of this kind of testing elements are the ability to measure complex fluids as well as avoiding wall-slip effects (see [1] for a review on this technique).

The shear rate is estimated from the values of the rotation rate ( $\Omega$ ). The general formula to compute the value of the shear rate is based on the assumption that it acts uniformly on an equivalent fluid cylinder of radius  $R$ . This radius corresponds to a 360° cycle of the vanes (see [1]-[3]). There are some discussions on the validity of this estimation and Keenkok [4] stated, basing his studies in photographs of grease samples, that this radius could be up to 5% greater than the theoretical value, depending on the liquid analyzed. However, other authors [5] reported that this equivalent fluid cylinder had exactly the same radius of the vanes, using numerical simulations for viscoplastic liquids, e.g. Herschel-Bulkley, Bingham and Casson models. In this paper we visualize the flow for Newtonian and non-Newtonian fluids to investigate whether the estimation of the shear rate in a vane configuration is suitable in comparison to the assumption of the equivalent inner fluid cylinder for viscoplastic materials.

## Experimental setup and materials

### Experimental setup

A sketch of the vane rheometer is shown in Figure 1 (a). A vane geometry adapted to a VT550 Haake Viscotester has been designed and built. The external radius of each vane was  $R=17.5\text{mm}$  and its thickness was  $e=1\text{mm}$ . This vane geometry was introduced in a cylindrical container of radius  $R_0 = 20\text{mm}$  made of borosilicate. This transparent material was used to allow the lighting by means of a laser sheet. The pictures were obtained from the bottom of the container. The full experimental setup is shown in Figure 1 (b). The vane rotor was introduced in the transparent cylindrical container and connected to the viscosimeter axis. To light the setup a  $532\text{nm}$  continuous green laser of  $500\text{ mW}$  was used. The laser passed through a cylindrical lens that generated a laser sheet that was projected perpendicular to the axis of the viscosimeter. This sheet is better appreciated in figure 1 (a) in which one can observe the opening angle as it passes through the optics. The images were obtained from the bottom by means of a mirror set at a  $45^\circ$  angle and a High Speed camera Photron SA3. The typical frame rate depends on the rotation rate of the viscosimeter. Typical values of  $125$  frames per second were used for a rotation rate close to  $20\text{ rpm}$ .

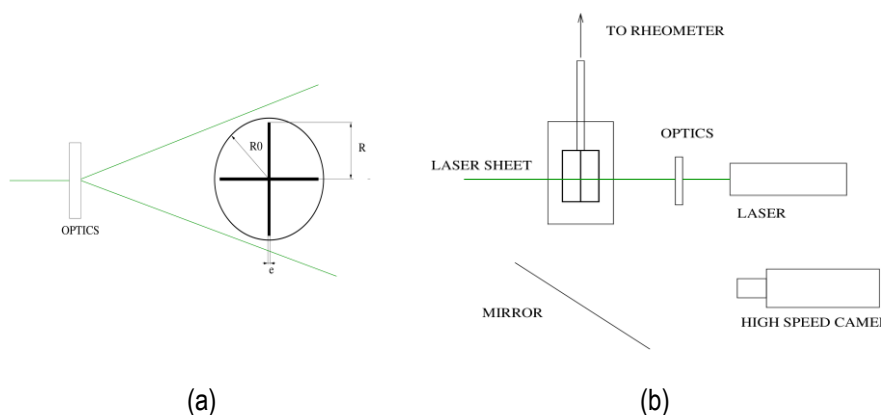


Figure 1. Sketch of the vane rheometer (a) and sketch of the experimental setup (b).

To process the images we added silver coated particles with an effective spherical diameter of  $15\text{-}30$  microns. These images were used for PIV applications, but a small amount of them also allowed us flow visualizations. Though kalliroscope flow visualizations have been also tested, the silver coated particles were more suitable for this work. Once the images have been obtained, we created a video in which we observed the vanes rotating at certain constant angular speed. This velocity was set by the viscosimeter for a constant shear rate mode. Special care was taken with the shadows generated when the vanes passed through the laser

sheet, so only one quadrant of the circumference has been analysed in the visualizations. To that end, we assumed that all the quadrants behave in the same way, although possible differences in the four quadrants should be tested in a future work. To process these images, we have imported them into Matlab. Consequently, we calculated the centre of the vanes, and then we rotated the images with respect to this centre at the same constant angular velocity of the viscosimeter. This procedure allowed us to set a reference frame fixed to the vanes. Thus, we obtained the position of the particles between two vanes. Once we processed the images corresponding to a temporal evolution in one quadrant of the circumference, we were able to compute the mean picture of a set of frames, getting the trajectories of each particle in the flow. Therefore, we observed the expected recirculation region between the vanes (see below).

### *Materials*

The reason of this research is to check qualitatively the flow behaviour in viscoplastic materials. To have something standard to compare with, we had first check our method with a Newtonian fluid (Glycerol 99%). We also used a transparent viscoplastic fluid (Aerosil R805 in PPG2000 10% w/w). The flow curve for the Glycerol and R805PPG2000 are shown in figure 2 for a constant temperature of 25°C. Note that the non-Newtonian fluid has a viscosity one order of magnitude greater than the Glycerol in the high shear rate region. Moreover, the viscosity of the non-Newtonian fluid is extremely high at a very low shear rate, showing a viscoplastic behaviour.

## **Results and Discussion**

The problem depends on three non dimensional parameters: Reynolds number,

$$\text{Re} = \frac{\rho \Omega^2 R}{\eta} \quad (1)$$

with  $\rho$  the density and  $\eta$  the viscosity; a gap ratio  $\varepsilon = (R_0 - R) / R_0$ ; and a parameter to define the degree of nonlinearity of the non-Newtonian fluid. This parameter is a relation between the time to vary the viscosity when the shear rate changes and the viscous time,

$$\Delta = \frac{d\eta / d\dot{\gamma}}{\eta / \dot{\gamma}} \quad (2)$$

It is null for the case of a Newtonian flow, negative for shear thinning and positive for shear thickening fluids.

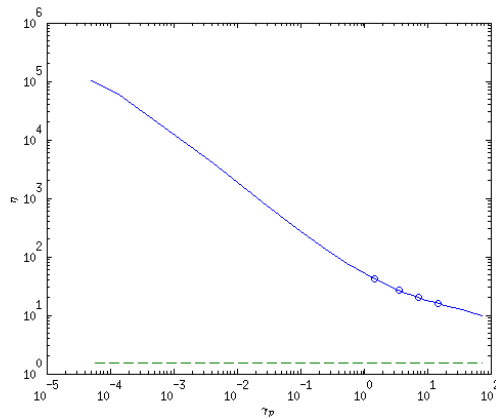


Figure 2. Apparent viscosity of Glycerol in dashed line and of PPG2000 in solid line.

We used a constant shear rate mode in the viscosimeter. We also imposed several constant speeds for both fluids at  $\Omega = 2, 5, 10$  and  $20$  rpm.

The mean images that characterise qualitatively the flow behaviour for the two tested fluids are depicted in figure 3. Rotation is clockwise. On the top row, the results for R805PPG2000 are shown. The values of  $Re = 0.1, 0.4, 1.1$  and  $2.9$ . Because of the higher viscosity, the vortex inside the two vanes was difficult to appreciate. This means that the flow had a solid body rotation movement. On the bottom row we show the four mean pictures for Glycerol. These images correspond to  $Re = 3.05, 7.6, 15.3$  and  $30.5$ . It can be observed in figure 3 how the lines formed a vortex that extends between two consecutive vanes. In addition, the outer line of the vortex is the threshold between the inner and the outer regions. This is explained below.

One can compute the line that separates the inner region and the outer regions, in other words, one can estimate the experimental value of  $R$ . The results for this threshold (or experimental line) are shown in figure 4 for the two fluids tested and the same rotation  $\Omega = 10$  rpm. In the case of the Newtonian fluid, the first vane that encountered the fluid forced a slight separation of the flow, so the line was almost parallel to the flow. On the other side, when the fluid encountered the second vane, due to fact that the inertial terms were not negligible in this case, the streamline was deformed. One can analyse the case of the non-Newtonian fluid, so that behaviour was found: the flow has been modified on both vanes, where the highest shear rates were located. However, the flow had a circular trajectory in the rest of the section with a smaller radius (3.4% of the radius of the blade). This corroborates the experiments of [4] but for viscoplastic materials.

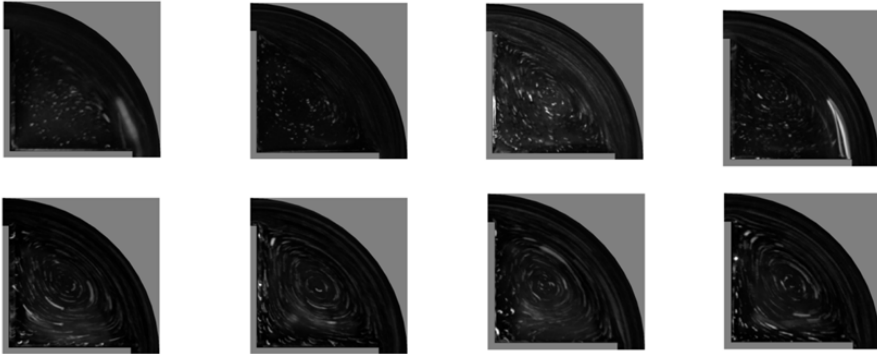


Figure 3. Sketch of the fluid flow characteristics of Glycerol on the first row and PPG2000 on the second row. From left to right the flow for  $W=2,5,10$  and  $20$  rpm

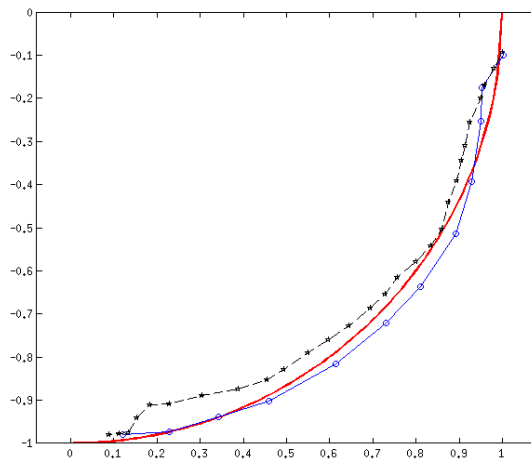


Figure 4. Position in non dimensional variables (using the radius of the vane  $R$ ) of the separating line between the inner flow and the outer flow. On thick line the unity radius, on solid line the Glycerol results and in dashed line the PPG2000 results.

### Conclusions

In this paper we have shown how the flow visualization technique used in other fields of Fluid Mechanics is suitable to analyse the complex flow generated with a vane geometry. The Newtonian and Non-Newtonian transparent flows, seeded with particles were recorded with a high speed camera. Those images were later processed to change artificially the reference of the frames. This method allows us to observe the flow behaviour inside a rheometer with a vane geometry. It has been shown that this technique works perfectly for Newtonian fluids as Glycerol, and the flow obtained had a vortex generated between the vanes. We observed structures with high velocity in the outer region of the vortex core that finally decreases suddenly at the outer wall due to slip boundary conditions. The separating line between the inlet and outer region (or the threshold of a fluid cylinder) was not exactly a circumference because the flow had previously lost its symmetry due to inertial effects (high Reynolds number). On the other hand, applying the same technique to a viscoplastic fluid, the region between the vanes had a quasi-solid body rotation movement, and the external flow presents the same characteristics as the Newtonian case, whereas the separating line between the interior and exterior regions was symmetric in this case (that can be expected also for the Newtonian case at low Reynolds numbers). Finally, it has been shown for a given case that the theoretical line used to estimate the shear rate is up to a 3.4 % different from the real line obtained from flow visualizations.

### References

1. H.A. Barnes, Q.D. Nguyen. *J. Non-Newtonian Fluid Mech.* 98, 1-14 (2001).
2. Q.D. Nguyen, D.V. Boger. *J. Rheology* 27 (4) 335-347 (1983).
3. Q.D. Nguyen, D.V. Boger. *J. Rheol.* 29 (3) 335-347 (1985).
4. M. Kenkook. *Rheol. Acta* 21 325-332 (1982).
5. J. Yan, A.E. James. *J. Non-Newtonian Fluid Mech.* 70 (3) 237-253 (1997).

### Contact Address:

Luis Parras ([lparras@uma.es](mailto:lparras@uma.es))  
Mecánica de Fluidos , E.T.S. Ingenieros Industriales  
Universidad de Málaga, Escuela de Ingenierías,  
C/ Doctor Ortiz Ramos S/N  
Telf.:+34 951952383

## CHAPTER 7

# Separation and deformation of red blood cells in PDMS microchannels

*Raquel O. Rodrigues<sup>1</sup>, Vera Faustino<sup>1,2</sup>, Diana Pinho<sup>1,2</sup>, Elmano Pinto<sup>1,2</sup>, Diana Cidre<sup>1</sup>, Raquel Rodrigues<sup>1</sup>, Tomoko Yaginuma<sup>1</sup>, Bruna Taboada<sup>1,2</sup>, David Bento<sup>1,2</sup>, Rui Lima<sup>1,2</sup>*

<sup>1</sup> ESTIG, Polytechnic Institute of Bragança, C. Sta. Apolónia, 5301-857 Bragança, Portugal.

<sup>2</sup> CEFT, Faculty of Engineering, University of Porto, R. Dr. Roberto Frias, 4200-465 Porto, Portugal.

### Introduction

Over the years, several experimental techniques were performed in *in vitro* environments, in an attempt to understand the flow behaviour of blood in microcirculation. Several of these studies were performed in glass capillaries, and have produced significant results with respect to rheological properties of blood [1, 2]. Another way to perform *in vitro* blood studies is to use microchannels fabricated by soft- lithography [3, 4] and xurography [5]. With these techniques several studies have focused in the formation of the cell-free layer (CFL) that is caused by the tendency of red blood cells (RBCs) to migrate toward the centre of the microchannel, in that the physical reason is known as the Fahraeus Lindqvist. The presence of this CFL at the regions adjacent to the wall is affected by the geometry of the microchannel [4] and the physiological conditions of the working fluid, such as the hematocrit (Hct) [6], and the RBC deformability [7]. The formation of CFL can be used for separation of diseased cells from healthy blood cells [8]. The aim of this paper is to show briefly the importance of the microfluidic devices to study several physiological phenomena that happens *in vivo* environments with special focus on the CFL behaviour and RBC deformability.

## Materials and Methods

### *Working fluids*

Generally several working fluids were examined: dextran 40 (Dx-40) containing 1%, 5%, 9% and 12% of RBCs. The hematocrits (Hcts) correspond to the feed reservoir Hct and it was measured by using a hematocrit centrifuge. Detailed description of the samples preparation can be found elsewhere [4, 5, 9-11].

### *Microchannels fabrication*

The microchannels tested were fabricated by means of two different microfabrication techniques, i. e., the soft-lithography [3, 4] and soft-xurography [5]. All the microchannels tested with dimensions less than 200  $\mu\text{m}$  were fabricated by standard soft-lithography techniques from a SU-8 photoresist mold [4, 9-11]. Recently we have developed a low cost microfabrication technique to study blood flow phenomena at a microscale level. This process uses vinyl mold masters fabricated by a cutting plotter. By using this technique we do not need a clean room facility and as a result it is possible to reduce significantly the production cost. Figure 1 shows the vinyl mold master and the correspondent PDMS microchannel fabricated by a soft-xurography. Detailed description of this fabrication process can be found elsewhere [5].

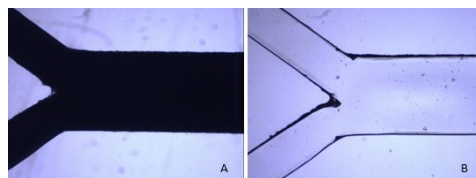


*Figure 1. Images obtained using an inverted microscope with a 4x objective lens: A - The vinyl mold master fabricated by a cutting plotter; B - PDMS microchannel of the confluence.*

### *Experimental set-up.*

The high-speed video microscopy system used in our experiments consists of an inverted microscope combined with a high-speed camera (see Figure 1). The PDMS microchannel was placed on the stage of the microscope where the flow rate of the working fluid was kept constant by means of a syringe pump.

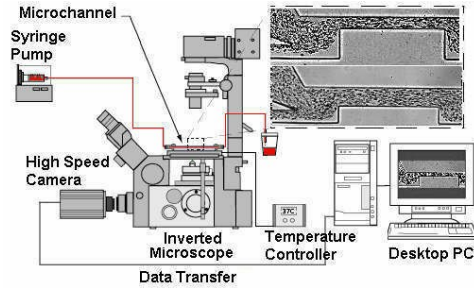


Figure 2. High-speed video microscopy system.

### *Image analysis*

Overall, the recorded images were transferred to the computer and then evaluated in Image J (NIH). To measure the CFL thickness the captured videos were converted to a sequence of static images (stack). Then, for each pixel, the maximum intensity of all the images in the stack was selected using the “Z project” function in ImageJ, which results in a region of RBCs core brighter than the background. To obtain quantitative measurements the grey scale images were converted to binary images with thresholding.

The RBC deformation measurements in hyperbolic microchannels were possible by using the following image analysis procedure. First, the captured videos were converted to a sequence of static images. Then, in order to reduce the noise in the images, a background image was created and subtracted from all original images. This process resulted in images having only the RBCs visible. To enhance its quality, image filtering was applied using ImageJ (NIH). Finally, the grey scale images were converted to binary images adjusting the threshold level. Detailed description of the image analysis procedure can be found elsewhere [10].

## **Results and Discussion**

### *CFL and RBC separation*

By using a microchannel with a confluence fabricated by a soft lithography technique we have obtained a very interesting blood flow phenomenon that happens at microscale level. Figure 3 shows flow visualizations around the confluence on the both trace particles in pure water and human RBCs containing about 14% Hct [4].

From Figure 3 we can clearly observe a CFL in middle of the microchannel after the apex of the confluence. In contrast this flow phenomenon is not observed with pure water. Recently, this phenomenon was also observed in microchannels fabricated by a soft xurography technique [5]. Detailed studies about this phenomenon are currently under way and will be published in due time. Figure 4 shows an image with the flow of RBCs through a 75% constriction for a constant

flow rate of  $1 \mu\text{L}/\text{min}$ . Measurements on the CFL thickness were also performed in a 25% constriction.

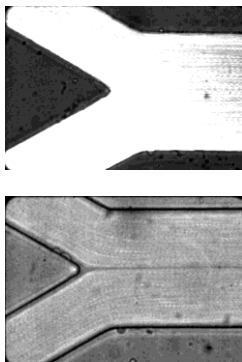


*Figure 3. Image of trace particles in pure water (up) and in vitro blood (down) obtained after “Zproject” (maximum intensity function). This microchannel was fabricated by a soft lithography technique.*

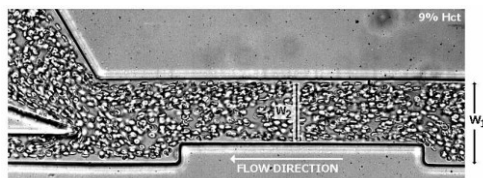


*Figure 4. Flow visualization of in vitro blood in a microchannel with the following dimensions:  $W_1 = 100 \mu\text{m}$  and  $W_2 = 75 \mu\text{m}$ .*

By using a combination of image analysis techniques we are able to automatically measure the CFL thickness before and after the artificial contractions. Figure 5 shows clearly that in both cases the constriction enhances CFL thickness. Furthermore, it is also clear that the enhancement is more pronounced for the channel with a contraction ratio ( $W_2/W_1$ ) equal to 0.25 than 0.75 [11]. This separation strategy will be crucial to obtain a low Hct and consequently perform cell deformability measurements.

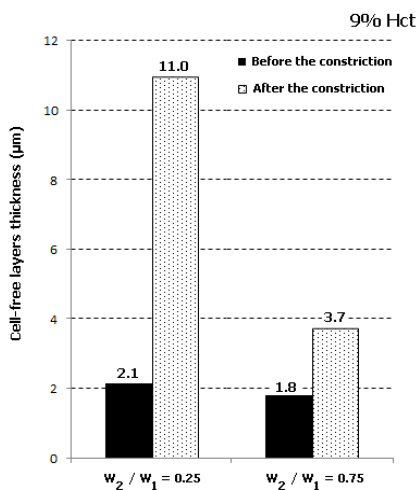


Figure 5. CFL thickness before and after artificial constrictions with different contraction ratios (Hct = 9%) [11].

### RBC deformation

To analyze the deformability of RBCs, the cells were measured in two pre-defined regions, (A) and (B) as shown in Figure 6. Region (A) is located upstream of the hyperbolic contraction and region (B) comprises a narrow part of the contraction region. Both regions are located axially along the centerline of the channel.

The flowing cells selected for measurement are measured twice in region (A) and (B). The RBC deformation was defined by the deformation index (DI) as  $(L_{Major} - L_{Minor}) / (L_{Major} + L_{Minor})$ , where  $L_{Major}$  and  $L_{Minor}$  refer to the major (primary) and minor (secondary) axis lengths of the ellipse best fitted to the cell. These values were obtained by using ImageJ (NIH).

Figure 6 shows an original image of the PDMS hyperbolic microchannel and the view of flowing RBCs at different flow rates (9.45  $\mu\text{l}/\text{min}$  and 66.15  $\mu\text{l}/\text{min}$ ) and in two pre-defined regions, (A) and (B). In Figure 7 the average deformation index calculated are shown for each case.

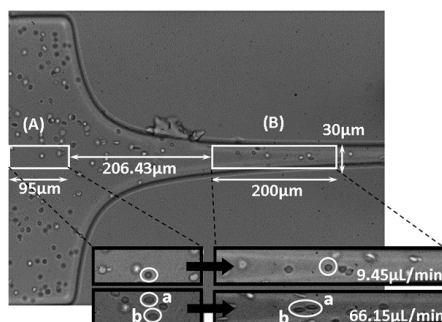


Figure 6. RBC deformation at different flow rates in region A and B [9].

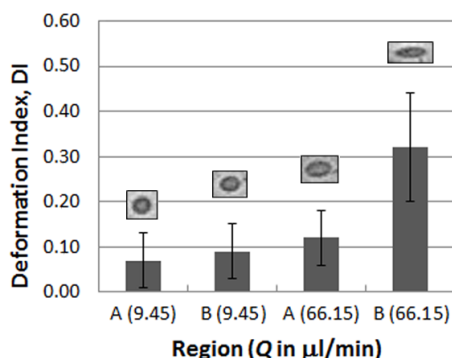


Figure 7. Comparison of deformation index at different flow rates in different regions.

As can be seen in Figure 7, for both flow rates, DI is higher in the hyperbolic contraction region (B) where the RBCs are submitted to a strong extensional flow. In the contraction region (B), DI increases substantially with the flow rate as a consequence of the higher strain rate to which the RBCs are submitted. These results evidence the highly deformable nature of RBCs under strong extensional flows and the present hyperbolic-shape microchannel is suitable for RBC deformability examination.

### Acknowledgment

The authors acknowledge the financial support provided by: PTDC/SAU-BEB/108728/2008, PTDC/SAU-BEB/105650/2008, PTDC/EME-MFE/099109/2008 and PTDC/SAU-ENB/116929/2010 from FCT (Science and Technology Foundation), COMPETE, QREN and European Union (FEDER).

## References

1. Lima, R., Ishikawa, T., Imai Y., and T., Yamaguchi T. (2012). In Single and two-Phase Flows on Chemical and Biomedical Engineering (Dias, R., Martins, A.A., Lima, R. and Mata, T.M. eds.), 513–547, Bentham Science Publishers: Netherlands.
2. Garcia, V., Dias, R. and Lima, R., (2012). In Applied Biological Engineering – Principles and Practice (Ganesh, R. Naik ed.), Vol. 17, 394-416, InTech.
3. Lima, R., Wada, S., Tanaka, S., Takeda, M., Ishikawa, T., Tsubota, K., Imai, Y. and Yamaguchi, T. (2008). Biomedical Microdevices. 10, 153-167.
4. Leble, V., Lima, R., Dias, R.P., Fernandes, C.S., Ishikawa, T., Imai, Y., and Yamaguchi T. (2011). Biomicrofluidics. 5, 044120.
5. Pinto, E., Pinho D., Bento, D., Correia, T., Garcia, V., Dias, R., Miranda, J.M. and Lima, R. (2013). 5<sup>o</sup>CNB, 301-306.
6. Kim, S., Ong, P.K., Yalcin, O., Intaglietta, M., and Johnson, P.C. (2009). Biorheology. 46, 181-189.
7. Fujiwara, H., Ishikawa, T., Lima, R., Matsuki, N., Imai, Y., Kaji, H., Nishizawa, M. and Yamaguchi, T. (2009). J. Biomech. 42, 838-843.
8. Hou, H.W., Han, J. and Lima, C.T. (2010). Lab.Chip. 10, 2605-2613.
9. Yaginuma, T., Oliveira, M.S.N., Lima, R., Ishikawa, T., Yamaguchi, T. (2011). Microtech Conference and Expo Boston, MA, USA, 2, 505.
10. Yaginuma, T., Oliveira, M.S.N., Lima, R., Dias, R., Ishikawa, T., Imai, Y., Yamaguchi, T. (2012). ECCOMAS Thematic Conference on Computational Vision and Medical Image Processing 209-211.
11. Lima, R., Oliveira, M.S.N., Yaginuma, T., Ishikawa, T., Imai, Y., Yamaguchi, T. (2011) Japan-Portugal Nano-Biomedical Engineering Symposium. 1, 49-50.

*Contact Address: ruimec@ipb.pt*

*Rui Lima (ruimec@ipb.pt)*

*Department: Mechanical Technology*

*Faculty/School of Engineering: ESTiG*

*University: Polytechnic Institute of Bragança (IPB)*

*Address: Campus de Santa Apolónia - Apartado 134 - 5301-857 Bragança - Portugal*



## **PART VII**

# **Suspensions and Colloids**



## CHAPTER 1

### Rheology of ethylene glycol based TiO<sub>2</sub> (anatase and rutile) nanofluids at high concentrations

*D. Cabaleiro, M.J. Pastoriza-Gallego, M.M. Piñeiro, J.L. Legido, L. Lugo*

*Departamento de Física Aplicada, Facultade de Ciencias, Universidade de Vigo, E-36310 Vigo, Spain*

#### Introduction

The understanding of the effect of nanoadditives on the rheology and dynamics of Newtonian fluids is of considerable importance and it is subject of great current interest. The early studies focused on the effective viscosity of the suspension as it was believed that the only effect of the nanoparticles was to enhance the viscosity of the suspension. Although a reduced number of studies about the rheological behaviour of nanofluids can be found in the literature, it has been recognized that above certain concentrations nanofluids may present remarkable shear thinning behaviour. However, there are inconsistencies such as Newtonian and non-Newtonian behaviours reported for nanofluids designed by using the same type of nanoparticles and base fluid. Hence, it is necessary to consider parameters as the nanocrystalline phase, shape or size of the nanoparticles in order to explain the discrepancies between some reported results as well as the temperature dependence of shear viscosity values.

The rheological behaviour is studied in this work for homogeneous stable suspensions obtained by dispersing mass concentrations up to 25 wt % of two TiO<sub>2</sub> nanocrystalline structures (Rutile, R-TiO<sub>2</sub>, and Anatase, A-TiO<sub>2</sub>) in pure ethylene glycol, EG. The study includes both flow curves and linear viscoelastic oscillatory tests, using a cone-plate rotational rheometer.

#### Experimental

##### *Materials and Sample Preparation*

Two different commercial TiO<sub>2</sub> nanopowders with pure anatase and rutile nanocrystalline phases were studied in pure ethylene glycol. Both types of nanoparticles were supplied by SkySpring Nanomaterials whilst ethylene glycol was provided by Sigma Aldrich. In order to analyse the influence of nanoparticle

shape, size and nanocrystalline phase on the final shear viscosity, the two dry nanopowders were previously characterized. The first step was an analysis of the dry nanoparticles by using the scanning electron microscopy (SEM) technique, with a JEOL JSM-6700 F field emission gun-SEM operating at an acceleration voltage of 20 kV in backscattering electron image. Both samples of nanoparticles presented nearly spherical shapes with average particles sizes of  $35\pm 17$  nm and  $47\pm 18$  nm for A-TiO<sub>2</sub> and R-TiO<sub>2</sub>, respectively. The samples were also chemically characterized by an energy dispersive X-ray (EDS) spectrometer incorporated in the SEM microscope. The A-TiO<sub>2</sub> sample only presents the chemical elements Ti and O in detectable quantities. For the R-TiO<sub>2</sub>, Si was also found but in an amount lower than 1% in mass. The powder was dispersed with a mass uncertainty lower than 0.02 wt % into a predetermined volume of the base fluid to obtain the desired mass fractions (5.00, 10.00, 15.00, 20.00 or 25.00 wt %) by using an ultrasonic homogenizer Bandelin Sonoplus HD 2200. These percent mass concentrations correspond to percent volume concentrations of 1.51, 3.13, 4.88, 6.77 and 8.83% for A-TiO<sub>2</sub>/EG nanofluids and of 1.36, 2.83, 4.43, 6.16 and 8.05% for R-TiO<sub>2</sub>/EG.

### *Rheological Measurements*

Flow curves and oscillatory experiments were performed by using a rotational Physica MCR 101 rheometer (Anton Paar, Graz, Austria) equipped with a cone-plate geometry. The cone, with a diameter of 25 mm and an angle of 1°, works at an imposed gap of 0.048 mm from the plate. Temperature, in the range from 283.15 to 323.15 K, was controlled with a Peltier P-PTD 200 with a diameter of 56 mm, placed at the lower plate and without groove. A constant amount of 110 μl of sample was employed [1] for the analysis. More details about the experimental setup and operating conditions can be found in our previous papers [1, 2].

## **Results and Discussion**

### *Rotational Tests*

Viscosity as a function of shear rate was determined for both sets of nanofluids at 303.15 K and at the five different mass fractions. The applied torques started from 0.1 μN·m, covering shear rate ranges from 0.1 to 1000 s<sup>-1</sup>. Figure 1 shows the flow curves for base fluid and several concentrations of both nanofluids.

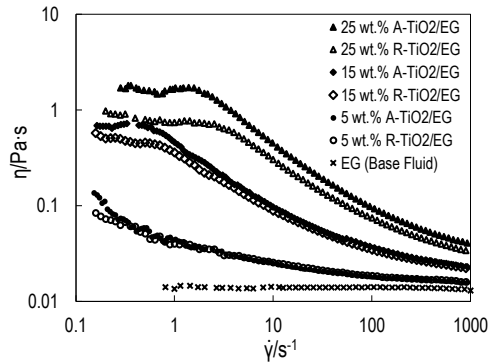


Figure 1. Shear viscosity,  $\eta$ , vs. shear rate,  $\dot{\gamma}$ , for base fluid and several concentrations of both nanofluids at the temperature of 303.15 K.

Unlike the base fluid, both set of nanofluids present a clear shear thinning behaviour, with higher shear viscosities for A-TiO<sub>2</sub>/EG nanofluids at the same shear rate and concentration. In the lowest shear rate region, Newtonian plateaus are easily identified as concentration rises. The Ostwald-de Waele model (Power law),  $\eta = K \cdot \dot{\gamma}^{n-1}$ , was used to describe the experimental shear viscosity data,  $\eta$ , as a function of the shear rate,  $\dot{\gamma}$ , in the shear-thinning region. The flow index,  $n$ , decreases exponentially with the nanoparticle concentration up to 0.27 for A-TiO<sub>2</sub>/EG and 0.33 for R-TiO<sub>2</sub>/EG. We should mention that no evidence of wall depletion phenomena were observed in the flow curves obtained.

The influence of temperature on the flow curves between 283.15 and 323.15 K was also studied for the highest mass concentration (25 wt %) of both nanofluids. Shear viscosity decreases as temperature increased. However, this temperature dependence is strongly influenced by the shear rate value. Thus, at a shear rate of ca. 10 s<sup>-1</sup> and for both nanofluids, shear viscosity is nearly temperature independent, which is not the case at high or low shear rate. At the same concentration A-TiO<sub>2</sub>/EG nanofluids also present higher shear viscosities than R-TiO<sub>2</sub>/EG nanofluids for all temperatures. At each shear rate, the influence of temperature on the viscosity can be described by an Arrhenius-type equation,  $\eta = A \cdot e^{E_a/(R \cdot T)}$ . Figure 2 shows the values obtained from the Arrhenius-type equation for the energy of activation,  $E_a$ , and pre-exponential factor,  $A$ , versus shear rate.

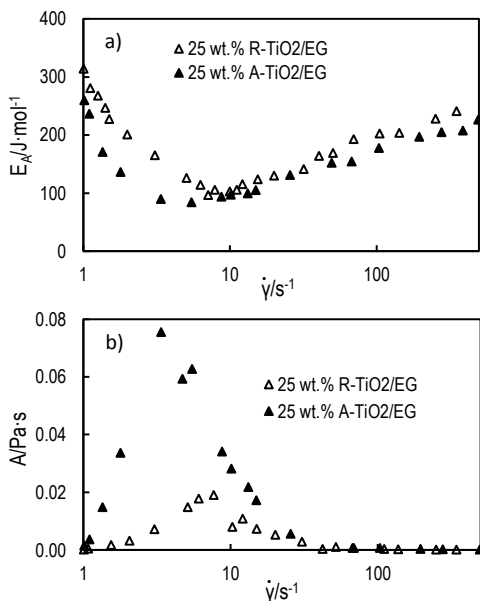


Figure 2. Energy of activation,  $E_a$ , and pre-exponential factors,  $A$ , vs. shear rate,  $\dot{\gamma}$ .

A minimum of the energy of activation and a maximum of the pre-exponential factor were found at shear rates around 6 s<sup>-1</sup> for A-TiO<sub>2</sub>/EG and around 8 s<sup>-1</sup> for R-TiO<sub>2</sub>/EG as can be observed in Figure 2.

### Oscillatory Tests

Linear viscoelastic oscillatory experiments were performed for A-TiO<sub>2</sub>/EG at 303.15 K in order to study their mechanical properties under small amplitude oscillatory shear. First, the linear viscoelastic region was identified through strain sweep tests for strains between 0.01 and 1000% at an angular frequency of 10 rad·s<sup>-1</sup>. Shear stress vs. strain is presented in Figure 3 for the 5 wt % and 25 wt % concentrations.

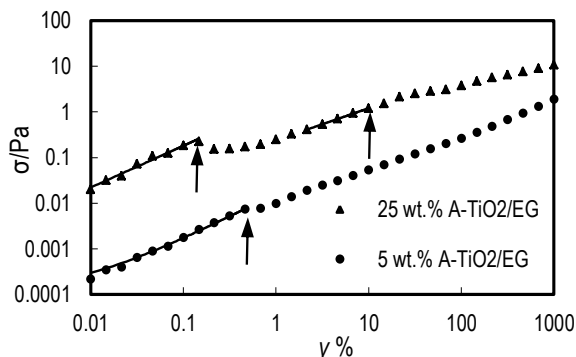


Figure 3. Shear stress,  $\sigma$ , vs. strain,  $\gamma$ , at an angular frequency of 10 rad/s and 303.15 K.

The strain increases linearly with the shear stress up to a strain of 0.7% for the 5 wt % concentration and up to 0.2% for the 25 wt %. After these critical strains, another strain-shear stress linear dependence appeared which became more evident at higher concentrations. This behaviour, which was previously described in literature as related to an attractive gel structure [3, 4], corresponds to a two two-step decrease of storage and loss modulus connected by two regions where  $G'$  and  $G''$  remain constant. The first decrease may correspond to a first break of the structure which is followed by an alignment of the nanoparticle clusters. Finally, at large deformations there is a second decrease due to the breaking of these clusters [3, 5].

Frequency sweep tests (for angular frequencies between 0.1 and 600 rad·s<sup>-1</sup>) were performed for A-TiO<sub>2</sub>/EG nanofluids at a strain of 0.1%. Storage and loss moduli increase with concentration at a given angular frequency, which means that the hydrodynamic interactions as well as the probability of collisions increase with the mass concentration of nanoparticles. The storage modulus is higher than the loss one at low frequencies for all studied nanofluids while the contrary is true at high frequencies. The crossover  $G'=G''$  moved towards higher angular frequencies when the concentration increases. This is in agreement with the fact that the degree of agglomeration of the particles is more important at highest concentrations but the alignment with the flow of the aggregates is achieved in a shorter time for higher concentrations. Finally, differences between the viscosities determined from steady,  $\eta(\dot{\gamma})$ , and oscillatory shear experiments,  $|\eta^*(\omega)|$ , at lower shear rates and angular frequencies were found for all mass concentrations. These differences which were higher with increasing concentrations, proved that the Cox-Merz is not valid for the studied suspensions.

## Conclusions

Both sets of the studied nanofluids, A-TiO<sub>2</sub>/EG and R-TiO<sub>2</sub>/EG, present a shear thinning non-Newtonian behaviour. At the lowest shear rate region, Newtonian plateaus were found for mass concentrations higher than 5 wt %. A-TiO<sub>2</sub>/EG nanofluids show higher shear viscosity for all studied shear rates, temperatures and concentrations. Minimum values of the energy of activation and maximum values of the pre-exponential factors were found at shear rates around 6 s<sup>-1</sup> for A-TiO<sub>2</sub>/EG and 8 s<sup>-1</sup> for R-TiO<sub>2</sub>/EG at the 25 wt % concentration. The deformation tests evidence attractive gel behaviour of the studied A-TiO<sub>2</sub>/EG nanofluids. Finally, it was found that the Cox-Merz rule does not hold even for the 5 wt % A-TiO<sub>2</sub>/EG nanofluid, departures becoming more important with increasing nanoparticle concentrations.

## Acknowledgements

This work was supported by the “Ministry of Economy and Competitiveness” and the FEDER program through the Project ENE2012-32908. The authors also acknowledge the financial support from Fundación Iberdrola and Univ. Vigo. D.C and L.L acknowledges the financial support under the FPU and Ramón y Cajal program provided by the “M. Education, Culture and Sport”, and “Science and Innovation M.”, respectively.

## References

1. Pastoriza-Gallego, M.J., Lugo, L., Legido, J.L., and Piñeiro, M.M. (2011). *Nanoscale Res. Lett.* 6, 560.
2. Cabaleiro, D., Pastoriza-Gallego, M.J., Piñeiro, M.M., and Lugo, L. (2013). *J. Chem. Thermodyn.* 58, 405-415.
3. Pham, K.N., Petekidis, G., Vlassopoulos, D., Egelhaaf, S.U., Pusey, P.N., and Poon, W.C.K. (2006). *Europhys. Lett.* 75, 624.
4. Tanaka, H., Meunier, J., and Bonn, D. (2004). *Phys. Rev. E Stat. Nonlin.* 69, 031404.
5. Tesfai, W., Singh, P.K., Masharqa, S.J.S., Souier, T., Chiesa, M., and Shatilla, Y. (2012). *J. Appl. Phys.* 112, 11.

## Contact Address:

*Luis Lugo (luis.lugo@uvigo.es)*

*Dpto. Física Aplicada, Facultad de Ciencias. Universidad de Vigo*

*Lagoas-Marcosende, s/n, 36310, Vigo (Spain)*

*Tel.: 986813771*

## CHAPTER 2

### Scouting the rheology of aqueous dispersions of a food-grade advanced performance xanthan gum

*J.A. Carmona, P. Ramírez, N. Calero, M.C. García, J. Muñoz*

*Departamento de Ingeniería Química. Facultad de Química. Universidad de Sevilla c/ P. García González, 1, E41012, Sevilla, Spain.*

#### **Introduction.**

Xanthan gum is a well-known non-gelling microbial biopolymer which exhibits ordered rigid chain conformation in aqueous media. It is able to form highly viscous dispersions even at low concentrations, their stability to temperature, pH and ionic strength being responsible for xanthan gum applications in many fields. In recent years the fermentation process has been improved by CP Kelco in order to supply the market with a xanthan gum sample exhibiting better rheological properties than the standard one. The supplier claims that this enhanced xanthan gum is able to endure the shear and turbulent flows typically found in high-shear mixers and homogenizers. The overall objective of this work was to explore the rheology (SAOS, steady shear flow and time-dependent properties) of an advanced performance xanthan gum.

#### **Experimental.**

##### *Materials and solution preparation*

The sample used was KELTROL® Advanced Performance “Food Grade” xanthan gum, gently donated by CP Kelco. The solutions studied were prepared with ultrapure Milli-Q water, following a standard procedure.

##### *Rheological measurements*

Rheological measurements were carried out with a CS AR2000 rheometer (TA Instruments). A smooth surface Aluminium plate & plate (60mm diameter) geometry of low inertia was used. All tests were performed at 20 °C, using a Peltier system and a solvent trap to inhibit evaporation. The upper plate reached the measuring gap at down speed (20µm/s) at a maximum normal force of 1N. This experimental set up was selected to minimize the sample structural breakdown as a consequence of the loading process.

Multistep step flow curves from 1 to 50 Pa were run fixing a steady state approximation of 0.05 for a maximum measuring time of 5 minutes. The viscoelastic characterization involved stress sweeps at 1 Hz and frequency sweeps in the linear viscoelastic region (LVR) from 20 to 0.5 rad/s. Time sweep tests in SAOS were conducted to monitor the structural recovery after a non-linear creep step at 8 Pa for 40 s. The LVR of the oscillatory time sweeps was checked by conducting kinetics experiments at different stress amplitudes.

**Results and Discussion**

Figure 1 shows that the critical stresses limiting the LVR at 1 Hz increased with gum concentration from 0.30 to 3 Pa.

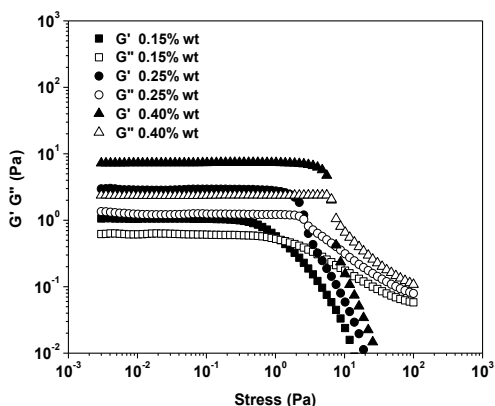


Figure 1. Stress sweeps (0.03-100 Pa) at 1 Hz of aqueous xanthan gum solutions with different gum concentration 0.15, 0.25 and 0.4% wt at 20°C.

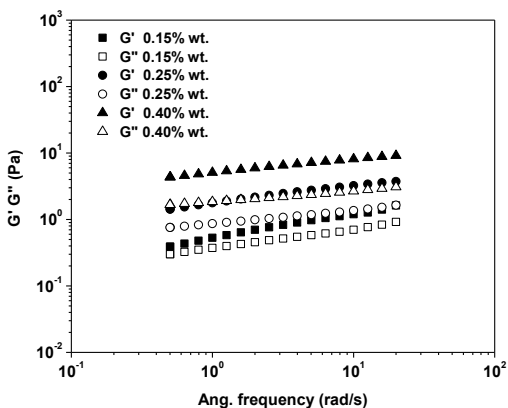


Figure 2. Frequency sweeps (20-0.5 rad/s) in AR2000 of aqueous xanthan gum solutions with different gum concentration 0.15, 0.25 and 0.4% wt at 20°C.

Figure 2 shows that the xanthan gum sample studied exhibited a weak frequency dependence of  $G'$  and  $G''$ , the former being dominant over the latter throughout the whole frequency range covered. This weak-gel behaviour was observed from a gum concentration as low as 0.15 wt%. It is noteworthy that a standard xanthan gum from Sigma Co. would have shown fluid-like viscoelastic behaviour, which is typical of macromolecular solutions instead of weak gels [1-2]. As expected while  $G'$  and  $G''$  increased with gum concentration, the loss tangent decreased. The values of both modules ( $G'$  and  $G''$ ) at 6,28 rad/s showed an exponential increase with gum concentration (Figure 3). This figure clearly illustrates that the  $G''/G'$  ratio was lower and lower as xanthan concentration increased.

Figure 4 demonstrates that all xanthan gum dispersions studied showed shear thinning behaviour.

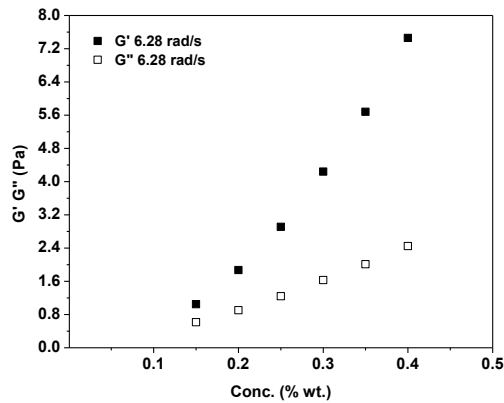


Figure 3. Values of  $G'$  and  $G''$  at 6.28 rad/s calculated from frequency sweeps (20-0.5 rad/s) in AR2000 of aqueous xanthan gum solutions with different gum concentration (0.15, 0.20, 0.25, 0.30, 0.35 and 0.4% wt) at 20°C.

The flow curves fitted the Carreau model (equation (1)).

$$\eta - \eta_{\infty} = \frac{\eta_{\infty} - \eta_0}{\left(1 + \left(\frac{\dot{\gamma}}{\dot{\gamma}_c}\right)^2\right)^{\frac{1-n}{2}}} \quad (1)$$

The corresponding fitting parameters are presented in Table 1.

While the zero-shear viscosity showed an exponential increase with gum concentration, the flow index remained fairly stable around 0.30. This means that these dispersions were significantly non-Newtonian and that the flow curves may be possibly superimposed on a single master curve.

Table 1. Carreau model parameters.

Conc. %Wt.	$\eta_0$ (Pas)	$\gamma_c$ (s <sup>-1</sup> )	n	R <sup>2</sup>
0.15	8.62	2.5E-2	0.32	0.99
0.2	28.9	1.2E-2	0.31	0.99
0.25	73.6	7.5E-3	0.30	0.99
0.3	149	6.1E-3	0.29	0.99
0.35	274	4.9E-3	0.29	0.99
0.4	542	3.1E-3	0.28	0.99

Non-linear creep experiments were conducted at a reference shear stress of 8Pa. This shear stress was optimised to obtain a clear shear flow, without the risk of sample migration out of the parallel plate used. The results showed an initial non-linear increase of strain with time and the onset of a steady-state response around a shear time of 10 s (Figure 5). These results are consistent with a fast drop of viscosity with time (thixotropy), which shortly leads to a steady-State value.

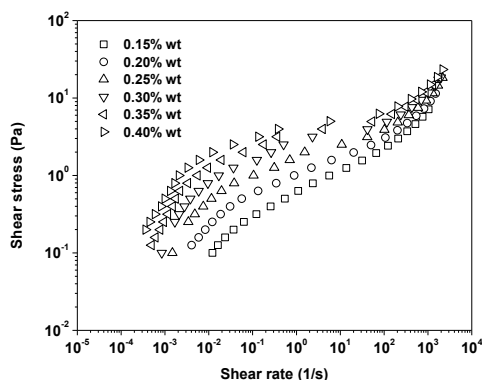


Figure 4. Flow curves under steady shear in AR2000 of aqueous solutions of xanthan gum with different gum concentration (0.15, 0.20, 0.25, 0.30, 0.35 and 0.4% wt) at 20°C.

Figure 6 illustrated the kinetics of structural recovery for the 0.15 wt% xanthan solution, which turned out to be quite fast. The stress amplitude of the oscillatory shear test made as a function of recovery time must be carefully chosen, since the structure of the system may be dependent of the recent shear history. This was confirmed by the fact that the response at 0.1 Pa was probably out of the new LVR. On the other hand, the kinetics of structural recovery for 0.4 wt % xanthan was slower (figure 7) due probably to the higher density of transient junction

zones to be rebuilt. A first-order equation was used to fit the kinetics of  $G'$  (equation 2) such that the reciprocal of the rate constant defines a characteristic time for 63.2% structural recovery.

$$G' - G'_o = (G'_\infty - G'_o)(1 - e^{-kt}) \quad (2)$$

Table 2 showed that the characteristic times ranged from 48 s for 0.15 wt % to 165 s for 0.4 wt % xanthan gum. Parameter  $G'_o$  predicts an instantaneous value of  $G'$ , which is linked to null recovery time. This may be considered as a fingerprint of the structural damage caused by shear.  $G'_\infty$  is the value of  $G'$  associated with a completed recovery. The ratio between  $G'_\infty$  and  $G'_o$  provides a value for the shear-induced structural breakdown.

Table 2. Parameters of the simple exponential fitting equation for  $G'$  growth with rest time after shearing solutions with 0.15, 0.20, 0.25, 0.30, 0.35 and 0.40 wt % gum concentration at 20°C.

Conc %Wt.	$G_\infty$ (Pa)	$G_o$ (Pa)	$k$ (s <sup>-1</sup> )	R <sup>2</sup>
0.15	1.23	1.12	2.1E-2	0.96
0.20	2.11	1.85	2.1E-2	0.95
0.25	3.30	2.77	1.5E-2	0.96
0.30	4.64	3.70	1.3E-2	0.96
0.35	6.29	5.80	5.7E-3	0.99
0.40	6.28	5.79	6.1E-3	0.99

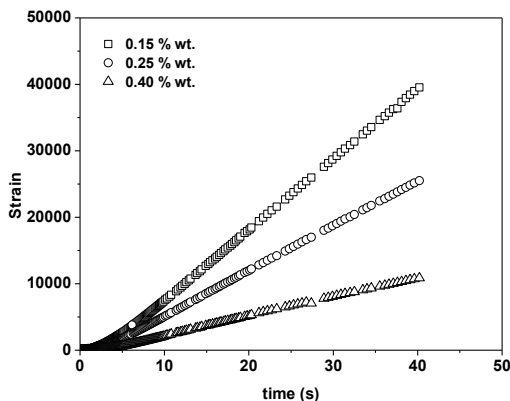


Figure 5. Strain versus time from non-linear creep test at 8 Pa of xanthan gum with different gum concentration 0.15, 0.25, 0.4% wt at 20°C.

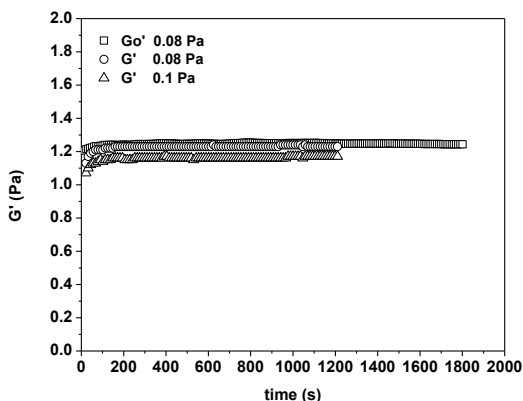


Figure 6. Dependence of the linear dynamic viscoelastic function,  $G'$ , on rest time after shearing at 8 Pa. System: 0.15 wt % xanthan gum solution at 20°C. Shear stress amplitudes: before non-linear creep: 0.08 Pa ( $\square$ ), after non-linear creep: 0.08 Pa ( $\circ$ ) and 0.1 Pa ( $\triangle$ ).

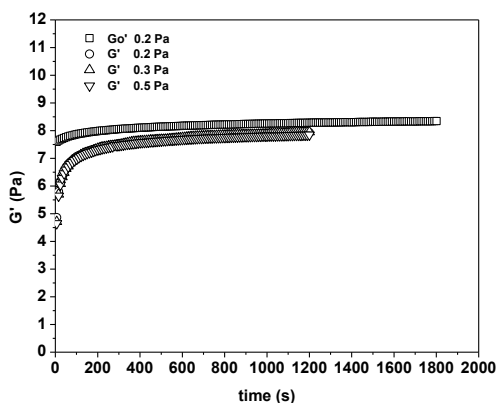


Figure 7. Dependence of the linear dynamic viscoelastic function,  $G'$ , on rest time after shearing at 8 Pa. System: 0.40 wt % gum concentration at 20°C. Shear stress amplitudes: before non-linear creep: 0.2 Pa ( $\square$ ), after non-linear creep: 0.2 Pa ( $\circ$ ), 0.3 Pa ( $\triangle$ ) and 0.5 Pa ( $\nabla$ ).

### Concluding Remarks

The Advanced performance xanthan gum presented a weak gel viscoelastic behaviour even at very low concentration (0.15 wt %). The high zero-shear viscosity and strong shear thinning response along with a fast drop of viscosity with shear time and also of structural recovery support the excellent applications of this enhanced xanthan gum as thickening agent and stabilizer of dispersions.

### **Acknowledgements**

The financial support received (Project CTQ2011-27371) from the Spanish MINECO and from the European Commission (FEDER Programme) is kindly acknowledged.

### **References**

1. Muñoz, J., Hudson, N.E., Velez, G., Alfaro, M.C., and Ferguson, J. *Rheol Acta* 40, (2001) 162.
2. Alvez, G. Ph.D. Thesis. University of Seville (2002).



## CHAPTER 3

### Viscosity empirical model for suspensions considering the effects of the shear rate and the concentration of particles

A.I. Gómez-Merino<sup>1</sup>, J.F. Velázquez-Navarro<sup>2</sup>, F.J. Rubio-Hernández<sup>1</sup>, C. Jiménez-Agredano<sup>1</sup>

<sup>1</sup> Department of Applied Physics II, University of Málaga (Spain)

<sup>2</sup> Department of Mechanical Engineering and Fluid Mechanics, University of Málaga (Spain)

#### Introduction

Titanium dioxide nanoparticles are used in a wide range of applications. In some cases, as in biomedical, optical or electronic, the precursor material must be in the colloidal state. In this case their effectiveness depends largely on of the rheological behaviour of TiO<sub>2</sub> suspensions. However, the maximization of the properties of the material can come into conflict with the need for low-cost manufacturing processes [1].

One of the parameters that determine the rheological behaviour of the suspensions is the volume fraction occupied by the solid particles ( $\phi$ ). The first  $\eta(\phi)$  relationship was proposed by Einstein assuming hard spherical particles in a mono-disperse and very diluted suspension,

$$\eta = \eta_0(1 + 2.5\phi) \quad (1)$$

In Eq. (1)  $\eta$  is the viscosity of the suspension and  $\eta_0$  the viscosity of the liquid phase. The intrinsic viscosity  $\left([\eta] = \lim_{\phi \rightarrow 0} \frac{\eta - \eta_0}{\phi}\right)$ , which expresses the contribution of particles to the viscosity of the suspension, is 2.5 for an isolated spherical particle. For concentrated suspensions the particle interactions must be considered. In this case more sophisticated expressions for the function  $\eta(\phi)$  have been proposed. For example, Krieger and Dougherty [2] and Mooney [3] proposed two expressions, in which the maximum packing fraction of particles ( $\phi_m$ ) appears as a second parameter,

$$\eta = \eta_0 \left(1 - \frac{\phi}{\phi_m}\right)^{-[\eta]\phi_m}; \quad \text{KD-equation (2)}$$

$$\eta = \eta_0 \exp\left(\frac{[\eta]\phi}{1 - \frac{\phi}{\phi_m}}\right); \quad \text{M-equation (3)}$$

All proposals for the function  $\eta(\phi)$  assume that there is not any dependence of the viscosity with shear rate. In this paper, we propose an empirical model of viscosity that captures the dependence of viscosity with the solid volume fraction and with the shear rate. For that, the dependence of the intrinsic viscosity and the maximum packing fraction of particles with the shear rate in TiO<sub>2</sub> suspensions will be determined.

### Experimental

The titanium oxide (anatase), supplied by Sigma Aldrich, had a purity of 99.9 %, density of 3.9 g/cm<sup>3</sup>, a BET area of 10 m<sup>2</sup>/g, and an average primary particle size (TEM) of 100 nm. It was used as it was supplied. The water was doubly distilled and deionised with a column of mixed bed exchange ions (Millipore).

The rheological measurements were performed in a Thermo-Haake RS600 rheometer. Cone-plate geometry of 20 mm and 1° was used. To avoid the undesirable influence of different mechanical histories, freshly prepared samples were homogenized to 50 s<sup>-1</sup> for 1 min. After this they were left to stand for 1 min. before starting the test rheological. The steady flow curves were obtained by applying successive shear-rates from 10<sup>-2</sup> up to 10<sup>4</sup> s<sup>-1</sup>. All measurements were carried out at 25.0±0.1 °C.

### Results and Discussion

Figure 1 shows the steady shear behaviour of concentrated suspensions of anatase. It is observed a shear-thinning behaviour and a trend towards a plateau viscosity at high shear rates. This result has been obtained in many other concentrated ceramic powder suspensions [4]. It may be justified as a result of the alteration of the suspension structure due to the shear. At low shear rates the suspension structure is close to the structure at rest because the colloidal interactions dominate over the hydrodynamic forces. The structure at rest can be aggregates of particles or even a structural network if the attraction forces are higher than the repulsive ones. When the shear rate increases the hydrodynamic forces break the suspension structure and shear-thinning is observed. At very high shear rates it appears a plateau because the hydrodynamic forces dominate. The plateau is a measure of the resistance to flow of a suspension with a structure

completely hydro-dynamically controlled.

As it can be seen in Figure 1, the degree of shear-thinning and the viscosity at high shear-rate increase with the solid volume fraction. On the other hand, as it is suggested by the Eqs. (2) and (3) the viscosity must be run to the highest value when  $\phi$  increases, and must be infinite when the  $\phi_m$ -value is reached. The maximum volume fraction is determined by geometrical arrangement in the suspension, i.e. the shape and size of the particles and can be used as a measure of the suspension microstructure. This is to say that different geometric parameters must provide different values of  $\phi_m$ .

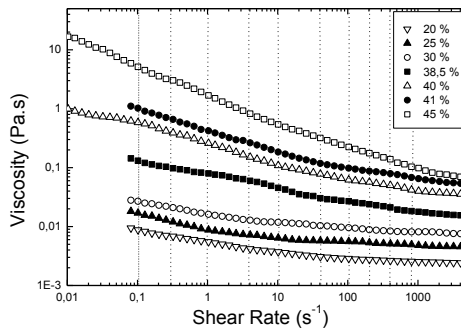


Figure 1. Flow curve of anatase suspensions at different solid volume fraction. Dot lines show the selected shear rates.

The intrinsic viscosity is a measure of the contribution of the particle shape to the distortion of the flow field. Einstein obtained a theoretical value  $[\eta] = 2.5$  for hard spheres, which has been experimentally confirmed. A number of studies [6] have shown that the deviation from spherical particles leads to greater  $[\eta]$  due to the increasing disruption of flow field.

It is important to note that models KD and M were formulated assuming Newtonian behaviour of the suspension. Therefore, as starting point we have obtained the values of  $\phi_m$  and  $[\eta]$  in the high shear region where clearly there is a Newtonian plateau. The results are shown in Table 1. Taking into account the values of the correlation coefficient, an acceptable fit for the two models can be assumed.

When the shear rate increases, the rest structure progressively erodes. It can be accepted that the Newtonian plateau at the higher shear rates results from the formation of ordered sheets formed by basic units. Between them the liquid phase can easily flow. The value  $\phi_m = 0.64$  supplied by KD model supports this conclusion. However, the extremely high value  $\phi_m = 0.90$  obtained with the use of M model, only can be justified if an extremely high polydispersion of the suspension is generated when it is strongly sheared. As the viscosity decrease with the shear rate observed in Fig 1 is consistent with the first explanation but not

with the second one, the KD model will be accepted as the start point for the development of the model that will be here proposed. Both the values  $[\eta] = 6$  supplied by KD model, and  $[\eta] = 5.4$  supplied by M model, suggest that the basic unit formed by the aggregation of  $\text{TiO}_2$  particles is not spherical but ellipsoidal [7].

*Table 1. Values of maximum packing fraction and intrinsic viscosity of anatase suspensions in the high shear Newtonian plateau.*

	$\phi_m$	$[\eta]$
KD-model	$0.64 \pm 0.12$	$6 \pm 3$
	$R^2=0.9343$	
M-model	$0.90 \pm 0.02$	$5.4 \pm 1.2$
	$R^2=0.9359$	

According with the erosion effect before described some dependence with the shear rate of the parameters  $[\eta]$  and  $\phi_m$  must be expected. As our aim is to find an empirical equation that relates viscosity with volume fraction and shear rate, the study of  $[\eta](\dot{\gamma})$  and  $\phi_m(\dot{\gamma})$  dependences is proposed to be included in KD model. The procedure is summarized as follows:

- The region of non-Newtonian behaviour is divided into equidistant intervals of shear rate (shown in Figure 1).
- The viscosity is plotted against the solid volume fraction for the selected shear rate.
- The KD equation is fitted to the experimental points to obtain the maximum packing fraction and intrinsic viscosity that correspond to the selected shear rates.
- The values of  $\phi_m$  and  $[\eta]$  obtained are plotted versus the selected shear rates. From these results, the empirical model is proposed.

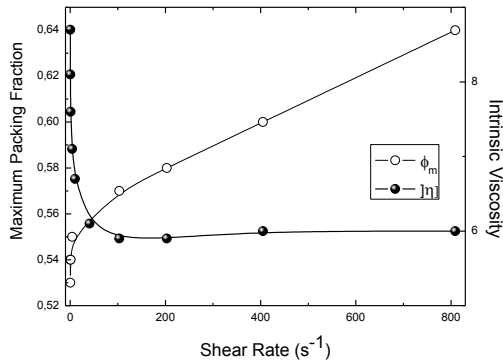


Figure 2.  $[\eta](\dot{\gamma})$  and  $\phi_m(\dot{\gamma})$  obtained using KD equation.

Figure 2 shows the dependence of  $\phi_m$  and  $[\eta]$  with the shear rate obtained by means of Eqn. (2). Other authors [6] also found that both parameters are shear rate dependent. It is remarkable that the intrinsic viscosity decreases while the maximum volume fraction increases with the shear rate. When the shear rate increases the aggregates erodes and tends to a spherical shape. This mechanism can explain the decrease observed in  $[\eta]$ . At a high enough shear rate value the aggregates cannot break anymore and maintain the same shape. This is why the intrinsic viscosity reaches a constant value  $[\eta] = 6$ . On the other hand, more different aggregate sizes coexist when the shear rate increases. This must favour the existence of a more dense packing. In other words, the maximum packing fraction should increase. The mathematical fits for both parameters, shown in Fig. 2, have been included in KD model. This results in the following empirical equation,

$$\begin{cases} \eta(\phi, \dot{\gamma}) = \eta_0 \left(1 - \frac{\phi}{\phi_m}\right)^{-[\eta]\phi_m} \\ \phi_m = 0.54 + 0.11 \cdot 10^{-6} \dot{\gamma} \\ [\eta] = 6 + 1.5 \exp\left(-\frac{\dot{\gamma}}{0.32}\right) + 1.6 \exp\left(-\frac{\dot{\gamma}}{12}\right) \end{cases} \quad (4)$$

### Concluding Remarks

The rheological behaviour of anatase aqueous suspensions with different solid concentrations has been presented. Two Newtonian models for the dependence of the viscosity with the solid volume fraction have been used to obtain the maximum packing volume fraction and the intrinsic viscosity in the high shear rate region, where a Newtonian plateau is always obtained.

M model has been rejected because an unacceptable  $\phi_m$ -value is obtained. Then, KD model has been assumed as reflecting the true concentration dependence of the suspension viscosity. Then, following the same process but in the shear-thinning region, i.e., fitting the shear rate value, these parameters have been also obtained and a combined shear rate and concentration dependence of the suspension viscosity has been concluded. Despite the  $\eta(\phi)$  models assume Newtonian behaviour, which is an obvious weak-point of this proposal, the  $\eta(\phi, \dot{\gamma})$  dependence here obtained could be use as an empirical relationship that could help to predict the behaviour of a suspension.

### References

1. Ridley, M.K., Hackley, V.A., Machesky, M.L. (2006). *Langmuir* 22, 10972-10982.
2. Krieger, I.M., Dougherty, T.J. (1959). *Trans Soc Rheol* 3, 137–52.
3. Mooney, M. (1951). *J. Colloid Interface Sci.* 6, 162-170.
4. Larson, R.G. (1999). *The structure and Rheology of complex fluids*. Oxford University Press. New York.
5. Stickel, Qi F, Tanner R. *Rheol Acta* 2012;51:289–302.
6. De Kruif, C. G., van Iersel, E. M. F., & Vrij, A. (1985). *Journal of Chemical Physics*, 83,4717-4725.
7. Rubio-Hernández, FJ, Ayúcar-Rubio, MF, Velázquez-Navarro, JF, Galindo-Rosales, FJ (2006). *J Colloid Interface Sci.* 298, 967-972.

### Contact Address:

A.I Gómez-Merino ([aimerino@uma.es](mailto:aimerino@uma.es))

*Dpto. Física Aplicada II, Escuela de Ingenierías, Universidad de Málaga, Avda Dr Ortiz Ramos s/n, 29071, Málaga, Spain.*

*Telf.:+34951952294*

# Author Index

## A

Aguilar J.M.	143
Alejandro I.	383
Alfaro M.C.	31, 247, 265, 291, 391
Almeida A.	205
Almeida A.J.	45, 149
Almeida P.L.	27
Alonso G.	3
Álvarez M.D.	173
Alves M.A.	339
Alves V.D.	69
Arancibia C.	217
Aranda M.A.G.	301
Arteaga J. F.	3, 15
Arufe S.	197

## B

Bargiela V.	135, 157, 181
Batista I.	165
Bayarri S.	217
Beirão-da-Costa S.	81, 87
Bengoechea C.	21, 51, 271
Bento D.	357, 407
Berasategui J.	383
Bica A.	205
Borderías A.J.	135, 157, 189
Borges J.P.	307
Bou-Ali M.M.	383
Brehm T.	307

## C

Cabaleiro D.	417
Calafell I.	57

Calero N.	31, 233, 423
Camacho C.	81, 87
Campo-Deaño L.	351
Canales J.	313
Canejo J.	325
Canet W.	173
Carballo J.	181
Carmona J. A.	247, 423
Chenlo F.	123, 197
Choplin L.	277
Cidade M.T.	27, 149, 307
Cidre D.	357, 363, 377, 407
Coelho M.R.	87
Contreras-de Villar F.	319
Cordobés F.	143
Costell E.	217
Cox P.	247
Crumeyrolle O.	345
Cuadri A.A.	241

## D

Davila D.	371
de la Fuente J.	143
de la Torre A.G.	301
de Sousa H.C.	253
del Pino C.	401
del Rio C.	371
Delgado M.A.	259
Diañez I.	63
Dias A.M.A.	253
Dias R.	357, 377
Díez-Sales O.	105

# Perspectives in Fundamental and Applied Rheology

Durán J.D.G.	383	Hilliou L.	325
<b>E</b>		Hu Q.	253
Elejabarrieta M.J.	383	<b>I</b>	
<b>F</b>		Irazu L.	383
Faustino V.	357, 363, 377, 407	<b>J</b>	
Félix M.	9, 21	Jiménez-Agredano C.	431
Fernandes C.S.	357	<b>L</b>	
Fernandes S.N.	325	Leal C.R.	27, 325
Fernández M.	99	Legido J.L.	417
Fernández-Espada L.	143, 271	Leiza J.R.	99
Fradinho P.	93	Lima R.	357, 363, 377, 407
Franco I.	181	Lobo I.	253
Franco J.M.	3, 15, 73, 225, 259, 391	López-Castejón L.	51
Fuentes R.	173	López-López M. T.	383
<b>G</b>		Lucio-Villegas A.	9
Galindo-Rosales F.J.	339	Lugo L.	417
Gallego R.	15	<b>M</b>	
Gallegos C.	225, 259	Mancini G.	205
García M.C.	31, 233, 247, 391, 423	Marceneiro S.	253
García V.	377	Marchal P.	277
García-Maté M.	301	Martí-Bonmatí E.	211
García-Morales M.	51, 63, 241, 285, 391	Martínez I.	51, 63
García-Zapateiro L.A.	259	Martínez-Arias B.	345
Godinho A.	69	Marto J.	45, 111, 149
Godinho M.H.	325	Masoudian M.	351
Gómez-Merino A.I.	431	Mata P.	93
Gonçalves LMD.	205	McNally T.	285
Gouveia L.	45, 111, 149, 205	Mejia P.	57
Gracia-Fernández C.	371	Meyer F.	397
Guerrero A.	9, 271, 277	Militão M.	111
Gutiérrez-Barranco E.	401	Miranda J.	377
Gutiérrez-Solís M.J.	21	Moldão-Martins M.	69
<b>H</b>		Moral M.	383
Haward S.J.	37, 339	Moreira R.	123, 197
Hernández M.J.	105, 117, 129, 211	Moret-Tatay A.	211
Hernando I.	211		31, 233, 247, 265, 291,
Herranz B.	135, 157, 189	Muñoz J.	391, 423

Muñoz M.E.	99, 313	Rodrigues R.	377, 407
Murillo-González S.	333	Rodrigues R.O.	357, 363, 407
Mutabazi I.	345	Rodríguez Belenguer P.	105
<b>N</b>		Rodríguez-García J.	211
Nácher A.	105	Romero A.	9, 21, 225, 277
Navarro F.J.	241, 285	Rubio-Cintas M.D.	319
<b>O</b>		Rubio-Hernández F.J.	319, 333, 401, 431
Olivares M.D.	173	Ruiz D.	225
Oliveira E.	45, 111, 149	Ruiz M.	271
Ortega F.J.	285	<b>S</b>	
Ortega-Casanova J.	333	Salvador A.	129
<b>P</b>		Sánchez R.	3, 73
Parras L.	401	Sánchez-Vicent A.	117
Partal P.	63, 225, 241	Sangroniz L.	313
Pastoriza-Gallego M.J.	417	Santacruz I.	301
Patrício P.	27	Santamaría A.	57, 99, 313
Peixinho J.	345	Santos J.	31, 233
Pereira A.I.	363	Santos J.C. P.	307
Pérez-Mosqueda L.M.	265, 291	Sanz T.	129
Peris J.	117	Silva S.	69
Picó J. A.	117	Sobral R.G.	27
Pinho D.	357, 363, 407	Soergel F.	397
Pinho E.	253	Sousa I.	69, 81, 87, 165
Pinho F.T.	351	<b>T</b>	
Pinho S.	81	Taboada B.	377, 407
Pinto E.	357, 363, 377, 407	Tarancón P.	129
Piñeiro M.M.	417	Teixeira P.	325
Pires C.	165	Tomé A.S.	165
Portela R.	27	Tonin F.	45
<b>R</b>		Torres M.D.	123, 197
Rama B.	123, 197	Tovar C. A.	135, 157, 181, 189
Ramírez P.	265, 291, 423	Trujillo L.A.	233, 265, 291
Ramos S.	93	<b>V</b>	
Rasteiro M. G.	253	Valencia C.	3, 15, 73, 259
Raymundo A.	93, 165	Velázquez-Navarro J.F.	431
Ribeiro B.	69	<b>Y</b>	
Ribeiro H. M.	45, 111, 149, 205	Yaginuma T.	363, 407





